LANTHANIDE BORIDE SYSTEMS AND PROPERTIES

Part I: Lanthanide-Boron-Carbon Systems

Part II: Vaporization and Stabilities of Lanthanide Borides

by

P. Kent Smith
B.S., University of Virginia, 1957

Submitted to the Department of Chemistry and the Faculty of the Graduate School of the University of Kansas in partial fulfillment of the requirements for the degree of Doctor of Philosophy.

Advisory Committee:

Redacted Signature

Chairman

Redacted Signature

Redacted Signature

May, 1964

ABSTRACT

This dissertation presents the results of experimental studies on the rare earth borides and rare earth borocarbides. The work consisted of six parts: (1) the ternary phases and equilibria in Ln-B-C systems; (2) the structure of the phase, LnB_2C_2; (3) the discovery of the new hectoboride phase; (4) the vaporization characteristics of the rare earth borides; (5) the decomposition pressures and the heat of sublimation of GdB_4; and (6) ternary Ln-M-B compatibility studies and the boron potential series.

The ternary Ln-B-C systems were investigated by arc melting and X-ray diffraction techniques. Emphasis was placed on the metal-deficient portion of the ternary Gd-B-C system. Five ternary phases were identified: GdB_2C_2, $Gd_{0.35}B_{0.19}C_{0.46}$, $Gd_7B_9C_4$, $Gd_3B_4C_3$ and $Gd_8B_7C_5$.

The LnB_2C_2 phase was prepared for the lanthanides, Nd, Gd, Tb, Dy, Ho, Er, and Yb, by reaction of their tetraborides with graphite. It is proposed that the tetragonal LnB_2C_2 structure contains continuous planar sheets of alternate boron and carbon atoms arranged in eight- and four-membered aromatic rings between which lie the metal atoms.

A primitive cubic phase of composition near LnB_{100} was found for Gd and Yb. The cell parameters were 16.50 and 16.56 Å, respectively.

By free evaporation and Knudsen effusion techniques, it was found that tetraborides of the light lanthanide metals, La, Ce, Pr, Nd and Sm,

lose metal gas preferentially to produce a hexaboride residue, which vaporizes congruently. Hexaborides of Gd, Tb, Dy, and Y vaporize with preferential loss of boron gas to a tetraboride residue, which vaporizes congruently. Ytterbium gas is lost from YbB_4, YbB_6 and YbB_{12} to a YbB_{100} residue. A mass spectrometric study revealed only atomic species in the gas phase.

The decomposition pressures of congruently vaporizing GdB_4 from ZrB_2 crucibles were measured in the range 1599-2403°K. by Langmuir, mass spectrometric and Knudsen effusion techniques.

It was demonstrated that variation in metal volatility alone was not sufficient to account for the difference in the vaporization behaviors of the borides. The stability of the borides with respect to condensed elements decreases with increasing atomic number, and the hexaboride becomes less stable faster than the tetraboride.

Ternary compatibility studies between the lanthanide borides and Ta, Zr, W and C were performed with arc melting and X-ray diffraction techniques to define the limits on the free energy of formation of the lanthanide borides. Emphasis was placed on the gadolinium borides. The concept of a boron potential series was developed to order the boride systems with respect to their ability to give up boron.

ACKNOWLEDGMENTS

The author is especially indebted to Professor Paul W. Gilles for his guidance and assistance in the direction of this research.

The counsel of Dr. Sven Westman on the LnB_2C_2 structure analysis and of Professor Richard L. Schowen on the interpretation of the bonding possibilities in LnB_2C_2 was greatly appreciated.

The financial assistance of the United States Atomic Energy Commission under contract number AT(11-1)-1140 and its predecessor AT(11-1)-83 is gratefully appreciated. Further, the author is indebted for the support of the Office of Naval Research, which provided equipment under contract Nonr-2760(00).

Many individuals have contributed immeasureably to the development of this research. The author is particularly indebted to his colleagues in the High Temperature Laboratory for their interest and constructive criticisms, and for the rapport of the laboratory. Considerable indebtedness is due to the multitude of technical personnel without whose able assistance in shop work, glass blowing, sample preparations, chemical analyses, data reduction, computer usage and typing, this research could not have been done.

The author dedicates this dissertation to his wife, Sarah, in recognition of her patience and support throughout this period.

TABLE OF CONTENTS

TABLES

PART I

FIGURES

PART I

PART II

INTRODUCTION

General and Long-Range Incentives

Chemistry is a science which characterizes matter and its interactions. From observations of the behavior of countless chemical systems, chemists have developed increasingly complex tools to categorize these observations and allow predictions of chemical behavior under many conditions. The formulations of quantum mechanics, kinetics, statistical mechanics, and thermodynamics are among the tools that have been developed in an attempt to explain the nature of the chemical bond.

The application of quantum theory to simple systems of gaseous matter has been most fruitful in lending insight into the role of electrons in determining bond strengths in molecules. However, in complex chemical systems where many atomic interactions are present, as in the condensed state, the tool of quantum mechanics is not nearly as well developed in its ability to define those factors which determine bond strength. In order for the theoretician to expand his tools for use in the condensed state, many experimental observations must be made on the effects of varying environments on condensed systems.

One such environmental variable is temperature. The influence of temperature on the equation of state of materials accounts for behaviors at high temperature considerably different from the behavior of materials at low temperatures. Unusual oxidation states, varied structures

and different kinetic effects exist at high temperatures. Further, chemical reactions which are not energetically favored at ordinary temperatures may become important at elevated temperatures because of the enhanced $T\Delta S$ contribution to the free energy available for the reaction.

At sufficiently high temperatures any material can be made to vaporize to gaseous atoms or molecules. If one measures the rate of vaporization as a function of temperature, information concerning the stability of the solid with respect to the gas phase is gained. Further, if the volatility of the constituents of the gas is known, information concerning the stability of the solid with respect to its condensed components is available. Still further, the observation of the process by which a material vaporizes contributes to the understanding of the bond strengths in the solid and the gas phases.

With the above framework this thesis was undertaken to study the factors which contribute to the stability of the lanthanide borides. From this information and many, many more experiments on related systems, our understanding of chemical bonding will increase. More specifically, from many such experiments, theory describing the equations of state for condensed materials will eventually be developed.

Immediate Incentives

Borides

In the last twenty years the demands of our rapidly expanding curiosity, and the development of nuclear and space sciences have forced inter-disciplinary focus on the physical and chemical behavior of materials at high temperatures. In the field of materials science,

inorganic and physical chemists, solid state physicists, ceramists, metallurgists and chemical engineers are losing their identities in their common efforts to contribute to the understanding and development of refractory materials.

Among the materials most suited for applications at high temperatures are carbides and borides. Very little is known concerning the existence of boride and carbide phases, much less their stabilities and interactions at high temperatures. Schwarzkopf and Kieffer (01) discuss the preparations, phases and structures of transition metal borides and carbides. Heat capacity data and heats of formation are being determined, with most emphasis to date placed on carbides. In the past ten years some thermochemical information, based on low temperature heat capacity measurements and vaporization studies, has been presented for the Periodic Groups IVB, VB and VIB metal borides. The high temperature behavior and thermodynamics of B_4C and BN have been fairly well characterized. Some thermochemical data are available for MgB_4, UB_4, UB_{12} and SiB_6. Other than these few data, information on the high temperature behavior of borides is woefully absent.

Borides, in general, are extremely interesting from the viewpoint of their structures and high stability. The complex cages, nets and sheets that boron atoms assume in elemental boron and in borides have been described by X-ray structure analysis. Using quantum mechanics, chemists have attempted to describe the boron covalent binding in metal borides. In general, their interpretations are supported by experiment. However, considerable additional experimental work must yet be done to provide a foundation for expansion of their theories. The factors which

influence the boride structures and stabilities must be ascertained.

In this Laboratory some experiments on the preparation of, and the determination of precise lattice parameters for, some lanthanide tetra- and hexaborides were performed by Dr. H. A. Eick (02). His work initiated a program to study the influence of metal volatility on the vaporization processes of metal borides, which is developed as the principal subject of this thesis.

The lanthanides were chosen for study not only because of their extreme variance in metal volatility, but also because the lanthanide series is long and because the compounds existing for one lanthanide generally exist for all. This fact affords an opportunity to compare the effects of many different lanthanides on boride stability with the same foundation of structure and composition. In effect, this similarity of structure and composition for the solid minimizes the heat effects of breaking up structures in which coordination spheres are different for different lanthanides, and allows the effect of metal volatility to be isolated from other factors. With such a wide choice of metal volatility and relatively fixed boride heats of formation, perhaps two constant vaporizing single phase compositions at the same temperature in the same metal-boron system may be found.

Borocarbides

An obvious extension of the work on boride and carbide refractory materials is the study of M-B-C ternary compounds. No thermochemical data exist for M-B-C ternary compounds. In fact, while researchers have been looking for such ternary compounds for twelve years, only in the last four years have any ternary compounds been found. In Vienna, as noted

later, Nowotny has found borocarbides of uranium, thorium and molybdenum.

In view of the similarity between the metal-boron and metal-carbon systems of thorium and uranium and those of lanthanide metals, ternary compounds might exist in lanthanide systems that are similar to those in the actinide systems. Further incentive for an examination of the lanthanide-boron-carbon system for refractory phases arises from the observation of a gadolinium borocarbide formed on interaction of gadolinium borides with graphite crucibles.

Structure of the Thesis

This work deals with phase relations, stabilities and high temperature properties of refractory lanthanide borides and borocarbides. The thesis is divided into two parts. Part I is concerned with the solid phases in the lanthanide-boron-carbon system. Phase relations were established from fifty synthetic compositions in the Gd-B-C field. The structure of LnB_2C_2 is discussed. Part II, the principal effort of this work, discusses the existence and stability of lanthanide borides both with respect to condensed elements and with respect to gaseous elements from an examination of the vaporization properties and from ternary compatibility studies with transition metals and graphite. As a reference point for the relative stabilities, the decomposition pressures of GdB_4 are determined as a function of temperature.

PART I

LANTHANIDE-BORON-CARBON SYSTEMS

CHAPTER 1

BACKGROUND

1. 1 Transition Metal Borocarbides

Steinitz (03) in 1951 studied the interaction of titanium borides with titanium carbides and tantalum borides with tantalum carbides without finding any ternary phases. Similarly, Nelson, Willmore and Womeldorph (04), and Greenhouse, Accountius and Sisler (05), investigated the Ti-B-C system and reported no ternary phases. Glaser (06) in 1952 surveyed the metal-boron-carbon fields for Ti, Zr, V, Nb, Ta, Cr, Mo, W and Th and found no ternary compounds in any of these systems. More recently, Nowotny, Benesovsky, Brukl, Schob, Rudy and Toth (07, 08, 09, 10), have investigated in detail the systems Zr-, Hf-, Mo-, V-, Nb-, Ta- and W-B-C. Only one ternary compound was found, Mo_2BC. This phase has been found by Nowotny to melt congruently at $2800 \pm 10^{o}C$. (11). Jeitschko, Nowotny and Benesovsky (12) determined the crystal structure of Mo_2BC as D_{2h}^{17}, orthorhombic, with all atoms in position 4(c). The atoms are located at (0, y, 1/4; 0, $\bar{y}$, 3/4)+(0, 0, 0; 1/2, 1/2, 0) with $y_B = 0.027$ and $y_C = 0.192$. The cell parameters are 3.086, 17.35 and 3.047Å for a_o, b_o and c_o, respectively. The phase, W_2BC, could not be made. An iron phase of composition $Fe_{23}C_3B_3$ has been reported by Stadelmaier (13).

1. 2 Alkaline Earth Borocarbides

Markovskii and Vekshina (14) reported the existence of an alkaline earth borocarbide of composition Ca-, Sr-, and $BaBC_2$. This phase was formed on reaction of metal oxide, B_2O_3 and graphite. A more detailed study (15) set the composition at MB_2C_4, rather than MBC_2. This phase appeared in reaction products at 1300°C. along with MC_2, B_4C and MB_6. At higher temperatures only borates, borides, graphite and/or B_4C appeared. They attempted to prepare this phase in the lanthanide system, but produced only the LnB_x phase, noted in Chapter 1.4, along with LnB_6 for the reaction of CeO_2 or La_2O_3 with B_2O_3 and graphite (16).

1. 3 Actinide Borocarbides

The investigations of Nowotny, Benesovsky and Rudy (17), in the U-B-C system revealed a single ternary phase, UBC, with extensive solid solution. This phase is orthorhombic, D_{2h}^{17}, with a_o, b_o and c_o, 3.591, 11.95 and 3.372 Å, respectively. Further research by Nowotny, Toth, Benesovsky and Rudy (18), in the Th-B-C system exposed, in addition to ThBC with the UBC symmetry and extensive solid solution, Th_2BC_2 which oxidizes in air and has a structure closely related to ThC_2; $ThBC_2$ which has a structure too complex for easy identification; and ThB_2C which was indexed as a C-32 type hexagonal phase with a_o and c_o, 3.872 and 3.812 Å, respectively. There is a summary of the M-B-C systems studied by Nowotny's group by Rudy (19) with a discussion of the use of phase relations to derive heats of formation and related thermochemical data for binary and ternary refractories.

1. 4 Lanthanide Borocarbides

The existence of ternary borocarbide phases with the lanthanide and actinide metals has been partially studied by Brewer and Heraldsen (20) in their nitride, boride, carbide compatibility studies. Much of the behavior among unfilled d-orbital transition metals noted in Chapters 1.1 and 1.3 was confirmed. In addition they found that CeB_6 and carbon will not react, but that CeB_4 reacts with carbon to form some uncharacterized Ce-B-C compound. The CeC-CeB_4, Ce_2C_3-CeB_4 and CeC_2-CeB_4 two phase joins which they have inferred must be corrected in view of the ternary phases found in the present work.

Hoyt, Chorne and Cummings (21) hot pressed lanthanide tetra- and hexaborides with carbon in graphite dies. However, the only products they observed were B_4C and lanthanide carbides. The attempts of Post, Moskowitz and Glaser (22) to prepare lanthanide borides by reaction of lanthanide sesquioxides with boron in the presence of carbon at 1500 to 1800°C. in graphite crucibles under inert atmospheres produced the phases listed in Table 1.

Table 1

LnB_x Lattice Parameters and Symmetry

Ln	a_o (Å)	c_o (Å)	Symmetry
La	3.82	3.96	tetragonal
Pr	3.81	----	cubic or pseudocubic
Gd	3.79	3.63	tetragonal
Yb	3.77	3.56	tetragonal
Y	3.78	3.55	tetragonal

The cubic phase, PrB_x, occurs when the a_o and c_o variations with atomic number cross at Pr, making a_o nearly equal to c_o. The phase, YB_x, was made by Binder in a similar study of yttrium borides (23). These LnB_x phases were suggested as borides ($3 < x < 4$) stabilized by carbon or oxygen. Later, Binder (24) suggested that carbon was needed to stabilize this phase, and that the composition might better be described as MB_2C. In the work of Johnson and Daane (25) on the La-B system, an unindexed ternary phase was found, whose composition was estimated as LaBC.

In view of the close similarity between Ln-B, Th-B and U-B and between Ln-C, Th-C and U-C binary systems, similar ternary phases might be expected to be formed in the lanthanide systems. For example, ThBC and UBC were found by Nowotny, et al. (18), and have the same structure. However, the analagous counterparts to Th_2BC_2, $ThBC_2$ and ThB_2C in the U-B-C ternary field were absent. The Th-B-C phases were studied in the same 800 to 1400°C. temperature range as the U-B-C system study. Tetragonal and cubic phases in the Ln-B-C system reported by Post cannot be indexed with the ThBC, UBC or ThB_2C symmetry. The investigation of the Gd-B-C ternary field was undertaken with the above observations in mind.

CHAPTER 2

PREPARATION AND CHARACTERIZATION OF SAMPLES

2. 1 Materials

Gadolinium rod, 32 g., was obtained from Michigan Chemical Corp. The assay provided with the sample specified Gd content as 99+ percent. This sample, lot 8859, was designated Gd-1.

Amorphous boron, grade AA, 325 mesh, was obtained from Cooper Metallurgical Associates. The assay accompanying the sample specified B content at 99.5%, Fe at 0.15% and carbon at 0.10%. This sample, lot number 1414, lab sample B-8, was used in preparing GdB_4 samples, 16 GdAM, 17 GdAM and 51 GdAM, and in preparing GdB_6 samples, 15 GdAM and 50 GdAM.

Spectroscopic grade graphite, SP-1, from Lots 329 and 513, was obtained from National Carbon Co., Inc.

The samples of GdB_4, 16 GdAM, 17 GdAM and 51 GdAM, and of GdB_6, 15 GdAM and 50 GdAM, were prepared as indicated in Chapter 2. 2. 2. of Part II. Preparations and materials of other lanthanide borides in Table 3. 1 are specified in Part II, Chapter 2. 2. 1 and 2. 2. 2. Emission spectrographic analysis of GdB_4, 16 GdAM, showed Cr, Cu and Fe, less than 0.1%; Si, barely detectable; and no other impurities.

2. 2 Preparation and Characterization

Synthetic compositions in the ternary field on the boron side of the GdB_4-C join were prepared with GdB_6, B and C or with GdB_4, B and C. About 0.2g of sample was prepared from 325 mesh powdered reagents for each synthetic ternary composition. The blended mixture was compacted at 2000 psi in a one-quarter inch hardened steel die. The resultant cylindrical pellet was twice melted on a water-cooled copper hearth under an oxygen-purged, argon atmosphere in an arc melter. Heating cycle durations were typically 30 seconds to two minutes at 200 amperes for each melting. On and around some cooled buttons for a radius of one or two inches was a light vapor deposit of mostly graphite. While this deposit could be wiped from the buttons before they were crushed and ground, the graphite contamination of adjacent samples in the arc melter was observed in some cases discussed later. The resultant cooled button was crushed in a diamond mortar (hardened steel), ground in an agate mortar and X-rayed by Guinier focusing or Debye-Scherrer powder diffraction cameras with Cu-K_{α_1} (1.54050Å) radiation from a Philips Electronics, Inc., generator.

The Guinier (26) forward focusing camera employed the $10\bar{1}1$ reflection from a curved quartz crystal to focus and separate Cu-$K\alpha_1$ (1.54050Å) or Cu-$K\alpha_2$ (1.54434Å) from the primary beam. The primary copper radiation passed through the line source side of the Philips Electronics X-ray tube mounted horizontally and driven externally from the generator. The focusing cameras have a film radius of 83.9mm. Slits, monochromator, sample holder and rotating motor and film cassette were mounted inside a sealed box capable of being evacuated to 10^{-4}mm. during

the exposure. These two cameras were purchased from Försvarets, Forskningsanstalt, Avdelning 1, Stockholm, Sweden.

From computational methods with IBM 653 and 1620 machines d-spacings were generated from the reading of X-ray powder films. From these d-spacings and by comparison of these films with films made on reference binary phases, all the lines on the film of the sample could be assigned to their appropriate phases in most cases in spite of the complexity of the sample composition.

The preparations in the ternary field on the metal-rich side of the GdB_4-C join were done with B, C and Gd reactants. All gadolinium handling was done in a nitrogen atmosphere dry box, in view of the air oxidation characteristic of lanthanide metals. Gadolinium metal filings, from which iron contamination was magnetically removed, were collected in a tared weighing bottle. This weight of gadolinium was matched with the proper amount of boron and graphite to produce the desired synthetic stoichiometry. Total sample weights were about 0.5 to 1.2g. After being mixed in the weighing bottle, the material was loaded into a three-eighths inch hard steel die, removed from the glove box, and, in a time interval of no more than five minutes, pressed at 6000 psi. The pellet was mounted in the arc furnace, melted twice under oxygen-purged argon, and the cooled button returned into the glove box. The button was crushed and ground as above, but in the glove box. A portion of the sample was removed from the box and loaded into the Guinier camera, which was then pumped out to 10^{-3}mm. The bulk of the sample was sealed into a weighing bottle with paraffin while still in the dry box.

The care to exclude oxygen is probably not very important with gadolinium, but some of the carbon-rich products were quite pyrophoric. For instance, GdC_2 powder will oxidize completely to Gd_2O_3 and carbon in one hour in air. The maximum time these preparations were exposed to air between melting and X-ray analysis was five minutes.

Chemical analyses of the ternary preparations generally were not performed. The preferential loss of constituents after mixing during handling and arc melting was thought to be less than one percent by weight.

CHAPTER 3

PHASE DIAGRAM RESULTS AND DISCUSSION

3. 1 Ternary Diagram and Experimental Observations

Table 3. 1 contains a listing of the synthetic metal-boron-carbon compositions for gadolinium and for other lanthanide metals. The first column contains the sample identification. The atomic proportions of the components in the synthetic composition in thousandths are listed in the second column. Columns three and four reveal the diffraction camera used, the photograph number and the phases identified in the reaction product. The weights of the starting materials are shown in the fifth column.

Figure 3. 1 summarizes the fifty synthetic compositions listed in Table 3. 1 for the gadolinium-boron-carbon field. In view of the heavy concentration of experimental compositions in the GdB_4-C-B triangle, a key is provided with the figure to identify the equilibria observed at each synthetic composition in this region.

Figure 3. 2 is a non-isothermal phase diagram derived from the observations of Table 3. 1 and Figure 3. 1. The phases on the gadolinium side of the GdB_4-GdB_2C_2 and GdB_2C_2-C joins were not investigated in nearly the detail of the metal deficient portion of the ternary field. Thus, much of this portion of the diagram is assumed. In addition to the GdB_2C_2 phase, which is discussed in great detail in Chapter 4, four

TABLE 3. 1

Synthetic Lanthanide-Boron-Carbon Compositions and Observed Phases

D = Guinier film
C = Debye-Scherrer film

mjr = major
mnr = minor

tr = trace
eqc = equal concentrations

Sample	Composition Ln	B	C	Film	Product Phases	Starting Material		NB page
2LaAM	091	546	363	C-2401	LaB_6 only	.11336g .02618	LaB_6(1LaAM) C	467
7NdAM	105	526	369	C-2353	NdB_2C_2, mjr NdB_4, mnr NdB_6, tr	.16452 .02650 .00953	NdB_4(5NdAMb) C B	451
8NdAM	105	526	369	C-2355	NdB_2C_2, mjr NdB_4, mnr C, mjr	.1500 .00106	NdB_4, NdB_6, NdB_2C_2, (7NdAM) C	464 451
2SmAM	091	546	363	C-2357	SmB_6 only	.12018 .02710	SmB_6(1SmAM) C	456
20GdAM	167	688	164	C-2274	GdB_4, mjr GdB_2C_2, tr	.20244 .01195	GdB_4(16GdAM) C	428
21GdAM	181	725	094	C-2276	GdB_4, mjr GdB_2C_2, tr	.20002 .00623	GdB_4(16GdAM) C	428
22GdAM	143	570	287	C-2277	GdB_2C_2 GdB_4, eqc	.20134 .02432	GdB_4(16GdAM) C	429
23GdAM	112	447	441	C-2278	GdB_2C_2 GdB_6, eqc C, tr	.19315 .04572	GdB_4(16GdAM) C	429
24GdAM	091	363	546	C-2308	GdB_2C_2 GdB_6 C, eqc	.14898 .05379	GdB_4(16GdAM) C	439
25GdAM	091	544	366	C-2298	GdB_2C_2, mjr GdB_6, tr	.16505 .03608	GdB_6(15GdAM) C	439
26GdAM	066	398	535	C-2309	GdB_2C_2, mjr GdB_6 C, eqc, mnr	.17588 .07680	GdB_6(15GdAM) C	439
27GdAM	111	556	332	C-2299	GdB_2C_2, mjr GdB_6 C, eqc, tr	.17046 .00924 .03055	GdB_4(16GdAM) B C	439

TABLE 3. 1, continued

Sample	Composition Ln	B	C	Film	Product Phases	Starting Material		NB page
28GdAM	077	536	387	C-2302	GdB_2C_2, mjr GdB_6, mnr	.13262 .02149 .04015	GdB_4(16GdAM) B C	440
29GdAM	063	428	509	C-2310	GdB_2C_2, mjr GdB_6 C, eqc, mnr	.12205 .01856 .05931	GdB_4(16GdAM) B C	440
30GdAM	126	503	372	C-2313 C-2316	GdB_2C_2, mjr GdB_6, mnr to tr	.17067 .03027	GdB_4(16GdAM) C	440
32GdAM	132	795	073	C-2319	GdB_6 only	.19391 .00579	GdB_6(15GdAM) C	440
33GdAM	124	744	132	C-2320	GdB_6 only	.19012 .01096	GdB_6(15GdAM) C	440
34GdAM	111	668	221	C-2318	GdB_6, mjr GdB_2C_2, mnr	.17945 .01933	GdB_6(15GdAM) C	445
35GdAM	122	732	146	C-2323	GdB_6, mjr GdB_2C_2 C, eqc, mnr	.11780 .07643	GdB_6(15GdAM) C	445
36GdAM	066	267	667	C-2324	GdB_2C_2 GdB_6, eqc, mjr C, tr	.12939 .07765	GdB_4(16GdAM) C	445
40GdAM	125	500	375	C-2574	GdB_2C_2, mjr GdB_4 GdB_6, eqc, mnr C, tr	3.30808 .58724	GdB_4(16GdAM) C	492
41GdAM	143	572	286	D-1092	GdB_2C_2 GdB_4, eqc	1.00065 .12055	GdB_4(17GdAM) C	576 581
42GdAM	133	533	334	D-1111	GdB_2C_2, mjr GdB_6, mnr GdB_4, tr	.57512 .08637	GdB_4(17GdAM) C	586
43GdAm	100	600	300	D-1112	GdB_2C_2, mjr GdB_6, mnr	.73548 .11946	GdB_6(15GdAM) C	586
44GdAM	100	500	400	D-1113	GdB_2C_2, mjr GdB_6, mnr	.52525 .02839 .12619	GdB_4(17GdAM) B C	586

TABLE 3. 1, continued

Sample	Composition In	B	C	Film	Product Phases	Starting Material		NB page
45GdAM	118	529	353	D-1116	GdB_2C_2, mjr GdB_6, mnr	.58123 .01571 .10461	GdB_4(17GdAM) B C	587
52GdAM	050	800	150	D-1220	GdB_6, mjr GdB_2C_2, mnr B_4C, mnr C, tr	.12119 .05912 .01969	GdB_6(15GdAM) B C	618 628
53GdAM	050	900	050	D-1221	GdB_6, mjr B_4C, mnr GdB_{100}, mnr	.12199 .07140 .00660	GdB_6(15GdAM) B C	618 629
54GdAM	040	160	800	D-1222	GdB_2C_2 GdB_6 C, eqc	.09090 .10917	GdB_4(51GdAM) C	618
55GdAM	130	610	260	D-1223	GdB_2C_2, mjr GdB_4, mnr GdB_6, mnr	.17279 .00647 .02074	GdB_4(51GdAM) B C	618
56GdAM	130	610	260	D-1224	GdB_2C_2, mjr GdB_6 GdB_4, eqc, mnr	.17280 .00647 .02073	GdB_4(51GdAM) B C	618
57GdAM	080	470	450	D-1225	GdB_2C_2 GdB_6, eqc, mjr GdB_4, tr	.13898 .01409 .04692	GdB_4(51GdAM) B C	618
72GdAM	020	960	020	D-1269	GdB_{100} GdB_6, eqc, mjr C, tr	.0968 .1981 .0052	GdB_6(15GdAM) B C	644
73GdAM	050	650	300	D-1324	GdB_2C_2, mjr GdB_6 C, eqc, tr	.18003 .06147 .05849	GdB_6(15GdAM) B C	644
74GdAM	050	580	370	D-1328	GdB_2C_2, mjr GdB_6, mnr C, tr	.17922 .04896 .07181	GdB_6(15GdAM) B C	644
75GdAM	040	450	510	D-1329	GdB_2C_2, mjr GdB_6, mnr C, tr	.15413 .03947 .10640	GdB_6(15GdAM) B C	644
76GdAM	030	300	670	D-1330	GdB_2C_2, mjr GdB_6 C, eqc, mnr	.12478 .02434 .15088	GdB_6(15GdAM) B C	644

TABLE 3. 1, continued

Sample	Composition Ln	B	C	Film	Product Phases	Starting Material		NB page
77GdAM	010	900	090	D-1331	GdB_6	.05372	GdB_6(15GdAM)	644
					B_4C	.22011	B	
					GdB_{100}, eqc	.02618	C	
					C, mnr			
78GdAM	070	920	010	D-1332	GdB_{100}, mjr	.06579	GdB_6(15GdAM)	644
					GdB_6	.22917	B	
					C, eqc, mnr	.00508	C	
79GdAM	010	980	010	D-1333	GdB_{100}, mjr	.05413	GdB_6(15GdAM)	644
					C, mnr	.24294	B	
					GdB_6, tr	.00293	C	
94GdAM	333	333	333	D-1671	GdKS9	.54815	Gd	766
				C-2871	lines	.03780	B	998
				C-2874		.04196	C	
95GdAM	400	200	400	D-1675	GdKS5, mjr	.58115	Gd	766
				C-2872	GdC_2, tr	.02004	B	998
				C-2875		.04449	C	
96GdAM	250	250	500	D-1681	GdB_2C_2, mjr	.71256	Gd	766
				D-1683	GdC_2, tr	.04914	B	998
				C-2873		.10909	C	
				C-2876				
97GdAM	250	500	250	D-1674	GdKS9, mjr	.35235	Gd	766
				C-2879	GdB_4, mnr	.04860	B	998
					lines	.02697	C	
98GdAM	200	400	400	D-1672	GdB_2C_2, mjr	.82980	Gd	774
				D-1676	GdC_2, tr	.11445	B	998
				C-2893		.12704	C	
98aGdAM	200	400	400	D-1668	GdB_2C_2only	3.92105	Gd	774
				D-1670		.54079	B	998
						.60031	C	
99GdAM	400	400	200	D-1669	Gd	.77347	Gd	774
				C-2899	GdKS10, eqc	.05334	B	998
						.02961	C	
100GdAM	600	200	200	D-1677	Gd	.50529	Gd	774
					GdKS10, eqc	.01170	B	998
						.01292	C	

TABLE 3. 1, continued

Sample	Composition Ln	B	C	Film	Product Phases	Starting Material		NB page
101 GdAM	200	400	400	D-1682 C-2913	GdB_6 GdB_2C_2, mjr C, tr (O_2 present on melting)	1.08993 .15028 .16687	Gd B C	774 998
102GdAM	750	125	125	D-1684 D-1673 D-1679	Gd only	.56000 .00663 .00722	Gd B C	774 998
103GdAM	333	167	500	D-1680	GdKS5 only	.51023 .01756 .05860	Gd B C	783 998
104GdAM	333	500	167	D-1678	GdKS7, mjr GdB_4, mnr	.50296 .05026 .01928	Gd B C	783 998
105GdAM	200	400	400	D-1691	GdB_2C_2 only	4.02112 .55424 .61575	Gd B C	783 998
3TbAM	118	588	294	C-2352	TbB_2C_2, mjr TbB_4, tr to mnr	.16910 .02533 .00885	TbB_4 (2TbAMa) C B	451
2DyAM	091	546	363	C-2375	DyB_2C_2, mjr DyB_4, mnr C, tr	.20399 .04324	DyB_6 (1DyAMb) C	482 475 467
2HoAM	112	555	333	C-2501	HoB_2C_2 only	.2361 .0388	$HoB_{4,6,12}$ (1HoAM) C	511 489, 509
2ErAM	112	555	333	C-2498	ErB_2C_2, mjr ErB_4, tr	.1155 .0198 .0059	$ErB_{4,12}$ (1ErAM) C B	507 504 490
2YbAM	091	546	363	C-2356	YbB_2C_2, mjr YbB_6, mnr	.12056 .02425	$YbB_{6,4}$ (1YbAM) C	456
5YbAM	091	546	363	C-2567	YbB_2C_2, mjr YbB_6, mnr C, tr	1.0439 .2098	$YbB_{6,4}$ (1YbAM) C	523
5YbAMa	091	546	363	C-2571	YbB_2C_2 YbB_6, eqc	remelt of 5YbAM		528

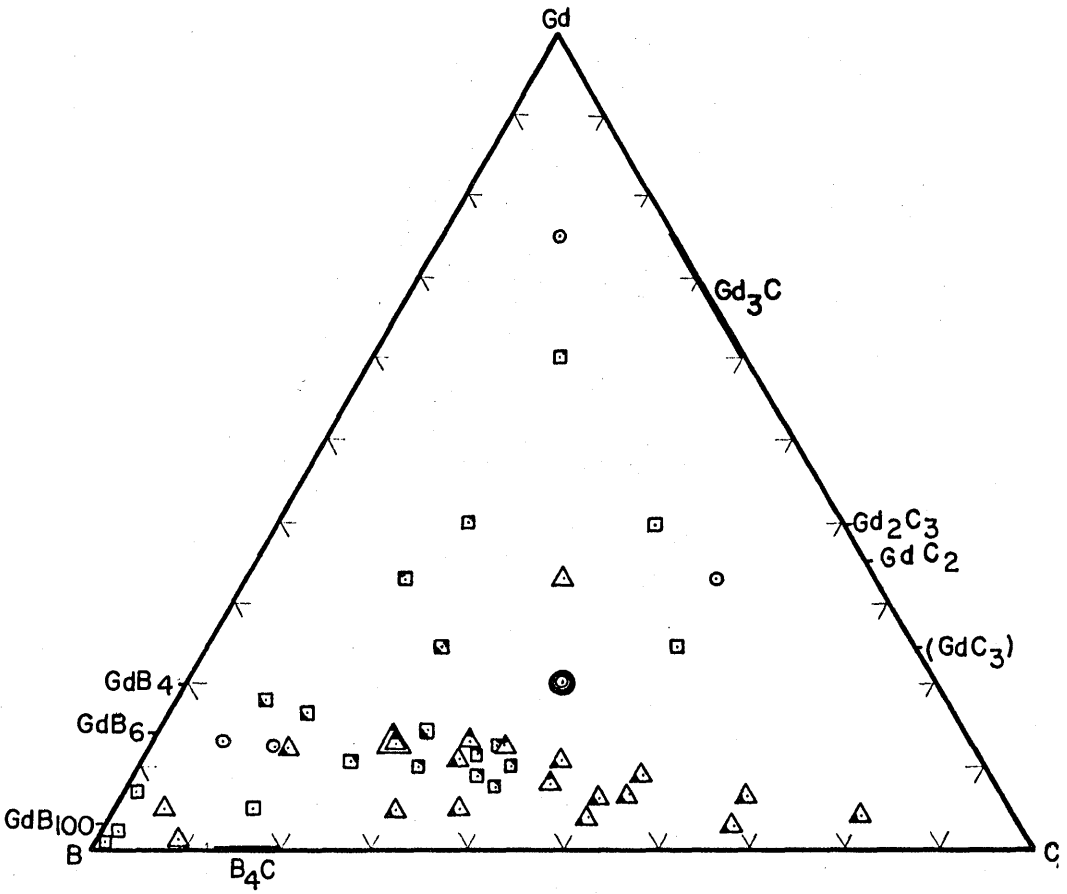

SYNTHETIC COMPOSITIONS IN THE Gd-B-C FIELD

FIGURE 3.1

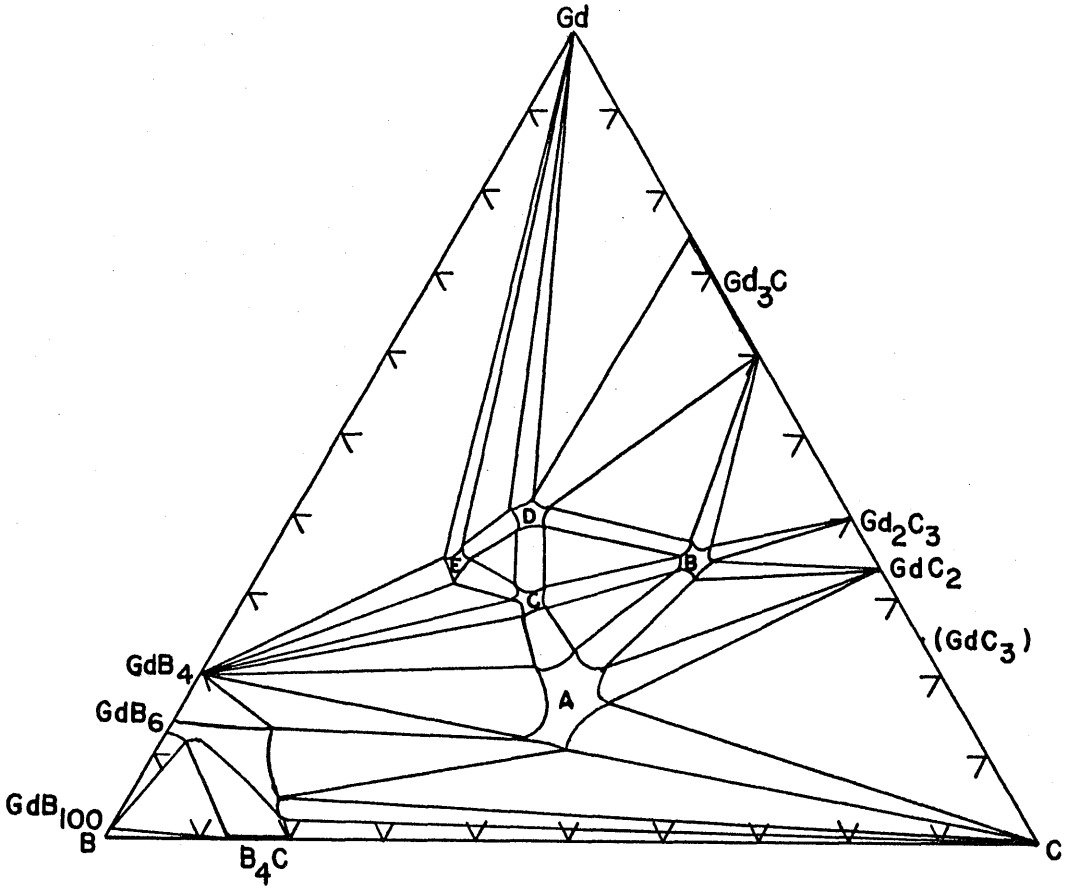

A	GdB_2C_2		$Gd_{0.20}B_{0.40}C_{0.40}$
B	"Gd_2BC_2"	GdKS5	$Gd_{0.35}B_{0.19}C_{0.46}$
C	$Gd_3B_4C_3$	GdKS9	$Gd_{0.30}B_{0.40}C_{0.30}$
D	$Gd_8B_7C_5$	GdKS10	$Gd_{0.40}B_{0.35}C_{0.25}$
E	$Gd_7B_9C_4$	GdKS7	$Gd_{0.35}B_{0.45}C_{0.20}$

GADOLINIUM-BORON-CARBON PHASE DIAGRAM

FIGURE 3. 2

other ternary Gd-B-C phases were found. These are called GdKS5, GdKS7, GdKS9 and GdKS10. Their compositions are estimated at $Gd_{0.35}B_{0.19}C_{0.46}$, $Gd_7B_9C_4$, $Gd_3B_4C_3$ and $Gd_8B_7C_5$, respectively.

The gadolinium borides, GdB_4, GdB_6 and GdB_{100}, are discussed in Part II, Chapter 2. Crystallographic information on all binary compounds is listed in Table 5. 8 and in Table 2. 1, Part II.

3. 2 Gadolinium Deficient Region

The two-phase region, GdB_4-GdB_2C_2, is established clearly by preparations 41GdAM, 22GdAM, 21GdAM and 20GdAM. Carbon solubility in GdB_4 is at most 10 atomic percent, as indicated by 21GdAM. The three-phase equilibria field, GdB_6-GdB_4-GdB_2C_2, is established by 55GdAM, 56GdAM, 57GdAM, 42GdAM and 40GdAM. The presence of graphite in 40GdAM is attributed to contamination from neighboring pellets during their melting in the same copper hearth (cf. Chapter 2. 2).

The GdB_6-GdB_2C_2 two-phase region was found in 45GdAM, 43GdAM, 44GdAM, 25GdAM, 28GdAM, 30GdAM and 34GdAM. Apparently, there is much more solid solubility of graphite in GdB_6 than in GdB_4. This fact is revealed by 32- and 33GdAM. An estimate of 15 atomic percent graphite solution in GdB_6 is also reflected in the considerable carbon content of the GdB_6-GdB_{100} two-phase region. Comparison of the d-spacings of back reflection Debye-Scherrer powder pattern lines indicated no change in GdB_6 lattice parameter as a function of carbon content. However, Johnson and Daane (25) observed no change in lattice parameter for LaB_6 as they varied the boron content from 85 to 88 atomic percent through the homogeneity range of LaB_6.

The GdB_6-C-GdB_2C_2 ternary phase field is demonstrated in 73-, 74-, 75-, 76-, 54-, 24-, 26-, 27-, 29-, 35-, 36- and 23GdAM. Proper compositions were not investigated to demonstrate the GdB_6-B_4C-C equilibrium, but it is implied by other observed triangles. In 52GdAM GdB_6, GdB_2C_2 and a single B_4C line were observed. But graphite was also observed, and the overwhelming evidence for a GdB_6-GdB_2C_2-C triangle prohibits a GdB_6-B_4C-GdB_2C_2 triangle. This weak B_4C line and graphite are attributed to contamination or incomplete reaction. The GdB_6-B_4C two-phase field was not demonstrated. But the GdB_6-B_4C-GdB_{100} field is established by 77- and 53GdAM. Further, the GdB_6-GdB_{100} two-phase equilibrium is revealed by 72-, 78- and 79GdAM, as well as additional binary preparations discussed in Part II, Chapter 2. 3. 4. Samples 72-, 78- and 79GdAM contained small amounts of graphite. Either a GdB_{100}-B_4C-GdB_6 equilibrium or a GdB_{100}-C-GdB_6 equilibrium exists. The beautiful match of $\sin^2\theta$ values for the phases in 77- and 53GdAM with reference film and literature values is convincing evidence in favor of the GdB_{100}-B_4C-GdB_6 equilibrium. Further support of this conclusion lies in the observation of the CeB_6-B_4C-C equilibrium by Brewer and Heraldsen (20). The presence of graphite in 72-, 78- and 79GdAM is, again, explained by incomplete reaction or contamination from neighboring pellets during the arc melting. No attempt was made to demonstrate GdB_{100}-B_4C and GdB_{100}-B_4C-B equilibria; however, these equilibria must exist.

3. 3 Gadolinium Rich Region

3. 3. 1 GdKS5

The X-ray pattern of GdKS5 is fairly simple, i.e., it contains relatively few lines. Excellent patterns of GdKS5 were obtained in 95-

and 103GdAM. Even though these patterns do not overlap exactly, their symmetries appear quite similar. The differences might be explained by extensive anisotropic solid solution ranges. From the synthetic composition and the phases observed in equilibrium with GdKS5, the composition of this phase is estimated as $Gd_{0.35}B_{0.19}C_{0.46}$, close to Gd_2BC_2. This material is black and very brittle.

Since Nowotny (17) did not report a diffraction record for Th_2BC_2, the symmetries cannot be compared. Nowotny stated that the structure of Th_2BC_2 is closely related to ThC_2, which is monoclinic (17). However, from its diffraction record, $Gd_{0.35}B_{0.19}C_{0.46}$ is not at all similar to GdC_2, which is reported by Spedding, Gschneidner and Daane (28) to be body-centered tetragonal of the C-11a type. The $Gd_{0.35}B_{0.19}C_{0.46}$ cell is either of lower symmetry or has a large unit cell compared to GdC_2.

Nowotny reported that Th_2BC_2 oxidizes quickly in air similarly to ThC_2. The same behavior occurs with $Gd_{0.35}B_{0.19}C_{0.46}$; however, $Gd_{0.35}B_{0.19}C_{0.46}$ is more stable in air than GdC_2. The crushed arc melted buttons containing Gd_2BC_2 turn to a white chalky powder in a few hours exposed to air. The sample, 103GdAM (Gd_2BC_3), must have contained more GdC_2 than did 95GdAM (Gd_2BC_2), even though the X-ray pattern revealed none. The powdered sample of 103GdAM had oxidized to almost white; but the carbon deficient sample, 95GdAM, on being exposed for the same length of time, was still nearly black. The inability to see GdC_2 in 103GdAM probably arises from oxidation to finely divided oxides during the Guinier exposure.

An attempt has been made to index GdKS5. It is not cubic, tetragonal or hexagonal in symmetry. It is believed that the phase can be indexed on orthorhombic axes. A partial indexing was achieved with

a_o and c_o, 6.09 and 8.56 Å, respectively. The b-axis must be at least as large as eight Angstroms to fit the low angle lines. Table 3. 2 contains the diffraction record of both 95- and 103GdAM.

3. 3. 2 GdKS7

The X-ray pattern of GdKS7 is given by 104GdAM (Gd_2B_3C). This preparation clearly shows a significant amount of GdB_4. In view of the complexity of the GdKS7 diffraction record (cf. Table 3. 2) no attempt was made to index the pattern. On the basis that this phase must have a composition richer in metal and carbon than Gd_2B_3C, the stoichiometry has been estimated as $Gd_7B_9C_4$. This choice was made considering how the overall ternary phase equilibria can best be made to agree with the observed experimental results. However, the stoichiometry of this phase might well be Gd_2B_2C, for which there is no Th-B-C counterpart. The phase, GdKS7, is a brittle black material, apparently stable to air at room temperature.

3. 3. 3 GdKS10

The diffraction record of GdKS10, taken from 99- and 100GdAM, is very complex, and the powder photographs are of poor quality. This phase is also black, brittle and stable to air at room temperature. While comparison is difficult, GdKS10 and GdKS7 are obviously different phases. The stoichiometry of GdKS10 is estimated at $Gd_8B_7C_5$. GdKS7 and GdKS10 diffraction records appear in Table 3. 2 along with the lines of the minor phases present.

TABLE 3. 2

GdKS5, GdKS7 and GdKS10 Diffraction Records.
$CuK\alpha_1$, 1.54050Å, Radiation.

95GdAM---GdKS5 Film D-1675			103GdAM---GdKS5 Film D-1680		
I/I_o	d, Å	$\sin^2\theta$	I/I_o	d, Å	$\sin^2\theta$
S	3.490	0.04868	M	3.515	0.04803
VS	3.044	.06403	S	3.155	.05960
M	2.712	.08071	W	3.089	.06220
S	2.606	.08737	S	2.738	.07915
S	2.586	.08876	S	2.587	.08869
S	2.532	.09257	S	2.535	.09231
VW	2.113	.13292	VW	2.186	.12412
M	1.877	.16847	M	1.979	.15145
M	1.840	.17522	W	1.825	.17809
M	1.813	.18044	W	1.807	.18169
M	1.665	.21393	W	1.782	.18693
VW	1.625	.22471	M	1.578	.23833
M	1.574	.23934	VW	1.518	.25757
W	1.520	.25686	VW	1.468	.27522
W	1.497	.26466			
VW	1.425	.29204			
VW	1.403	.30153			

TABLE 3. 2, continued

104GdAM---GdKS7 Film D-1678			99GdAM---GdKS10 Film D-1669		
I/I_o	d, Å	$\sin^2\theta$	I/I_o	d, Å	$\sin^2\theta$
W	3.981	0.03744	M	3.375	0.05207
M	3.509	.04817	W	3.091	.06205
M	3.414	.05091	M	3.004	.06576
M	3.380	.05193	M	2.967	.06738
M	3.133	.06046	M	2.921	.06956
W	3.071	.06290	W	2.848	.07314
W	3.044	.06403	W	2.822	.07448
M	2.991	.06632	M	2.714	.08057
W	2.979	.06728	M	2.646	.08474
M	2.916	.06978	W	2.611	.08706
W	2.853	.07294	VW	2.486	.09597
VW	2.733	.07945	W	2.274	.11475
W	2.670	.08321	VW	2.240	.11824
M	2.626	.08607	W	2.214	.12109
M	2.544	.09170	M	1.784	.18640
M	2.482	.09627	W	1.689	.20866
M	2.460	.09801	VW	1.652	.21738
M	2.214	.12100	W	1.529	.25397

3. 3. 4 GdKS9

GdKS9 also has a complex diffraction record (Table 3. 3) for which no indexing scheme has been obtained. The phase is observed in 94- and 97GdAM. It too is stable to air at room temperature. While the composition is estimated at $Gd_3B_4C_3$, GdBC is also possible. No agreement between the diffraction records of ThBC or UBC and GdKS9 was found. There apparently is quite a range of solid solution for GdKS9, as indicated by the variation in d-spacings between 94- and 97GdAM.

3. 4 Limitations and Qualifications

No Gd-B-C counterpart was found for Nowotny's hexagonal ThB_2C or for the orthorhombic ThBC (18). GdKS7 and GdKS10 did not contain any GdB_2 in view of the high temperature of the arc melting (cf. Part II, Chapter 2. 1. 2). None of these ternaries could be matched with the powder films or diffraction records of GdC_2, Gd_2C_3, Gd_3C, GdC_3, GdB_2, ThBC, ThB_2C, Gd or Gd_2O_3.

This survey of the Gd-B-C ternary field by the arc melting and X-ray techniques should not be regarded as representing an equilibrium temperature-composition study. The compositions, phase equilibria and temperatures are generally poorly defined. In the GdB_4-GdB_2C_2-C-B region it was the intention of this study to define the behavior of GdB_4, GdB_6 and GdB_{100} in graphite at high temperatures. The compositions and equilibria found in this region are those observed after rapid cooling of melted samples each of which melts at a different temperature. Certainly different solid solution ranges, phase transitions and other equilibria might exist at lower temperatures. However, it is believed

TABLE 3. 3

GdKS9 Diffraction Records. CuK_{α_1}, 1.54050Å, Radiation.

94GdAM---GdKS9 Film D-1671			97GdAM---GdKS9 Film D-1674		
I/I_o	d, Å	$\sin^2\theta$	I/I_o	d, Å	$\sin^2\theta$
M	3.782	0.04149	VW	4.118	0.03501
S	3.733	.04257	W	3.757	.04204
W	3.502	.04838	W	3.622	.04521
M	3.440	.05014	M	3.471	.04927
M	3.353	.05277	VW	3.391	.05160
M	3.141	.06016	VW	3.309	.05421
W	3.008	.06557	W	3.234	.05676
M	2.934	.06892	VW	2.968	.06738
S	2.753	.07830	VW	2.791	.07613
M	2.688	.08211	M	2.712	.08067
W	2.573	.08961	VW	2.599	.08787
W	2.537	.09217	M	2.545	.09159
S	2.522	.09330	M	2.510	.09417
M	2.491	.09564	VVW	2.284	.11375
W	2.212	.12125	W	2.241	.11808
W	1.950	.15605	W	1.872	.16922
M	1.855	.17238	W	1.746	.19456
S	1.720	.20044	W	1.730	.19829
VW	1.630	.22335	VW	1.646	.21914
W	1.618	.22675	VW	1.636	.22174
S	1.554	.24411	VW	1.604	.23069
			VW	1.574	.23945
			VW	1.566	.24197

that the behaviors in this region generally represent those at lower temperatures and may be used to catalogue relative stabilities (cf. Part II, Chapter 14). The even more cursory examination of the GdB_4-GdB_2C_2-C-Gd region was performed only to uncover the ternary phases that might exist.

CHAPTER 4

PREPARATION AND PROPERTIES OF LnB_2C_2

4. 1 Description and Properties

GdB_2C_2 has no counterpart in the phases of the Th-B-C system (18). This phase is a black brittle solid, stable in air at room temperature, and does not decompose or melt in the presence of graphite up to 2400°K. in vacuum. This refractory material is not soluble in acetone, ether, alcohol, carbon tetrachloride, ethylene trichloride or water. It is attacked very slowly by concentrated HCl and will dissolve slowly in hot concentrated nitric, sulfuric or perchloric acids.

Table 4. 1 contains the diffraction record of this ternary compound with the indexing. Column one contains the relative intensities estimated from the Debye-Scherrer film. Columns three and four contain the computed d-spacings and $\sin^2\theta$ values from the film reading. Calculated $\sin^2\theta$ values are based on the indexing in column two with tetragonal unit cell having a_o and c_o parameters, 3.7919Å and 3.6399Å, respectively. These parameters are in agreement with the lattice parameters and symmetry that Post (22) reported for GdB_x (cf. Table 1).

The crystallographic density calculated with one GdB_2C_2 unit in this cell is 6.44g/cm^3. The density determined on powdered GdB_2C_2, 98aGdAM, in a 10 ml. pycnometer was 6.1g/cm.^{3} in nitrobenzene and

TABLE 4. 1

GdB_2C_2 Diffraction Record. Cu-K_α Radiation. Film C-2047.

Calculated Values of $Sin^2\theta$ and Values of hkl are Based on Cell Parameters, a_o = 3.7919 and c_o = 3.6399Å.

I/I_o	hkl	d, Å	$\sin^2\theta_{obs.}$	$\sin^2\theta_{calc.}$
50	100	3.780	0.04159	0.04140
30	001	3.628	.04516	.04500
30	110	2.674	.08313	.08280
100	011	2.617	.08679	.08640
20	111	2.154	.12809	.1278
30	200	1.893	.16583	.1656
30	002	1.817	.18007	.1800
40	120	1.694	.20703	.2070
40	201	1.678	.21094	.2106
40	102	1.638	.22139	.2214
40	121	1.535	.25227	.2520
40	112	1.503	.26299	.2628
30	202	1.313	.34496	.3456
30	221	1.257	.37606	.3762
40	122	1.239	.38711	.3870
$30\alpha_1$ $20\alpha_2$	130	1.198	.41370 .41716	.4133 .4154
$30\alpha_1$ $20\alpha_2$	013	1.155	.44490 .44751	.4456 .4479
$30\alpha_1$ $20\alpha_2$	131	1.139	.45753 .46014	.4582 .4605
$20\alpha_1$ $10\alpha_2$	113	1.104	.48637 .48855	.4870 .4894
$30\alpha_1$ $20\alpha_2$	231	1.010	.58144 .58532	.5822 .5851
$30\alpha_1$ $20\alpha_2$	132	1.0005	.59264 .59522	.5930 .5960
$30\alpha_1$ $20\alpha_2$	123	.9857	.61064 .61149	.6110 .6140

TABLE 4. 1, continued

I/I_o	hkl	d, Å	$\sin^2\theta_{obs.}$	$\sin^2\theta_{calc.}$
$30\alpha_1$	140	0.9194	0.70192	0.7026
$20\alpha_2$			.70592	.7061
$40\alpha_1$	232	.9101	.71624	.7170
$30\alpha_2$			.71860	.7206
$30\alpha_1$	223	.9003	.73189	.7349
$20\alpha_2$			.73460	.7386
$30\alpha_1$	141	.8920	.74573	.7476
$20\alpha_2$			.74991	.7513
$20\alpha_1$	014	.8846	.75820	.7601
$10\alpha_2$			.76269	.7639
$30\alpha_1$	033	.8754	.77413	.7763
$20\alpha_2$			.77960	.7802
$30\alpha_1$	331	.8689	.78574	.7889
$20\alpha_2$			.79217	.7928
$30\alpha_1$	114	.8618	.79888	.8014
$20\alpha_2$			.80307	.8054
$40\alpha_1$	133	.8528	.81579	.8176
$30\alpha_2$			.81951	.8217
$40\alpha_1$	042	.8411	.83862	.8410
$30\alpha_2$			.84342	.8452
$40\alpha_1$	241	.8262	.86919	.8715
$30\alpha_2$			.87329	.8759
$40\alpha_1$	142, 024	.8209	.88048	.8823
$30\alpha_2$			.88527	.8867
$50\alpha_1$	332, 124	.8018	.92275	.9237
$40\alpha_2$			.92849	.9283
$40\alpha_1$	323	.7948	.93914	.9416
$30\alpha_2$			.94447	.9463

5.5g/cm.^{3} in water, glycerol and benzene, which is in sufficient agreement with the crystallographic density to preclude the occupancy of more than one GdB_2C_2 formula unit for this cell volume.

4. 2 Analysis and Composition

An analysis of 105 GdAM (Table 3. 1) for gadolinium and for boron was performed on a pair of one-gram samples. The borocarbide sample from the arc melter was crushed in a steel mortar, ground in an agate mortar, washed successively with warm 50% HCl to remove oxides, dried at 110°C. in air, weighed and dissolved into a warm perchloric-nitric acid mixture in a reflux vessel. The resultant solution was saturated with oxalic acid and digested overnight. Gadolinium oxalate precipitate was filtered and ignited in air to Gd_2O_3, from which the gadolinium content was calculated. After adjusting the filtrate to pH = 6.0 with NaOH or HCl solution, solid mannitol was added and the solution quickly titrated to the phenophthalein end point of the monoprotic boric acid complex with potassium acid phthalate-standardized sodium hydroxide solution. The carbon percentage was obtained by the difference of the sum of the gadolinium and boron analyses and the total sample weight. This analysis revealed a composition of $Gd_{1.00\pm.02}$ $B_{2.03 \pm .01}C_{2.66}$. If the sample had a three weight percent impurity, the Gd/B/C ratio would have been $Gd_{1.00}B_{2.03}C_{2.0}$. Further, evidence that this phase has appreciable carbon solid solution is given in Chapter 4. 3.

Additional information of the GdB_2C_2 stoichiometry and of the reproducibility of the arc melted compositions is given in Table 3. 1 by the four preparations of GdB_2C_2, 98-, 98a-, 101- and 105 GdAM. These

samples all were prepared with a synthetic composition of GdB_2C_2 and showed only GdB_2C_2 or principally GdB_2C_2 as the reaction product. A trace of GdC_2 was noted in 98 GdAM. Sample 101 GdAM was known to have been melted with a large air leak in the arc furnace, thus explaining the abstraction of carbon. Samples 98a- and 105 GdAM, gave no indications by X-ray analysis of anything but GdB_2C_2.

4. 3 Solid Solution

As discussed above, solid solution between tetragonal GdB_4 and tetragonal GdB_2C_2 is not large. Further, the solid solution between GdB_2C_2 and tetragonal GdC_2 is not extensive, as illustrated by the observation of both GdC_2 and GdB_2C_2 in 96 GdAM. The equilibrium between GdB_2C_2 and GdB_6 as well as graphite has also been demonstrated.

However, some solid solution effects are noted in GdB_2C_2. The variation of lattice parameters for three ternary compositions containing GdB_6 and/or GdB_4 as minor phases is illustrated in Table 4. 2. Column one lists the synthetic compositions and column two the phases present as identified in the film of column seven. Columns three and four contain the a_o parameter and its associated error. Similarly, columns five and six contain the c_o parameter with its error. These precise parameters and their errors were computed from diffraction records with an IBM 653 computer, using the least squares technique described by Hess (29). The variation in c_o is just outside the error and, therefore, not considered significant. The carbon-rich composition, however, has a value of the a_o parameter significantly smaller than the other preparations. This deviation can be explained by the substitution

of carbon atoms with a covalent radius of 0.77Å for boron atoms with a 0.87Å radius.

TABLE 4. 2

GdB_2C_2 Lattice Parameter Variation Demonstrating Solid Solution

Synthetic Solid Composition	Phases Present	a_o	delta a_o	c_o	delta c_o	film
$Gd_{.126}B_{.503}C_{.372}$	GdB_2C_2, mjr GdB_6, mnr	3.7757	.0058	3.6379	.0034	C-2047
$Gd_{.143}B_{.572}C_{.286}$	GdB_2C_2, mjr GdB_4, mnr GdB_6, tr	3.7992	.0017	3.6421	.0010	D-0884
Unknown	GdB_2C_2, mjr GdB_6, mnr	3.7919	.0007	3.6399	.0003	D-1092

4. 4 LnB_2C_2 Existence and Lattice Parameters

The existence of LnB_2C_2 for lanthanides other than GdB_2C_2 was investigated. Samples were prepared by the reaction of mixtures of LnB_6 and/or LnB_4 with graphite in the arc melter furnace (cf. Table 3. 1). Exceptions to this were erbium, where the reactants were ErB_4, ErB_{12} and graphite, and holmium, where the holmium reactant contained HoB_4, HoB_6 and HoB_{12}. An attempt to produce LaB_2C_2 (2 LaAM) by the reaction of LaB_6 with graphite yielded a product with an X-ray pattern containing only LaB_6 lines. Similarly, SmB_2C_2 could not be prepared by the reaction of SmB_6 and graphite (2 SmAM). The phase, LnB_2C_2, was observed with the metals, Nd, Gd, Tb, Dy, Ho, Er and Yb. No attempt was made to prepare this borocarbide for other lanthanides.

An investigation of the lattice parameters of LnB_2C_2 for different lanthanides is illustrated in Table 4. 3. Column one contains the particular lanthanide metal designation. Columns two and three and columns four and five contain the computed values of a_o with its error and of c_o with its error. Column six lists the increment in a_o as a function of the lanthanide. Similarly, column seven lists the c_o increment with lanthanide.

The parameters in Table 4. 3 were computed in the fashion described above. In this table, all compositions showed excess LnB_4 or LnB_6 as the minor phases except the holmium system, which showed only HoB_2C_2. Since the minor phases present are nearly the same in all cases, the compositions of the LnB_2C_2 phase may be considered the same in all cases. Thus, the variation in lattice parameters as a function of lanthanide may be determined.

Figure 4 graphically illustrates the lattice parameter variation over all the lanthanides and YB_2C_2. The parameters for La-, Pr- and YB_2C_2 are those reported by Post (22) (cf. Table 1). Parameters for the compound with other lanthanides determined in this work are listed in Table 4. 3. The scale on a_o and c_o are the same to dramatize the extreme variation in c_o compared to that in a_o. While a_o changes only one percent from La to Lu, c_o changes 13 percent. The variation in c_o is about twice that of a_o in LnB_6 and of a_o and c_o in LnC_2, and even greater than the parameter variation in the lanthanide metals (30).

TABLE 4. 3

Precise Lattice Parameters of LnB_2C_2 Determined by the Hess Method

Ln	a_o	delta a_o	c_o	delta c_o	a_o increment	c_o increment
Nd	3.803 Å	.008	3.794	.009	.011	.154
Gd	3.7919	.0007	3.6399	.0003	.0079	.0487
Tb	3.7840	.0016	3.5912	.0003	.0022	.0313
Dy	3.7818	.0019	3.5599	.0010	.0017	.0225
Ho	3.7801	.0003	3.5374	.0001	.0024	.0297
Er	3.7777	.0006	3.5077	.0003	.0025	-.0521
Yb	3.7752	.0014	3.5598	.0006		

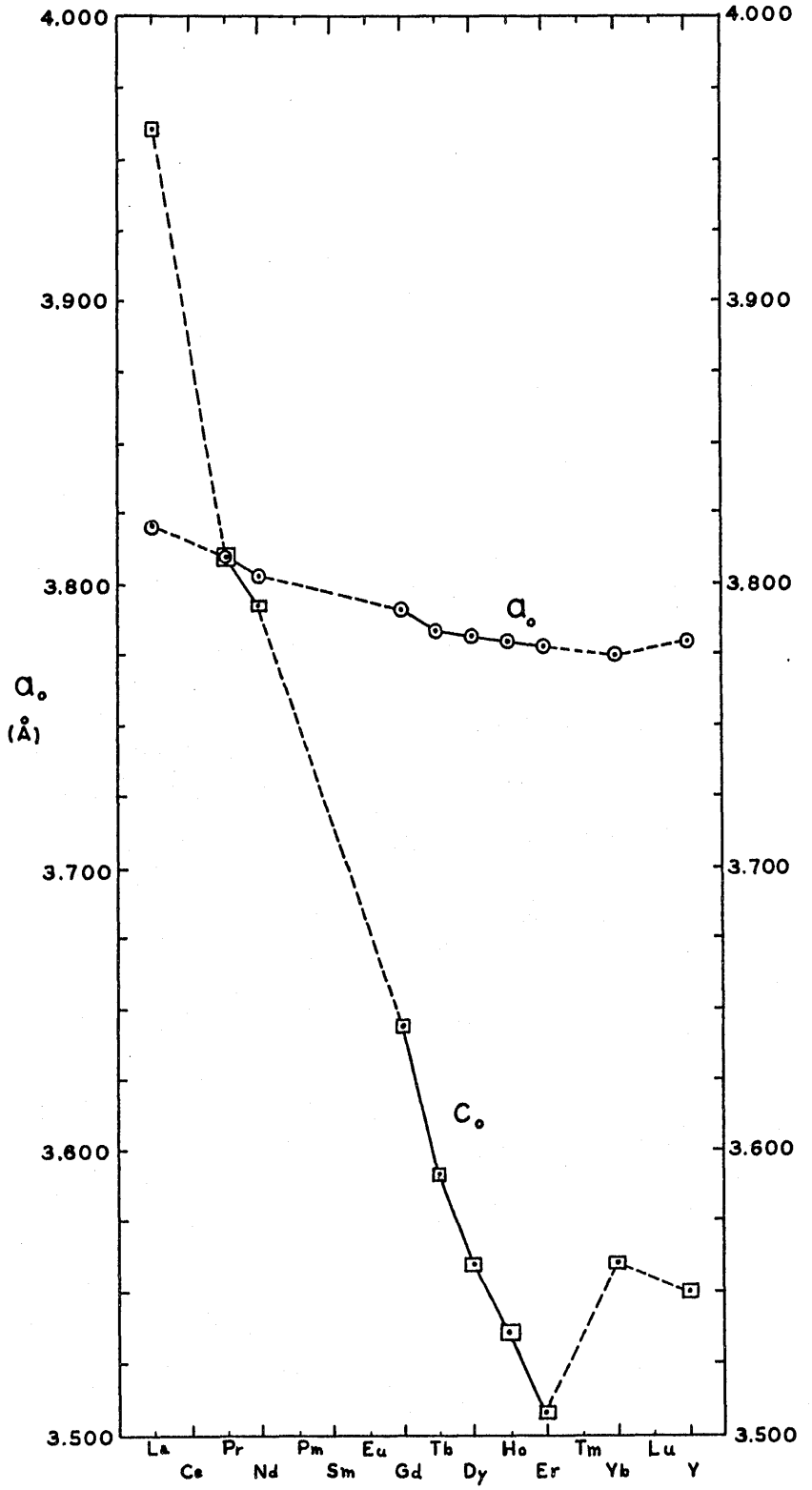

$Ln B_2 C_2$ Lattice Parameter Variation

FIGURE 4

CHAPTER 5

STRUCTURE OF LnB_2C_2

5. 1 Experimental

With the use of a Weissenberg single crystal camera with a 57.3 mm. diameter (Charles Supper Co., Newton Center, Massachusetts), a Philips Electronics Co. X-ray diffractometer and the employment of techniques discussed by Buerger (31, 32) for single crystal photograph interpretation and structure analysis, the structure of LnB_2C_2 has been fairly well established. Mo-K_α (MoK_α = 0.70926, 0.71354, 0.7107Å) radiation from a Philips Electronics Co. generator and tube was used in the single crystal studies, and Cu-K_α (Cu-K_α = 1.54050, 1.54434, 1.54180Å) radiation was employed to obtain an intensity record with the Philips diffractometer, which was equipped with a proportional counting system.

From the crushed, arc melted button of 3 TbAM (Table 3. 1), single crystals of TbB_2C_2 were found. Two crystals from this sample were chosen for single crystal analysis. Crystal no. 1 had dimensions, 0.1 x .05 x .01 mm. Crystal no. 2 had dimensions, 0.2 x 0.1 x 0.03 mm. While these crystals were not spherical, they had dimensions which were large enough to allow appreciable diffraction, but small enough so that absorption was not too great. More specifically,

$$-dI = \mu I dt \qquad (5.\ 1)$$

relates the linear absorption coefficient, μ , for a particular wavelength radiation, the intensity, I, and the thickness of the crystal, dt, to the attenuation of the beam. Further,

$$\mu = \rho \left[p_{Tb}(\mu/\rho)_{Tb} + p_B(\mu/\rho)_B + p_C(\mu/\rho)_C \right] , \qquad (5.\ 2)$$

where p is the fraction by weight of that element in the compound, ρ is the crystal density and (μ / ρ) is the mass absorption coefficient taken from the literature (33) for that particular element. For a crystal density of 6.62g/cm.^{3}, μ (TbB_2C_2) is 347 cm.$^{-1}$ for Mo radiation. An optimum size crystal has linear dimensions such that the beam travels through a path distance of $2/\mu$. The intensity of diffracted radiation increases to this thickness and decreases beyond this thickness (31, p. 180). Thus, the dimensions of the crystal should be near 0.05 mm. to an order of magnitude, which matches the size of crystal from which the TbB_2C_2 symmetry properties were determined.

With a 400-mesh powdered sample of HoB_2C_2 (2 HoAM) and with the use of the Philips diffractometer, an intensity record containing thirty diffraction angles was determined on charts C-2553, C-2555 and C-2557. The sample was mixed with a small amount of powdered gum arabic and a drop of water. In this fashion preferred orientation of the microcrystals was avoided. Integrated areas under the one-eighth degree per minute diffractometer trace were determined with a Keuffel and Esser

calibrated planimeter (Ser. No. 98759). It is believed that these relative intensities are determined with at least ten percent precision and generally to better than five percent.

5. 2 Single Crystal X-ray Analysis and Point Group

Oscillation and rotation photographs were taken to align crystal no. 1 along each of two different directions. Normal beam, zero-layer, Weissenberg photographs about the crystal [110] axis (film D-0886) and the [100] axis (film D-0889) were taken. These films allowed the mapping of reciprocal lattice planes on cylindrical coordinates, ξ and γ, from the film coordinates, x and y. From these reciprocal lattice mappings the value of c_o was calculated as 3.61 Å and a_o as 3.82 Å to be compared with powder photograph parameter values of 3.59 and 3.78 Å, respectively.

A rotation photograph about [001] (D-0911), equiinclination Weissenberg photographs for the (kh0), (hk1), (hk2), (hk3) and (hk4) layers (films D-0914, D-0915, D-0917, D-0918 and D-0919) and an anti-equiinclination photograph of the (hk0) layer (film D-0920) were taken on TbB_2C_2 crystal no. 2. The layer line coordinates were determined from the [001] rotation film (D-0911). Table 5. 1 summarizes the films, layers, layer line coordinates, inclination angles, exposure times and layer screen settings. Figure 5. 1 illustrates these mappings with the size of the lattice point increasing with the intensity of the reflection.

Figure 5. 1. 1 is the reciprocal lattice determined with [110] rotation from the normal beam Weissenberg film, D-0886. Figure 5. 1. 2 is the reciprocal lattice mapped from the (0kl) layer Weissenberg film, D-0889. Figure 5. 1. 3 shows the tetragonal axis from a graphing of the

spots on the (hk0) layer Weissenberg film, D-0920. Reciprocal cell dimensions are shown on each figure.

TABLE 5. 1

TbB_2C_2 Single Crystal Analysis Photographs; Mo-K_α Radiation

Crystal No. 1:

D-0885 Oscillation about [110].

D-0886 Weissenberg, Rotation about [110], normal beam. Nine hours.

D-0887 Oscillation about [100].

D-0888 Rotation about [100], normal beam, 14 hours.

D-0889 Weissenberg, rotation about [100], normal beam, (0kl) layer, three films.

Crystal No. 2:

D-0910 Oscillation about [001].

D-0911 Rotation about [001], normal beam.

Layer line coordinates determined as:

Layer	y (mm.)	ζ
(hk1)	5.30	.19
(hk2)	12.35	.39
(hk3)	21.15	.59
(hk4)	36.9	.78

D-0912 Weissenberg, anti-equiinclination, μ =11.5°, X=5.2mm. (hk0), 12 hrs.

D-0913 Weissenberg, normal beam, (hk0), 190-390°, 12 hrs.

D-0914 Weissenberg, normal beam, (hk0), 0-200°, 20 hrs.

D-0915 Weissenberg, equiinclination, μ =5.2°, X=2.3mm, (hk1), 20 hrs.

D-0916 Weissenberg, equiinclination, μ =11.4°, X=5.1mm, (hk2), 20 hrs.

D-0917 Weissenberg, equiinclination, μ =11.4°, X=5.1mm, (hk2), 20 hrs.

D-0918 Weissenberg, equiinclination, μ =17.3°, X=7.9mm, (hk3), 20 hrs.

D-0919 Weissenberg, equiinclination, μ =23.2°, X=10.9mm, (hk4), 20 hrs.

D-0920 Weissenberg, anti-equiinclination, μ =-17.3°, X=7.9mm, (hk0), 20 hrs.

X, layer screen setting

μ, inclination angle

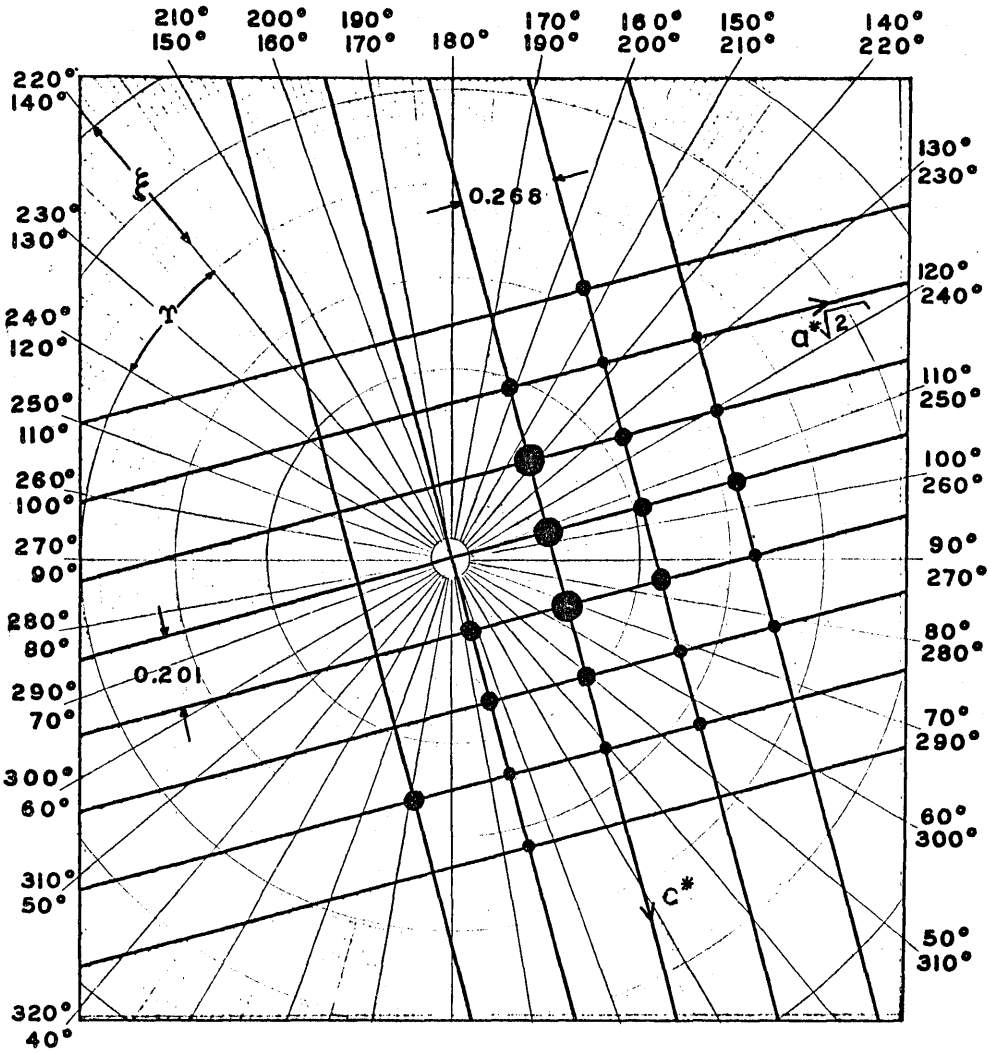

Tb B_2 C_2 RECIPROCAL LATTICE

[110] ROTATION AXIS

FIGURE 5. I. I

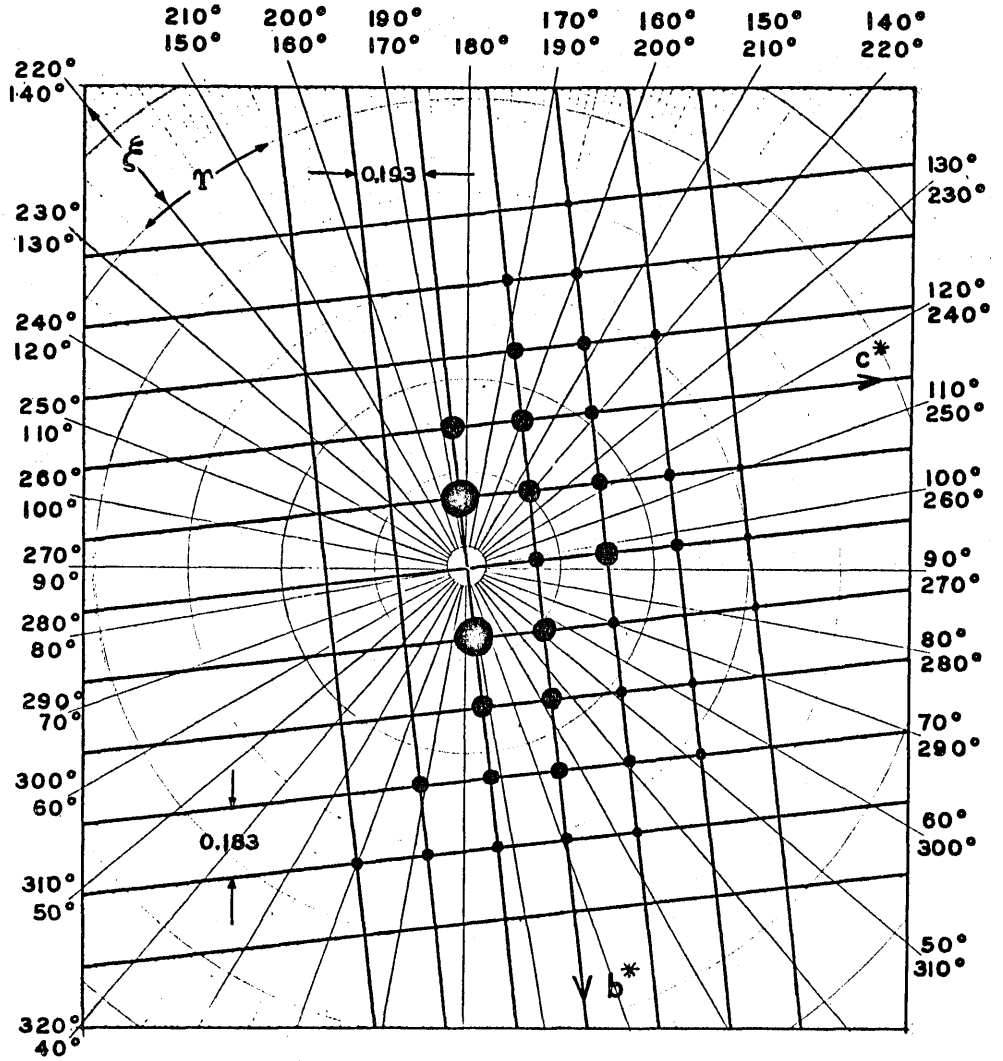

TbB_2C_2 RECIPROCAL LATTICE

$[0\bar{1}0]$ rotation axis

FIGURE 5. I. 2

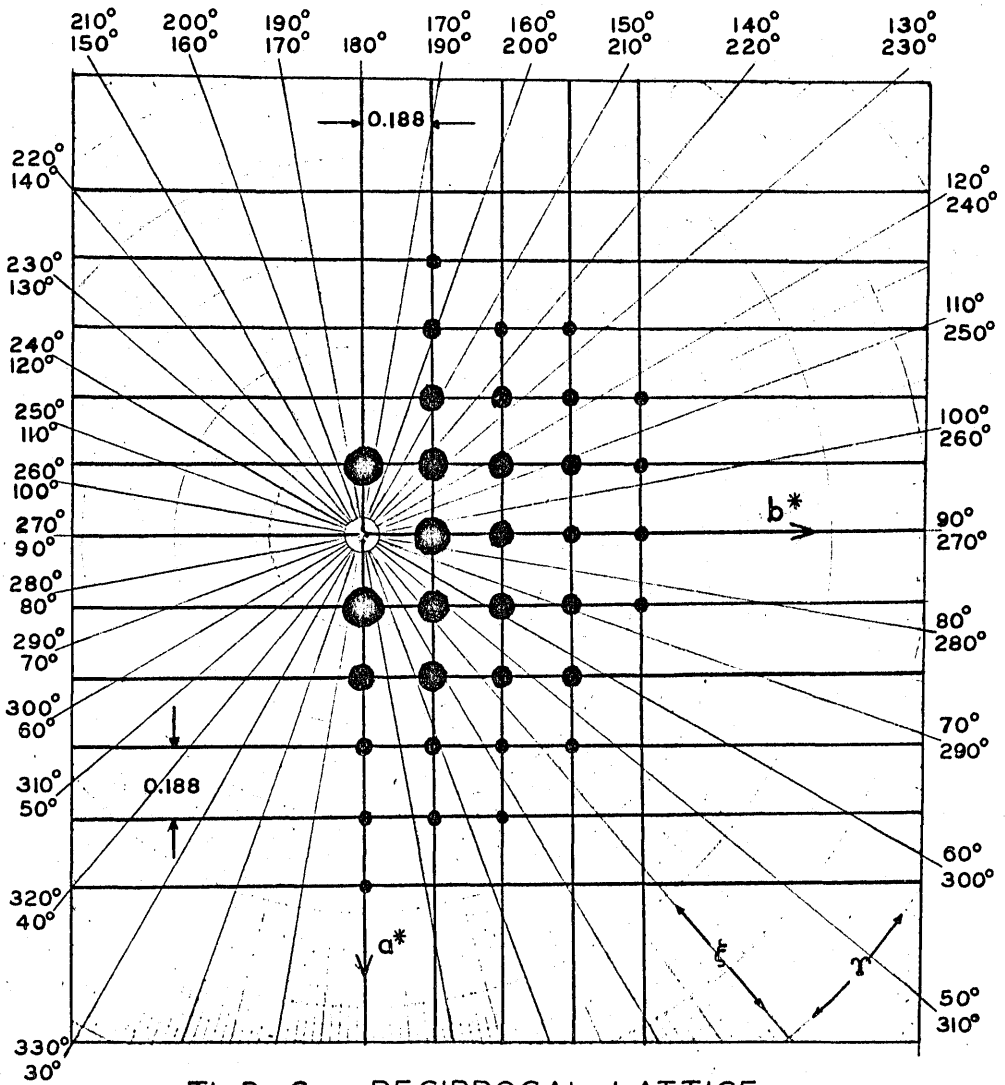

Tb B_2 C_2 RECIPROCAL LATTICE

[00l] rotation axis

FIGURE 5. I. 3

These films confirm the symmetry and unit cell dimensions assigned to the powder photographs. In addition, they reveal that there are no extinctions among the reciprocal lattice points for the cell chosen (cf. Figures 5. 1. 1, 5. 1. 2 and 5. 1. 3). The absence of an extinguished class implies the absence of any symmetry element with a translation component, i.e., glide planes or screw axes, and also implies that the cell is primitive.

The point group from X-ray diffraction observations is 4/mmm. The symmetry elements of the point group are summarized in Figure 5. 2. There is a four-fold axis of rotation on the [001] axis, vertical mirror planes both diagonal and perpendicular to the cell edges, and a horizontal mirror which reflects any point above the plane through the plane. The possible space groups that this phase might have are P422-No. 89, P4mm-No. 99, $P\bar{4}2m$-No. 111, $P\bar{4}m2$-No. 115 and P4/mmm-No. 123 (33). The first four of these space groups exhibit no center of symmetry. If a center of symmetry were added to each of these, P4/mmm would result.

5. 3 Intensity, Structure Factor and Phase Problem

In order to decide among these space groups and to ascertain the locations of the atoms in the structure, a measurement of the intensities from the diffracting planes must be made. The intensity is given by

$$I = KLpmA \mid F(hkl) \mid^2 \qquad (5.\ 3)$$

where I is the intensity of the diffracted beam in arbitrary units; K is the proportionality constant for the experiment; L is the Lorentz factor; p, the polarization factor; m, the multiplicity; A, the absorption

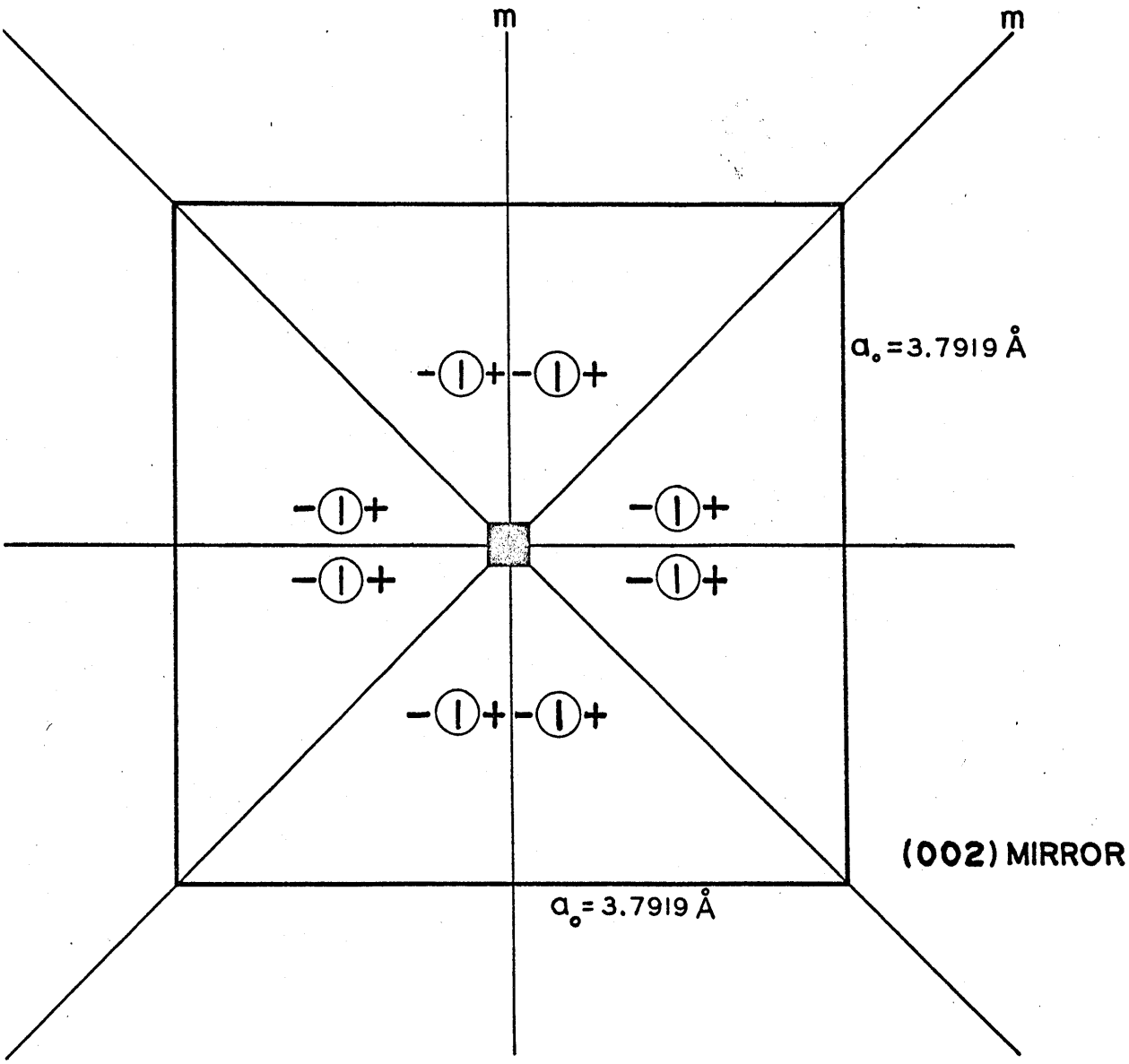

LnB_2C_2 APPARENT POINT GROUP

4/m mm.

FIGURE 5. 2

factor; and F, the structure factor. The structure factor is given by

$$F(hkl) = \sum_j f_j \, e^{i2\pi(hx_j+ky_j+lz_j)} , \qquad (5.\ 4)$$

where f_j is the atomic scattering factor for the j^{th} atom; x_j, y_j and z_j are the position parameters for the j^{th} atom in the cell as fractions of the unit cell lengths; and the sum is over all atoms in the cell. Obviously, the quantities we wish to determine are x_j, y_j and z_j. The structure factor may be considered a resultant vector of vectors, $f_j e^{i2\pi(hx_j+ky_j+lz_j)}$, whose amplitudes for scattering are f_j, and whose directions into the complex plane are determined by the phase of the scattered wave, i.e.,

$$e^{i2\pi(hx_j+ky_j+lz_j)} = \cos 2\pi(hx_j+ky_j+lz_j) + i \sin 2\pi(hx_j+ky_j+lz_j). \qquad (5.\ 5)$$

$$F(hkl) = \left(\sum_j f_j \cos 2\pi(hx_j+ky_j+lz_j)\right) + i\left(\sum_j f_j \sin 2\pi(hx_j+ky_j+lz_j)\right) . \qquad (5.\ 6)$$

$$|F(hkl)| = \left\{\left[\sum_j f_j \cos 2\pi(hx_j+ky_j+lz_j)\right]^2 + \left[\sum_j f_j \sin 2\pi(hx_j+ky_j+lz_j)\right]^2\right\}^{1/2} , \qquad (5.\ 7)$$

From equations 5. 6 and 5. 7, it is apparent that when one computes $|F(hkl)|^2$ from measured intensities he obtains only the scattering amplitude of the structure factors and not the phase angles. The inability to measure experimentally a quantity which will allow one to calculate

the phases of the diffraction spectra is the so-called "phase problem" of crystallography.

Buerger (32) discusses this problem and summarizes the many methods that have been devised to extract the most information about the phases of scattering centers from intensity measurements. Very often a knowledge of the number of atoms per cell and their radii will allow one to guess the position parameters of the atoms. From this guess, the structure factors and their absolute values may be computed. When the quantity,

$$R = \frac{\Sigma \left| |F(hkl)_{obs.}| - |F(hkl)_{calc.}| \right|}{\Sigma |F(hkl)_{obs.}|} , \qquad (5.8)$$

is less than 0.4, the structure is assumed solved (32, p. 586).

5.4 Electron Density and Patterson Functions

One powerful tool for the location of scattering maxima in a crystal was devised by Patterson (32, p. 554; 34). One can consider that the structure exhibits an electron density, $\rho(XYZ)$, which varies continuously over the cell volume and has a value at any XYZ in the cell as well as at x_j, y_j and z_j. Then equation 5.4 may be replaced by

$$F(hkl) = \int_0^V \rho(XYZ)\, e^{2\pi i(hX+kY+lZ)}\, dV \qquad (5.9)$$

$V = abc$ and $dV = dxdydz$. Hence, $dV = V\,(dx/a)(dy/b)(dz/c)$. Then in fractional coordinates,

$$dV = V\, dX\, dY\, dZ. \qquad (5.10)$$

Thus,

$$F(hkl) = \int_0^1\int_0^1\int_0^1 \rho\,(XYZ)e^{2\pi i(hX+kY+lZ)}VdXdYdZ \qquad (5.11)$$

Generally, a three dimensional Fourier series is given by

$$\rho\,(XYZ) = \sum_{h'k'l'=-\infty}^{+\infty} K(h'k'l')e^{-2\pi i(h'X+k'Y+l'Z)}, \qquad (5.12)$$

where K(h'k'l') is a Fourier coefficient. Substituting equation 5.12 into equation 5.11, one derives the relation,

$$F(hkl)=\int_0^1\int_0^1\int_0^1 \sum_{h'k'l'=-\infty}^{+\infty} K(h'k'l')e^{-2\pi i(h'X+k'Y+l'Z)}e^{2\pi i(hX+kY+lZ)}VdXdYdZ. \qquad (5.13)$$

Rearranging equation 5.13,

$$F(hkl)=\sum_{h'k'l'=-\infty}^{+\infty}\int_0^1\int_0^1\int_0^1 K(h'k'l')e^{2\pi i[(h-h')X+(k-k')Y+(l-l')Z]}VdXdYdZ. \qquad (5.14)$$

For h = h', k = k' and l = l'

$$\int_0^1\int_0^1\int_0^1 K(hkl)e^{0}\,VdXdYdZ = VK(hkl). \qquad (5.15)$$

If one or more pairs of indices are not equal,

$$\int_0^1\int_0^1\int_0^1 K(h'k'l')e^{2\pi i(h-h')X}e^{2\pi i(k-k')Y}e^{2\pi i(l-l')Z}\,VdXdYdZ \qquad (5.16)$$

will vanish on integration from zero to one. Therefore, in the non-vanishing condition of equal indices,

$$F(hkl) = VK(hkl) \quad . \tag{5.17}$$

Substituting equation 5.17 into equation 5.12, one finds the following expression for electron density:

$$\rho(XYZ) = \frac{1}{V} \sum_{hkl}^{+\infty}\sum\sum\sum_{-\infty} F(hkl)e^{-2\pi i(hX+kY+lZ)} . \tag{5.18}$$

This is the electron density function.

Patterson noted that if two Fourier series, each representing the electron density of a crystal, are multiplied together, terms such as $F(hkl)\cdot F(\bar{h}\bar{k}\bar{l})^*$ occur.

$$F(hkl) \cdot F(\bar{h}\bar{k}\bar{l})^* = F(hkl) \cdot F(hkl)^* = |F(hkl)|^2, \tag{5.19}$$

which is the phaseless quantity determined by experimental intensity measurements. Therefore, a Fourier synthesis with coefficients, $|F(hkl)|^2$, defines a relation between the phase dependent structure factor and its complex conjugate. The general Patterson function is given in equation 5.20.

$$P(XYZ) = \frac{1}{V^2} \sum_{h}^{+\infty}\sum_{k}\sum_{l}\sum_{-\infty} |F(hkl)|^2 e^{-2\pi i(hX+kY+lZ)} \tag{5.20}$$

The electron density map will have maxima at atomic positions. But the Patterson synthesis map will have maxima at the ends of vectors between the atomic positions revealed by the electron density map. Thus,

for every pair of electron density maxima one Patterson maximum will exist. As a result, the Patterson map will reveal many maxima only a specific few of which would be observed as atomic positions in the electron density map. The population of the cell and steric considerations will force a choice for atomic positions from these Patterson maxima that, for simple structures, may be unequivocable.

A point should be made about the possibility of positioning the light atoms, boron and carbon, in the presence of lanthanide atoms by the use of the Patterson function. The scattering amplitude, f_j, decreases as $\sin \theta / \lambda$ increases. The relative scattering power of one atom compared to another is in the same relation as their atomic number, Z. In particular, the contribution to the amplitude of diffraction of X-rays from planes, (hkl), by the terbium, boron and carbon atoms, which populate that plane to equal atomic concentrations, will be, to a first approximation, in the ratio of their atomic numbers or 65:5:6. In the case of a Patterson function, which involves the scattering power squared, the ratio of the atomic scattering amplitudes in their contribution to the function will be 4225:25:36. Obviously, unless planes which contain large numbers of the light atoms relative to terbium can be included in the synthesis and unless precise intensity measurements can be made, there is little chance of locating the light atoms in the structure, much less distinguishing between the boron and carbon equivalent positions.

Another problem with the Patterson synthesis is its inherent centrosymmetry. For each interatomic vector there exists the reverse interatomic vector. Thus, the Patterson function for each of the five

possible space groups will contain many equivalent positions related not only by the space group symmetry, but by centrosymmetry. Again, one cannot decide the space group from a Patterson synthesis alone.

5. 5 Experimental Intensity Measurement

Without a single crystal diffractometer the determination of accurate intensities from (hkl) reflections from single crystals is difficult. When precise intensities are needed, as is the case for LnB_2C_2, multiple film techniques are not very useful. An examination of the intensities of spots on three film layers for each of the Weissenberg films of Table 5. 1 demonstrated that all spots, which represent planes that reflect at the same Bragg angle in powder diffraction, had equal intensity (cf. Figure 5. 1). This is a consequence of Friedel's Law (32) and the point group. Friedel's Law states that, since phases cannot be measured in X-ray diffraction experimentation, it follows that reflections from (hkl) and $(\bar{h}\bar{k}\bar{l})$ have the same intensities. Thus, with the four-fold rotation axis of Figure 5.2,

$$|F(hkl)|=|F(\bar{h}kl)|=|F(h\bar{k}l)|=|F(hk\bar{l})|=|F(\bar{h}\bar{k}l)|=|F(\bar{h}k\bar{l})|=|F(h\bar{k}\bar{l})|=|F(\bar{h}\bar{k}\bar{l})|. \tag{5.21}$$

Therefore, the number of planes contributing to each element of the powder diffraction record is known, and the extent of their contribution to the intensity is equal. This observation enables one to measure intensities precisely with the use of a diffractometer and proportional counting equipment.

Using the appropriate multiplicities and measuring the intensities on a powdered specimen on a Philips Electronics Co. diffractometer with a

proportional counter (cf. Chapter 5. 1), one may calculate the intensity from each reflecting plane, (hkl). Table 5. 2 contains these data taken from diffraction charts, C-2553, C-2555 and C-2557. Column one contains the indices based on a primitive tetragonal cell with a_o and c_o, 3.7801 and 3.5374Å, respectively. Column two contains the diffraction angle in degrees. Relative intensity in units of square centimeters as determined with the planimeter are listed in column three. The statistical deviations from the mean of the four measurements of relative intensity for a particular diffraction angle are listed in column four. Column five contains the Lorentz and polarization factors at the diffraction angle of column two for powdered samples taken from Henry, Lipson and Wooster (35, Table 9). The multiplicity determined from the point group is listed in column six. Finally, the square of the absolute structure factor, as calculated from equation 5. 3 , is contained in column seven. The absorption factor was assumed unity.

5. 6 Patterson Synthesis

Since the space group will be decided finally by choosing likely positions for the atoms from many possible equivalent positions, the Patterson function for the centrosymmetric space group P4/mmm, No. 123, was used to treat the data in order to expose all possible maxima. From the International Tables of Crystallography (33) the Patterson function is

$$P(UVW) = \frac{8}{V_c^2} \sum_{hkl}^{\infty\infty\infty} |F(hkl)|^2 \cos 2\pi hU \cos 2\pi kV \cos 2\pi lW. \qquad (5.22)$$

The $|F(hkl)|^2$ values were not normalized to absolute values by applying

TABLE 5. 2

Powder Intensity Record for HoB_2C_2

Obtained with Diffractometer and Proportional Counter, Copper Radiation

hkl	2θ,(°)	$I_{obs.}$	$\sqrt{\frac{(I-I_m)^2}{N}}$	$\frac{1+\cos^2 2\theta}{\sin^2\theta\cos\theta}$	m	$\lvert F(hkl)_{obs.}\rvert^2$
100	23.52	11.9	0.2	38.14	4	0.780
001	25.17	5.0	.1	39.22	2	.637
110	33.44	5.2	.3	21.40	4	.0607
101	34.75	17.9	.1	19.67	8	.114
111	42.37	7.4	.2	12.71	8	.0728
200	48.14	1.28	.01	9.516	4	.0336
002	51.70	1.49	.09	8.090	2	.0921
210	54.25	2.50	.05	7.248	8	.0431
201	55.11	1.78	.02	6.998	8	.0318
102	57.51	1.85	.02	6.354	8	.0364
211	60.72	2.08	.02	5.622	16	.0231
112	62.98	1.18	.06	5.185	8	.0284
220	70.42	0.38	.02	4.095	4	.0232
202	73.38	.835	.015	3.779	8	.0276
030	75.41	.199	.024	3.594	4	.0138
221	76.18	1.322	.154	3.529	8	.0468
122	78.22	1.658	.194	3.374	16	.0307
130	80.35	0.636	.074	3.233	8	.0246
031	81.00	.747	.087	3.194	8	.0292
131	85.81	.858		2.962	16	.0181
103	86.39	.829		2.939	8	.0353
113	91.31	.492		2.799	8	.0220
222	92.58	.178		2.775	8	.00802
230	94.67	.340		2.747	8	.0155
032	97.44	.141		2.729	8	.00646
231	100.14	.361		2.732	16	.00826
023	100.67	.363		2.734	8	.0166
132	102.25	.604		2.748	16	.0137
123	105.75	.492		2.798	16	.0110
040	109.36	.262		2.884	4	.0286
232	117.46	.588		3.198	16	.0115
141	120.75	.502		3.377	16	.00929
223	121.45	.662		3.420	8	.0242
014	127.19	.748		3.828	8	.0244
133	133.54	.790		4.416	16	.0112
042	135.44	.476		4.645	8	.0128

scale and temperature factors. This omission does not change the location of the maxima. The values of $|F(hkl)|^2$ for reflections for which there was no observed intensity were set equal to zero. The quantity, $|F(000)|^2$, was also set equal to zero; although, $|F(000)|^2 = Z^2$, where Z is the total number of electrons in the unit cell (32, p. 375). The effect of setting $|F(000)|^2$ to zero is to subtract out a constant from each vector. The relative peaks are affected uniformly.

One must be careful in using the multiplicity. The multiplicity generated from Friedal's Law and the 4/mmm point group is already included in the Patterson function by the factor eight (cf. Chapter 5. 5). However, this eight-fold multiplicity inherent in the Patterson function is not the correct multiplicity for all (hkl) reflections. As noted in Table 5. 2, column six, the point group multiplicity may be 1, 2, 4, 8 or 16, depending on the orientation of the reflecting planes. Since the Patterson map is generated from relative $|F|^2$ values, the factor eight in equation 5.22 may be effectively treated as a scale constant affecting the Patterson maxima amplitude at each point of generation in the unit cell to the same extent without affecting the position of the maxima. Thus, the values of $|F(hkl)|^2$ used in the Patterson function calculations were taken as those of Table 5. 2, column seven, multiplied by the multiplicity of column six, Table 5. 2.

There is yet another complicating factor in determining the proper multiplicity. The procedure for introduction of the (hkl) values and their accompanying $|F(hkl)|^2$ values into the computer causes reflections (hkl) and (khl) to be picked up separately. However, these two sets represent planes reflecting at the same Bragg angle and, therefore,

are considered together in the multiplicity of Table 5. 2. Thus, the $|F(hkl)|^2$ values, with the appropriate multiplicity factor of Table 5. 2 already included, must be divided by two on introduction into the computer for reflections of the type hkl, $h \neq k$. For h=k, (hhl), the computer only reads one $|F(hhl)|^2$ value; and no additional computer multiplicity factor is needed.

Table 5. 3 contains a record of the Patterson input data in the order of introduction to the computer. The hkl values are listed in column one from 000 to 444. The accompanying $|F(hkl)|^2$ values are listed in column two and include all the multiplicity considerations discussed above.

The three-dimensional Fourier synthesis was programmed generally for hkl from 000 to 555 to compute the Patterson function in sixteenths of the unit cell. An IBM 653 computer was employed for these computations. Only one-eighth of the unit cell was computed, since the rest of the cell can be generated by symmetry. These computed values are listed by layers in Table 5. 4. The nine layers are taken at increments of one-eighth of the c-axis. Since there is a diagonal mirror perpendicular to the XYO plane and passing through the origin, the field for Y greater than X need not be shown. Negative values arise from failure to scale the $|F(hkl)|^2$ values.

The conclusions to be drawn from this Fourier synthesis are these: First, and most important, there can be no possibility of holmium atoms in any position other than the corners of this unit cell of a_o and c_o dimensions, 3.7801 and 3.5374Å, respectively. Second, with such a dominating influence on the positions displayed by the large scattering holmium

TABLE 5. 3

Input Data for HoB_2C_2 Patterson Synthesis for Space Group P4/mmm.

hkl	$\lvert F(hkl)_{obs.} \rvert^2$	hkl	$\lvert F(hkl)_{obs.} \rvert^2$	hkl	$\lvert F(hkl)_{obs.} \rvert^2$	hkl	$\lvert F(hkl)_{obs.} \rvert^2$
000	0	113	.1760	231	.0661	344	0
001	.637	114	0	232	.0920	400	.0572
002	.0921	120	.1724	233	0	401	0
003	0	121	.1848	234	0	402	.0512
004	0	122	.2456	240	0	403	0
010	1.560	123	.0880	241	0	404	0
011	.456	124	0	242	0	410	0
012	.1456	130	.0984	243	0	411	.0743
013	.1412	131	.1448	244	0	412	0
014	.0976	132	.1096	300	.0276	413	0
020	.0672	133	.0896	301	.1168	414	0
021	.1272	134	0	302	.0258	420	0
022	.1104	140	0	303	0	421	0
023	.0664	141	.0743	304	0	422	0
024	0	142	0	310	.0984	423	0
030	.0276	143	0	311	.1448	424	0
031	.1168	144	0	312	.1096	430	0
032	.0258	200	.0672	313	.0896	431	0
033	0	201	.1272	314	0	432	0
034	0	202	.1104	320	.0620	433	0
040	.0572	203	.0664	321	.0661	434	0
041	0	204	0	322	.0920	440	0
042	.0512	210	.1724	323	0	441	0
043	0	211	.1848	324	0	442	0
044	0	212	.2456	330	0	443	0
100	1.560	213	.0880	331	0	444	0
101	.456	214	0	332	0		
102	.1456	220	.0928	333	0		
103	.1412	221	.3744	334	0		
104	.0976	222	.0642	340	0		
110	.2428	223	.1936	341	0		
111	.5824	224	0	342	0		
112	.2272	230	.0620	343	0		

TABLE 5. 4

Patterson Synthesis Output Data on HoB_2C_2 with Space Group P4/mmm

X/16 Y/16	0	1	2	3	4	5	6	7	8
0	1.84	1.58	1.02	0.544	0.309	0.202	0.121	0.0651	0.0475
1		1.35	.877	.485	.292	.192	.103	.0404	.0206
2			.590	.373	.262	.165	.0539	-.0240	-.0478
3				.296	.229	.111	-.0275	-.114	-.138
4					.147	-.0019	-.148	-.223	-.239
5						-.159	-.284	-.330	-.334
6		Z = 0/16					-.374	-.397	-.394
7								-.413	-.410
8									-.409

X/16 Y/16	0	1	2	3	4	5	6	7	8
0	1.56	1.35	0.884	0.498	0.301	0.200	0.118	0.0614	0.0440
1		1.16	.767	.445	.282	.187	.0985	.0373	.0184
2			.528	.345	.247	.154	.0485	-.0237	-.0454
3				.274	.208	.0982	-.0270	-.104	-.126
4					.130	-.0025	-.131	-.198	-.212
5		Z = 1/16				-.138	-.247	-.291	-.296
6							-.329	-.358	-.360
7								-.387	-.392
8									-.400

TABLE 5. 4, continued

X/16 Y/16	0	1	2	3	4	5	6	7	8
0	0.981	0.866	0.620	0.414	0.291	0.197	0.108	0.495	0.0318
1		.765	.553	.376	.269	.178	.0867	.0264	.0082
2			.414	.301	.221	.130	.0330	-.0306	-.0495
3				.235	.166	.0671	-.0357	-.0989	-.117
4					.0894	-.0152	-.113	-.168	-.183
5		Z = 2/16				-.113	-.196	-.240	-.252
6							-.267	-.311	-.324
7								-.365	-.385
8									-.409

X/16 Y/16	0	1	2	3	4	5	6	7	8
0	0.554	0.512	0.443	0.364	0.282	0.184	0.0889	0.0278	0.0088
1		.487	.415	.339	.259	.161	.0665	.0054	-.0137
2			.351	.280	.201	.104	.0098	-.0521	-.0717
3				.210	.128	.0304	-.0628	-.124	-.144
4					.0442	-.0494	-.137	-.196	-.216
5						-.133	-.211	-.267	-.287
6		Z = 3/16					-.283	-.340	-.362
7								-.402	-.428
8									-.454

X/16 Y/16	0	1	2	3	4	5	6	7	8
0	0.423	0.414	0.384	0.325	0.239	0.139	0.0522	-.0027	-.0207
1		.403	.368	.306	.219	.120	.0329	-.0228	-.0414
2			.324	.255	.166	.0681	-.0195	-.0782	-.0985
3				.182	.0925	-.0043	-.0941	-.158	-.180
4					.0055	-.0901	-.181	-.248	-.273
5						-.184	-.272	-.336	-.359
6		Z = 4/16					-.351	-.405	-.423
7								-.446	-.459
8									-.469

TABLE 5. 4, continued

X/16 Y/16	0	1	2	3	4	5	6	7	8
0	0.411	0.393	0.339	0.256	0.161	0.0744	0.0084	-.0330	-.0472
1		.375	.321	.239	.146	.0593	-.0078	-.0502	-.0649
2			.269	.193	.105	.0203	-.0496	-.0948	-.110
3				.127	.0475	-.0378	-.113	-.162	-.178
4					-.0297	-.121	-.204	-.255	-.272
5						-.222	-.310	-.358	-.371
6		Z = 5/16					-.392	-.426	-.432
7								-.442	-.438
8									-.431

X/16 Y/16	0	1	2	3	4	5	6	7	8
0	0.357	0.333	0.272	0.193	0.113	0.0407	-.0156	-.0509	-.0628
1		.310	.252	.175	.0947	.0212	-.0357	-.0692	-.0798
2			.199	.130	.0539	-.0209	-.0764	-.103	-.109
3				.0733	.0032	-.0718	-.124	-.140	-.139
4					-.0663	-.148	-.204	-.213	-.208
5						-.248	-.318	-.330	-.323
6		Z = 6/16					-.404	-.423	-.417
7								-.446	-.441
8									-.435

X/16 Y/16	0	1	2	3	4	5	6	7	8
0	0.273	0.259	0.224	0.181	0.126	0.0556	-.0115	-.0542	-.0676
1		.244	.207	.160	.0985	.0238	-.0419	-.0782	-.0878
2			.165	.111	.0405	-.0395	-.0951	-.110	-.108
3				.0523	-.0223	-.100	-.137	-.120	-.103
4					-.0985	-.178	-.207	-.172	-.143
5						-.274	-.328	-.305	-.280
6		Z = 7/16					-.424	-.444	-.434
7								-.505	-.512
8									-.527

TABLE 5. 4, continued

X/16 Y/16	0	1	2	3	4	5	6	7	8
0	0.236	0.228	0.212	0.189	0.145	0.0723	-.0041	-.0530	-.0680
1		.218	.196	.166	.113	.0337	-.0402	-.0804	-.0904
2			.161	.114	.0436	-.0424	-.102	-.114	-.109
3				.0514	-.0289	-.111	-.144	-.115	-.0896
4					-.112	-.193	-.211	-.157	-.119
5		Z = 8/16				-.289	-.334	-.300	-0.267
6							-.440	-.463	-.454
7								-.546	-.562
8									-.588

atoms, there is no chance to locate the light atoms from a Patterson map. Third, even though the structure is centrosymmetric with respect to the holmium atoms, the structure may not be centrosymmetric with respect to the light atoms too. Therefore, the space group is still unknown. The slight troughs and ridges may be due to diffraction rings arising from errors from cutting off the Fourier series before the limiting convergence has been reached.

5. 7 Light Atom Structure Factor

The position of the holmium atoms in the corners of the unit cell determines the phase of the holmium atoms. Thus, the structure factor becomes:

$$F(hkl) = f_{H_o} e^{2\pi i(ho+ko+lo)} + \sum_j f_j e^{2\pi i(hx_j+ky_j+lz_j)} , \qquad (5.23)$$

where the sum is now over equivalent positions for boron and carbon atoms only.

$$F(hkl) = f_{H_o} + \sum_j f_j e^{2\pi i(hx_j+ky_j+lz_j)} . \qquad (5.24)$$

$$F(hkl) - f_{H_o} = \sum_j f_j e^{2\pi i(hx_j+hy_j+lz_j)} = F'(hkl). \qquad (5.25)$$

This derivation points out the fact that if the sign of the total structure factor, F(hkl), could be ascertained, after scaling the intensity data and correcting for temperature, the scaled and corrected scattering factor of holmium could be subtracted out from the total structure factor. An electron density map (cf. equation 5.18 and

Chapter 5. 4) of the residual structure factor would be a function only of the positions of the boron and carbon atoms.

The total structure factor is always positive because the holmium atom dominates the diffraction pattern as can be seen from the following arguments. Consider Figure 5. 3. This graph is a plot of the atomic scattering factors for boron, carbon and holmium atoms versus $\sin\theta/\lambda$. The scattering factors for boron were taken from Ibers (36); for carbon, from Berghuis, et al. (37); and for holmium, from Internationale Tabellen (38). The scattering factors decrease with $\sin\theta/\lambda$. However, ${}^{o}f_{Ho}$ decreases less rapidly than either ${}^{o}f_{B}$ or ${}^{o}f_{C}$. Therefore, the amplitude of the structure factors for boron and carbon are most important relative to that of holmium at $\sin\theta/\lambda$ equal to zero. If in addition the phase contribution to the structure factor from the light atoms is taken to be minus one as the absolute minimum, the largest possible negative structure factor sum for the two boron and two carbon atoms per cell will be given by

$$\sum_{j} f_{j} e^{2\pi i(hx_j+ky_j+lz_j)} = -22. \qquad (5.26)$$

Therefore, from equation 5. 26

$$F(hkl) = 67 - 22 = 45 > 0. \qquad (5.27)$$

It is then possible to compute the electron density map from the temperature-corrected and scaled intensity measurements with the holmium contribution removed. If the intensity measurements were accurate enough and if sufficient terms in the Fourier series are available, the boron and carbon atomic positions can be revealed.

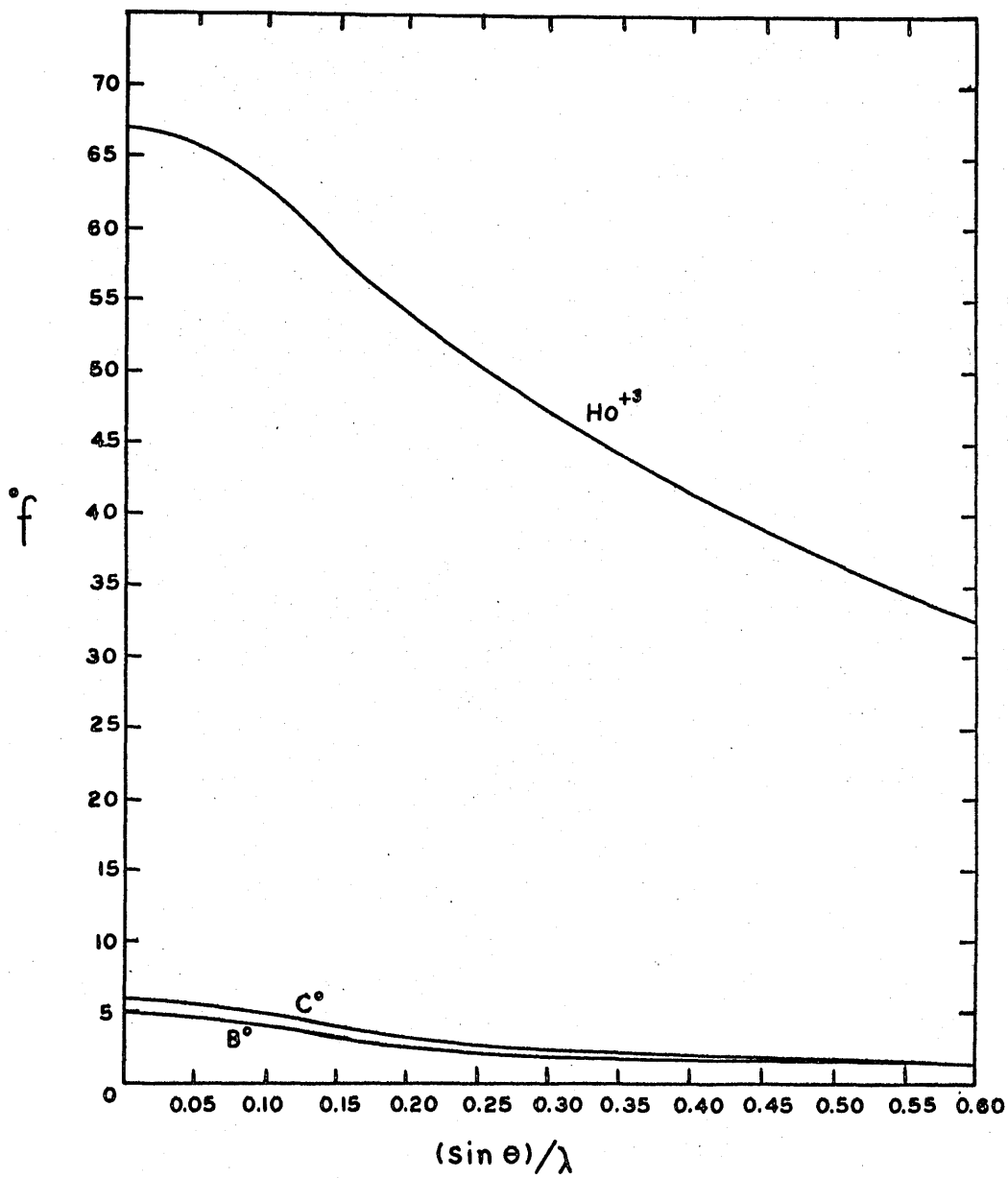

Atomic Scattering Factors For B°, C°, and Ho^{+3} Versus $(\sin\theta)/\lambda$

FIGURE 5. 3

5. 8 Light Atom Electron Density; Scale and Temperature Factors

It should be pointed out that this electron density map will include the inverse mapping as well as the real mapping.

$$|F(hkl)|^2 = F(hkl) \cdot F^*(hkl), \tag{5.28}$$

$$= (f_{Ho} + \sum_i f_i e^{2\pi i \phi_i})(f_{Ho} + \sum_j f_j e^{-2\pi i \phi_j}), \tag{5.29}$$

$$= f_{Ho}^2 + f_{Ho}(\sum_i f_i e^{2\pi i \phi_i} + \sum_j f_j e^{-2\pi i \phi_j}) + \sum_{\substack{j \\ i=j}} f_j^2$$

$$+ \sum_{\substack{i \\ i \neq j}} \sum_j f_i f_j e^{2\pi i \phi_i} e^{-2\pi i \phi_j} . \tag{5.30}$$

If the sum or the average is taken over a large number of hkl values, the last term tends to zero, since it contains as many positive as negative components. Therefore,

$$(|F(hkl)|^2)^{1/2} = \left(f_{Ho}^2 + f_{Ho}(\sum_i f_i e^{2\pi i \phi_i} + \sum_j f_j e^{-2\pi i \phi_j}) + \sum_j f_j^2 \right)^{1/2} . \tag{5.31}$$

$$F(hkl) = f_{Ho} \left(1 + \frac{1}{f_{Ho}} (\sum_i f_i e^{2\pi i \phi_i} + \sum_j f_j e^{-2\pi i \phi_j}) + \frac{1}{f_{Ho}^2} \sum_j f_j^2 \right)^{1/2} . \tag{5.32}$$

Expanding the right hand side into a binomial series, one finds:

$$F(hkl) \cong f_{Ho} [1 + \frac{1}{2f_{Ho}} (\sum_i f_i e^{2\pi i \phi_i} + \sum_j f_j e^{-2\pi i \phi_j}) + \frac{1}{2f_{Ho}^2} \sum_j f_j^2 + \ldots\ldots] . \tag{5.33}$$

Hence,

$$F'(hkl) = F(hkl) - f_{Ho}$$

$$= \frac{1}{2}\left(\sum_j f_j e^{2\pi i \phi_i} + \sum_j f_j e^{-2\pi i \phi_j}\right) + \frac{1}{2f_{Ho}} \sum_j f_j^2 \quad . \tag{5.34}$$

The structure factor Fourier coefficients, F'(hkl), in the electron density synthesis will involve the inverse terms, $\frac{1}{2} \sum_j f_j e^{-2\pi i \phi_j}$, as well as the real terms. But, again, atomic size considerations will force a choice of the positions revealed by the electron density map.

A scale factor, which could be ignored in the Patterson synthesis, must be applied to the observed F(hkl) values and a temperature factor applied to ${}^{o}f_{Ho}$ in order that the F'(hkl) values represent the difference between numbers on the same scale and at the same temperature. These factors are determined in the following fashion: Recall equations 5.28 and 5. 4. In general,

$$|F(hkl)|^2 = \left(\sum_j f_j e^{2\pi i \phi_i}\right)\left(\sum_j f_j e^{-2\pi i \phi_j}\right), \tag{5.35}$$

$$= \sum_i \sum_j f_i f_j e^{2\pi i [h(x_i - x_j) + k(y_i - y_j) + l(z_i - z_j)]}, \tag{5.36}$$

$$= \sum_{\substack{j \\ i=j}} f_j^2 + \sum_{\substack{ij \\ i \neq j}} f_{ij} f_{ij} e^{2\pi i [h(x_i - x_j) + k(y_i - y_j) + l(z_i - z_j)]} \quad . \tag{5.37}$$

As pointed out in equation 5. 30, the last term of 5. 37 approaches zero for an average over all hkl. Therefore,

$$\overline{|F(hkl)|^2} = \overline{\sum_j f_j^2} \quad . \tag{5.38}$$

Further,

$$|F(hkl)_{obs.}|^2 = K\,|F(hkl)_{abs.}|^2 , \tag{5.39}$$

where K is the scale factor. From equation 5.38

$$\overline{|F(hkl)_{obs.}|^2} = K\,\overline{\sum_j f_j^2} . \tag{5.40}$$

The temperature factor correction (32) is given by

$$f^2 = {}^{o}f^2\, e^{f(\frac{\sin^2\theta}{\lambda^2})} . \tag{5.41}$$

where ${}^{o}f$ is the atomic scattering factor at zero degrees absolute. Consequently,

$$Ke^{f(\frac{\sin^2\theta}{\lambda^2})} = \frac{\overline{|F(hkl)_{obs.}|^2}}{\overline{\sum_j {}^{o}f_j^2}} ; \tag{5.42}$$

and

$$\ln \frac{\overline{|F(hkl)_{obs.}|^2}}{\overline{\sum_j {}^{o}f_j^2}} = \ln K + f\,(\frac{\sin^2\theta}{\lambda^2}) . \tag{5.43}$$

Equation 5.43 is of the form,

$$y = a + f\,(\frac{\sin^2\theta}{\lambda^2}) . \tag{5.44}$$

Thus, a plot of the left hand side of equation 5.43 versus $\sin^2\theta/\lambda^2$ in the limit of $\sin^2\theta/\lambda^2$ equal to zero produces the scale factor, K.

The temperature factor, $f(\frac{\sin^2\theta}{\lambda^2})$, can be calculated from this curve for each $\sin^2\theta/\lambda^2$ desired.

Figure 5. 4 is a graph of equation 5.43 for HoB_2C_2. The data were taken from Table 5. 5, columns five and seven. The five numbers arranged horizontally halfway up the figure represent the average values for the vertical coordinates of experimental points lying between the brackets on either side of the average value.

Normally, such a curve as defined by equation 5.43 is a straight line with slope equal to -2B. This factor is the Debye-Waller temperature factor. However, in this case (Figure 5. 4) a parabolic plot resulted. The parabolic behavior is attributed to an error in the ${}^{o}f_{Ho}$+3 literature values (38). However, a scale and temperature correction can still be made.

The corrections applied are of the form,

$$F'(hkl) = F(hkl) - f_{Ho} = \frac{|F(hkl)_{obs.}|}{K^{1/2}} - {}^{o}f_{Ho}\, e^{f(\frac{\sin^2\theta}{\lambda^2})/2}, \qquad (5.45)$$

where $f(\frac{\sin^2\theta}{\lambda^2})$ is taken from Figure 5. 4 as the difference between the two curves on the graph.

For F'(hkl) values below the series cut-off point where $\sin^2\theta/\lambda^2$ is .360 at 444 and for which no experimental intensity was observed,

$$F'(hkl) = F(hkl) - f_{Ho}, \qquad (5.46)$$

$$= 0 - {}^{o}f_{Ho}\, e^{f(\frac{\sin^2\theta}{\lambda^2})/2},$$

$$= -{}^{o}f_{Ho}\, e^{f(\frac{\sin^2\theta}{\lambda^2})/2}. \qquad (5.47)$$

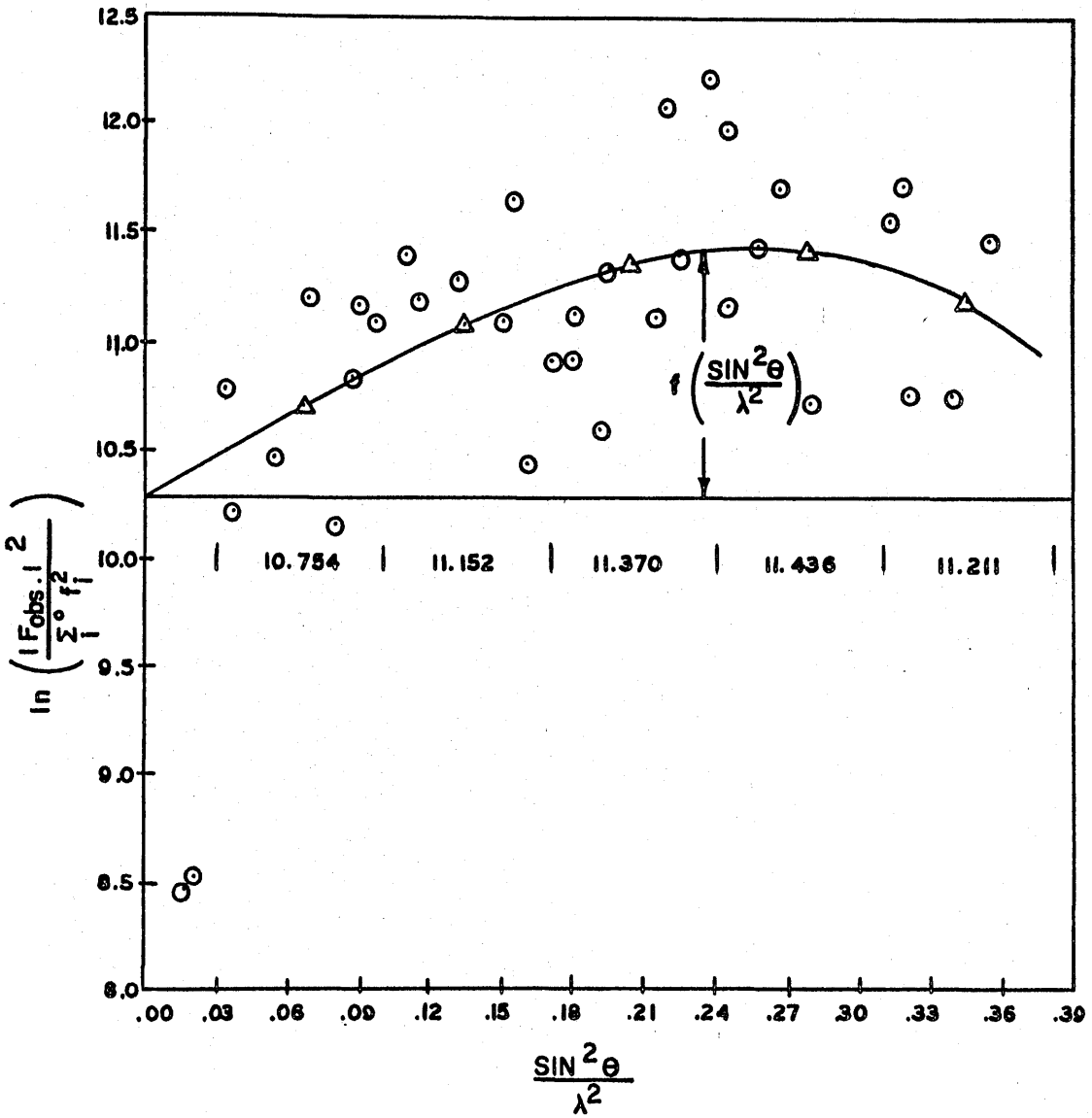

$$\ln\left(\frac{|F_{obs.}|^2}{\sum_i^o f_i^2}\right) \text{ vs. } \frac{SIN^2\theta}{\lambda^2} \text{ for } HoB_2C_2$$

FIGURE 5. 4

The F'(hkl) values should be small positive or negative numbers. Any small error in the measured intensities will be amplified considerably in F'(hkl) after subtracting f_{Ho}. Thus, the maxima in the electron density map due to the light atoms may be obscured by series termination maxima, and the location of the maxima representing atomic positions may be shifted from their real position because of intensity measurement error.

The light atom structure factor data are listed in Table 5. 5. The indexing applies to the cell with a_o and c_o dimensions, 3.7801 and 3.5374Å, respectively. Columns one through five contain the indices of the reflecting planes, the atomic scattering factors at 0^oK. for covalent boron and carbon atoms and for trivalent holmium ions, and $(\sin^2\theta)/\lambda^2$. Column six lists $|F(hkl)|^2$ observed experimentally from Table 5. 2. In addition, hkl values, such that sin θ is less than one and for which no reflection was observed, are listed with $|F(hkl)|^2$ set equal to zero. Column seven lists the left side of equation 5.43. Column eight contains scaled structure factors at the room temperature of the intensity data collection. Column nine contains the holmium structure factor at room temperature, and column ten contains the absolute light atom structure factor at room temperature.

The 100 and 001 values in Table 5. 5 were omitted from the electron density computations because of their obviously too large size. As in the Patterson synthesis, this omission will have some effect on the amplitude of the maxima, but not on the position of the electron density maxima.

For the same reasons discussed in the Patterson synthesis, the electron density functions for space group, P4/mmm, were computed rather

TABLE 5. 5

HoB_2C_2 Light Atom Structure Factors Corrected for Scale and Temperature Factors. K = 3.439 x 10^{-5}

hkl	$^{o}f_{Ho}$	$^{o}f_{B}$	$^{o}f_{C}$	$\frac{\sin^2\theta}{\lambda^2}$	$\lvert F(hkl)_{obs.}\rvert^2$	$-\ln\frac{\lvert F(hkl)_{obs.}\rvert^2}{\sum_i {}^{o}f_i^2}$	$F(hkl)_{abs.}$	f_{Ho}	$F(hkl)_{abs.}$-f_{Ho}
000	67.00	5.00	6.00	.00000	.00000		.000	67.0	-67.0
100	59.67	3.575	4.50	.01748	.780	8.449	151.	55.83	95.2
001	58.98	3.44	4.37	.01996	.637	8.625	136.	54.66	81.3
110	55.49	2.84	3.85	.03482	.0607	10.851	42.0	48.63	-6.57
101	54.96	2.76	3.65	.03752	.114	10.200	57.6	47.91	9.69
111	52.05	2.38	3.24	.05490	.0728	10.538	46.0	42.62	3.38
200	49.82	2.17	2.80	.06996	.0336	11.222	31.3	38.76	-7.46
002	48.52	2.07	2.65	.07998	.0921	10.160	51.8	36.64	15.16
210	47.59	2.01	2.55	.08750	.0431	10.880	35.4	35.17	.23
201	47.30	1.98	2.54	.09000	.0318	11.173	30.4	34.65	-4.25
102	46.56	1.94	2.44	.09734	.0364	11.006	32.5	33.40	-.90
211	45.56	1.88	2.37	.10745	.0231	11.417	25.9	31.80	-5.90
112	44.88	1.84	2.30	.11492	.0284	11.181	28.7	27.81	.89
220	42.71	1.75	2.08	.13988	.0232	11.260	26.0	27.56	-1.56
202	41.84	1.72	2.03	.15015	.0276	11.068	28.3	26.40	1.90
030	41.29	1.70	1.99	.15724	.0138	11.734	20.0	25.70	-5.70
221	41.10	1.69	1.98	.16008	.0468	10.504	36.9	25.42	11.52
122	40.65	1.68	1.93	.16736	.0307	10.903	29.9	24.81	5.09
130	40.15	1.66	1.90	.17514	.0246	11.123	26.7	24.18	2.52
031	40.05	1.66	1.89	.17741	.0292	10.924	29.1	23.99	5.11
003	39.8			.17981	.0000		.000	23.8	-23.8
131	39.00	1.62	1.85	.19492	.0181	11.350	22.9	22.79	.11
103	38.90	1.62	1.83	.19714	.0353	10.676	32.0	22.64	9.36
113	37.90	1.59	1.80	.21511	.0220	11.120	25.3	21.62	3.68

TABLE 5. 5, continued

hkl	$^{o}f_{Ho}$	$^{o}f_{B}$	$^{o}f_{C}$	$\frac{\sin^2\theta}{\lambda^2}$	$\lvert F(hkl)_{obs.}\rvert^2$	$-\ln\frac{\lvert F(hkl)_{obs.}\rvert^2}{\sum_i {}^{o}f_i^2}$	$F(hkl)_{abs.}$	f_{Ho}	$F(hkl)_{abs.}-f_{Ho}$
222	37.65	1.58	1.79	.21977	.00802	12.093	15.3	21.38	-6.08
230	37.25	1.57	1.76	.22753	.0155	11.413	21.2	21.02	.18
032	36.75	1.56	1.74	.23756	.00646	12.262	13.7	20.60	-6.90
231	36.25	1.54	1.72	.24741	.00826	11.989	15.5	20.28	-4.78
023	36.10	1.54	1.71	.24930	.0166	11.281	22.0	20.17	1.83
132	35.93	1.53	1.71	.25502	.0137	11.464	20.0	20.07	-.07
123	35.52	1.52	1.68	.26750	.0110	11.661	17.9	19.86	-1.96
040	35.11	1.50	1.67	.28005	.0286	10.681	28.8	19.71	9.09
140	34.9			.29741	.00000		.000	19.9	-19.9
401	34.7			.29991	.00000		.000	19.8	-19.8
232	34.26	1.47	1.63	.30736	.0115	11.544	18.3	19.77	-1.47
330	34.4			.31492	.00000		.000	20.0	-20.0
141	33.92	1.45	1.62	.31787	.00929	11.739	16.4	19.94	-3.54
004	34.2			.31966	.00000		.0000	20.1	-20.1
223	33.86	1.44	1.61	.32013	.0242	10.753	26.5	19.95	6.55
331	33.6			.33491	.00000		.000	20.6	-20.6
033	33.6			.33727	.00000		.000	21.1	-21.1
014	33.35	1.43	1.58	.33756	.0244	10.737	26.6	20.54	6.06
240	33.1			.34991	.00000		.000	21.2	-21.2
114	33.0			.35465	.00000		.000	21.6	-21.6
133	32.84	1.41	1.56	.35522	.0112	11.486	18.0	21.46	-3.46
042	32.70	1.40	1.55	.36024	.0128	11.341	19.3	21.83	-2.53

$$F(hkl)_{abs.} = +\sqrt{\frac{\lvert F(hkl)_{obs.}\rvert^2}{K}} \qquad f_{Ho} = {}^{o}f_{Ho}\, e^{f(\sin^2\theta/\lambda^2)/2}$$

than one of the other four possible space groups. Minor changes in the computer program discussed above, mostly concerned with the adaptation of the program to the IBM 1620 computer, were made. The expression for the electron density function for space group P4/mmm is given by

$$\rho(XYZ) = \frac{8}{V} \sum_{hkl}^{+\infty}\sum\sum F'(hkl) \cos 2\pi hX \cos 2\pi kY \cos 2\pi lZ \ . \qquad (5.48)$$
$$o$$

This function was computed in units of sixteenths of the unit cell edges for one-eighth of the cell. Again the rest of the cell is obtained by symmetry.

The computer input data are listed in Table 5. 6 in the same format and with the same multiplicity considerations of Table 5. 3. The computer output data are listed in Table 5. 7 again in the same format and unit cell choice as for the Patterson computations of Table 5. 4. These electron density data are mapped by layers up the c-axis in Figure 5. 5. Contour lines on the nine layers define the positions of the centers of electron concentration. Figure 5. 6 is a {XY0} projection of the maxima of Figure 5. 5 with the radius of the circles indicative of the size of the maxima. The fractional heighth up the c-axis is indicated with each circle.

While there are many more maxima than there are atoms to put in them, the four maxima at 1/4, 1/2, 1/2; 1/2, 1/4, 1/2; 3/4, 1/2, 1/2 and 1/2, 3/4, 1/2 do stand out as nearly twice as intense as the next most intense maxima.

TABLE 5. 6

Input Data for HoB_2C_2 Light Atom Electron Density Synthesis for Space Group P4/mmm.

hkl	$F(hkl)_{abs}$ - f_{Ho}	hkl	$F(hkl)_{abs}$ - f_{Ho}	hkl	$F(hkl)_{abs}$ - f_{Ho}	hkl	$F(hkl)_{abs}$ - f_{Ho}
000	-8.38	113	3.68	231	-4.78	344	.000
001	.000	114	-21.6	232	-1.47	400	2.27
002	3.79	120	.12	233	.000	401	-9.90
003	-5.95	121	-5.90	234	.000	402	-1.27
004	-5.03	122	5.09	240	-10.6	403	.000
010	.000	123	-1.96	241	.000	404	.000
011	4.85	124	.000	242	.000	410	-9.95
012	-.45	130	1.26	243	.000	411	-3.54
013	4.68	131	.11	244	.000	412	.000
014	3.03	132	-.07	300	-1.43	413	.000
020	-1.83	133	-3.46	301	2.56	414	.000
021	-2.13	134	.000	302	-3.45	420	-10.6
022	.95	140	-9.95	303	-10.5	421	.000
023	.915	141	-3.54	304	.000	422	.000
024	.000	142	.000	310	1.26	423	.000
030	-1.43	143	.000	311	.11	424	.000
031	2.56	144	.000	312	-.07	430	.000
032	-3.45	200	-1.83	313	-3.46	431	.000
033	-10.5	201	-2.13	314	.000	432	.000
034	.000	202	.95	320	.09	433	.000
040	2.27	203	.915	321	-4.78	434	.000
041	-9.90	204	.000	322	-1.47	440	.000
042	-1.27	210	.12	323	.000	441	.000
043	.000	211	-5.90	324	.000	442	.000
044	.000	212	5.09	330	-10.0	443	.000
100	.000	213	-1.96	331	-20.6	444	.000
101	4.85	214	.000	332	.000		
102	-.45	220	-.78	333	.000		
103	4.68	221	11.5	334	.000		
104	3.03	222	-6.08	340	.000		
110	-3.29	223	6.55	341	.000		
111	3.38	224	.000	342	.000		
112	.89	230	.09	343	.000		

TABLE 5. 7

HoB_2C_2 Light Atom Electron Density Synthesis Output Data with Space Group, P/4mmm

X/16 Y/16	0	1	2	3	4	5	6	7	8
0	-23.0	-12.0	4.11	3.00	-7.91	-9.33	-2.30	1.04	0.680
1		-4.37	5.62	2.32	-6.43	-5.96	.103	1.19	-.236
2			5.53	.356	-2.92	.653	3.77	.307	-3.00
3				-1.23	.183	3.17	2.48	-2.76	-6.01
4					.508	-1.92	-4.70	-6.00	-6.20
5						-9.56	-11.5	-7.01	-3.81
6		Z = 0/16					-11.7	-6.45	-3.29
7								-6.20	-6.31
8									-8.45

X/16 Y/16	0	1	2	3	4	5	6	7	8
0	-17.5	-7.91	5.72	3.97	-5.78	-6.25	-1.45	-.766	-2.38
1		-1.57	6.26	2.47	-5.16	-4.22	.362	-.825	-3.32
2			4.58	-.803	-3.02	1.10	3.35	-1.55	-5.52
3				-2.44	.078	3.87	2.92	-3.04	-6.64
4					1.78	.611	-1.98	-3.74	-4.22
5						-5.32	-6.85	-2.81	.075
6		Z = 1/16					-6.48	-1.70	1.15
7								-1.77	-2.12
8									-4.45

TABLE 5. 7, continued

X/16 Y/16	0	1	2	3	4	5	6	7	8
0	-9.65	-2.88	6.18	4.14	-2.05	-1.09	1.68	-2.04	-5.72
1		1.02	5.04	1.26	-3.10	-.488	1.95	2.84	-6.98
2			.911	-3.99	-3.57	1.78	2.74	-4.09	-8.86
3				-5.17	-.437	4.57	3.15	-3.60	-7.47
4					3.69	4.35	1.75	-.734	-1.54
5						1.01	-.363	2.51	4.76
6		Z = 2/16					.133	3.60	5.73
7								2.50	1.62
8									-1.10

X/16 Y/16	0	1	2	3	4	5	6	7	8
0	-9.82	-4.98	1.60	1.03	-.919	2.63	5.29	0.811	-3.11
1		-2.47	.048	-1.98	-2.82	1.58	3.92	-.945	-4.92
2			-3.86	-6.72	-4.35	1.13	1.93	-3.78	-3.66
3				-6.35	-.847	3.26	1.41	-3.94	-5.74
4					3.89	3.93	.554	3.93	-1.82
5						.622	-1.83	.232	2.30
6		Z = 3/16					-2.73	-.437	1.34
7								-2.30	-3.22
8									-5.78

X/16 Y/16	0	1	2	3	4	5	6	7	8
0	-12.7	-8.57	-2.50	-1.88	-2.61	0.983	4.41	2.54	0.244
1		-6.12	-2.99	-3.55	-4.00	-.573	3.25	.641	-1.35
2			-4.33	-5.29	-4.17	-1.66	-.801	-2.53	-3.84
3				-3.20	.210	.417	-1.99	-3.64	-3.95
4					3.47	.528	-3.74	.528	-2.27
5						-4.36	-7.69	-4.79	-1.95
6		Z = 4/16					-9.44	-6.46	-4.01
7								-6.86	-6.64
8									-7.75

TABLE 5. 7, continued

X/16 Y/16	0	1	2	3	4	5	6	7	8
0	-9.38	-5.94	-1.01	-1.22	-3.66	-2.84	-.601	-.961	-1.99
1		-3.64	-.611	-1.64	-4.42	-4.40	-2.49	-1.89	-2.16
2			-.116	-.856	-3.06	-5.03	-4.82	-2.81	-1.62
3				1.90	2.15	-1.91	-4.56	-2.12	.212
4					4.02	-1.21	-5.27	-2.07	1.20
5		Z = 5/16				-6.17	-8.80	-3.95	.050
6							-9.54	-4.61	-1.07
7								-2.18	-.349
8									.469

X/16 Y/16	0	1	2	3	4	5	6	7	8
0	-3.65	-1.62	1.03	0.200	-1.96	-2.10	-1.98	-3.94	-5.45
1		-.311	1.13	-.356	-3.28	-4.47	-4.05	-3.93	-4.12
2			1.25	.270	-2.85	-6.27	-6.16	-2.42	-.077
3				2.79	2.14	-2.79	-4.40	.910	4.88
4					4.31	-.358	-3.00	2.38	6.79
5		Z = 6/16				-3.63	-5.14	.486	4.83
6							-5.45	-.423	3.16
7								2.32	4.45
8									5.77

X/16 Y/16	0	1	2	3	4	5	6	7	8
0	-2.91	-2.29	-1.46	-.874	1.10	3.83	3.20	-1.46	-4.37
1		-2.22	-2.35	-2.56	-1.78	-.184	.167	-1.39	-2.48
2			-3.59	-3.84	-4.25	-5.04	-3.63	.451	2.85
3				-1.59	-.426	-2.87	-2.38	4.34	8.84
4					3.16	.721	-.333	5.69	10.2
5		Z = 7/16				-1.02	-2.50	2.00	5.68
6							-4.63	-2.15	.244
7								-2.52	-1.67
8									-1.58

TABLE 5. 7, continued

X/16 Y/16	0	1	2	3	4	5	6	7	8
0	-4.17	-4.20	-3.87	-2.11	2.58	7.46	6.97	1.10	-2.52
1		-4.59	-5.27	-4.44	-1.16	2.56	3.32	.965	-.657
2			-7.17	-6.79	-5.23	-4.04	-1.69	2.40	4.66
3				-4.58	-2.10	-2.83	-1.23	5.90	10.5
4					2.18	1.00	.608	6.62	11.0
5		Z = 8/16				-.270	-2.06	1.54	4.73
6							-5.56	-4.77	-3.16
7								-7.25	-7.28
8									-8.08

HoB_2C_2 LIGHT ATOM 3-D ELECTRON DENSITY CONTOURS

SPACE GROUP P4/mmm

FIGURE 5. 5

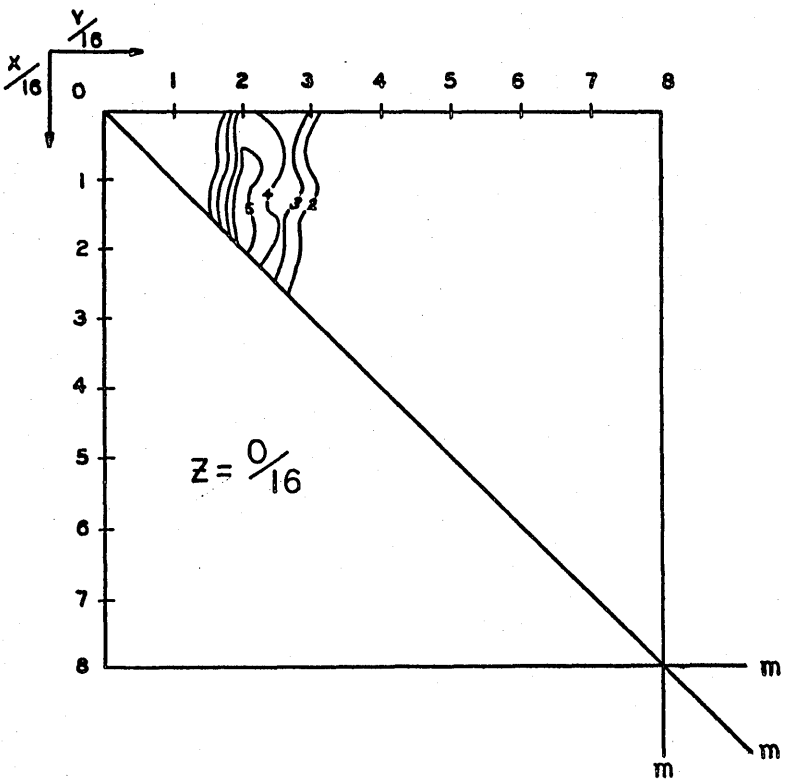

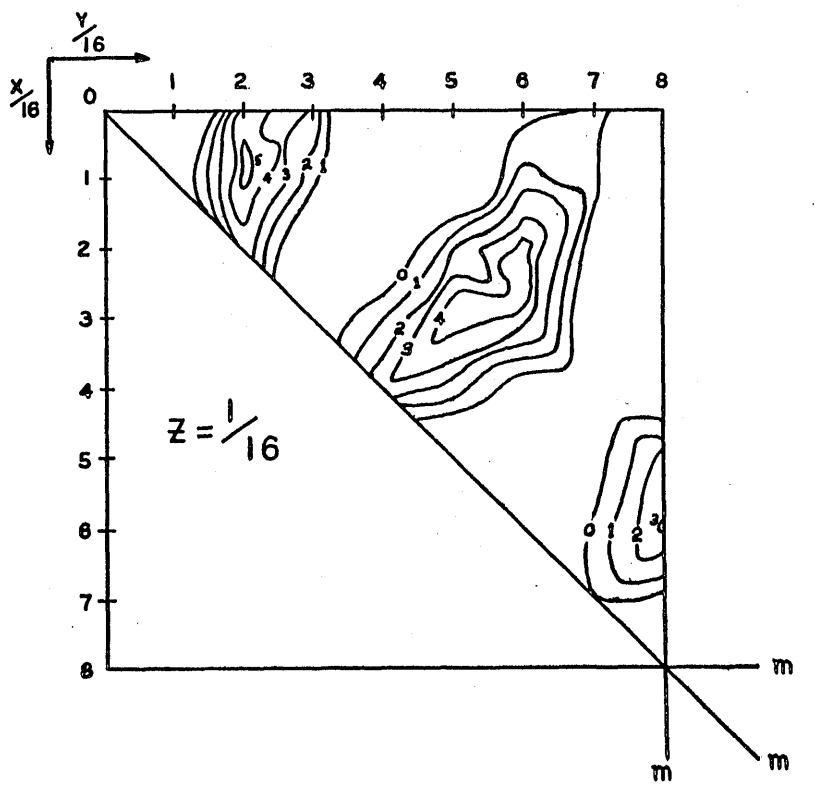

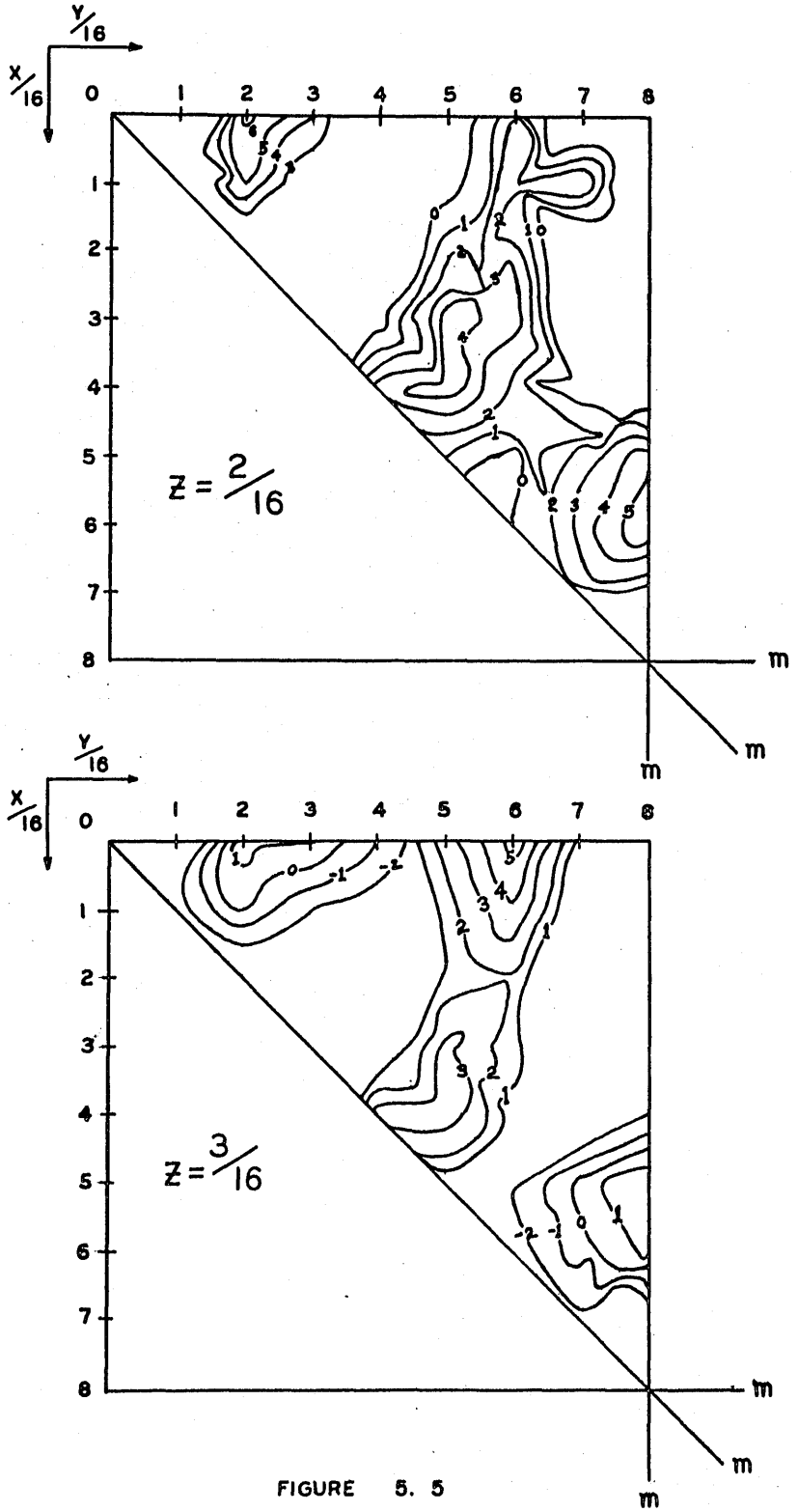
Y/16
X/16
0 1 2 3 4 5 6 7 8
1 2 3 4 5 6 7 8
Z = 2/16
m
m
m
Y/16
X/16
0 1 2 3 4 5 6 7 8
1 2 3 4 5 6 7 8
Z = 3/16
m
m
m

FIGURE 5. 5

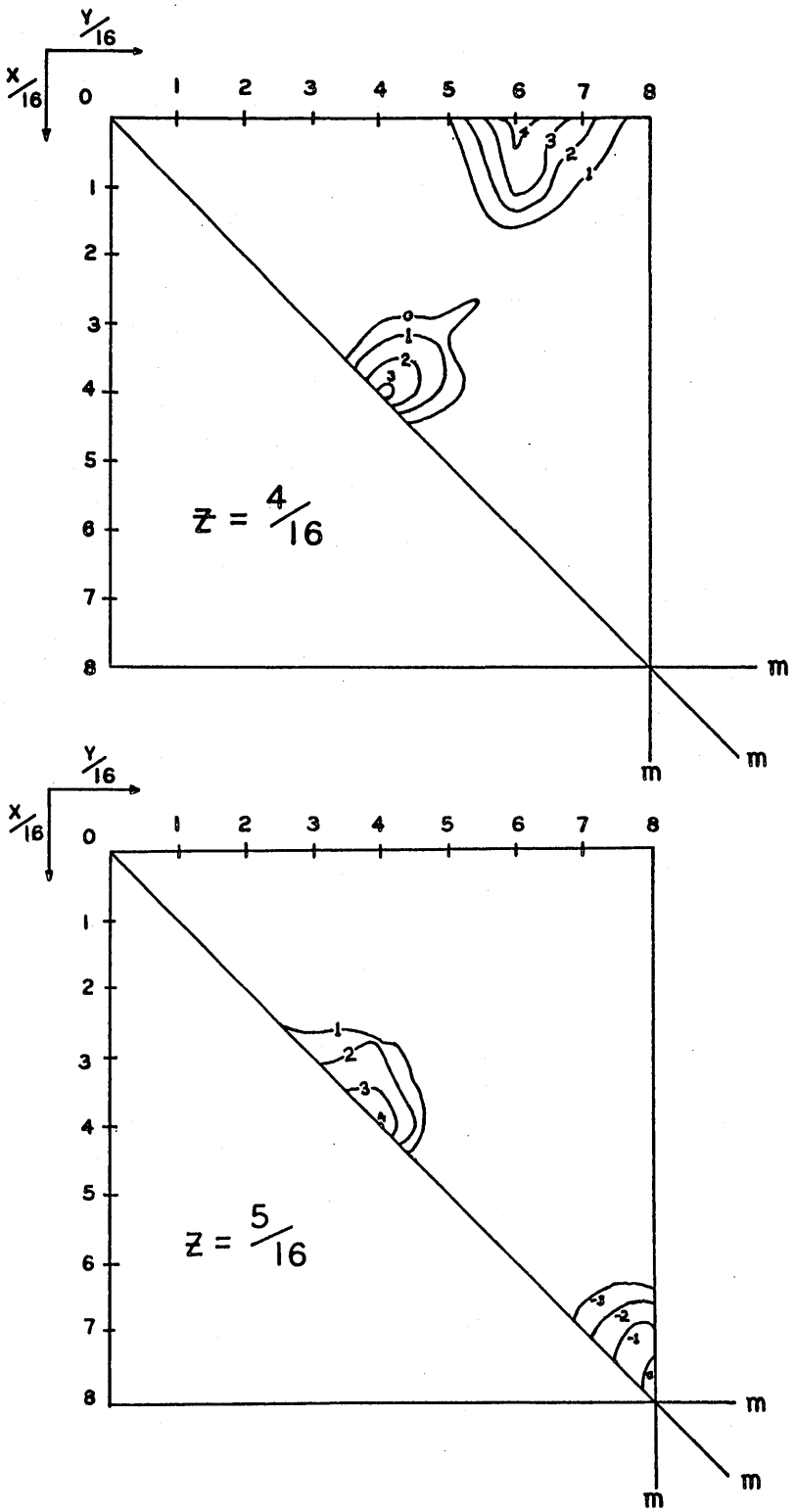
Y/16
X/16
0 1 2 3 4 5 6 7 8
1 2 3 4 5 6 7 8
Z = 4/16
m
m
m
Y/16
X/16
0 1 2 3 4 5 6 7 8
1 2 3 4 5 6 7 8
Z = 5/16
m
m
m

FIGURE 5. 5

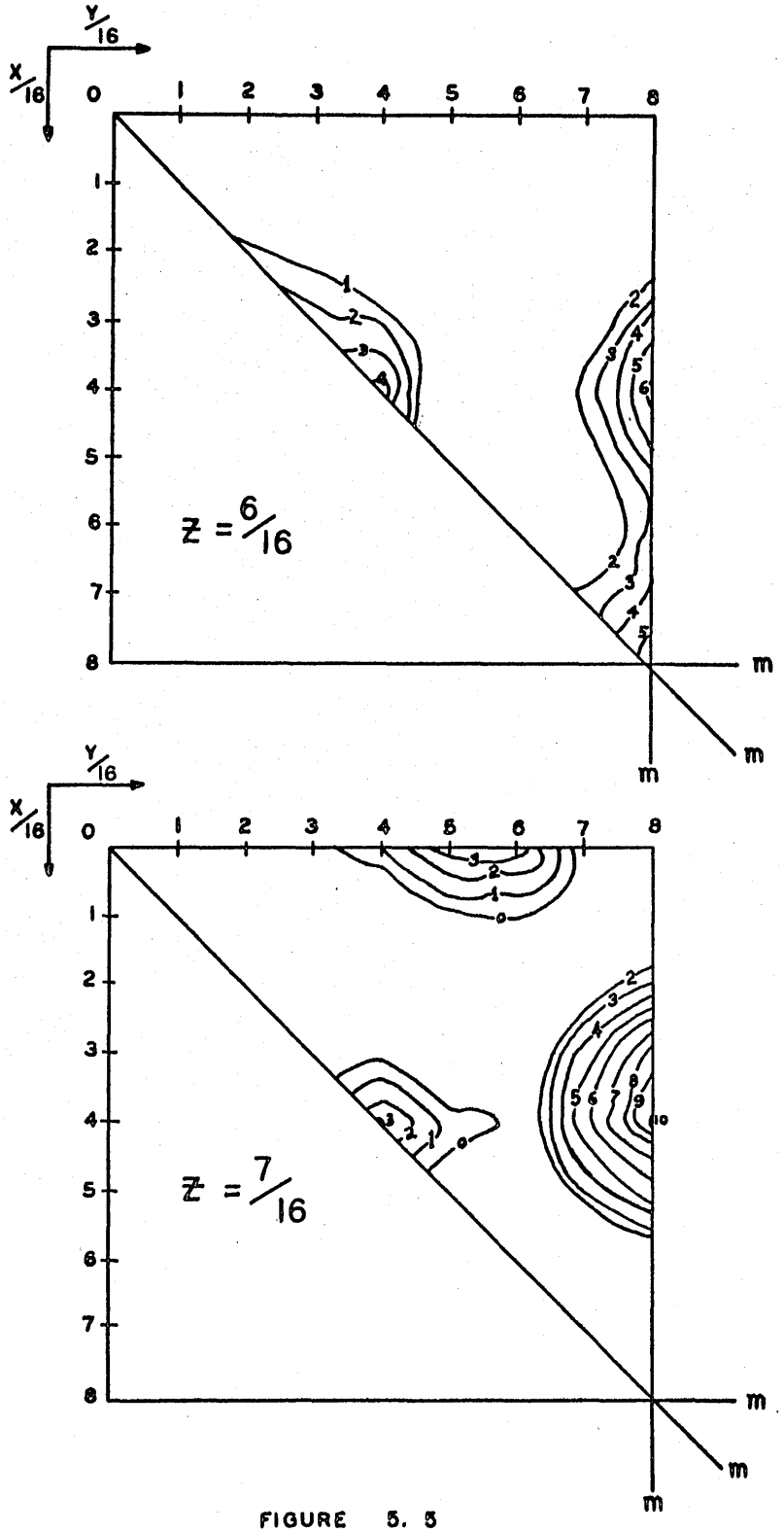

FIGURE 5. 5

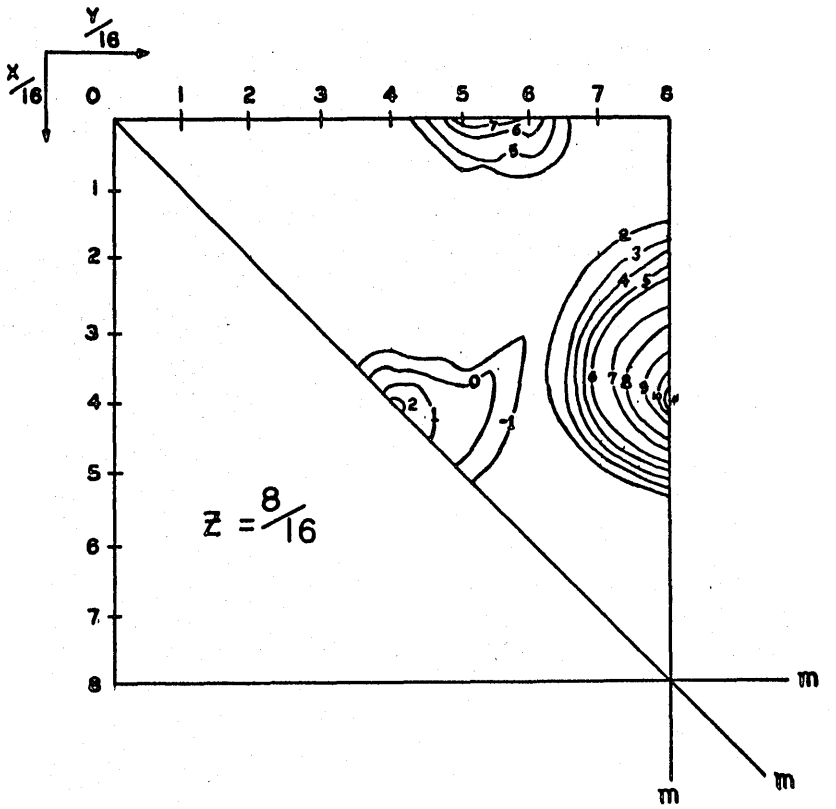

FIGURE 5. 5

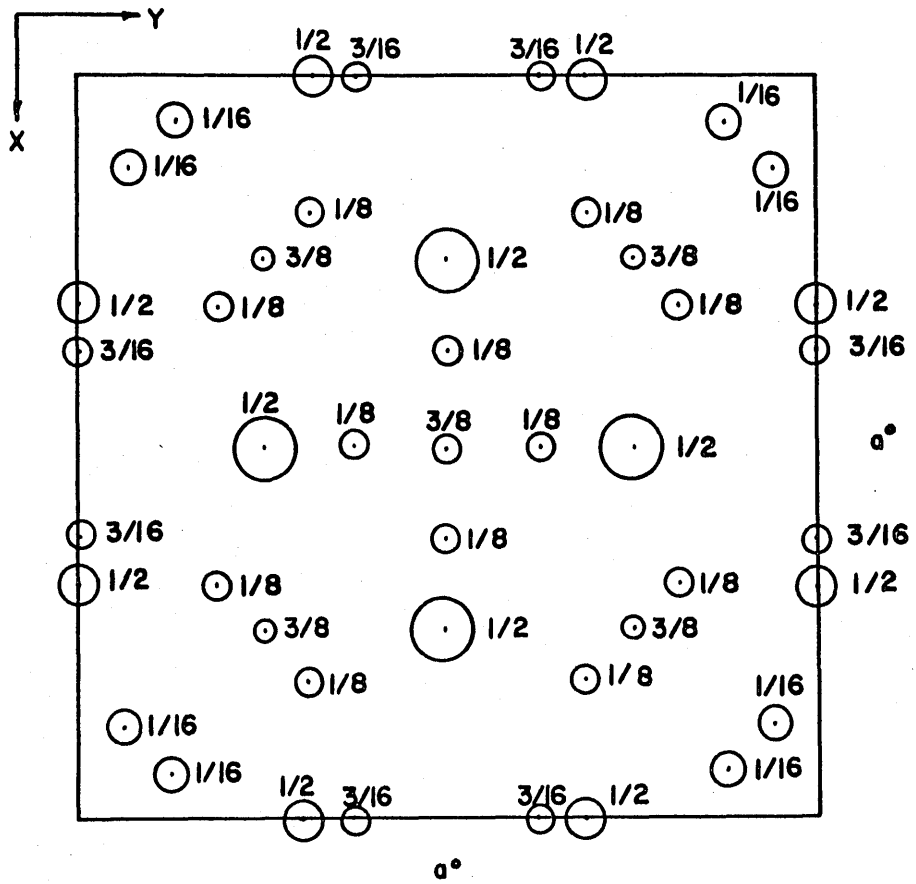

Ln B_2C_2 LIGHT ATOM ELECTRON DENSITY PROJECTION

{ oow }

FIGURE 5. 6

5. 9 Light Atom Positions; Space Group; General Structure Discussion

There are several arguments and observations which define the space group of LnB_2C_2 and the boron and carbon positions. First, the chemical analysis and preparative techniques discussed in Chapter 4. 2 fix the boron to metal and carbon to metal ratios at two. Second, the density measurements of Chapter 4. 1 fix the unit cell content at one formula unit -- one metal, two boron and two carbon atoms -- for a cell with a_o and c_o, 3.7801 and 3.5374Å, respectively.

Third, the X-ray information is quite restrictive on the atomic positions. In Chapter 5. 6 a Patterson synthesis left no doubt that the metal atoms were located only in the corners of the primitive cell chosen for the analysis. It is very inviting to place the two boron and two carbon atoms in the four (o) equivalent positions, $\pm$(x, 1/2, 1/2; 1/2, x, 1/2), found for the light atom electron density map of Chapter 5. 8. However, one must appreciate that the symmetry demands of the computations force the equivalence of these possible positions and the equivalence of other maxima observed in the mapping.

There are three distinct symmetry considerations. The first is the inherent centrosymmetry of the reciprocal lattice. This centrosymmetry arises from the phase problem (cf. Chapter 5. 3, Friedel's Law) involving inverse as well as real structure factors in the $|F(hkl)|^2$ values measured, and introduces both structure factors into the point group. Thus, the use of the centrosymmetric 4/mmm point group in generating the electron density map is required. A second consideration, related to the first, is the unavoidable inclusion of inverse light atom

structure factors in the synthesis from the light atom phase problem, even with the phase problem of the metal atoms solved. Finally, there is the inability of X-rays to distinguish between carbon and boron atoms.

Selection of other maxima in the electron density map at which four atoms may be located was attempted. In order to limit the choices to a total of four positions, symmetry elements were removed, i.e., the diagonal mirror planes, the four-fold axis, and each of the mutually perpendicular mirror planes of Figure 5. 2. All combinations of four maxima with different point groups could be rejected with steric arguments except the obvious equivalent positions described above.

If these four equivalent positions had not occurred along the lines representing the intersection of two mutually perpendicular mirror planes, then the number of observed equivalent maxima in Figure 5. 6 would have been eight or sixteen, depending on whether the maxima were located in a mirror plane or not. Then the choice for atomic positions would have been more difficult. Thus, since the light atoms have two position coordinates equal to 1/2, the point group must contain three mutually perpendicular mirror planes. No diagonal mirrors are required.

Fourth, the agreement between the atomic position arrangement in the LnB_2C_2 structure and those of LnB_6 and LnB_4 is remarkable. Figure 5. 7 illustrates structures reported for LnB_4, LnB_6, LnB_{12}, LnC_2 and Ln_2C_3. In the cubic hexaboride described by Blum and Bertant (39) the cell is primitive with respect to the metal ions. Boron positions are observed at $\pm$(1/2, 1/2, .207; 1/2, .207, 1/2; .207, 1/2, 1/2). Four of these six positions agree precisely with the four largest maxima found in the HoB_2C_2 light atom electron density map. While the tetragonal

tetraboride structure discussed by Blum and Bertant and by Zalkin and Templeton (39, 40) is more complex than LnB_2C_2, a tetragonal cell can be chosen that is primitive with respect to the metal ions and contains a boron octahedron, which has four boron sites in positions equivalent to those for the light atoms in LnB_2C_2 just as in LnB_6. There is no such striking similarity to the icosahedral boron structure of LnB_{12} (39, 41), to LnC_2 (42, 28, 43), to Ln_2C_3 (42-3, 28) or to Ln_3C (28). It is apparent, then, since there are four positions needed and four obvious maxima available, and since the resemblance to LnB_4 and LnB_6 structures is so striking, that the boron and carbon atoms are probably located at $\pm$(1/2, x, 1/2; x, 1/2, 1/2) with x approximately 1/4.

The questions of a four-fold, two-fold or one-fold axis must be resolved. It should be noted that because of the inaccuracy in the light atom structure factors the remaining light atom position parameter to be specified need not be fixed at 1/4, but could vary as much as one-eighth of the unit cell dimension in either direction, staying in the mirror planes. Further, if one recalls that the four-fold axis was an assumption included in the tetragonal P4/mmm space group application, the possibility that only a two-fold axis exists cannot be overlooked. This would define two sets of equivalent positions, $\pm$(x, 1/2, 1/2) and $\pm$(1/2, y, 1/2). A one-fold axis would arise, if the equivalent positions were (x, 1/2, 1/2; 1/2, 1-x, 1/2) and (1/2, y, 1/2; 1-y, 1/2, 1/2).

There are six possible arrangements of the boron and carbon atoms to be considered. These are illustrated in Figure 5. 8 by projections on the (XYO) plane. Sheets of metal atoms are at the zero level and sheets of boron and carbon atoms are located between metal sheets at

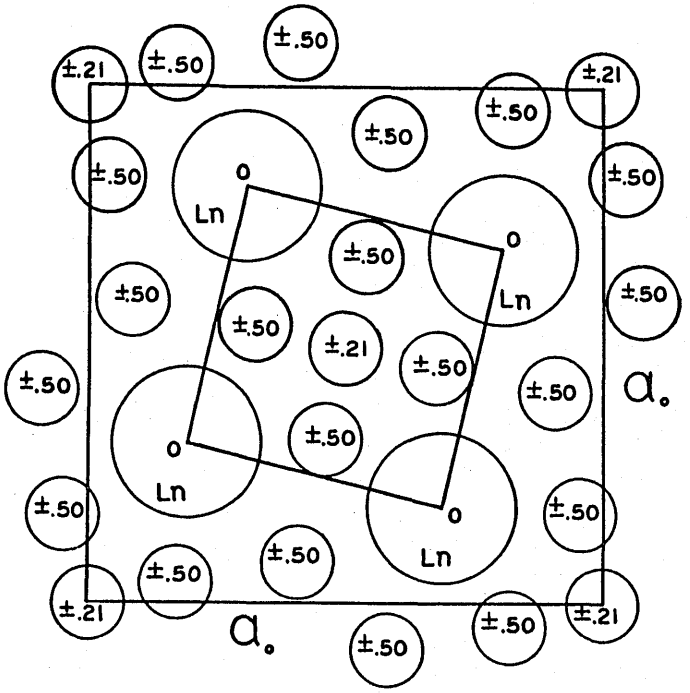

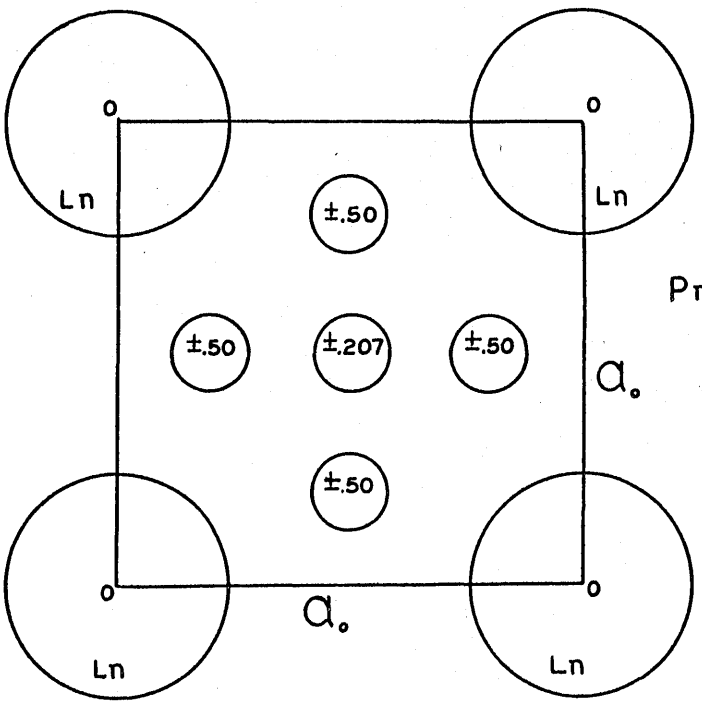

LnB_4, LnB_6, LnB_{12}, LnC_2, and Ln_2C_2 ⟨00w⟩ Structure Projections

FIGURE 5. 7

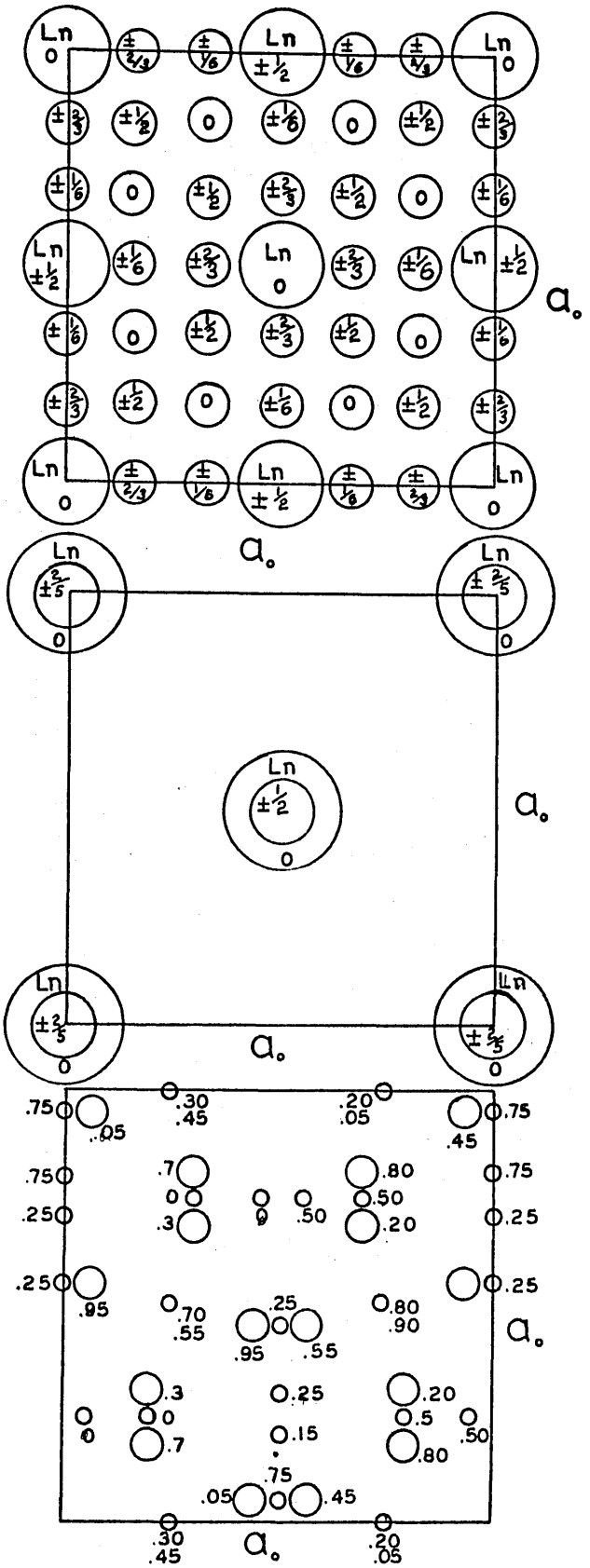

LnB_{12}

$Fm3m - O_h^5$

CUBIC

LnC_2

$I4/mmm - D_{4h}^{17}$

TETRAGONAL

Ln_2C_3

$I\bar{4}3d - T_d^6$

CUBIC

FIGURE 5. 7

a heighth of one-half of the c_o dimension. The two carbon and two boron sites might be adjacent (one-fold axis), as in Figure 5. 1. 1, or opposite (two-fold axis), as in Figure 5. 8. 2. All four of these positions might contain only boron atoms or only carbon atoms, and an adjacent cell would contain only carbon atoms or boron atoms (two-fold axis), as in Figure 5. 8. 3. Necessarily, then, a larger unit cell to define the crystal motif would be needed. A fourth possibility would be a random ordering of boron and carbon atoms into these four sites (four-fold axis), as shown in Figure 5. 8. 4. Fifth, the boron and carbon atoms could be arranged in an alternating arrangement going around light atom rings. This arrangement would necessitate the choice of the larger unit cell shown in Figure 5. 8. 5. Finally, there may be a screw axis applied to all these possibilities, depending how each light atom sheet is oriented with respect to another.

The choice between these sets of equivalent positions would be easy if the boron and carbon atoms could be distinguished in the electron density map. Intensity data are not accurate enough to distinguish these possibilities. Recall from above that with such a disparity in the scattering power between the dominant lanthanide atom and the boron and carbon atomic scattering power and with such a limited set of measured intensities in the diffraction record, it is difficult to locate the positions of the light atoms at all, much less distinguish between carbon and boron atoms.

Let us examine the light atom arrangements in Figure 5. 8 in more detail. From the average boron-boron separation indicated in borides of Table 5. 8 the boron covalent radius is about 0.87Å. Also,

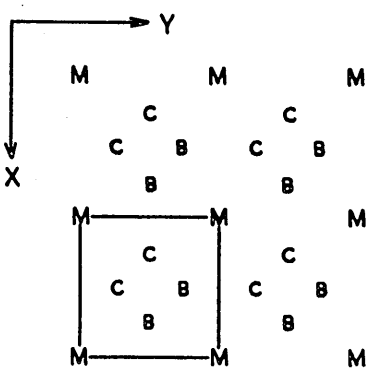

LIGHT ATOMS ADJACENT

5. 8. 1

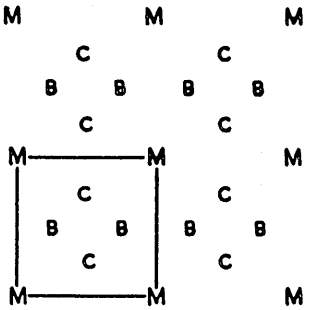

LIGHT ATOMS OPPOSITE

5. 8. 2

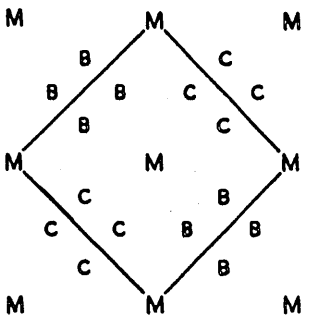

LIGHT ATOMS CLUSTERED
IN GROUPS OF FOUR-OF-A-KIND

5. 8. 3

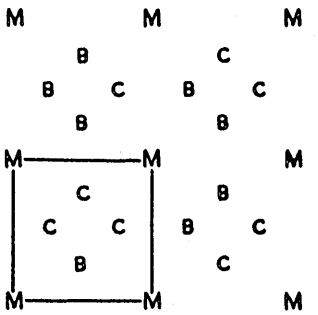

LIGHT ATOMS RANDOM

5. 8. 4

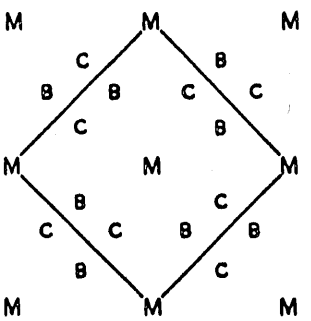

LIGHT ATOMS ALTERNATING

5. 8. 5

POSSIBLE LnB_2C_2 LIGHT ATOM ARRANGMENTS

FIGURE 5. 8

from Table 5. 8, the covalent carbon radius is about 0.70Å. In Figure 5. 8. 1, then, the boron-boron distance will be greater than the carbon-carbon separation. Thus, even though carbon and boron atoms are indistinguishable by X-ray diffraction, this arrangement can be eliminated as a possible structure on the basis of the structure's failure to exhibit any four-fold axis. While it might be a coincidence that TbB_2C_2 would exhibit this apparent tetragonal symmetry, it is fortuitous that all the lanthanides which have wide ionic radius variation should show the tetragonal symmetry as discussed in Chapter 4. 4. Never in the high angle powder photographs or in the single crystal studies were superlattice lines or spots observed indicative of lower symmetry than a four-fold axis.

Similarly, the light atom arrangement in Figure 5. 8. 2 can be eliminated. The metal separation in the Y-direction should be larger than that in the X-dimension because of the disparity in boron-boron and carbon-carbon distances. This disparity does not allow any four-fold axes.

While there are four-fold axes in the center of the light-atom, four-membered rings of the arrangement in Figure 5. 8. 3, there is no four-fold axis at the metal ions, as is demanded by the Weissenberg photographs coupled with the positioning of the metal atoms in the corner of the primitive tetragonal cell chosen for the Fourier analyses.

The arrangements in Figures 5. 8. 1, 5. 8. 2 and 5. 8. 3, with their screw axis counterparts are, hence, all eliminated as possible structures. However, both the random orientation of Figure 5. 8. 4 and the alternating arrangement of Figure 5. 8. 5 with its screw counterpart

meet the requirements of a four-fold axis and the light atoms positioned as required by the electron density analysis. Since boron and carbon have equal numbers of core electrons, the differences in their scattering amplitude will depend on the valence electrons. It is conceivable that bonding requirements would set the scattering abilities equal or even reversed from the atomic number ratio. Also, as discussed in the above paragraph, from the centrosymmetric space group for which the computations were done, vectors in the synthesis contributed from carbon sites and those contributed from boron sites were set equal by symmetry. Therefore, the intensities of the four electron density maxima must be equal.

If a random filling of these positions is allowed, it would appear that a solid solution range from the tetragonal tetraboride to the tetragonal dicarbide ought to exist. While there is some evidence of solid solution in GdB_2C_2 there is not anything like the solid solution range one might expect for such random filling. If such were the case, the space group would be P4/mmm, D_{4h}^1, No. 123 (33). However, the random arrangement seems very improbable.

Therefore, the only possible light atom arrangement remaining is that of Figure 5. 8. 5 with its screw axis counterpart. This alternating arrangement of boron and carbon atoms in eight- and four-membered rings satisfies the symmetry and position requirements established by X-ray analysis.

This structure belongs to the tetragonal space group P4/mbm, No. 127 (33). There are two LnB_2C_2 formula units per cell. The atoms and their

equivalent positions are:

Two Ln at 2(a); 000; 1/2, 1/2, 0;

Four B at 4(h); x, 1/2+x, 1/2; $\bar{x}$, 1/2-x, 1/2; 1/2+x, $\bar{x}$, 1/2;
1/2-x, x, 1/2;

Four C at 4(h); x, 1/2+x, 1/2; $\bar{x}$, 1/2-x, 1/2; 1/2+x, $\bar{x}$, 1/2;
1/2-x, x, 1/2;

Figure 5. 9 contains the symmetry elements of this space group and Figure 5.10 is a projection onto the (XYO) plane of the actual structure. There are four-fold inversion axes at the corners of the cell and at the center of the cell. Two-fold inversion axes are found half-way along the cell edges. There are diagonal mirror planes between adjacent two-fold inversion axis positions and a mirror plane perpendicular to and half-way up the c-axis. There are two-fold rotation axes parallel to the paper half-way up the c_o dimension and defined by the mirror plane intersections. Perpendicular glide planes passing through 1/4, 0, 0 and 0, 1/4, 0 and cell diagonal glide planes exist. Diagonal and perpendicular screw diads parallel to the paper and half-way up the c_o dimension also exist.

The possibility of light atom sheets being alternately in or out of phase with respect to superposition down the c-axis must be considered, i.e., will a boron atom of one light atom sheet superimpose onto the boron atom of the adjacent sheet on projection, or will a carbon atom superimpose on a boron atom? As a matter of fact, many alternate orientations up the c-axis are possible. The space group considered above would be an AAAAA . . . arrangement of light atom sheets. For an ABABAB . . . arrangement, the point group would involve two-fold screw axes. In particular, the space group would be P4/mnc, No. 128, with

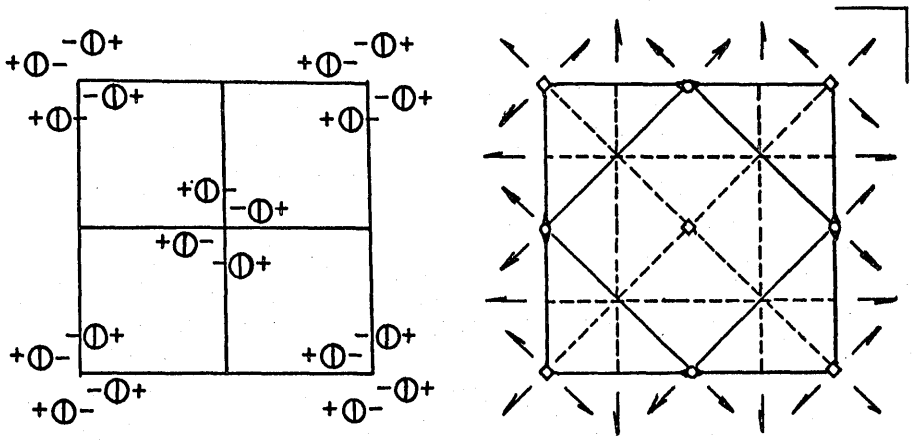

Origin at centre (4/m)

LnB_2C_2 SPACE GROUP, P4/mbm, TETRAGONAL

FIGURE 5. 9

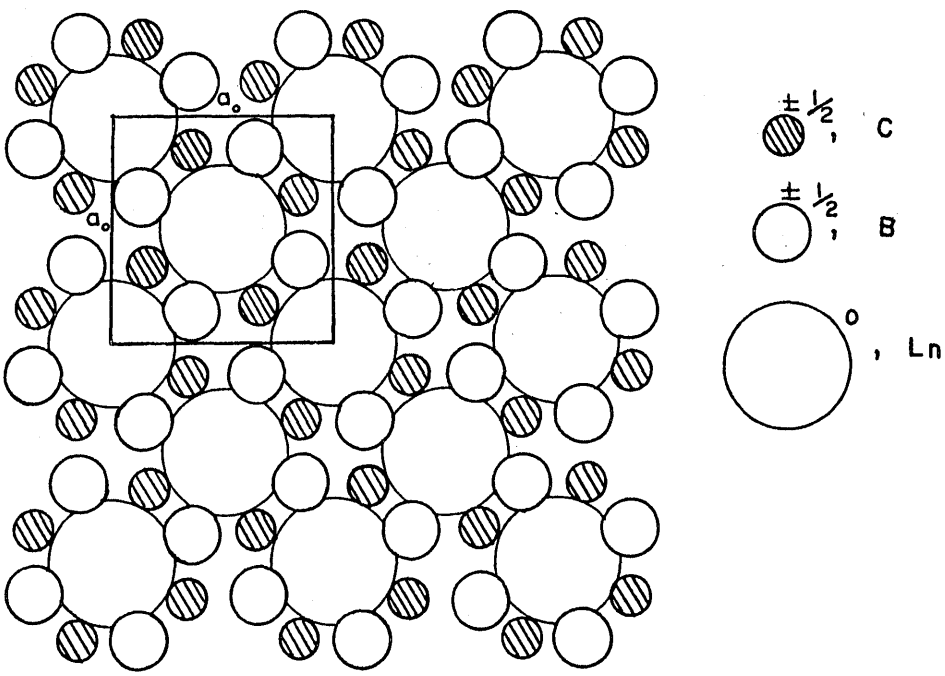

LnB_2C_2 Structure ; {oow} Projection

FIGURE 5. 10

four formula units per cell. The metals would be at 2(a) and 2(b) positions; eight boron atoms, at 8(g); and eight carbon atoms, at 8(g). More complex sheet ordering is possible. In an effort to choose the smallest cell the space group is assumed to be P4/mbm with an AAAA . . . light atom plane orientation. The bonding considerations of Chapter 6 and the above discussion constitute a fifth argument favoring the selection of this space group.

It is now necessary to fix the boron position parameter, x_B, and the carbon position parameter, x_C, in order to completely define the structure. The electron density map does not fix these parameters any better than $0.25 \pm .1$. These parameters for HoB_2C_2 have been established by comparing interatomic distances in related compounds.

Table 5. 8 summarizes crystallographic information for α-B, B_4C, tetragonal-B, HoB_4, HoB_6, HoB_{12}, Ho_3C, Ho_2C_3, HoC_2, UBC, ThB_2C, and HoB_2C_2. The table lists space groups, symmetries, lattice parameters, formula units/cell and interatomic distances. All data, except for HoB_2C_2, were taken from the literature references cited at the heads of the columns. The space group assignment for ThBC is tentative and interatomic distances are nominal.

The boron-carbon distance in B_4C is 1.64Å and in UBC is 1.64Å. The boron-carbon distance in HoB_2C_2 is assumed to be that distance required by a regular octagon of light atoms all in the diagonal mirrors. Thus, the boron-carbon distance is 1.58Å, which agrees quite well with the 1.64Å spacing expected. With this assumption, the holmium-boron and holmium-carbon distances will be equal at 2.70Å. This metal-light atom distance is in excellent agreement with metal-boron distances in related compounds,

but a little higher than metal-carbon distances in carbides. The boron-boron and carbon-carbon separations across the square four-membered rings are both 2.23Å. Arguments are presented in Chapter 6 for aromatic eight-membered boron-carbon rings. Aromaticity would account for the decrease in the boron-carbon separation in HoB_2C_2 compared to 1.64Å. The interatomic distances in HoB_2C_2 are in striking agreement with the expected separations (cf. Table 5. 8). The excellent agreement between the interatomic distances in HoB_2C_2 and those of the related compounds is the sixth argument confirming the structure.

Optimization of the position parameters within the restrictions of the above space group and the required light-atom regular octagon produced the distances for HoB_2C_2 in Table 5. 8. As a result, the boron parameter, x_B, is 0.352; and the carbon parameter, x_C, is 0.148. These position parameters are not outside the variation allowed by the electron density map in terms of the smaller cell.

Finally, a seventh point in support of this structure is found in the variation of the $a_o = b_o$ and the c_o lattice parameters for LnB_2C_2. In Figure 4, it was observed that the a_o parameter of the smaller unit cell chosen at first changes only a total of one percent as atomic number increases through the lanthanides. This change compares to lattice parameter changes in tetraboride parameters of six percent and in hexaborides parameters of seven percent (02). On the other hand, the c_o parameter decreases by thirteen percent, a rate greater than the pure metal lattice parameter decrease with increasing atomic number (30).

This disparity in a_o and c_o behavior in LnB_2C_2 is not at all surprising if the structure is examined. Consider LnB_2C_2 to be made up

of sheets of interconnected alternate boron and carbon atoms interspersed by metal ions centered between holes in the eight-membered boron-carbon rings. It is very easy for these sheets, separated by 3.5 Å and thus too far for much light atom bonding between sheets, to get closer together as the radius of the lanthanide decreases. However, the metal atoms lying in a plane parallel to the light atom sheet are fairly well constrained to their respective positions regardless of the metal radius, since they are required to stay centered with respect to the holes in the eight-membered light atom rings whose dimensions do not change with metal.

This effect is dramatically illustrated in the case of YbB_2C_2. Normally, both parameters would show alkaline earth deviation from the lanthanide contraction at ytterbium. In the case of YbB_2C_2, c_o is no exception. However, a_o deviates only very slightly.

The crossing of the a_o and c_o parameters at praseodymium produces an interesting situation. Where c_o was larger than a_o for lanthanum, the reverse situation occurs at Pr or Nd with increasing diversity through the lanthanides beyond Nd. The cubic symmetry that would result if a_o equals c_o would explain Post's cubic or pseudocubic PrB_x observation (Table 1). Even NdB_2C_2 has an apparent cubic symmetry unless high angle lines are available or long wavelength radiation is used to detect line splitting.

With the assignment of the tetragonal cell defined in the above discussion, it is necessary to re-index the data in Tables 4. 1, 5. 1, 5. 2, 5. 3, 5. 4, 5. 5, 5. 6 and 5. 7 for this end-centered cell with twice the volume of the unit cell chosen for these data. This new indexing scheme is listed in Table 5. 9. As prescribed by the P4/mbm space

TABLE 5. 8

Crystallographic Data and Interatomic Distances in Lanthanide Borides and Carbides and Related Compounds

	α-B (44)	B_4C (44,45)	B (44)	HoB_4 (39,40,46, 30,31)	HoB_6 (39, 46)	HoB_{12} (39,41, 46)	Ho_3C (28)	Ho_2C_3 (42,28, 43)	HoC_2 (42,28, 43)	UBC (17)	ThB_2C (18)	HoB_2C_2
Space Group	$R\bar{3}m$	$R\bar{3}m$	$P4_2/nnm$	$P\frac{4}{m}bm$	$Pm3m$	$Fm3m$	$Fm3m$ ($F\bar{4}3m$)	$I\bar{4}3d$	$I4/mmm$	$Cmcm$	($P\bar{6}/mmm$)	$P/4mbm$
Symmetry	Rhombo-hedral	Rhombo-hedral	Tetrag-onal	Tetrag-onal	Cubic	Cubic	Cubic	Cubic	Tetrag-onal	Ortho-rhombic	Hexag-onal	Tetrag-onal
Lattice Parameters (Å) (deg.)	a_o;5.057	5.19	8.75	7.086	2.096	7.492	5.061	8.176	3.643	3.591	3.872	5.3459
	b_o;									11.95		
	c_o;		5.06	4.008					6.139	3.372	3.812	3.5374
	α;58.06	65.3										
Formula Weights/Cell	12	15	50	4	1	4	4Ln	8	2	4	1	2
Interatomic Distance, (Å)												
M-B;				2.78 2.72	3.02	2.792				2.57 2.75	(2.70)	2.70
M-C;							2.53	2.51	2.47	2.35 2.40	(2.70)	2.70
M-M;				3.64 4.01	4.096	3.818	3.578	3.34	3.64	3.58 3.74		3.537 3.780
B-C;		1.64								1.64	(1.95)	1.58
B-B;	1.74-1.80	1.74	(1.68) (1.81)	1.73 1.78 1.77	1.704	1.766				1.92	(1.95)	2.23
C-C;		1.39					1.53	1.226	1.28			2.23

group, there are two classes of possible reflections, h + k = 2n for general hkl and k = 2n for 0kl.

Further, new unit cell parameters must replace those assigned in Tables 1, 4. 2 and 4. 3, and in Figure 4. 1 and 5. 8. These corrected parameters are contained in Table 5.10. The c-axis has the same length as that in Tables 1 and 4. 2; but the a-axis of the correct unit cell is $(2)^{1/2}$ times the a_o parameter of the primitive unit cell of Tables 1 and 4. 2.

Final confirmation of the LnB_2C_2 structure is shown by a comparison of the observed and calculated structure factors listed in Table 5.11. Columns one and two contain hkl values for the original tetragonal cell and the correct larger cell, respectively. Column three lists the observed, scaled structure factors from Table 5. 5 taken at room temperature. The structure factors at absolute zero, calculated with the position parameters described above for space group no. 127, are listed in column four. Column five contains the observed structure factors corrected to absolute zero with the same temperature factor used to correct $^{o}f_{Ho}$ in Table 5. 5. A corrected scale factor, K' = 1.98, was chosen, which minimized R of equation 5. 8 on application to $^{o}F(hkl)_{obs.}$. These rescaled, observed structure factors are listed in column six. The agreement between observed and calculated structure factors is indicated in column seven.

The residual, R, calculated from equation 5. 8, was found to be 0.13, which is considerably less than 0.4, the maximum for which the structure can be considered solved (cf. Chapter 5. 3). Hence, the

structure is fairly well defined. In view of the uncertainties in the measured intensities, the poor data on $^{o}f_{Ho}+3$, the small contributions of the light atoms to the structure factors (< 15%), the few terms in the Fourier series and the variance in the difference between observed and calculated structure factors, refinement to define the light atom position parameters more precisely is not worth doing. The exact positions of the light atoms must await neutron diffraction on a B-11 preparation of this phase or X-ray diffraction studies with a lighter metal in the phase, such as with ScB_2C_2.

The GdB_6-C equilibrium and the CeB_6-C equilibrium (cf. Chapter 3) lead one to infer that all LnB_6 phases exist in equilibrium with graphite. The inability to prepare LaB_2C_2 or SmB_2C_2 by reaction of LaB_6 or SmB_6 with graphite supports this argument. It is almost certain that the LnB_2C_2 phase can be made for all the lanthanides and certain other metals as well.

TABLE 5. 9

Corrected Tetragonal Unit Cell Indexing of LnB_2C_2

hkl Small Cell	hkl Correct Cell	hkl Small Cell	hkl Correct Cell	hkl Small Cell	hkl Correct Cell
100,010	110	122,212	312,132	232,322	512,152
001	001	130,310	420,240	223	403,043
110	200,020	031,301	331	141,411	531,351
101,011	111	031,103	113	014,104	114
111	201,021	131,311	421,241	033,303	333
200,020	220	113	203,023	331	601,061
002	002	222	402,042	114	204,024
120,210	310,130	230,032	510,150	133,313	423,243
201,021	221	032,302	332	042,402	442
102,012	112	231,321	511,155	241,421	621,261
121,211	311,131	123,203	223	142,412	532,352
112	202,022	132,312	422,242	024,204	224
220	400,040	123,213	313,133	332	602,062
202,022	222	040,400	440	124,214	314,134
030,300	330	140,410	530,350	323,233	513,153
221	401,041				

TABLE 5.10

Corrected Unit Cell Lattice Parameters for LnB_2C_2

Ln	a_o(Å)	c_o(Å)
La	5.40	3.96
Pr	5.39	3.81
Nd	5.378 ± 0.011	3.794 ± 0.009
Gd	5.3625 ± 0.0010	3.6399 ± 0.0003
Tb	5.3514 ± 0.0023	3.5912 ± 0.0003
Dy	5.3483 ± 0.0027	3.5599 ± 0.0010
Ho	5.3459 ± 0.0004	3.5374 ± 0.0001
Er	5.3425 ± 0.0008	3.5077 ± 0.0003
Yb	5.3389 ± 0.0020	3.5598 ± 0.0006
Y	5.35	3.55

TABLE 5.11

HoB_2C_2 Calculated and Observed Structure Factors. K' = 1.98.

hkl	h'k'l'	$^{T}F(hkl)_{obs}$	$^{O}F(hkl)_{cal}$	$^{O}F(hkl)_{obs}$	$K'^{O}F(hkl)_{obs}$	$^{O}F_{cal}-{}^{O}F_{obs}K'$
100	110	151.0	107.8	161.3	--	--
001	001	136.0	86.7	146.6	--	--
110	200	42.0	103.4	47.9	94.8	8.6
101	111	57.6	119.1	66.1	130.9	-11.8
111	201	46.0	110.5	56.1	111.1	-.6
200	220	31.3	101.3	40.2	79.6	21.7
002	002	51.8	115.9	68.5	135.7	-19.8
210	310	35.4	105.4	47.9	94.8	10.6
201	221	30.4	93.1	41.5	82.1	11.0
102	112	32.5	86.9	45.3	89.7	-2.8
211	311	25.9	81.6	37.1	73.4	8.2
112	202	28.7	85.0	41.9	82.9	2.2
220	400	26.0	75.9	40.3	79.8	-3.9
202	222	28.3	84.9	44.8	88.8	-3.9
030	330	20.0	69.6	32.1	63.6	6.0
221	401	36.9	94.5	59.6	118.1	-23.6
122	312	29.9	89.4	49.0	96.9	-7.5
130	420	26.7	83.7	44.3	87.8	-4.1
031	331	29.1	92.6	48.6	96.1	-3.6
131	421	22.9	74.7	39.2	77.6	-2.9
103	113	32.0	82.7	55.0	108.8	-26.1
113	203	25.3	79.7	44.3	87.8	-8.1
222	402	15.3	44.0	26.9	53.3	10.7
230	510	21.2	75.0	37.6	74.4	.6
032	332	13.7	62.1	24.4	48.4	13.7
231	511	15.5	72.0	27.7	54.8	17.2
023	223	22.0	71.2	39.3	77.9	-6.7
132	422	20.0	74.9	35.8	70.9	4.1
123	313	19.5	63.9	34.9	69.0	-5.1
040	440	17.8	79.1	31.7	62.8	16.3
232	512	23.1	69.0	40.0	79.2	-10.2
141	531	25.5	68.6	43.4	85.9	-17.3
223	403	8.8	57.5	14.9	29.5	27.9

TABLE 5.11, continued

hkl	h'k'l'	$^{T}F(hkl)_{obs}$	$^{O}F(hkl)_{cal}$	$^{O}F(hkl)_{obs}$	$K'^{O}F(hkl)_{obs}$	$^{O}F_{cal}-^{O}F_{obs}K'$
014	114	13.2	62.4	21.4	42.4	20.0
133	423	24.5	62.8	37.5	74.2	-11.3
042	442	31.8	73.7	47.6	94.2	-20.5

$$\Sigma \left| {}^{O}F_{cal} - {}^{O}F_{obs}K' \right| = 368.7$$

$$\Sigma \left| {}^{O}F_{obs}K' \right| = 2798$$

$$R = \frac{\Sigma \left| \left| {}^{O}F_{cal} \right| - \left| {}^{O}F_{obs}K' \right| \right|}{\Sigma \left| {}^{O}F_{obs}K' \right|} = 0.132 \text{ (cf. equation 5. 8)}$$

$$^{O}F(hkl)_{obs} = e^{\frac{f(\sin^2\theta/\lambda^2)}{2}} \, {}^{T}F(hkl)_{obs}$$

CHAPTER 6

CHEMICAL BINDING IN LnB_2C_2

The bonding possibilities in LnB_2C_2 are extremely exciting. Trigonal sp^2 and tetrahedral sp^3 covalent bonding in boron and carbon allotropes, in B_4C, between boron atoms in metal borides and between carbon atoms in metal carbides are well known.

Consider the bonding between the boron and carbon atoms in Figure 6. Each unit cell contains an eight-membered ring of alternate boron and carbon atoms. Trigonal sp^2 hybrid bonds for the boron and carbon atoms, resulting in an interlocking net of σ-bonds, would account for 24 of the 28 valence electrons contributed by the four boron and four carbon atoms in each cell. The remaining four electrons could form two π-bonds in the eight-membered ring.

However, this arrangement is insufficient to satisfy the Octet Rule for two of the carbon atoms in the ring. Further, such a non-conjugated eight-membered ring would not be planar because of bond-angle strain. Yet, from Chapter 5. 9, the light atoms were demonstrated to lie in parallel planes.

In order to overcome the bond-angle strain, to insure a planar eight-membered ring network, and to satisfy the Octet Rule for all atoms in the net, additional electrons are needed to conjugate the ring and

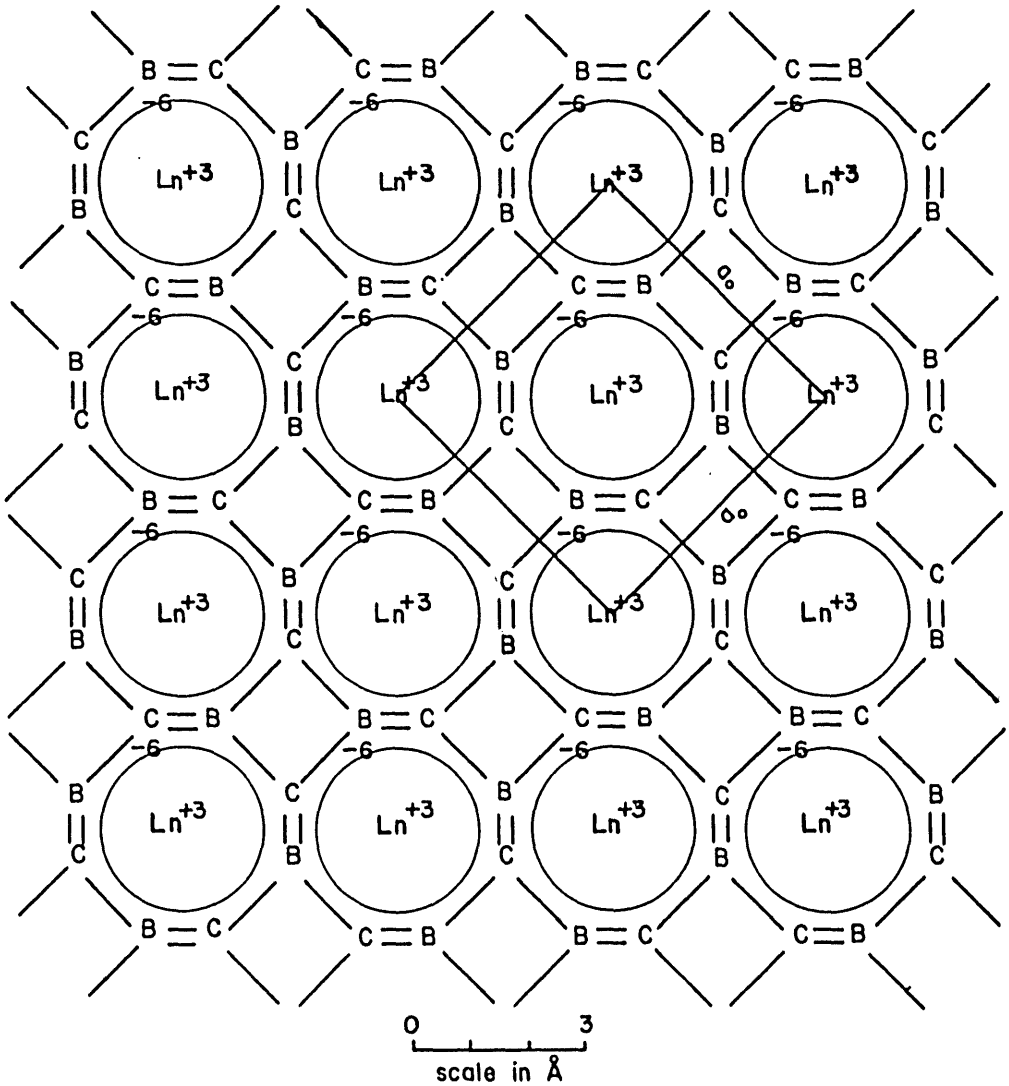

SCHEMATIC OF LnB_2C_2 BONDING

FIGURE 6

provide resonance stabilization. More specifically, the rings must be aromatic and, therefore, obey the Huckel Rule (47) demanding (4n + 2) π-electrons, where n is an integer. The system is not aromatic with only four π- electrons. Hence, the metal atoms must contribute their valence electrons to the light atom rings. This demand on the metal accounts for the necessity of metal in the structure.

If n = 1, six π-electrons would satisfy the aromaticity rule. However, the addition of only two more π-electrons to the ring is not sufficient to satisfy the Octet Rule for all members of the ring. Further, very little resonance stabilization is added.

A more obvious choice of n = 2 or ten π-electrons in each eight-membered ring can be satisfied. If both lanthanide atoms in the unit cell contribute three valence electrons each, or a total of six electrons, to each eight-membered ring, a total of ten π-electrons will be available to aromatize the light atom sheet. Since the lanthanides are normally trivalent, the demand of three electrons from each metal is reasonable. Further, the inability to prepare MB_2C_2 for divalent alkaline earth metals (cf. Chapter 1. 2) can be explained by the inability of the light atom sheets to gain aromatic character and, hence, sufficient resonance stabilization to overcome angle strain.

Consider the interatomic distances and bond angles in the light atom sheets. The carbon-carbon distances in ethane, ethylene, acetylene, benzene and ferrocene are 1.54, 1.34, 1.20, 1.39 and 1.4Å, respectively. The boron-carbon separation was set at 1.58Å in the eight-membered ring, the boron-carbon distance between rings in the same sheet is also 1.58Å. In view of the aromatic character and high resonance stabilization of

the bonding of Figure 6, the interatomic separations in the large ring are expected to be less than the 1.64Å separation in sp^3 tetrahedrally-bound boron and carbon in B_4C. However, the Coulombic repulsion of six negative charges per eight-membered ring would compromise the expected decrease in eight-membered ring size somewhat, accounting for the failure to decrease the boron-carbon ring to the same extent that the carbon-carbon distance contracts in benzene compared to ethane. Generally, the boron-carbon distances expected are in quite satisfactory agreement with separations in related aromatic organic systems.

The sp^2 trigonal bond angle in C_2H_4 and BX_3 is 120°. The bond angles in the LnB_2C_2 eight-membered rings are 135°, and the angles in the four-membered rings are 90°. Cyclooctatetraene, although conjugated, is not aromatic and not planar. The resonance stabilization provided by the conjugated system is insufficient to allow the bond angles to deviate from 120° to 135° without puckering the eight-membered ring. Apparently, the added two π-electrons in LnB_2C_2 rings provide sufficient resonance stabilization to overcome the angle strain problem.

The absence of bonds between light atoms in different light atom sheets is supported by the large separation of 3.6Å and the metal-like variation of c_o with lanthanide (cf. Chapter 5.9). Consequently, as for graphite, the electrical conductivity of LnB_2C_2 in the c_o dimension should be quite low if all lanthanide valence electrons are involved in σ- and π-bonds between light atoms. Further, one would expect very large ring currents in the a_ob_o-plane, which should be manifested by a very high electrical conductivity in this dimension.

The concept of metal atoms donating valence electrons to satisfy the orbital requirements of boron-boron covalent bonds is

fairly well established in metal borides of high boron content. Electrical conductivity and Hall coefficient measurements on borides reported by Johnson and Daane (25), particularly hexaborides of the lanthanide and alkaline earth metals, indicate that the lanthanide borides are metallic in nature while the alkaline earth hexaborides are semiconductors. This conductance behavior would be expected if only two metal valence electrons were needed to satisfy bonding requirements between boron atoms. Theoreticians, using molecular orbital and atomic orbital treatments, have demonstrated that tetra-, hexa- and dodecaborides all require two electrons per metal atom to satisfy the full complement of electrons needed in the covalently-bound boron structure. The realization that LnB_2C_2 is no exception is convincing evidence for the bonding and structure proposed.

The analogy between LnB_2C_2 and the ferrocene-type compounds in the field of organic chemistry is striking. These sandwich compounds gain aromaticity by donation of metal valence electrons into π-orbitals of the multi-membered carbon rings. These π-electrons, then, are in orbitals which overlap with the vacant d-orbitals of the electrophilic metal ion. The extremely significant difference between ferrocene-type compounds and LnB_2C_2, however, lies in the infinite sheets of electrophilic metals coupled to continuous boron-carbon aromatic sheets in LnB_2C_2 as opposed to the existence of isolated single molecules in sandwich compounds. This distinction, of course, accounts for the thermal degradation of ferrocenes at relatively low temperature while LnB_2C_2 cannot be melted up to $2500^{o}K$.

Ferrocene-type compounds exist for metals in the center of the Periodic Table, particularly those metals in Group VIII. Apparently, sandwich compounds have not been observed for the Group IIIB metals or the lanthanides. It is interesting to speculate that the LnB_2C_2-type phase will be found for the metals of Group VIII. It is further interesting to ask why the metals in Group IVB, which are capable of trivalency, do not exhibit the LnB_2C_2 phase (cf. Chapter 1. 1). Perhaps the five d-orbitals of the transition metals do not possess the radial distribution necessary to overlap with the π-orbitals of the eight-membered rings, whereas the seven 4f-orbitals of the lanthanides and the five 5d-orbitals provide a better possibility of orbital overlap. Recall from above that the lanthanide-boron and lanthanide-carbon distances are significantly shorter in LnB_2C_2 than in lanthanide borides and lanthanide carbides. This closer approach allows for close orbital overlap. However, the existence of YB_2C_2 in which 4f-orbitals are unimportant casts doubt on the above speculation. Perhaps the inability to prepare transition metal analogs of LnB_2C_2 is merely a matter of difficulty in removing the third metal valence electron compared to Group IIIB metals and a matter of ionic size.

The existence of the eight- and four-membered, conjugated, aromatic rings in continuous sheets involving a trivalent electrophilic metal, the refractory nature of this phase, the unusual electrical properties expected, and the possibility of analogous phases existing for other metals all are considerations generating a very significant problem in the elucidation of the theory of chemical bonding. The subtle variations between fourteen lanthanide metals and lanthanum afford a wonderful opportunity to determine second-order effects on the bonding in this phase.

CHAPTER 7

LANTHANIDE ORTHOBORATES

7. 1 Experimental

Powdered samples containing mostly LnB_2C_2 were sintered in evacuated quartz tubes at 1050°C. for two weeks in a Hereaus rhodium-wound resistance furnace. It was the purpose of this sintering to grow single crystals of the LnB_2C_2 phase for X-ray crystallographic studies. Debye-Scherrer X-ray powder photographs, using Cu-K_α (1.54180Å) radiation, taken of the powdered residues for the gadolinium, terbium and ytterbium samples indicated that the LnB_2C_2 phase had oxidized to $LnBO_3$.

7. 2 Background

Felten (48) has studied the $LnBO_3$-type borates and assigned the structure of the orthoborates of yttrium and the smaller of the lanthanide trivalent ions (samarium through lutetium) to be isostructural with vaterite (μ -$CaCO_3$). Felten pointed out the close similarity between the X-ray powder patterns of $LnBO_3$ phases and the transition metal diborides. Both have hexagonal symmetry. The patterns are identical except for the presence of a weak 101 line in the borate pattern. Therefore, the c-axis of the borate is twice that of the transition

metal diborides. The metal atom separation is the same in the diboride structure as in $LnBO_3$. Felten further pointed out that the hexagonal YB_2 phase reported by Binder (23) with a reported AB_2 structure could have been YBO_3 if the 101 line was not observed in the diffraction record. Since YB_2 was observed as a minor phase in an yttrium-boron agglomerate, the 101 line could have been overlooked. Since borate formation persists on fabrication of lanthanide borides (24), interpretation of $LnBO_3$ as LnB_2 is quite possible. The 101 reflection was observed in the thirty-two line powder pattern of all the oxidized LnB_2C_2 samples in this work.

Felten determined the lattice parameters for $LnBO_3$ compounds from two lines of the diffraction record. His graph of lattice parameters versus atomic number showed a linear lanthanide contraction even for the $YbBO_3$ phase.

7. 3 Lattice Parameters and Discussion

The precise lattice parameters for gadolinium, terbium and ytterbium orthoborates were computed by a least squares technique developed by Hess (29) for use with X-ray powder diffraction data. An IBM 653 computer was employed. The lattice parameters and their errors calculated from this work are compared with those of Felten in Table 7.

The a_o parameter for $GdBO_3$ agrees with Felten's value quite well. However, the c_o parameter of this work for $GdBO_3$ is 0.05 Å smaller than that of Felten. This disagreement is inexplicable. As a matter of fact, the lattice parameters of GdB_4, GdB_6 and Gd_2O_3 are found to be slightly larger than would be expected from a linear slope in the variation of

TABLE 7

Lattice Parameters of $LnBO_3$.

	Felten		This Work			
Orthoborate	a_o	c_o	a_o	delta a_o	c_o	delta c_o
Y	3.77_8	8.81_4				
Sm	3.86_2	8.97_8				
Eu	3.84_2	8.93_7				
Gd	3.83_9	8.90_6	3.8400	.0113	8.8532	.0084
Tb			3.8128	.0022	8.8824	.0018
Dy	3.79_3	8.84_7				
Ho	3.78_4	8.83_6				
Er	3.76_7	8.80_7				
Tm	3.75_3	8.78_9				
Yb	3.73_5	8.74_7	3.7447	.0007	8.7470	.0004
Lu	3.72_7	8.72_2				

parameters with atomic number (30). Both experimental a_o values for $GdBO_3$ in Table 7 confirm this trend; however, both c_o values are below the linear slope instead of above.

The a_o and c_o parameters of $TbBO_3$, for which Felten had no information, fall very well on the linear slope lattice parameter variation. The parameter, c_o, for $TbBO_3$ is less than Felten's c_o for $GdBO_3$ as expected, but greater than the c_o value for $GdBO_3$ from this work. This observation coupled with the large discrepancy between the c_o values for $GdBO_3$ casts considerable doubt on the accuracy of the c_o of $GdBO_3$ from this work. The parameters computed from this work for $YbBO_3$ agree quite well with those reported by Felten.

7. 4 Lattice Parameter-Valence Relationship

It is interesting to note that the samarium, europium and ytterbium parameters also fall on a linear lattice parameter variation slope. This behavior is greatly in contrast to the behavior of lanthanide metal and of LnB_6, but in better agreement with the LnB_4, LnC_2 and LnB_2C_2 behavior, and in perfect harmony with the lattice parameter behavior of Ln_2O_3 (30). A plot of the lattice constant for the cubic C-type of the lanthanide sesquioxide is linear through europium, samarium and ytterbium. The trivalency of the lanthanide ions in each of these sesquioxides except for cerium has been confirmed by magnetic studies (30).

A comparison of the tetragonal LnC_2 lattice parameter variation with the variation for $LnBO_3$ reveals some differences. The average valence of ytterbium in YbC_2 has been found from magnetic studies to be

less than three and, accordingly, the a_o and c_o lattice parameters are larger than that predicted from a linear slope extrapolation through Yb (30). The fact that samarium in SmC_2 has a measured valence less than +3 even though its lattice parameters fall on the linear slope is an anomaly which needs investigation.

In the case of LnB_4(30), SmB_4 has no lattice parameter deviation from a linear slope. But both a_o and c_o for ErB_4 are larger than the values expected from a linear slope; and, further, a_o for YbB_4 is quite a bit larger than the linear slope value. If this deviation at erbium and ytterbium is explained by an ytterbium valency below +3, then samarium ought to show a lattice parameter deviation also. Gschneidner pointed out that a plot of unit cell volume versus atomic number for ErB_4, YbB_4 and LuB_4 defines a straight line, which implies that the valency of ytterbium is still +3. No magnetic data are available. Tetragonal LnB_2C_2 lattice parameters show a nearly linear lattice parameter variation for a_o through ytterbium; but c_o increases at ytterbium, indicative of the alkaline earth character of the ytterbium ion.

The differences in the lattice parameter variation for LnB_6 and lanthanide metal (30) compared with $LnBO_3$ are quite large. The lattice parameter variation for cubic LnB_6 is not linear. Large positive deviations occur for europium and ytterbium hexaboride. Less positive deviations are observed for samarium, erbium and lutetium hexaborides. Magnetic susceptibility measurements confirm that the valency of samarium is less than trivalent in SmB_6. All such deviations are attributed to divalent character. There are many modifications for the lanthanide metals (30). If a lattice parameter plot of the cubic parameter for the

A2-W modification of these metals is constructed, europium and ytterbium deviate from a linear slope with extremely large differences. These deviations, confirmed by magnetic susceptibility measurements, are interpreted as an exhibition of divalent character.

As the strong ionic character of O^{-2} and BO_3^{-3} ions is replaced by the covalent or metallic character of the non-metal entities in lanthanide compounds, and if the lanthanide ions are not separated by too large distances or insulated from each other by non-metal cages, the rigid demands on the valence electrons are relaxed and the lanthanides show valence behavior similar to the metals alone. Thus, it would seem that as one compares phases in which a rigid requirement of trivalency in all the lanthanides is maintained to those in which the lanthanides take on a radius more typical of their value in pure lanthanide metals, the bonding characteristics change from ionic to metallic.

CHAPTER 8

SUMMARY AND CONCLUSIONS

A rough survey of the Gd-B-C system with emphasis on the boron- and carbon-rich regions of the ternary diagram and on the phase relations in the system was performed, using arc melting and X-ray diffraction techniques. Five ternary phases were revealed. No relation was found among these phases and those of the Th-B-C or U-B-C systems. Four of these phases, called $Gd_{0.35}B_{0.19}C_{0.46}$, $Gd_7B_9C_4$, $Gd_8B_7C_5$ and $Gd_3B_4C_3$, are characterized only by their X-ray powder patterns. The stoichiometry estimate could be in error by as much as ten atomic percent in each element.

The fifth phase, LnB_2C_2, was characterized by chemical analysis of gadolinium and boron, phase relationships, multiple preparations, density, lattice parameters and crystal structure. This phase was made by reaction of LnB_4 with graphite for neodymium, gadolinium, terbium, dysprosium, holmium, erbium and ytterbium metals. Lanthanum and samarium did not form this phase on reaction of the hexaborides with graphite. Some evidence for carbon solid solution in LnB_2C_2 is shown.

With Weissenberg single crystal techniques and diffractometer intensity measurements, the structure of LnB_2C_2 was determined. The symmetry is tetragonal with space group, P4/mbm, No. 127. The two metal atoms are at 2(a). The four boron atoms are positioned at 4(h) with

$x_B = 0.352$. The four carbon atoms are also located in the 4(h) positions with $x_c = 0.148$. The assignment of the light atom positions was based to some extent on the expected interatomic distances in related compounds.

This structure can be described as composed of parallel sheets of eight-membered and four-membered rings of alternate boron and carbon atoms that are interspersed with parallel planes of metals centered between the holes in the eight-membered rings of the light atom sheets. Further confirmation of the structure was derived from lattice parameter variation, similarity to boride structures, bond distances, electronic requirements and general bonding considerations. The probability of σ - and π-bonds between boron and carbon atoms with conjugated, aromatic, planar, four- and eight-membered light atom rings extending throughout the structure in two dimensions was discussed.

Precise lattice parameters of $GdBO_3$ and $YbBO_3$ were determined and compared with previous work. The lattice parameters of $TbBO_3$ were also reported. A discussion of the bonding as indicated by variation in lattice parameters for various lanthanide compounds leads to a conclusion of ionic bonding in $LnBO_3$ compounds.

CHAPTER 9

SUGGESTIONS FOR FUTURE RESEARCH

By far the most significant future research that arises from this study is the further investigation of LnB_2C_2. Eight- and four-membered boron and carbon conjugated ring structures and the possibility of ferrocene- or bridge-bonds are extremely exciting.

The concept of sheets of aromatic boron and carbon atom rings similar to graphite, except needing trivalent metal ions for aromaticity, is a new concept in bonding in solids that establishes a bridge between the electron interpretation tools of organic chemistry and the study of bonding in solid refractory materials.

Simple experiments can be performed to note whether two or more electrons per metal are needed in bonding. For instance, alkaline earth borocarbides might exist. In particular, CaB_2C_2, where the radius of divalent calcium ion is compared to trivalent lanthanide ions, may exist. Possibly the MB_2C_4 alkaline earth phase, reported by Russian investigators, is really MB_2C_2. Electrical conductivity and Hall coefficient measurements will provide insight into how many electrons are involved in localized bonding and how many in conduction. Electrical conductivity measurements on single crystals of LnB_2C_2 will confirm or deny the anisotropic conductivity predicted. A test for metal solid solution will determine the extent metals are involved in bonding in LnB_2C_2. It would be useful to

determine the extent of alkali metal substitution for lanthanide and to follow changes in electrical properties or c_o parameter with alkali metal content. Quantum mechanical treatments of the bonding, such as were done in metal borides, ought to contribute understanding of the bond types. More detailed studies of properties which vary with metal or temperature should be investigated. A single crystal structural study of ScB_2C_2 will more clearly fix the boron and carbon position parameters and define any deviation from planar light atom sheets.

As more information on composition, symmetry and structure becomes available on other M-B-C compounds, perhaps other aromatic light atom ring systems will be identified. In fact, the criterion of aromaticity in continuous light atom sheets in metal deficient borocarbides may allow the prediction of other metal borocarbides.

Obviously a more detailed survey of the ternary lanthanide-boron-carbon system in the region on the lanthanide side of the LnB_4-LnB_2C_2-C joins should be performed with arc melter techniques. The primary purpose here would be to fix the composition and phase relations of the four ternary compounds in this field. Characterization of these phases by chemical analysis, density, and crystal structure will make it possible to compare the lanthanide borocarbides with the actinide borocarbides. Attempts to prepare these ternary compounds for other lanthanides will reveal the influence of the size of the metal ion on the phase stability. Variation of lattice parameters of these ternary phases with atomic number and magnetic susceptibility studies will possibly reveal the kind of bonding in these phases.

Once the general characteristics of these phases have been surveyed, a more detailed study of the temperature-composition phase diagrams for two or three of these ternary systems, whose behavior is widely divergent, might be ascertained in detail with such a tool as high-temperature X-ray diffraction. This investigation would fix melting points, eutectics, transition temperatures, disproportionation behavior and other thermal effects which determine the refractory quality of these solids. These characteristics should contribute further to an understanding of the size effect on phase stability.

As of yet, no research has revealed a gaseous metal-boron-carbon molecule. Of all of the factors which determine the stability of a solid phase the presence of a stable gaseous molecule is the greatest. Only recently have investigators been able to find stable solid borocarbides. The possibility of a ternary Ln-B-C molecule over one of these ternary phases is very interesting. A mass spectrometric study of LaB_2C_2, perhaps the most stable of the LnB_2C_2 compounds, in graphite crucibles could quickly be done. Thermal properties of any species found in the gas phase could be determined. In the binary metal-boron systems there are no metal-boron gaseous molecules, but $GdC_2(g)$ and $LaC_2(g)$ are reported by Jackson, Barton, Krikorian and Newbury in the metal-carbon system (49). Over boron carbide solid the molecules BC_2, B_2C and BC were found by Drowart in a mass spectrometer up to ten percent in intensity compared to atomic boron gas (50).

Another interesting ternary molecule possibility is the $LnBO_2$ gaseous molecule over $LnBO_3$ solid. The alkali metal borates were studied in a mass spectrometer by Büchler and Berkowitz-Mattuck (51). They found

ABO_2 and $(ABO_2)_2$ molecules. Should such lanthanide borate molecules be found, a behavior such as White, Walsh, Ames and Goldstein found in the vaporization of lanthanide sesquioxides (52, 53) might be looked for. White found that the importance of LnO molecule decreased with respect to formation of the gaseous elements as atomic number increased across the lanthanides.

The general pressure-composition phase diagrams for the ternary lanthanide-boron-carbon systems could be predicted from the behavior of the binary systems currently being investigated. Because of the extreme volatility of lanthanide metals compared to boron or carbon, and since LnC_2(s) loses Ln(g) preferentially (49) on heating, and since LnB_4(s) is either congruently vaporizing or loses Ln(g) preferentially (cf. Part II), and if there are no exceptionally stable ternary molecules, all lanthanide ternary borocarbides probably will lose metal preferentially on vaporization. From measured pressures of metal gas over these ternary systems, thermodynamic data on the stability of the solid may be computed. For instance, the temperature coefficient of the gadolinium partial pressure over GdB_2C_2 (s) could be measured on vaporization of gadolinium from GdB_2C_2 in a graphite crucible. From this measured heat of vaporization of GdB_2C_2 to graphite a value for the stability of GdB_2C_2 can be determined.

In all of these suggestions concerning lanthanide chemical behavior, the one characteristic which makes the lanthanides extremely interesting is the similarity of chemical behavior for fifteen different metals. In no other group or period in the Periodic Table is there provided such an opportunity to simplify the number of variables which effect the chemical behavior of so many elements. Small changes in the

electron population of the 4f orbitals accompanied by small radius changes for these metals are manifested by slightly different metal activities in these compounds, and yet the gross chemical characteristics such as structure, composition and general bond types are preserved. Chemists, ceramists, physicists and metallurgists could contribute a considerable understanding to the theory of the solid state from a detailed investigation of the subtle variations of behavior among similar lanthanide compounds.

PART II

VAPORIZATION AND STABILITIES OF LANTHANIDE BORIDES

CHAPTER 1

STATEMENT OF PROBLEM

1. 1 Purpose and Organization

Generally, this work intends to evaluate the factors influencing the stability of lanthanide borides with respect to gaseous and to solid elements. More specifically, it is the purpose of this work to relate the volatility of the lanthanide metals to the vaporization processes exhibited by the lanthanide borides. Since the lanthanide metals exhibit an extremely wide range of volatility, quite different vaporization behavior can be expected for corresponding compounds of the different lanthanide metals.

Typically, there are five major steps in the organization of a vaporization study. First, the solid phases in the system are characterized as to composition and structure and a crucible choice is made. The second stage is an investigation of the vaporization processes by noting phase and/or compositional changes in vaporization residues and analyzed sublimates. In order to establish the net process being investigated, the third stage is the identification of the gaseous species in the process and the confirmation of the stoichiometry of the process. In the fourth stage the actual pressures are measured as a function of temperature. Thermochemical data are calculated. Most vaporization studies stop at this point, as is the case with this study. But a fifth stage would be

a quantitative study of the kinetic factors which govern the vaporization process and establishment of its mechanism.

1. 2 Factors Influencing Vaporization Processes

The principal vaporization process exhibited by a particular boride is that process which develops the highest total pressure, i. e., the process which has the smallest standard free energy of vaporization for formation of one total mole of gas. Several factors influence the vaporization processes and the their pressures. The most important of these factors are the composition and stability of gaseous molecules in the system. The second factor is the stability of the solid compound with respect to the solid elements. The third factor is the stability of other condensed phases in the system. Component volatility is a fourth factor.

Fifth, the composition of the compound must be considered in properly balancing a chemical equation written to form one total mole of gaseous atoms. Consider borides of composition MB_x and MB_{x_o} with MB_{x_o} having some specific stability with respect to formation of one total mole of gaseous atoms. For a given MB_x stability with respect to formation of one total mole of gaseous atoms the proximity of x to x_o, which depends on the composition of the borides in the system, increases the influence of the stability of MB_x on the vaporization behavior of MB_{x_o}. Thus, not only are the relative stabilities of the condensed phases in the system important on fixing the vaporization behavior, but also their compositions.

A sixth factor would be the curvature in the free energy-composition diagram, particularly for a solid phase with wide solid solution. Finally, if one is using kinetic methods to measure equilibrium pressures,

the nature of the method used is important in defining the principal vaporization process.

Let us consider the extent that each of these factors influences the vaporization of lanthanide borides. It is shown in Chapter 5 that only atomic species are found in the vapor over lanthanide borides. Thus, no stable molecule is influencing the gas phase composition. It might be supposed that, to a first approximation, corresponding solid compounds might have about the same stability for all the lanthanides. Hence, under this supposition, variation of the heat of formation of corresponding borides is not important in establishing the relative vaporization processes for the lanthanide borides.

Generally, for vaporization processes written to form one total mole of gas, the principal contribution to the entropy change will be the entropy of the gas. It might be supposed that essentially all the entropy of the gaseous atoms is translational entropy; and, therefore, the entropy of the vaporization processes is independent of the composition of the gas and a constant for processes written to form one total mole of gas. In the light of this supposition, the process with the smallest enthalpy change, as well as free energy change, will predominate. The volatility of the component, boron, is a constant in these studies. Therefore, the volatility of the lanthanide metal will be extremely important in defining the principal vaporization processes.

In view of the supposition of constant heats of formation of corresponding borides and since the same compositions occur for all lanthanide borides, the composition factor is not important in an ordering of volatilities of corresponding lanthanide compounds all vaporizing by the same

process. However, the choice of the principal vaporization process for a particular lanthanide boride would depend on a knowledge of the presumed constant values for the heats of formation of the various borides in the processes. Thus, on intercomparison of different vaporization processes, the composition factor will be important.

Since the borides studied have essentially no detectable solid solution range, the shape of the free energy curve is relatively unimportant in defining the principal vaporization process. However, the technique employed to determine the gas pressures in these systems could be an important factor influencing the principal vaporization process exhibited by these borides. The problems arising from the kinetic measurements of the Knudsen and Langmuir pressure measurement techniques are discussed in Chapters 4 and 6.

In summary, the factors presumed to be most important in establishing the vaporization behavior of the lanthanide borides are: first, and most important, metal volatility; second, composition; and third, experimental methods.

1. 3 Vaporization Behavior Expected

The five possible vaporization modes that metal borides may exhibit are summarized in Table 1. 1. The composition factor is important here; however, in general, as metal volatility increases there is a change from loss of boron from all metal borides to loss of metal from all metal borides. Leitnaker (54) has shown that all tantalum borides lose boron preferentially. He has also demonstrated that ZrB loses boron to the gas phase on vaporization to form $ZrB_{1.96}(s)$, which vaporizes congruently to the

Table I. 1

Possible Modes Of Vaporization Of Metal Borides

Process	Example	$\Delta H^{o}_{298\,^{o}K}$ (vap.) (kcal/gr.-at.)
$MB_x \xrightarrow{-M(g)} MB_y \xrightarrow{-M(g)} B$	Mg	35.6
$MB_x \xrightarrow{-M(g)} MB_y \xrightarrow{-[M(g)+yB(g)]}$	Ln	40 to 97
$\xleftarrow{-[M(g)+xB(g)]} MB_x \qquad MB_y \xrightarrow{-[M(g)+yB(g)]}$	Unknown	
$\xleftarrow{-[M(g)+xB(g)]} MB_x \xleftarrow{-B(g)} MB_y$	Zr	146.0
$M \xleftarrow{-B(g)} MB_x \xleftarrow{-B(g)} MB_y$	Ta	186.8

Volatility Increasing

gaseous elements (131). An example of a metal-boron system, which loses metal from all borides, is the magnesium-boron system (cf. Chapter 15. 2. 3). The requirements that allow two single-phase solid compositions in the same system to develop a ratio of partial pressures of the components in the gas phase with the same values as their atomic ratios in the solids are extremely restrictive, and no binary refractory system has yet been found with such behavior. Perhaps, such a set of conditions might be found in the lanthanide-boron systems. The lanthanide tetra- or hexaborides generally develop the lowest pressures in the lanthanide-boron system. Some lanthanides, it will be shown, exhibit loss of metal gas from the tetraboride to form hexaboride, which then vaporizes congruently, and vice versa.

Table 1. 2 contains a summary of some physical and thermochemical data on the alkaline earth, group IIIB, lanthanide and actinide elements. Notice that the heats of sublimation for the lanthanides vary from 40.0 to 97.3 kcal./g.-at. at 298°K. With this large variation in the volatility of the metal and with other factors in the heat of vaporization of the boride fairly constant, as the atomic number of the lanthanide is varied, the vaporization processes expected for these borides could be quite different for different lanthanides. Figure 1. 1 is a plot of metal volatility versus atomic number. It could be postulated that a horizontal line could be drawn in this graph at some height above which the involatile lanthanides will show preferential loss of boron from lanthanide hexaborides, and below which the relatively volatile lanthanides will lose metal to the gas phase from lanthanide tetraborides. If suitable conditions prevail, a metal of intermediate volatility might show congruent vapori-

TABLE 1. 2

Physical and Thermochemical Data of Metals

M	m.p. (°C.)	I.P. (I) (ev.)	I.P. (II) (ev.)	I.P. (III) (ev.)	$r(M^{o})$ (Å)	$r(M^{+2})$ (Å)	$r(M^{+3})$ (Å)	$r(M^{+4})$ (Å)
B	2025k							
Be	1283k	9.32n	18.21n	154.n	1.110q	0.38n		
Mg	650k	7.64n	15.03n	80.1n	1.595q	0.66n		
Ca	850k	6.11n	11.87n	51.2n	1.97q	0.99n		
Sr	770k	5.69n	11.03n		2.148q	1.15n		
Ba	710k	5.21n	10.00n		2.171q	1.37n		
Sc	1539j	6.54r	12.80r	24.75r	1.645j		0.81n,0.68j	
Y	1509j	6.38r	12.23r	20.5r	1.7780j		0.96n,0.88j	
La	920j	5.61r	11.43r	19.17r	1.8852j		1.16n,1.04j	
Ce	795j	6.91r		20r	1.8248j	(1.2)n	1.14n,1.02j	1.01n,0.92j
Pr	935j	5.76r			1.8363j		1.12n,1.00j	0.99n,0.90j
Nd	1024j	6.31r			1.8290j		1.10n,0.99j	
Pm							1.08n,0.98j	
Sm	1072j	5.51r	11.4r		1.8105j	(1.16)n,1.11j	1.07n,0.97j	
Eu	826j	5.66r	11.22r		1.994j	(1.14)n,1.09j	1.05n,0.96j	
Gd	1312j	6.16r			1.810j		1.03n,0.94j	
Tb	1363a,1356a,j	6.74r			1.8005j		1.02n,0.92j	0.91n,0.84j
Dy	1407j	6.82r			1.7952j		1.00n,0.91j	
Ho	1461j				1.7887j		0.99n,0.89j	
Er	1497j				1.7794j		0.98n,0.87j	
Tm	1545j				1.7688j		0.96n,0.86j	
Yb	824j	6.24r	12.08r		1.9397j	(1.06)n,0.93j	0.95n,0.85j	
Lu	1661,1652j	6.15r	14r		1.7516j		0.93n,0.84j	
Th	1695k				1.795q		1.08pn	0.95p,0.99n
U	1133k				1.38q		1.04p,1.03n	0.89p,0.93n

TABLE 1. 2, continued

M	$\Delta H^{\circ}_{298^{\circ}K.}$ vap. (kcal./gfw.)	$S^{\circ}(s)_{298^{\circ}K.}$ (eu.)	$S^{\circ}(g)_{298^{\circ}K.}$ (eu.)	$S^{\circ}(l)_{2200^{\circ}K.}$ (eu.)	$S^{\circ}(g)_{2200^{\circ}K.}$ (eu.)	$\Delta S^{\circ}_{2200^{\circ}K.}$ vap. (eu.)	$\Delta H^{\circ}_{2200^{\circ}K.}$ vap. (kcal./gfw.)	$\Delta F^{\circ}_{2200^{\circ}K.}$ vap. (kcal./gfw.)
B	132.6s	1.392s	36.65s	12.40(s)	46.58s	34.18s	125.0s	45.05
Be	77.90k	2.28k	32.55k	16.29k	42.48k			
Mg	35.60k	7.81k	35.51k	45.43(g)k	45.43k			
Ca	42.20k	9.95k	36.99k	46.93(g)k	46.93k			
Sr	39.10k	12.50k	39.32k	49.27(g)k	49.27k			
Ba	41.74k	15.50k	40.67k	51.13(g)k	51.13k			
Sc	82.0k	(8.5)g	41.75k	24.79k	51.87k	27.09k	72.2k	12.6k
Y	102.0k	10.63g	42.87k	26.70k	53.90k	27.20k	94.7k	34.9k
La	97.3c	13.64g	43.56k	30.79k	57.20k	26.8k	95.9k	36.9k
Ce	96.4c	16.68g		35.03k	(57)	(22)	(91)	(42.6)
Pr	85.2d,85.1b 77.9a	17.49g		35.00k	(57)	(22)	(80)	(32)
Nd	75.0d,75.0b 76.3a	17.54g	45.24k	37.08k	58.00k	21.0k	70.0k	23.8k
Pm		(17.2)g		34.70k				
Sm	49.9d,49.9b	16.64g	43.72k	(34.02)k	57.96k	(24.0)	45.4k	(-7.4)
Eu	42.1e,43.1b	(17.0)g	45.10k	(34.39)k	55.06k	(20.6)	35.6k	(-8.8)
Gd	83.6a,81.2b	15.77g	46.42k	33.66k	58.79k	25.1k	75.3k	20.1k
Tb	86.9a,71.4d 87.2a,91.9b	17.48g		34.78k	(57)	(22.2)	(85)	(36.2)
Dy	61.6a,71.4b (67)a	17.87g		35.12k	(57)	(21.9)	(66)	(17.8)
Ho	69.5a,75.0b	18.00g		35.02k	(57)	(22.0)	(70)	(21.6)
Er	66.4a,75.4b	17.52g		34.89k	(57)	(22)	(70)	(21.4)
Tm	58.4a,57.5b 57.6d	17.37g		34.07k	(57)	(22.9)	(52)	(1.6)
Yb	40.0d,40.0b	(15.0)g	41.35k	(31.40)k	51.28k	(19.8)	36.0k	(-7.6)
Lu	94.7a,70.0a 102.8b	12.19g	44.14k	28.78k	55.71k	26.9	(95)	(35.8)

TABLE 1. 2, continued

M	$\Delta H^{\circ}_{298^{\circ}K.}$ vap. (kcal./gfw.)	$S^{\circ}(s)_{298^{\circ}K.}$ (eu.)	$S^{\circ}(g)_{298^{\circ}K.}$ (eu.)	$S^{\circ}(l)_{2200^{\circ}K.}$ (eu.)	$S^{\circ}(g)_{2200^{\circ}K.}$ (eu.)	$\Delta S^{\circ}_{2200^{\circ}K.}$ vap. (eu.)	$\Delta H^{\circ}_{2200^{\circ}K.}$ vap. (kcal./gfw.)	$\Delta F^{\circ}_{2200^{\circ}K.}$ vap. (kcal./gfw.)
Th	137i,137.7m	12.76k		33.25k				
U	115.2h,126h 117.2k,118h 114h,122h	12.03hk	48.1h,47.73k	33.69k	59.42k	25.73	106.0k	49.4

a = 55
b = 56
c = 57
d = 58
e = 59
f = 60
g = 61
h = 62
i = 63
j = 64
k = 65
m = 66
n = 67
p = 45
q = 68
s = 69
( ) = estimated

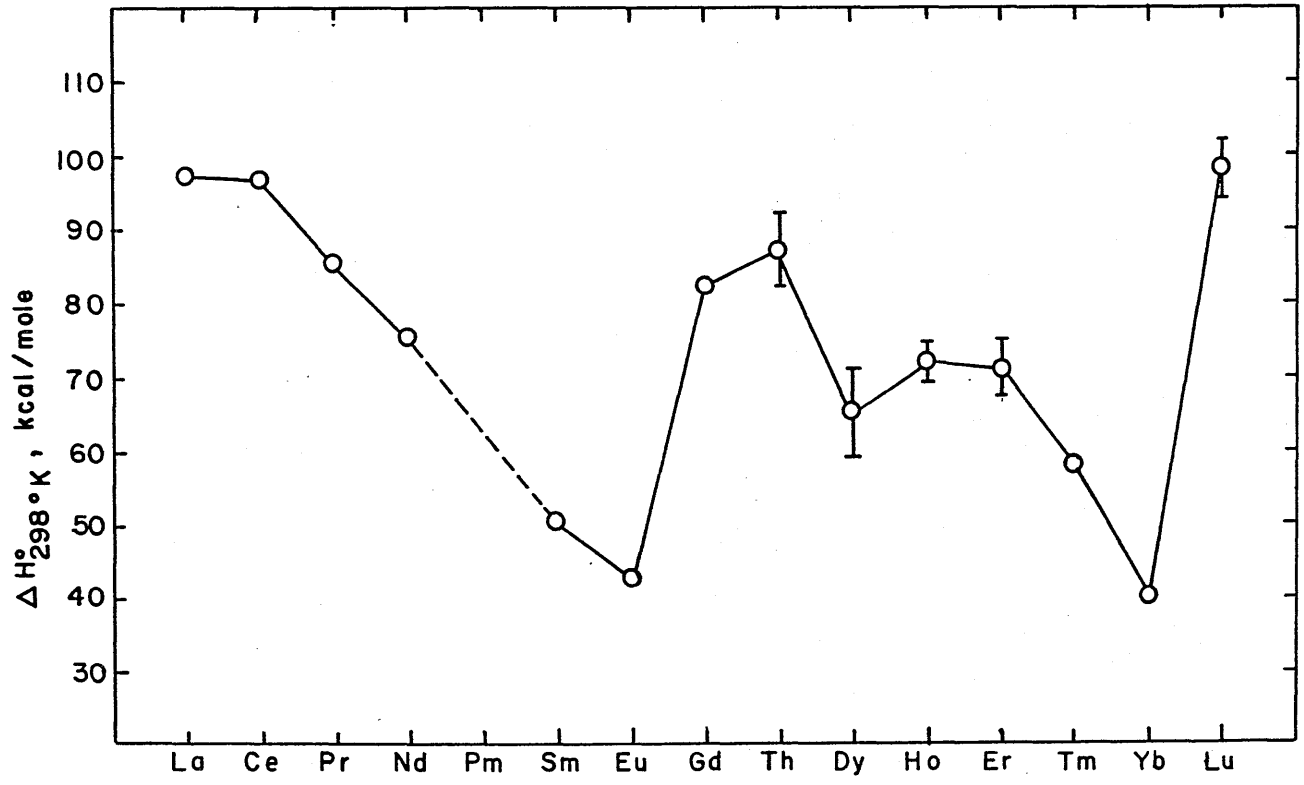

HEATS OF VAPORIZATION OF LANTHANIDE METALS AT 298° K

FIGURE I. I

zation of both tetra- and hexaboride. This investigation is concerned principally with tetra- and hexaborides since these exhibit the least volatility among the lanthanide borides. Figure 1. 2 contains pressure-composition diagrams schematically illustrating these behaviors in addition to loss of metal from all lanthanide borides and loss of boron from all lanthanide borides.

In the consideration of which of the possible vaporization processes is the principal process, it is important to find the process with the smallest heat of vaporization per mole of gas for a particular boride (70). Only in this way can the total pressures be compared with the equilibrium constants and the entropy change be considered nearly constant for all processes. The process developing the highest total pressure will be designated by the smallest heat of vaporization, assuming entropy changes identical for different processes forming one total mole of gas. The possible processes to be considered for LnB_4 and LnB_6 compounds are:

$$3\ LnB_4(s) = 2\ LnB_6(s) + Ln(g) \qquad (1.\ 1)$$

$$1/5\ LnB_4(s) = 1/5\ Ln(g) + 4/5\ B(g) \qquad (1.\ 2)$$

$$1/4\ LnB_4(s) = 1/4\ Ln(l) + B(g) \qquad (1.\ 3)$$

for the tetraboride, and:

$$2\ LnB_6(s) = LnB_{12}(s) + Ln(g) \qquad (1.\ 4)$$

$$1/7\ LnB_6(s) = 1/7\ Ln(g) + 6/7\ B(g) \qquad (1.\ 5)$$

$$1/2\ LnB_6(s) = 1/2\ LnB_4(s) + B(g) \qquad (1.\ 6)$$

for the hexaboride. Which two of these are most important for various lanthanides will be determined.

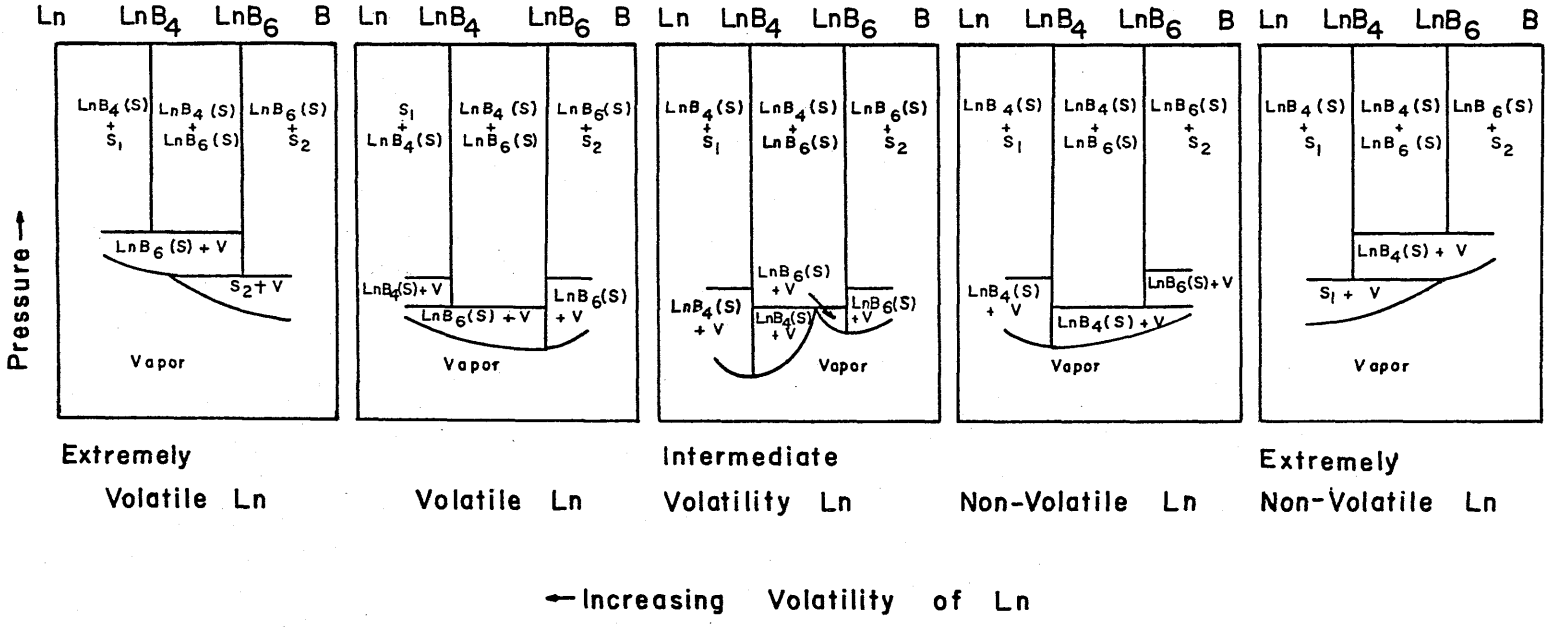

POSSIBLE PRESSURE COMPOSITION DIAGRAMS FOR LANTHANIDE BORIDES

FIGURE I. 2

CHAPTER 2

SOLID PHASES IN THE LANTHANIDE-BORON SYSTEM

2. 1 Previously Established Phases

The solid phases of the lanthanide-boron system that are reported in the literature are lanthanide metal, LnB_2, $LnB_{3<x<4}$, LnB_4, LnB_6, LnB_{12}, LnB_{50}, LnB_{70} and boron.

2. 1. 1 Ln

Table 1. 2 contains some physical and thermochemical information for the lanthanide metals. Gschneidner (30) summarizes the many solid state transformations and structures for these metals.

2. 1. 2 LnB_2

The compounds, GdB_2, TbB_2, DyB_2, HoB_2, ErB_2, ScB_2 and YB_2, have all been reported in the literature (46). These compounds were indexed with hexagonal symmetry and are of the C-32, AlB_2-type. The phase, GdB_2, is reported to disproportionate above 1300°C. to gadolinium metal and GdB_4 (71). A DyB_2 phase was found by the same investigators. Both these phases are questioned by Gschneidner (30) as possible borates (cf. Part I, Chapter 7). The compounds, GdB_2, TbB_2, DyB_2, HoB_2 and ErB_2, are reported by Post (46) with no preparative details. The phase, ScB_2, was identified by Russian investigators (72) from X-ray powder techniques. The inter-

pretation of YBO_3 as "YB_2" (23) has been discussed previously in Part I, Chapter 7. Binder (24), who reported the "YB_2" phase, admitted that this diboride phase is a "ternary boroxide." However, Johnson and Daane (73) prepared single crystals of YB_2 on which electrical properties were measured. The compounds, ScB_2 and YB_2, appear to be well established Group IIIB borides. Lattice parameters for the diborides are found in Table 2. 1. The lanthanide diborides reported must await further characterization to remove the possibility of their being borates of similar symmetry.

2. 1. 3 LnB_x

Existence of an LnB_x phase with x between three and four was erroneously reported by Post, et al. (22), and by Binder (23). As discussed in Part I, Chapter 4. 4, this phase is LnB_2C_2.

2. 1. 4 LnB_4

After discovery of the lanthanide hexaborides, the tetraborides of Ce, U and Th were discovered by Brewer, Sawyer, Templeton and Dauben (74). Zalkin and Templeton (75) in 1953 and Blum and Bertaut (39) in 1954 determined the structure of this boride. The symmetry is tetragonal with four formula units per cell and has a space group, $P4/mbm - D_{4h}^5$. Four metal ions are found in positions 4(g) at $\pm$ (u, u + $\frac{1}{2}$, 0; $\frac{1}{2}$ - u, u, 0) with u = 0.310. The sixteen boron atoms in the cell are in positions 4 (e) at $\pm$ (0,0,v;$\frac{1}{2}$,$\frac{1}{2}$,v) with v = 0.214, 4 (h) at $\pm$ (w,w+$\frac{1}{2}$, $\frac{1}{2}$; $\frac{1}{2}$-w,w,$\frac{1}{2}$) with w = -0.086, and 8 (j) at $\pm$(x,y,$\frac{1}{2}$;x + $\frac{1}{2}$,$\frac{1}{2}$-y,$\frac{1}{2}$; $\bar{y}$,x,$\frac{1}{2}$;y + $\frac{1}{2}$, x +$\frac{1}{2}$, $\frac{1}{2}$) with x = 0.174 and y = 0.042. This structure defines a three dimensional network of covalently-bound boron atoms. These borides are a metallic gray

TABLE 2. 1

Lattice Parameters, Densities and Melting Points of Lanthanide Borides (46).

Ln	LnB_2			LnB_4				LnB_6			LnB_{12}		LnB_{100} (70)
	a_o (Å)	c_o (Å)	$D_{calc.}$ (g./cm.^{3})	a_o (Å)	c_o (Å)	$D_{calc.}$ (g./cm.^{3})	m.p. (°C.)	a_o (Å)	$D_{calc.}$ (g./cm.^{3})	m.p. (°C.)	a_o (Å)	$D_{calc.}$ (g./cm.^{3})	a_o (Å)
La				7.30	4.17	5.44	1800±15[c]	4.143	4.72	2530			
Ce				7.205	4.090	5.72	> 2100[b]	4.141	4.79	2190			
Pr				7.20	4.11	5.71	> 2250[b]	4.130	4.85	> 2250[b]			
Nd				7.219	4.102	5.84		4.126	4.94	2540			
Pm													
Sm				7.174	4.070	6.12		4.133	5.06	2540[a]			
Eu								4.178	4.94				
Gd	3.31	3.94	7.96	7.144	4.048	6.44	> 2250[b]	4.108	5.31	> 2100			16.50[b]
Tb	3.28	3.86	8.34	7.118	4.029	6.60	> 2100[b]	4.102	5.39	> 2100[b]	7.505	4.540	(23.5)
Dy	3.285	3.835	8.53	7.101	4.017	6.74	> 1950[b]	4.098	5.48	> 1950[b]	7.501	4.600	
Ho	3.27	3.81	8.80	7.086	4.008	6.86		4.096	5.55		7.492	4.655	(23.5)
Er	3.28	3.79	8.89	7.071	3.997	6.99		(4.102)	(5.58)		7.484	4.706	
Tm				7.05	3.99	7.10		(4.110)	(5.57)		7.476	4.756	

TABLE 2. 1, continued

Ln	LnB_2			LnB_4				LnB_6			LnB_{12}		LnB_{100} (?)
	a_o (Å)	c_o (Å)	$D_{calc.}$ (g./cm.^{3})	a_o (Å)	c_o (Å)	$D_{calc.}$ (g./cm.^{3})	m.p. (°C.)	a_o (Å)	$D_{calc.}$ (g./cm.^{3})	m.p. (°C.)	a_o (Å)	$D_{calc.}$ (g./cm.^{3})	a_o (Å)
Yb				7.01	4.00	7.30		4.147	5.54		7.469	4.818	16.56[b] (23.5)
Lu				7.00	3.94	7.50		(4.111)	(5.73)		7.464	4.868	
Sc	3.146	3.517	3.67					(4.435)	(2.1)				
Y	3.298	3.843	5.54	7.111	4.017	4.33		4.113	3.67	2300	7.500	3.444	11.75 23.5

a, 30. b, This work. c, 25.

in color. Figure 5. 7, Part I, contains a projection of the LnB_4 structure onto the (XYO) plane.

Since the discovery of the tetraboride phase, many researchers have discovered other tetraborides with the same structure (72, 22, 23, 76, 77, 78, 79, 80). Of the lanthanides only EuB_4 and PmB_4 have not been prepared. Apparently, EuB_4 cannot be obtained because of its instability with respect to formation of europium gas and EuB_6 (76).

Many investigators have studied the influence of size of the metal ions on the lattice parameters of LnB_4 (75, 22, 78-9, 02, 81). The variation of lattice parameter with atomic number reveals a fairly uniform lanthanide contraction for both a_o and c_o parameters, even through Sm and Yb, and is indicative of the same metal ion valency in all the tetraborides. Magnetic susceptibility measurements (30) established the valency as + 3. This behavior is quite different from the hexaboride behavior (30, 02, 81). While the variation in reported lattice parameters is great for particular tetraborides, this variation was thought by Eick and Gilles (02) and Gschneidner (30) not to be evidence of wide solid solution ranges, but, rather, evidence for impurities. Binder (24) pointed out that small amounts of oxygen or carbon help to stabilize tetraborides. Eick and Gilles prepared many compositions in the two phase regions on either side of the tetraboride with no measureable variation in the parameters. This behavior implies a narrow range of homogeneity for the tetraboride. Felten, Binder, and Post (76) reported a considerable solid solution effect in LaB_4; however, the detailed work of Johnson and Daane (25) denied this conclusion. Table 2. 1 contains a summary of the parameters and densities of the lanthanide tetraborides.

2. 1. 5 LnB_6

The discovery of the hexaborides of Ca, Sr and Ba was first made by Moissan in 1897 (82). At the turn of the century other investigators prepared these borides (83-5). Interest was renewed in 1929 by Andrieux (86) and by Allard (87) in 1932 with the discovery of ThB_6. In 1934 the hexaboride structure was determined by von Stackelburg and Neumann and also by Laves (88-9). These hexaborides have cubic symmetry, have one formula unit per cell, and belong to space group O_h^1-Pm3m. The metal atom is located in position 1 (a) at 0,0,0. Six boron atoms are found in positions 6 (f) at $\pm$ $(\frac{1}{2},\frac{1}{2},u;\frac{1}{2},u,\frac{1}{2};u,\frac{1}{2},\frac{1}{2})$ with u = 0.207. A projection of the structure onto the (XYO) plane is shown in Figure 5. 7, Part I. In this structure the metal ions are surrounded by boron cages in octahedral arrangement.

The hexaborides of all of the lanthanides except promethium have been reported (22, 39, 71, 74, 79, 80, 02, 87, 90-100). However, considerable doubt as to the existence of ErB_6, TmB_6 and LuB_6 has been cast recently by Sturgeon and Eick (101), who demonstrated that X-ray powder patterns of hexaboride preparations for these metals could be indexed as a mixture of tetra- and dodecaborides. The hexaborides vary in color from deep blue to purple.

A plot of the cubic lattice parameter for the lanthanide hexaborides as a function of atomic number reveals a behavior significantly different from that of the tetraboride (02). Large positive deviations at europium and ytterbium and a smaller positive deviation at samarium indicate significant alkaline earth character in these metal ions. On the other hand, in the tetraborides the nearly linear variation of lattice parameters even through

these metals indicates that the valency of the metal is more nearly constrained to trivalency. This behavior of the hexaborides is strikingly similar to the behavior found in lanthanide metals (102). Therefore, as suspected, the hexaborides are quite metallic in nature (24, 103, 22, 76). A quantum mechanical discussion of the bonding in hexaborides and the implications thereof is presented by several authors (104, 105, 106-8). Covalent boron-boron bonding in MB_2, MB_4, MB_6 and MB_{12} compounds is demonstrated by the above authors and by Johnson and Daane (73). Table 2. 1 summarizes the lattice parameters, densities and melting points of lanthanide hexaborides. Values for Er- Tm-, Lu- and ScB_6 are indicated by parenthesis, reflecting doubt as to their existence. The melting points listed for the borides of this table are taken, for the most part, from tables listing experiments with these borides performed in this work in which no melting was observed.

The problem of the extent of solid solution in these hexa- and tetraborides has not been resolved. Again, as in the case of the tetraborides, the wide disagreement in reported lattice parameters might indicate an extensive solid solution range. Eick and Gilles (02) and Gschneidner (30) believe a large part of this discrepancy may well be from impure preparations. Post, et al. (76), gave evidence supporting wide solid solution in EuB_6, and Johnson and Daane (25) determined a solid solution range for LaB_6 of 85.8 to 88% boron by X-ray diffraction, synthetic composition and density studies. However, Eick and Gilles were able to prepare boron-rich and metal-rick compositions for the tetraborides and hexaborides without finding a change in lattice parameters, implying narrow solid solution ranges. While these considerations are

not conclusive as to whether or not wide solid solution ranges exist in these borides, they seem to support a narrow homogeneity range. Conclusive studies of this problem must await high purity materials and precise boron analyses.

2. 1. 6 LnB_{12}

In 1949 Bertaut and Blum (109) and Andrieux and Blum (110) reported the discovery of UB_{12}. A second dodecaboride, ZrB_{12}, was identified in 1952 by Post and Glaser (111-2). Blum and Bertaut (109, 39) found that the structure of this body-centered-cubic boride contains four formula weights per unit cell and belongs to the space group, $Fm3m\text{-}O_h^5$. The four metal ions are in positions 4 (a) at $(0,0,0;0,\frac{1}{2},\frac{1}{2};\frac{1}{2},0,\frac{1}{2};\frac{1}{2},\frac{1}{2},0)$. The forty-eight boron atoms are in positions 48 (i) at $(0,0,0;0,\frac{1}{2},\frac{1}{2};\frac{1}{2},0,\frac{1}{2};\frac{1}{2},\frac{1}{2},0)$ + $(\frac{1}{2},x,x;x,\frac{1}{2},x;x,x,\frac{1}{2};\frac{1}{2},x,\bar{x};\bar{x},\frac{1}{2},x;x,\bar{x},\frac{1}{2};\frac{1}{2},\bar{x},\bar{x};\bar{x},\frac{1}{2},\bar{x};\bar{x},\bar{x},\frac{1}{2};\frac{1}{2},\bar{x},x;x,\frac{1}{2},\bar{x};\bar{x},x,\frac{1}{2})$. This structure is described by regular cubo-octahedra of boron atoms containing metal ions at the center. Figure 5. 7, Part I, is a projection of the MB_{12} structure onto one face of the cubic cell.

Unsuccessful efforts to prepare boride phases richer in boron than MB_6 for the larger radius lanthanides are described by Post, Moskowitz and Glaser (113). In 1959 Lundin (80) found YB_{12}. Seybolt (114) in 1960 confirmed that YB_{12} was isostructural with UB_{12}. La Placa, Binder and Post (41) were able to make the UB_{12}-type dodecaboride of the smaller radius lanthanides, Dy, Ho, Er, Tm and Lu, as well as YB_{12}. They pointed out that the size of the metal ion plays a critical role in the formation of these dodecaborides. In particular, an atom with metallic radius greater than 1.91 Å will not be accommodated by the size of the holes in the boron

cubo-octahedra. However, a later paper by La Placa, Noonan and Post (115) reported the existence of TbB_{12} and YbB_{12}.

Very little information on the physical properties of these compounds is available. ZrB_{12} melts at 2680°C. and exhibits metallic conduction (116). YB_{12} melts peritectically at 2200°C. (80). The lattice parameters for this cubic phase are presented in Table 2. 1.

2. 1. 7 LnB_{50}

In 1960 Seybolt (114) discovered an extremely boron-rich yttrium boride with metal content between one and two atomic percent yttrium. Metallographic studies revealed that this phase is cubic and has about 1700 atoms/cell. This composition was estimated to be YB_{50}. No lattice parameter was reported.

2. 1. 8 LnB_{70}

From an extensive metallographic study of the yttrium-boron system, Lundin (80) reported a tetragonal phase with an estimated 90% boron content and composition YB_{70}. This symmetry is tentative. The lattice parameters, a_o and c_o, were tentatively assigned as 11.75 and 12.62 $\pm$ .04 Å, respectively. Lundin believes the YB_{50} and the YB_{70} phases are probably the same and may be an allotrope of boron stabilized by yttrium. Recently, in a report by Post (46), Kasper found that the YB_{70} phase is primitive cubic with a_o about 23.50 Å. Post reported the existence of Tb-, Ho- and YbB_{70} (46).

2. 2 Experimental

2. 2. 1 Materials

The gadolinium metal used in attempts to prepare GdB_2 (cf. Chapter 2. 3. 1) is the same as that described in Part I, Chapter 2. 1.

Amorphous boron, grade AA, 325 mesh, was obtained from Cooper Metallurgical Associates. The assay accompanying the sample specified boron content at 99.5%, Fe at 0.15% and carbon at 0.10%. This sample, lot number 0361, lab sample B-13A, was used in the preparation of GdB_4 (81GdAM), GdB_6 (83GdAM), and all borides of other lanthanide metals and in the ternary compatibility studies of Chapter 14.

All of the metals listed below and ZrB_2 were used in the ternary compatibility studies of Chapter 14. Reactor-grade, zirconium, metal sponge was obtained from Columbia-National Corporation. An analysis of this sample showed oxygen content at 1129 ppm., Fe at 969 ppm., Mg at 385 ppm; Cr at 149 ppm., Cl at 118 ppm. and all other contaminants less than 50 ppm. The sample was denoted Zr-1. Tantalum powder, lot 1000B, lab sample Ta-2, type 268, 325 mesh, was purchased from Fansteel Metallurgical Corporation. The assay showed 99.88% Ta, 0.02% Fe, 0.01% C, 0.04% W and 0.05% Nb. Tungsten powder, lab sample W-1, with an assay of 99.9% W was purchased from Fansteel Metallurgical Corporation. Powdered ZrB_2, lot 112.8L, grade 100F, lab sample ZrB_2-3, was purchased from Norton Company. The ZrB_2 assay showed 76.0% Zr, 17.9% B and 0.8% C.

Lanthanide oxides, La_2O_3, Ce_2O_3, CeO_2, Pr_6O_{11}, Nd_2O_3, Sm_2O_3, Gd_2O_3, Tb_4O_7, Dy_2O_3, Ho_2O_3, Er_2O_3, Yb_2O_3 and Y_2O_3 were purchased from Lindsay Rare Earth Chemicals of American Potash and Chemical Corporation, from

Research Chemicals Division of Nuclear Corporation of America and from Vitro Chemical Company. The purities were designated as 99.9% oxide with less than 0.1% other lanthanide oxide content.

2. 2. 2 Preparation and Characterization

Many methods have been used to prepare metal borides. These are discussed in the references of Chapter 2. 1. Among these methods is the reaction of boron with metal oxides. With the use of an arc melting furnace the reaction of compacts of lanthanide oxides and boron under argon atmospheres produced the desired borides much more swiftly than the vacuum heating techniques other researchers employed, and removed the possibility of crucible interaction in the preparative scheme. Only tetra- and hexaborides were prepared in this work.

It was found that hexaboride preparations according to the stoichiometry,

$$Ln_2O_3(s,l) + 14B(s,l) = 2\ LnB_6(s) + B_2O_3(g), \qquad (2.\ 1)$$

produced principally hexaboride with tetraboride present in less abundance. Preparations of tetraborides according to the stoichiometry,

$$Ln_2O_3(s,l) + 10B(s,\ l) = 2LnB_4(s) + B_2O_3(g), \qquad (2.\ 2)$$

gave tetraboride as the principal phase with the hexaboride an appreciable contaminant. Single phase hexaboride resulted if the stoichiometry,

$$2Ln_2O_3(s,\ l) + 30\ B(s,\ l) = 4\ LnB_6(s) + 3\ B_2O_2(g), \qquad (2.\ 3)$$

was followed and the melted pellet was crushed, ground, pressed and re-melted several times. However, the stoichiometry,

$$2Ln_2O_3(s,\ l) + 22\ B(s,\ l) = 4\ LnB_4(s) + 3\ B_2O_2(g), \qquad (2.\ 4)$$

produced tetraboride severely contaminated with hexaboride. The boron

content had to be decreased by twenty atomic percent to generate single phase LnB_4. These observations were made for all the lanthanides in the materials list except for Sm and Yb, where pure tetraborides were never made.

Reactants in the form of 325 to 400 mesh powders were weighed to the stoichiometry desired, carefully blended, pressed into a hardened steel die and extruded as a cylindrical pellet. Total sample weights varied from 200mg. to 5g. Cylindrical dimensions varied from 1/4" to 1" diameter and from 1/8" to 1-1/2" length. The compacting pressure on the Carver hydraulic press (Fred S. Carver, Inc., New York) varied from 2000 to 10,000 lbs./in^2. These pellets were mounted on a 9" diameter copper hearth cleaned with nitric acid. After the hearth was mounted in the arc melting apparatus, the system was pumped out to a pressure of 5 microns with a mechanical forepump. Argon was introduced to a pressure of one atmosphere. The atmosphere in the melter was exchanged with argon successively for three cycles, leaving one atmosphere of argon in the melter. All surfaces which might heat during the melting were water-cooled. A DC arc was struck between the copper hearth anode and the flexible, bellows-mounted, 1/2", tungsten cathode with a high frequency arc start. While the operator viewed the melting through a glass viewport, zirconium metal was first melted to purge the system of residual oxygen, nitrogen and water; then the arc was moved onto the powder-compacted pellets and they in turn were arc melted with currents from 150 to 300 amp. and heating times of 1/4 to 2 minutes. The arc was then extinguished, samples cooled and turned over, and the melting cycle repeated. During these preparatory meltings, considerable material was vaporized throughout the melter chamber

and high pressures were developed during the heating. A large brass bellows with one cubic foot of volume in the relaxed position expanded with these pressure surges to allow the operator to maintain a steady arc position.

After the melted pellets cooled, they were removed from the arc melter, crushed in a hardened steel "diamond" mortar and ground in an agate mortar. If the melted button appeared free of B_2O_3 glass and was uniformly blue or gray, indicative of hexa- or tetraboride only, the ground material was examined for completeness of boride formation by X-ray diffraction. If reaction was obviously incomplete, the ground material was compacted again and the melting process repeated. When the X-ray powder photographs revealed only the boride of interest present, the finely ground boride was washed several times with warm 50% HCl followed by distilled water to remove oxide material. In a few cases, when the desired boride did not form to the exclusion of other borides after several remeltings, additional boron or lanthanide oxide was added and melting repeated.

Regardless of the initial stoichiometry, the boride first appearing on arc melting was LnB_6. Layer formation of blue hexaboride on a gray tetraboride core occurred initially in attempts to prepare tetraborides. The hexaboride was imbedded in a melt of oxide material. Continued heating of this mass vaporized B_2O_3 and Ln_2O_3 throughout the melter chamber without appreciably increasing the concentration of the boride desired. However, if the pellet was crushed, ground and pressed again, more intimate contact of the elemental boron and LnB_6 with Ln_2O_3 was favored, and the abundance of the desired boride increased. In an initial stoichiometry of

equation 2. 3, repeated melting, crushing, grinding, compacting and melting produced nearly oxide-free hexaboride after three or four cycles. However, in the case of the tetraboride preparation, because appreciable Ln_2O_3 was vaporized from the reaction medium after hexaboride was formed, but before the hexaboride and metal oxide could be remixed to allow further reduction to the tetraboride, the initial composition had to be rich in Ln_2O_3 to insure the formation of LnB_4. These observations were supported by visual and X-ray evidence. Many of the possible kinetic and competing processes in the preparation of lanthanide borides by oxide reduction with boron are discussed by Galloway (117).

X-ray evidence alone is not sufficient to demonstrate that the boride prepared in this fashion was pure. For instance, phases present in concentrations less than, say, 5% might not have produced structure lines on the powder photograph intense enough to allow observation of the phase. Further, glasses, which were a strong possibility with B_2O_3 present, have no structure and cannot be observed in X-ray patterns. In general, evaporation of the acid washing solutions revealed very little, if any, oxide residue. In the GdB_4 and GdB_6 preparations, analyses for metal and for boron were performed on the finished product material. This analysis is described in Chapter 7. Typical results for gadolinium and for boron analysis in GdB4 and GdB6 are shown in Table 7. The metal analysis was accurate to $\pm$ 1% and the boron analysis was accurate to $\pm$ 2%. The sum of the boron and gadolinium content routinely accounted for 95 to 100% of the sample. These analyses precluded the presence of appreciable quantities of metal oxide, boron oxides and/or borates. Excess elemental boron may have been observed in powder photographs because of the low

intensity of diffracted radiation and would not have been revealed in a total metal-boron content analysis. However, the gadolinium to boron ratio in these preparations was equal to, or greater than, the stoichiometry of the boride observed in the X-ray pattern. Emission spectrographic analysis of GdB_4 (16GdAM) prepared in the arc furnace showed Cr, Cu and Fe less than 0.1%; Si, barely detectable; and no other impurities.

If there were wide homogeneity ranges for these borides, large composition gradients might have been expected in these preparations, in view of the large temperatures inherent with arc melting. However, from the evidence discussed in Chapter 2. 1. 4 and 2. 1. 5, the tetra- and hexaborides apparently have narrow solid solution ranges. Therefore, with the assumption of narrow solid solution limits and considering the analytical observations above, it is felt that the phase observed in the boride preparation defined the composition fairly well. In addition, assuming that the tetra- and hexaborides of other lanthanides than gadolinium were identical in composition and solid solution characteristics, simple observation of the product boride by X-ray diffraction was sufficient to characterize all the boride preparations.

2. 3 Borides Observed

2. 3. 1 LnB_2

Never in the course of these studies was any diboride phase observed. A specific attempt to prepare GdB_2 or any boride phase existing between the metal and GdB_4 was made. Powdered GdB_4 was mixed with gadolinium metal filings, pressed into a 3/8" pellet, mounted into a copper

current concentrator on a ZrB_2 support and the entire assembly placed into a glass vacuum system capable of being pumped to a pressure of 2×10^{-5}mm. in two hours from atmospheric pressure. The vacuum assembly and heating technique are discussed in Chapter 8. 1. The pellet was heated by induction to about 1500°C. for 20 minutes. During the heating the gadolinium was observed to melt (m.p. 1312°C.), but a solid phase remained suspended in the viscous melt. On cooling and removing from the vacuum line, the globule was ground for X-ray analysis. No reaction between the cooler ZrB_2 base and the sample was observed. X-ray powder photographs (C-2864,5), while of poor quality, revealed GdB_4, Gd and Gd_2O_3. No AlB_2-type symmetry was observed. No other specific attempt to prepare lower lanthanide borides was made.

2. 3. 2 LnB_4 and LnB_6

Tetra- and hexaborides or two-phase tetra- and hexaboride mixtures were prepared with the elements, Y, La, Ce, Pr, Nd, Sm, Gd, Tb, Dy, and Yb. The symmetries and intensities exhibited by X-ray powder diffraction photographs for all the hexaborides and tetraborides were in agreement with previously reported information. Attempts to prepare single-phase LaB_4 and SmB_4 by reduction of the sesquioxide with boron or hexaborides in the arc melting apparatus were unsuccessful. In every case the predominant phase was hexaboride with tetraboride only present as a minor phase. YbB_4 was never observed in the arc melting preparations. Even samples with large excesses of Yb_2O_3, compared to the reactant ratios discussed above, produced only YbB_6 or YbB_6-YbB_{12} two phase mixtures. A preparation of ErB_4 in the stoichiometry of equation 2. 4 produced a

mixture of ErB_4 and ErB_{12}. An attempt to prepare HoB_6 produced an HoB_4-HoB_6-HoB_{12} mixture. For the lanthanides, Ce, Pr, Gd, Tb, Dy and for Y, both the tetra- and the hexaborides could be prepared easily.

Eick and Gilles (02) reported that they were unable to prepare ErB_6 and YbB_4 by this method. However, they were successful in preparing SmB_4. Binder (24) pointed out that EuB_4 cannot be prepared by any method and that La-, Eu- and YbB_4 are difficult to prepare probably because of their large metal radii. Difficulty in preparing single-phase SmB_4 was noted by Galloway and Eick (117). Further, as noted above, Eick and Sturgeon suggested that ErB_6 does not exist. Attempts to prepare ErB_6 produced ErB_4-ErB_{12} mixtures. These observations are corroborated by this research. No attempt was made to prepare Pm, Eu, Tm or Lu borides.

2. 3. 3 LnB_{12}

Specific attempts to prepare GdB_{12} by melting GdB_6/B compacts in the arc furnace revealed only a GdB_6-GdB_{100} two-phase region. An ErB_4 preparation, as noted above, produced ErB_4 as a major phase and ErB_{12} in lesser concentration. A similar preparation of HoB_6, in which reaction was not complete or in which large temperature gradients existed in the arc melting, produced HoB_6 as a major phase, and HoB_4 and HoB_{12} as minor phases. Further, a YbB_6 preparation according to the stoichiometry of equation 2. 3 produced YbB_6 as the major constituent and YbB_{12} as the minor constituent.

The inability to prepare GdB_{12} is in agreement with Post, et al. (41, 113), who were unable to prepare dodecaborides of lanthanides larger in radius than that of terbium. Further, Post, et al., did prepare ErB_{12}

by reducing Er_2O_3 with excess boron at 1400-1500°C. in helium. Post prepared HoB_{12} in a similar manner. However, Post's work failed to prepare YbB_{12} by reduction of sesquioxide with boron. This failure was explained, at first, by the large size of the ytterbium ion in its tendency to exhibit divalency. Only direct combination of the elements produced YbB_{12} (115).

The YbB_{12} X-ray pattern obtained from this work was identical in indexing and intensity to that reported by Post for TmB_{12}. In addition the (210), (301) and (321) reflections were observed. Table 2. 2 contains the diffraction record computed from a Debye-Scherrer powder photograph with an IBM 1620 computer. The unit cell edge of this cubic dodecaboride was calculated from high angle lines as 7.462 Å to be compared with 7.469 Å reported by Post. This value fits the lanthanide contraction of the parameters of other dodecaborides, as reported by Post, quite well (cf. Table 2. 1).

The large increase in cell dimensions which is observed for Yb in hexa- and tetraborides and in lanthanide metals is absent for the dodecaborides. This absence probably reflects the encirclement and insulation of metal atoms from one another by boron cages in the dodecaboride structure. Thus, the metal atoms are not free to interact in the fashion that they would if close metal-metal bonding were allowed. Apparently, the ytterbium ion is constrained to trivalency. This situation would account for the existence of YbB_{12} even though its metallic radius is greater than the 1.91 Å limiting value prescribed by Post for dodecaboride stability.

TABLE 2. 2

YbB_{12} Diffraction Record; Cu-$K\alpha_u$, 1.54178 Å,

Radiation; Debye-Scherrer Film C-2895.

hkl	I/I_o	d, Å	$\sin^2\theta$ (observed)
111	50	4.295	.03222
200	30	3.731	.04269
210	20	3.349	.05297
220	40	2.641	.08523
301	10	2.331	.10936
311	80	2.252	.11714
222	20	2.154	.12807
321	5	1.977	.15210
400	6	1.865	.17081
331	25	1.714	.20221
420	20	1.669	.21324
422	10	1.524	.25594
511/333	10	1.419	.29511
531	15	1.261	.37360
611	5	1.196	.41516
620	95	1.182	.42555
541	10	1.149	.44992
533	20	1.139	.45821
622	50	1.123	.47090
444	10	1.0786	.51079
711/551	10	1.0447	.54449
640	10	1.0356	.55410
612	10	1.0050	.58838
731/553	5	.9733	.62734

2. 3. 4 LnB_{100}

2. 3. 4. 1 GdB_{100}; Discovery and Composition. In arc melted preparations in the extremely boron-rich corner of the ternary Gd-B-C field, discussed in Part I, a large cell cubic phase was found, which was first thought to be an allotrope of boron. This phase has since been demonstrated to be a gadolinium boride, the composition of which is definitely between GdB_{100} and GdB_{200} and probably closer to GdB_{100}. This boride has been designated GdB_{100}.

Compositions in the extremely boron-rich region of the gadolinium-boron binary system are summarized in Table 2. 3. These samples were prepared by arc melting powder compacts of boron mixed with GdB_6 according to the synthetic stoichiometry indicated in Table 2. 3. The ground reaction products were examined for the phases present by X-ray powder diffraction techniques by use of the Guinier focusing cameras.

While ternary Gd-B-C preparations 53-, 72-, 77-, 78-, and 79GdAM of Table 3. 1, Part I, revealed the existence of GdB_{100}, it was not certain whether the phase was stabilized by carbon or was a boron allotrope. The preparations of Table 2. 3 clearly demonstrate that this phase is not a ternary carbon-stabilized phase. Further, 87GdAM demonstrates the two-phase region GdB_{100}-boron, indicating that this phase is definitely not a boron allotrope. The two-phase region, GdB_6-GdB_{100}, is revealed in 82- and 86GdAM. The absence of GdB_{12} is discussed above. Since the X-ray diffraction line intensities of the elemental boron phase in 87GdAM (GdB_{200}) are comparable to the intensities of the metal containing phase, GdB_{100}, it is assumed that the composition of the binary phase is considerably more boron deficient than GdB_{200}. Similarly, the line intensities

TABLE 2. 3

Boron-Rich Gadolinium Boride Compositions.

Sample	GdB_6, mg.	B, mg.	Composition	Film	Phases Present
82GdAM	96.85	203.15	$Gd_{.0200}B_{.9800}$	D-1447	GdB_{100}, mjr. GdB_6, mnr.
86GdAM	54.18	245.82	$Gd_{.0100}B_{.9900}$	D-1559 D-1563	GdB_{100}, mjr. GdB_6, mnr.
87GdAM	28.81	271.19	$Gd_{.0050}B_{.9950}$	D-1557 D-1479	GdB_{100} β-rhom. B, eqc.

of GdB_{100} compared to the line intensities of the GdB_6 phase in 86GdAM (GdB_{100}) imply that the GdB_{100} phase has a composition not much higher in boron content than GdB_{100}. Therefore, this phase has been labeled GdB_{100}. No attempts to prepare single-phase GdB_{100} or to analyze the prepared compositions has been made.

Only the use of a Guinier focusing camera, whose monochromatic radiation and extreme low angle utility range afford excellent resolution, could allow the analysis of complex diffraction records containing mixtures of β - rhombohedral boron, B_4C and GdB_{100}, all of which have large unit cells and complex structures. Reference patterns of β - rhombohedral boron (D-1373) and B_4C (D-1448) were prepared and their diffraction records computed. Intercomparison of these reference diffraction records with those computed from sample preparations made the interpretation of the phase relations quite simple.

2. 3. 4. 2 GdB_{100}; X-ray Character. Table 2. 4 contains the diffraction record of GdB_{100} (Guinier film D-1269). From an averaging of the a_o parameter determined from intense high angle diffraction lines, the primitive cubic cell edge dimension is $16.50 \pm .02$ Å. While the agreement between observed and calculated $\sin^2\theta$ values is not perfect, no other indexing scheme could be found without a choice of a larger unit cell. The small non-systematic deviations could easily arise from film reading errors, in view of the complexity of the pattern and the generally weak intensities.

An attempt was made to index the GdB_{100} diffraction record with the tetragonal symmetry and 11.75 and 12.62 Å axes of the YB_{70} phase found by Lundin (80). No agreement was found between computed $\sin^2\theta$ from the YB_{70} cell dimensions and the GdB_{100} observed $\sin^2\theta$ values. The cell

TABLE 2. 4

GdB_{100} and YbB_{100} Diffraction Records; Cu-K_{α_1}, 1.54050 Å, Radiation;

GdB_{100} Guinier Film D-1269, YbB_{100} Debye-Scherrer Film C-3187.

YbB_{100}					GdB_{100}				
hkl	I/I_o	d, Å	$\sin^2\theta_{obs}$	$\sin^2\theta_{cal}$	hkl	I/I_o	d, Å	$\sin^2\theta_{obs}$	$\sin^2\theta_{cal}$
110	60	12.05	0.004095	0.00434	110	20	11.75	0.00431	0.00436
111	05	9.459	0.00664	0.00651	211	60	6.732	0.01309	0.01309
200	05	8.301	0.008624	0.00867	220	80	5.832	0.01744	0.01744
210	12	7.789	0.009797	0.01084	310	20	5.236	0.02166	0.02181
211	11	6.748	0.01305	0.01300	222	20	4.771	0.02607	0.02617
220	12	5.855	0.01734	0.01735	401	20	3.948	0.03806	0.03674
221	07	5.526	0.01946	0.0195	330	20	3.897	0.03908	0.03926
301	04	5.249	0.02157	0.02167	331	10	3.792	0.04126	0.04144
222	20	4.796	0.02584	0.02599	420	10	3.696	0.04346	0.04344
321	20	4.415	0.03048	0.03033	332	20	3.525	0.04771	0.04777
401	07	4.036	0.03648	0.03687	501	40	3.243	0.05644	0.05633
411	05	3.896	0.03915	0.03903	530	10	2.843	0.07340	0.07368
420	20	3.726	0.04281	0.04338	600	50	2.758	0.07803	0.07799
421	10	3.599	0.04588	0.04552	611	10	2.684	0.08242	0.08234
332	10	3.529	0.04773	0.04773	621	10	2.577	0.08936	0.08889
430	15	3.351	0.05291	0.05204	541	10	2.556	0.09080	0.09076
501	20	3.249	0.05630	0.05639	622	30	2.493	0.09545	0.09527
333	04	3.169	0.05916	0.05858	630	10	2.454	0.09853	0.09810
600	15	2.761	0.07797	0.07802	444	20	2.393	0.10362	0.10373
611	20	2.680	0.08274	0.08240	700	30	2.372	0.10550	0.10579
622	07	2.491	0.09574	0.09535	701	20	2.342	0.10813	0.10793
630	07	2.462	0.09801	0.09755	640	30	2.296	0.11248	0.11244
701	10	2.335	0.10904	0.1084	730	30	2.173	0.12570	0.12541
640	07	2.294	0.1129	0.1127	801	10	2.055	0.14068	0.14050
721	12	2.247	0.1177	0.1171	811	45	2.035	0.14293	0.14284
632	04	2.208	0.1219	0.1214	820	30	2.006	0.14748	0.14715
731	10	2.162	0.1272	0.1278	653	10	1.979	0.15136	0.15179
650	07	2.116	0.1328	0.1323	822	10	1.951	0.15587	0.15559
811	10	2.043	0.1424	0.1431	662	40	1.898	0.16460	0.16449
820	10	2.006	0.1477	0.1474	921	20	1.787	0.18630	0.18615

TABLE 2. 4, continued

	YbB_{100}					GdB_{100}			
hkl	I/I_o	d, Å	$\sin^2\theta_{obs}$	$\sin^2\theta_{cal}$	hkl	I/I_o	d, Å	$\sin^2\theta_{obs}$	$\sin^2\theta_{cal}$
822	09	1.947	0.1568	0.1561	10,1,1	10	1.639	0.22106	0.22076
751	15	1.906	0.1636	0.1626	950	10	1.606	0.23006	0.22968
901	07	1.830	0.1774	0.1778	10,2,2	10	1.590	0.23455	0.23437
920	10	1.796	0.1842	0.1843	10,3,2	0	1.525	0.25500	0.25592
664	07	1.762	0.1914	0.1908					
932	14	1.710	0.2033	0.2038					
941	07	1.672	0.2125	0.2124					
10,2,1	04	1.614	0.2282	0.2275					
10,0,3	04	1.590	0.2352	0.2362					
944	04	1.564	0.2431	0.2427					
10,3,3	10	1.525	0.2556	0.2558					
10,5,3	04	1.437	0.2880	0.2881					
11,4,0	05	1.416	0.2964	0.2969					
12,2,1	02	1.355	0.3236	0.3230					
12,2,2	03	1.344	0.3289	0.3293					
11,6,3	05	1.287	0.3589	0.3598					

parameter of the cubic YB_{50} phase found by Seybolt (114) was not reported; however, it was estimated by him that the YB_{50} cell contains 1700 atoms/cell. Assuming closest packing of 0.87 Å radius covalently-bound boron atoms and ignoring the metal atom content, one calculates 1660 atoms/cell for GdB_{100}. It would appear that GdB_{100} and YB_{50} are identical structures. In view of Kasper's single crystal YB_{70} cell dimension of 23.50 Å (46), an attempt was made to index the GdB_{100} pattern to a cell of approximately this dimension. While the fit was as good as that obtained for the 16.50 Å cell, it is noted that almost any cell so large could be made to fit the observed diffraction record within the film reading errors involved. The 16.50 Å primitive cubic cell was chosen, since it is the smallest cell possible.

2. 3. 4. 3 YbB_{100}. While no specific attempt was made to prepare the LnB_{100} phase for other lanthanides than gadolinium, a Langmuir vaporiation experiment of a powder compact of a YbB_6-YbB_{12} mixture (cf. Table 4. 1) revealed a mixture of YbB_6 and YbB_{100} on the outer surface of the compact after heating. The pellet was mounted on a ZrB_2 stand in a copper current concentrator furnace (cf. Chapter 8. 1). Under vacuum of 10^{-5}mm. the pellet was heated by induction for one hour at 1920°C. The diffraction record of YbB_{100} computed from the reading of a Debye-Scherrer X-ray powder photograph (C-3187) is in Table 3. 5. The unit cell length of this cubic phase calculated from the high angle lines is 16.56 ± .01 Å, slightly larger than the cell parameter of GdB_{100}.

2. 3. 4. 4 Other LnB_{100} Phases. If the existence of a LnB_{100} phase is dependent on the size of the metal ion, and if Yb is constrained to a size typical of trivalency as in the dodecaboride, then the LnB_{100}

phase ought to exist for the lanthanides Gd, Dy, Ho, Er, Tm, Yb and Lu. If, on the other hand, Yb exhibits a radius indicative of that in the pure metal, then LnB_{100} ought to exist for lanthanides larger than gadolinium. Johnson and Daane (25) reported eutectic and eutectoid rejections of LaB_6 from rapidly cooled arc melted alloys between 89 and 99.5% boron. They estimated the composition of the eutectoid phase close to 99% boron and suggested the existence of a high temperature modification of elemental boron stabilized by lanthanum rather than a La-B phase. However, this behavior could easily be explained by a eutectic between LaB_6 and LaB_{100} followed by disproportionation at a lower temperature of LaB_{100} into LaB_6 and boron. The discovery of Tb-, Ho- and YbB_{100} by Post (46), coupled with the observations above, leads one to believe that the LnB_{100} phase will be found for all lanthanides and for Y.

2. 3. 4. 5 Boron Allotropes. It is interesting to compare the LnB_{100} phase with the polymorphic forms of boron. Hoard and others (118-9, 44) in 1960 and 1961 discussed the many boron structural forms. There are four polymorphs of boron currently given credence. These are the low temperature, α-rhombohedral form (120), the 1100 to 1300°C. tetragonal form (121), the high temperature β-rhombohedral allotrope (122), and more recently another tetragonal form (123). These allotropes and other reported forms (124, 125, 126) are summarized in Table 2. 5.

All of these allotropes except the α- and β-rhombohedral forms were found in the temperature range 1000-1300°C. and were all prepared by BX_3 deposition of boron on hot metal or graphite substrates. Stern and Lynds (126) found three different phases of boron in the 1075 to 1200°C. range, depending on whether BCl_3 was decomposed on titanium or graphite

TABLE 2. 5

Allotropic Modifications of Boron

Ref.	Modification	Conditions	Space Group	Cell Constants	Density (g./cm.^{3})	Atoms /Cell
120,118	α-Rhombohedral	Low temp., 750-1200°C.	$R\bar{3}m$ A = 4.908 Å C = 12.567 Å	a = 5.06 Å α = 58°4'	2.46	12
121,44,118	Tetragonal	1100-1300°C.	$P4_2/nnm$	a = 8.75 Å c = 5.06 Å	2.31	50
122,127,118	β-Rhombohedral	High temp., > 1200°C.	$R\bar{3}m$ A = 10.95 Å C = 23.73 Å	a = 10.12 Å α = 65°28'	2.35	108±1
44	Amorphous	< 800°C.			< 2.3	
118,123,44	Tetragonal	1250°C., BBr_3 dep.		a = 10.12 Å c = 14.14 Å	2.364	192
118,124	Tetragonal	1000-1300°C. BBr_3 dep. on W, Mo		a = 8.57 Å b = 8.13 Å	2.33	78
118,125	Hexagonal					90
118,126	Unknown	1075-1125°C. BCl_3 dep. on Ti			2.39-2.49	
118,126	Unknown	1075-1125°C. BCl_3 dep. on graphite			2.39-2.49	

and on the temperature. The phase of Szabo and Tobias (124) resulted from deposition from BX_3 on tungsten and molybdenum wires. In view of the existence of the extremely metal-rich borides noted above, and of the strong possibility of stabilization of the "boron allotropes", also discussed above, by reaction with the substrate material on pyrolytic decomposition of BX_3 gases, perhaps many more boron-rich metal borides exist. That these latter allotropes might be nonstoichiometric borides is suggested by Hoard (44).

CHAPTER 3

CRUCIBLE SELECTION

3. 1 General Requirements

The choice of a crucible in which the vaporization properties of the tetra- and hexaborides may be studied is dependent on several considerations. First, the crucible material must withstand high temperatures, in this case 2500°K., without melting or vaporizing significantly. Second the crucible material must not interact with the borides being studied at the temperatures of the experiment either in eutectic formation, eutectoid formation, in solid solution formation, or in oxidation or reduction of the sample phases to other binary or ternary compounds. Implied in this last requirement is the consideration that the chemical potential of boron and of lanthanide in the sample must be less than the chemical potential of these components in any compound that might exist between these components and the crucible material. More simply, if tungsten is the crucible material for the study of the vaporization of GdB_4, the pressure of boron over W_2B must be greater than the pressure of boron over GdB_4. Otherwise, W_2B will form on reaction of tungsten with GdB_4. However, even if crucible interaction does occur, thermochemical information concerning the vaporization of the lanthanide boride sample can be derived if thermochemical information for the crucible interaction products is available.

Since these lanthanide borides will be studied with Knudsen effusion techniques, porosity of the crucible material with respect to the vapor species is precluded. The fourth, fifth, sixth and seventh considerations require the crucible to withstand large rapid temperature changes, to be readily fabricated, to be readily available and preferably to be a metallic conductor to allow direct heating by induction.

3. 2 Exclusion of Unsuitable Materials

On the basis of thermochemical arguments and material compatibility studies, many possible crucible materials can be shown to be unsuitable for use as crucibles for the lanthanide boride study. Arc melted mixtures of each of tantalum, zirconium, tungsten and molybdenum with GdB_4 and X-ray analysis of the product demonstrated the reduction of GdB_4 to form metal borides by all of these metals. Limits on the heats of formation of the lanthanide borides can be estimated from such ternary studies. These ternary studies are discussed in detail in Chapter 14. Graphite or B_4C cannot be used as crucible materials in view of the ternary Ln-B-C phases discussed in Part I. If a metal crucible is to be used, the heat of formation per gram atom of boron of its lowest boride must be less than that of the lanthanide borides. This requirement may be met by metals in Group VIIB and Group VIII of the Periodic Table. However, the melting points of these metals are generally too low. Lanthanide metal or boron crucibles are excluded because of low melting points, air oxidation and oxidation of the sample.

Oxide crucibles are generally unsatisfactory because the high heats of formation of lanthanide oxides and B_2O_3 cause contamination of the

crucible, and because of the thermal and porosity characteristics of alumina, beryllia, cermets, etc. A crucible of BN is a possible choice. This material has been used in a study of the vaporization of samarium borides by Galloway and Eick (117). However, the volatility of BN is too high at the temperatures of interest.

3. 3 ZrB_2

3. 3. 1 Thermodynamic Compatibility

A crucible choice of overwhelmingly obvious advantages is a refractory metal boride, such as HfB_2 or ZrB_2. These are very high melting, 3250 (128) and 3040°C. (129), have high heats of vaporization per gaseous atom, 177 kcal. (130) and 156 kcal. (131), and large heats of formation per boron atom, -40 kcal. (130) and -36.5 kcal. (132), respectively. Lanthanide tetra- and hexaborides have heats of formation per boron atom estimated by Leitnaker (133) as -15 ± 3 kcal. and -12 ± 2 kcal., respectively. The largest heat of vaporization per gaseous atom would occur for congruent vaporization of LaB_6 and is estimated at 136 kcal. at 298°K. In general, a difference in the heat of vaporization per total gas atom of 9 kcal. at 2000°K. will produce a pressure change of a factor of ten. The smallest difference between $\Delta H^o_{vap.}$ of 1/3 ZrB_2 and $\Delta H^o_{vap.}$ of 1/7 LnB_6 occurs for La and is 156 kcal. less 136 kcal. or 20 kcal. Therefore, the lanthanide borides exhibit a volatility larger by at least a factor of 100 than ZrB_2, which satisfactorily labels ZrB_2 and HfB_2 as involatile compared to the lanthanide borides. Further, since the heat of formation of ZrB_2 per boron atom is much more negative than that of the lanthanide borides per boron atom, lanthanide gas or metal will not reduce ZrB_2.

Zirconium diboride over 1650°C. has been reported as being unstable with respect to the formation of ZrB_{12} in the presence of boron (134). Searcy and Myers (135) felt that a couple of kilocalories favoring ZrB_{12} formation over 1650°C. did not preclude their measurement of the heat of vaporization of boron in a ZrB_2 crucible up to 2400°K. Thus, the pressure of boron over a ZrB_{12}-B or a ZrB_2-ZrB_{12} mixture is not much less than the boron vapor pressure over a ZrB_2-B mixture. The boron pressures over two-phase mixtures of lanthanide borides generally should be much less than the boron vapor pressure. Thus, lanthanide borides should not oxidize ZrB_2 to ZrB_{12} at the expense of the lanthanide boride richer in boron. These preliminary thermodynamic estimations suggest that ZrB_2 or HfB_2 might be suitable crucible materials.

3. 3. 2 Arc Melter Test

Arc melted mixtures of ZrB_2 with Gd, Dy and Nd tetra- and hexaborides (Table 3) and the ternary studies of Chapter 14 confirm the prediction above that both LnB_4 and LnB_6 exist in equilibrium with ZrB_2.

Zirconium diboride has a hexagonal structure of the AlB_2-type. The lanthanide borides are tetragonal and cubic. Therefore, solid solution between ZrB_2 and the lanthanide borides is not expected to be significant. This expectation is confirmed by the arc meltings, summarized in Table 3, for meltings at both ends of the ZrB_2/GdB_4 and ZrB_2/GdB_6 joins. The GdB_6 sample (50GdAM) used in these investigations contained some GdB_4, which explains the appearance of GdB_4 in the GdB_6-ZrB_2 meltings. Duplicate X-ray patterns of the reaction products were taken, one at normal exposure times to examine the possible expansion or contraction of the

TABLE 3

Extent of ZrB_2 Reaction with LnB_4 and LnB_6 .

Sample	Composition	X-ray Film	Phases Present		GdB_4, mg. 51GdAM	GdB_6, mg. 50GdAM	ZrB_2, mg.
8NdAM	$(NdB_6)_{0.5}(ZrB_2)_{0.5}$	C-2869	NdB_6 ZrB_2, eqc.		Equal mixture of NdB_6(7NdAM) and ZrB_2.		
84GdAM	$(GdB_4)_{0.05}(ZrB_2)_{0.95}$	D-1446	ZrB_2 only		25.62		274.38
85GdAM	$(GdB_6)_{0.05}(ZrB_2)_{0.95}$	D-1445	ZrB_2, mjr. GdB_4, tr.			28.12	271.88
89GdAM	$(GdB_6)_{0.05}(ZrB_2)_{0.95}$	D-1475 D-1553	ZrB_2, mjr. GdB_6, mnr.			28.12	271.88
91GdAM	$(GdB_6)_{0.10}(ZrB_2)_{0.90}$	D-1478 D-1551	ZrB_2, mjr. GdB_6, mnr. GdB_4, tr.			53.77	245.23
92GdAM	$(GdB_6)_{0.90}(ZrB_2)_{0.10}$	D-1572	GdB_6, mjr. GdB_4, mnr. ZrB_2, mnr.	mech. mix.		18.53	286.56
		D-1573 D-1550	GdB_6, mjr. GdB_6, tr. ZrB_2, tr.	melt			

TABLE 3, continued

Extent of ZrB_2 Reaction with LnB_4 and LnB_6.

Sample	Composition	X-ray Film	Phases Present	GdB_4, mg. 51GdAM	GdB_6, mg. 50GdAM	ZrB_2, mg.
93GdAM	$(GdB_6)_{0.95}(ZrB_2)_{0.05}$	D-1574	GdB_6, mjr. mech. ZrB_2, tr. mix.		7.98	291.77
		D-1575 D-1546	GdB_6, mjr. ZrB_2, tr. melt GdB_4, tr.			
4DyAM	$(DyB_{4,6})_{0.5}(ZrB_2)_{0.5}$	C-2868	ZrB_2, mjr. DyB_6, mnr. DyB_4, mnr.	Equal amounts of ZrB_2 and 3DyAM (DyB_6 and DyB_4, eqc.)		

structure as manifested by a shift in the d-spacings, and one with twice the normal exposure to emphasize any minor phase present. The investigation of the minor phase was not done in experiment 84GdAM, which explains the failure to find GdB_4 in that sample although it was observed in others. From the results in Table 3 and the observations that the ZrB_2 structure contracts somewhat on GdB_4 and GdB_6 addition, it is concluded that the solid solution of GdB_4 in ZrB_2 at high temperature is greater than that of GdB_6 in ZrB_2 but both are soluble to less than five mole percent. Further, the solubility of ZrB_2 in GdB_6 and GdB_4 is considerably less than five mole percent.

3. 3. 3 ZrB_2 Solid Solution Effects

Some consideration ought to be given to the effect of a solid solution range in ZrB_2 on the vaporization of LnB_4 or LnB_6. If considerable solid solution exists, LnB_6 might be in equilibrium with boron-deficient ZrB_2. This behavior is shown diagrammatically in Figure 3 in an isothermal ternary phase diagram. Suppose LnB_6 were heated in a boron-rich ZrB_2 crucible of composition x' shown in the figure. Suppose further that LnB_6 vaporizes according to equation 1. 6 and LnB_4 vaporizes according to the reaction in equation 1. 2. Then, if the boron pressure over ZrB_2 of composition x' should be greater than the boron pressure in the equilibrium of process 1. 6, the crucible will lose boron preferentially until a ZrB_2 composition of x'' is reached. As the activity of boron decreases in this two condensed phase region, the gadolinium activity may increase appreciably. Only at this ZrB_2 composition can the boron pressure be fixed and its measurement characterize the process in equation 1. 6. If the

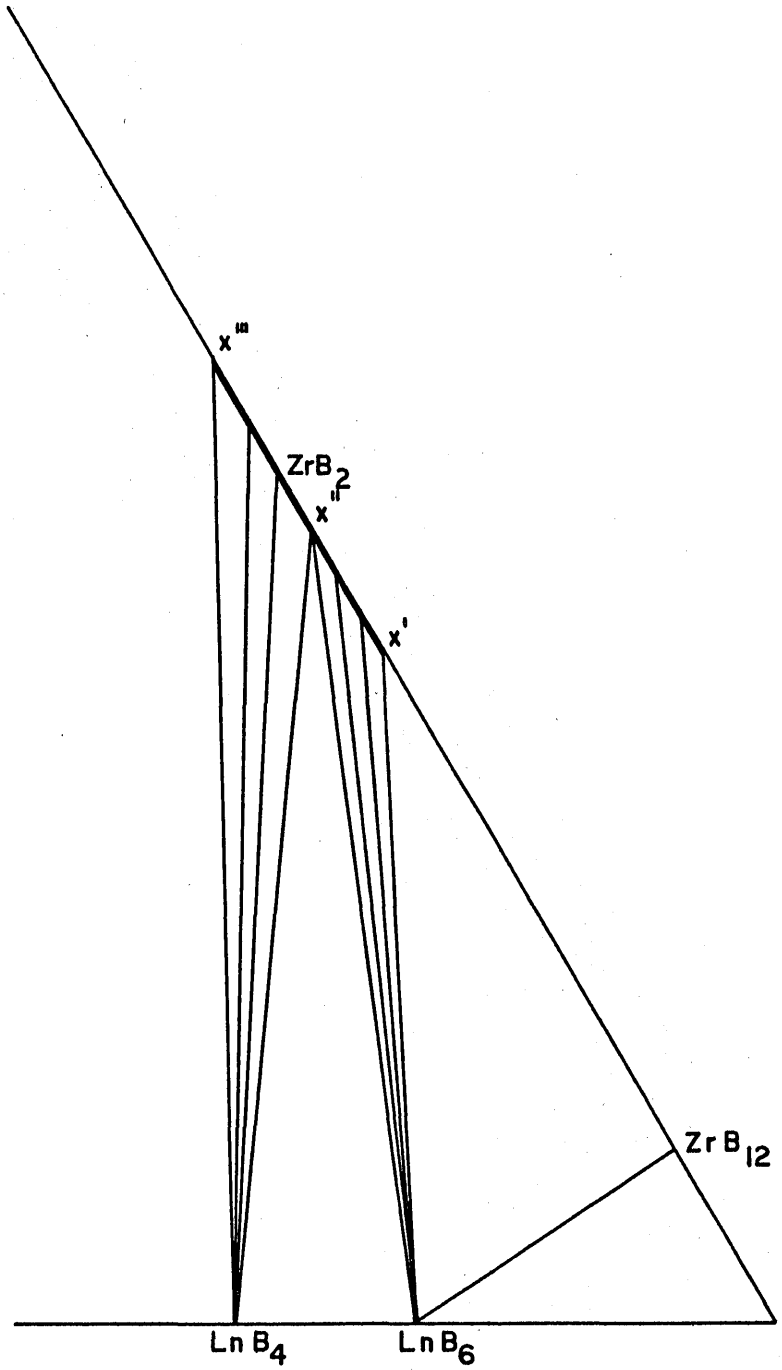

ZrB_2 SOLID SOLUTION EFFECTS

FIGURE 3

difference between x' and x'' is large, the system may not have time to lose boron to the univariant equilibrium of interest before a pressure measurement is made.

If the same crucible of ZrB_2 composition, x'', is now used in an investigation of the process in equation 1. 2, the same problem occurs. The boron pressure in process 1. 2 is lower than that in process 1. 6, so that ZrB_2 must again lose boron to a composition, x''', before meaningful pressure measurements can be made. If x'' - x''' is large and the temperature so low that evaporation is slow, one might measure a boron or gadolinium pressure widely different from those values at the univariant compositions. Of course, if both boron and gadolinium pressures are measured, the equilibrium constant for the lanthanide boride vaporization can still be obtained. However, to assume the boron pressure is four times the gadolinium pressure in process 1. 2 might lead to serious error.

In actual practice the attainment of a univariant condition can be determined from a plot of weight loss or gadolinium pressure versus time. When the weight loss is a constant with time at contant temperature, the system has equilibrated with the crucible.

However, ZrB_2 is thought to have a narrow range of homogeneity. Leitnaker (136) and Epel'baum and Gurevich (137) found no change in lattice parameters for compositions in the two-phase regions on either side of ZrB_2. Leitnaker's boron analyses indicated a homogeneity range no greater than $ZrB_{1.90}$ to $ZrB_{1.97}$. Consequently, ZrB_2 solid solution should be no problem in the lanthanide boride vaporization studies.

3. 3. 4 ZrB_2 Characterization

Finally, ZrB_2 was chosen as a crucible material, rather than HfB_2, because ZrB_2 Knudsen crucibles could be purchased (Borolite Corporation, Pittsburgh, Pa.) in a variety of sizes. These ZrB_2 crucibles required outgassing periods of 20 hours at 2250°C. in vacuum to reduce the vacuum line pressure to 5×10^{-6}mm. Heavy vapor deposits of what was probably a paraffin binding material appeared. An X-ray diffractometer scan (C-2758) revealed ZrB_2 with a small amount of ZrC or ZrB. In C-2762, an X-ray spectrographic analysis, the presence of small amounts of hafnium was revealed. Before these crucibles were used in lanthanide boride vaporization studies, small amounts of elemental boron were totally vaporized from the crucible to establish a uniform ZrB_2 composition. Never was diffusion of the crucible contents through the walls or between the lid and base of the crucible observed in any of the vaporization experiments.

CHAPTER 4

VAPORIZATION PROCESSES

4. 1 Free Evaporation Experiments

4. 1. 1 Scope of the Experiments

After the solid phases existing in the lanthanide-boron systems have been established, the principal vaporization processes exhibited by these borides must be established. For this purpose a series of Langmuir free evaporation experiments was made. With the use of an eddy-current concentrator furnace described in Chapter 8. 1, a survey of the general vaporization behavior of La, Ce, Pr, Nd, Sm, Gd, Tb, Dy, Yb and Y borides was made.

4. 1. 2 Experimental

Powder compacts of the borides, prepared according to the techniques described in Chapter 2. 2. 2, were prepared by pressing 325 mesh powders in 1/4", 3/8" or 1/2" hard steel dies at 2000, 6000 or 12,000 lbs./in.^{2}, respectively. These resulting cylinders, varying in height from 1/4" to 3/4", were mounted on a water-cooled copper hearth in the arc melting apparatus. Under an argon atmosphere purged of oxygen, the upper surfaces of these cylindrical compacts were glazed over by the arc. This partial melting provided a conducting region through which induced rf current could flow and initiate the heating of the compact by the induction

furnace. After a 1/16" black-body hole had been drilled into the top of the cylinder for temperature measurement, the sample was mounted into the current concentrator (cf. Chapter 8. 1) on a cylindrical ZrB_2 mounting stand. This ZrB_2 stand had a 1/4" diameter and was just tall enough to insure that the sample sat entirely within the core of the current concentrator without having the ZrB_2 penetrate the core (cf. Figures 8. 1 and 8. 2). This arrangement tended to decouple the ZrB_2 stand from the rf field. Consequently, the ZrB_2 stand normally was several hundred degrees cooler than the sample during heating.

After the current concentrator was placed in a vacuum line, the system was pumped to 10^{-5}mm. pressure. Sufficient rf power was applied to heat the sample to 1200-1400°C. and until the entire boride cylinder was heating uniformly. Then the power was increased until obvious vaporization occurred. After the walls of the apparatus were heavily laden with vapor deposits, the sample was cooled, removed from the furnace and examined visually and by X-ray diffraction for the phases present. An X-ray diffractometric analysis of the base of the sample cylinder and the top of the ZrB_2 stand was made in each case to reveal any ZrB_2-LnB_4 or ZrB_2-LnB_6 interaction. X-ray analysis of vapor deposits served only to demonstrate that both metal and boron were vaporizing.

4. 1. 3 Results

Table 4. 1 contains a summary of the experimental conditions and observations for the free evaporation of borides of La, Ce, Pr, Nd, Gd, Tb, Dy, Yb, and Y. No melting was observed in any of these heatings.

TABLE 4. 1

Free Evaporation Experiments; ZrB_2 stand.

Sample	Initial Phase Content	Film	Temp. (°C.)	Time (min.)	Pressure (10^{-6} mm.)	Weight Loss (%)	Final Phase Content	Film
6LaAM	LaB_6, mjr. LaB_4, mnr.	C-2897	1800-1950	25	200		ZrB_2/LaB_6 interface---ZrB_2, LaB_6 Outer surface---------LaB_6 only	C-2807a C-2807b
6LaAM1	LaB_6, mjr. LaB_4, mnr.	C-2807c	(2200)	6	100		LaB_6, La_2O_3 (air oxid. product)	D-1586
1CeAM	CeB_6, mjr. CeB_4, mnr.	C-2896	2100-2300	60	40		Inner core-----CeB_6, mjr.; CeB_4, mnr. Outer surface--CeB_6, mjr.; Ce_2O_3, tr. Vapor deposit--CeB_6	C-3120 C-2906 C-2907
1PrAM	PrB_6, mjr. PrB_4, mnr.	C-2902	2250-2350	60	30		Inner core-----PrB_6, mjr.; PrB_4, mnr. Outer surface--PrB_6 only Vapor deposit--PrB_6, mjr.; PrB_4, mnr.	C-3210 C-2909 C-2910
6NdAM	NdB_6	C-2048	1950-2050	30	40		ZrB_2/NdB_6 interface--ZrB_2, mjr.; NdB_6, mnr.; NdB_4, mnr. Outer surface--------NdB_6, mjr.; ZrB_2, tr.	C-2805a C-2805b
6NdAM1	NdB_6	C-2805	1950-2000	34	30	9	Inner core----------NdB_6 only Outer surface--------NdB_6 only ZrB_2/NdB_6 interface--ZrB_2, mjr.; NdB_6, mnr.; NdB_4, tr.; ZrB_{12}, tr. ZrB_2 stand core------ZrB_2 only	C-3201 C-2817 C-2818 C-3211
7NdAMa	NdB_6	C-2867	1950-2150	140	50		Inner core-----NdB_6, mjr.; NdB_4, tr. Outer scale----NdB_6 only	C-3206a C-3206b
81GdAM1 to a10	GdB_4, mjr. GdB_6, tr.	C-2859	1800-2100	535	50	20	Inner core-----GdB_4 only Outer scale----GdB_4 only	C-2861 C-2861a

TABLE 4. 1, continued

Sample	Initial Phase Content	Film	Temp. (°C.)	Time (min.)	Pressure (10^{-6} mm.)	Weight Loss (%)	Final Phase Content	Film
770GdAM	GdB_4 Gd, eqc.		1450-1550	20	100		Melted pellet----GdB_4, Gd, Gd_2O_3	C-2864 C-2865
15-50GdAM (59GdAM2)	GdB_6, mjr. GdB_4, tr.	D-1193 C-2215	2000-2150	60	3	3	Inner core-----GdB_6, mjr.; GdB_4, mnr. Outer scale----GdB_4 only Vapor deposit--GdB_6, mjr.; GdB_4, tr.	D-1407 visual D-1408
15-50GdAM2	GdB_6, mjr. GdB_4, mnr.	D-1407	2050-2300	50	6	18	Inner core-----GdB_6 only Outer scale----GdB_4, mjr.; GdB_6, tr.	visual D-1409
80GdAM1	GdB_4	D-1194	1500-1970	65	6	6	Outer scale----GdB_4 only Vapor deposit--GdB_6 and GdB_4, eqc.	C-2706 C-2705
80GdAM2	GdB_4	C-2706	1900-2100	285	5	5 to 10	Inner core-----GdB_4 only Outer scale----GdB_4 only Vapor deposit--GdB_6 and GdB_4, eqc.	visual D-1400 D-1402 D-1399 D-1401
1TbAM2	TbB_4, mjr. TbB_6, mnr.	visual	2000-2100	80	40	7	Inner core-----TbB_4 only Outer scale----TbB_4 only ZrB_2/TbB_4 interface--TbB_4 and ZrB_2, eqc.	C-2814 C-2813a C-2813b
2TbAM	TbB_6 TbB_4, eqc.	C-2894	2100-2300	50	50		Inner core-----TbB_6 and TbB_4, eqc. Outer scale----TbB_4 only Vapor deposit--TbB_6, mjr.; TbB_4, mnr.	C-2904 C-3220 C-2903 C-2814 C-2905

TABLE 4. 1, continued

Sample	Initial Phase Content	Film	Temp. (°C.)	Time (min.)	Pressure (10^{-6} mm.)	Weight Loss (%)	Final Phase Content	Film
741TbAM	TbB_4	visual	1600-2000	60	100		Outer scale----------TbB_4 only	C-2806
							ZrB_2/TbB_4 interface--TbB_4 and ZrB_2, eqc.	C-2813
								C-2815
								C-2816
3DyAMa	DyB_6, mjr. DyB_4, mnr.	C-2866	1950-2090	38	50		Inner core-----DyB_6, mjr.; DyB_4, mnr.	C-2881
							Outer surface--DyB_4, mjr.; DyB_6, tr.	C-2880
							Vapor deposit--DyB_6, mjr.; DyB_4, mnr.	C-3190
3YbAMa	YbB_6, mjr. YbB_{12}, mnr.	C-2895	(2000)	60	10		Inner core-----YbB_6, mjr.; YbB_{12}, tr.	C-3191
							Outer scale----YbB_6, mjr.; YbB_{100}, mnr.; YbB_{12}, mnr.	C-3187
							Vapor deposit--YbB_6, mjr.; YbB_4, mnr.	C-3196
1YAM	YB_6, mjr. YB_4, mnr. YB_{12}, tr.	C-2898	(2250)	108	20		Inner core-----YB_6 and YB_4, eqc.	C-3200
							Outer scale----YB_4, mjr.; YB_6, mnr.	C-2911
								C-3205
							Vapor deposit--YB_6, mjr.; YB_4, mnr.	D-1690

In the case of La, Ce, Pr and Nd, the vaporization of samples containing tetraborides produced sample cylinders with outer scales of hexaboride from which single crystals of hexaboride of about 0.5mm. length protruded. The inner cores of the pellets either had increased somewhat in hexaboride content or had remained unchanged in composition from the starting material. Mixtures of Gd, Tb, Dy and Y tetra- and hexaborides, when heated until appreciable vaporization had occurred, produced a layer of the tetraboride phase on each pellet. Protruding from this layer were small single crystals of tetraboride. Again the pellet core was either unchanged in composition or richer in tetraboride. For a YbB_6-YbB_{12} initial composition the resulting layer contained a phase mixture of YbB_6 and YbB_{100} with a trace of YbB_{12} present. Even though the hexaborides are ten to twenty percent more dense than the tetraborides, there was no visible evidence of spalling of the hexaboride layers or cracks in the tetraboride layers. The thickness of these insulating layers varied from one percent of the cylinder cross section to half the cross section radius, depending on the length of time and the temperature of the heating and on the lanthanide. The layer boundaries were quite apparent from the change in color from blue to gray.

4. 1. 4 Interpretation

4. 1. 4. 1 General Considerations.

The formation of a product layer of different composition from that of the bulk of the sample, a layer which completely covers the vaporizing solid as is found in the present work, could significantly retard the rate of vaporization. Even in congruent evaporation, where layer formation is absent, the rate of

free evaporation could be less than the rate of vaporization under closed-crucible or saturated-vapor conditions. A discussion of the associated kinetic problems is worthwhile.

Under equilibrium conditions in a Knudsen crucible, the rate limiting process in vaporization is the impingement on and escape through the crucible orifice (cf. Chapter 6. 3. 3) of the gaseous species in equilibrium with the solid. However, in the case of an infinitely large orifice, as in free evaporation experiments, the gas phase might be removed faster than it can be regenerated by decomposition of the solid. Then the rate limiting step may be any of a variety of processes in the mechanism by which the condensed structure decomposes on vaporization. It is clear that the rate limiting step in these Langmuir experiments is a process other than simple evaporation of gaseous species from the surface.

In the Langmuir theory, discussed in Chapter 6. 3. 1, one of the factors which has to be determined or a value of unity assumed is the evaporation coefficient. This coefficient is the manifestation of a non-equilibrium rate of escape of potential vapor species into the gas phase. Studies of the factors which contribute to a coefficient value different from unity are fundamental to appreciating the problems in determining equilibrium quantities from kinetic processes and to appreciating the general problems of surface chemistry.

There are at least two processes which could account for the behavior of La, Ce, Pr, Nd and Yb borides. The observation of hexaboride layers forming on the pellet, the boundaries of which move inward in the pellet, could be explained by a vaporization process limited by migration of metal to the surface or by movement of boron atoms toward the center of

the pellet. Similarly, the behavior of Gd, Tb, Dy and Y borides could be explained by rate limiting steps of metal movement toward the center of the pellet or by boron movement to the pellet surface.

It is not the intention of this work to define the vaporization mechanism, but to define the processes by which these borides vaporize under equilibrium conditions. It is sufficient to note that the product boride on vaporizing mixtures of hexaboride and tetraboride for the metals, La, Ce, Pr and Nd, was hexaboride; and that the product boride for similar mixtures of Gd, Tb, Dy and Y was the tetraboride. The product in the YbB_6/YbB_{12} mixture was YbB_{100}. Thus, even though these experiments are not equilibrium vaporization experiments, the interpretation of the vaporization processes is reliable.

The clear definition of phase boundaries, the absence of solid solution, the absence of spalling or cracking of layers, the availability of seventeen Group IIIB metals of widely different size and volatility, and the convenience of the experimental techniques, should provide a wonderful opportunity for future investigation to establish the factors influencing the vaporization mechanism and the vaporization kinetics for these borides.

4. 1. 4. 2 La and Ce. The final product in both the La and Ce boride vaporizations was the hexaboride (cf. Table 4. 1). While the disappearance of tetraboride in favor of a hexaboride product implies preferential loss of metal to the gas from the tetraboride, another explanation must also be considered because metal apparently was formed in two of the three experiments.

The X-ray pattern from experiments 6LaAm1 and 1CeAm showed small amounts of sesquioxide along with the hexaboride taken from the surface. Thus, lanthanum or cerium metal was probably present with the hexaboride in the vaporization residue. The metals are quite reactive with oxygen in the atmosphere at room temperatures. Indeed, the product of 6LaAm1 was observed to change texture from a purple-gray coherent body to a finely-divided low-density powder in a matter of a few hours on exposure to air.

The presence of metal in the product could be explained by the incongruent melting of LaB_4 or CeB_4 to the hexaboride and liquid metal followed by quenching and slow back reaction to tetraboride. Johnson and Daane (25) demonstrated incongruent melting of LaB_4 at 1800°C. Brewer, Sawyer, Templeton and Dauben (138) believe CeB_4 melts incongruently above 2000°C. The experimental temperatures in 6LaAM1 and 1CeAM were above the tetraboride melting temperatures. The presence of CeB_4 in the core of 1CeAM after heating above the CeB_4 incongruent melting temperature can be explained by a slower temperature drop on quenching in the pellet core than at the surface, allowing back reaction of metal and hexaboride to CeB_4 to occur.

While the incongruent melting of LaB_4 and CeB_4 does explain the presence of metal, it does not account for the appreciable weight loss during the vaporization experiment. The presence of CeB_6 in the vapor deposit of 1CeAM indicates vaporization of both metal and boron. While preferential loss of metal gas from the tetraboride is not precluded, the vaporization process in these two experiments is not clear. However, the disappearance of LaB_4 in favor of LaB_6 and the absence of metal in the product in experiment 6LaAM indicate preferential loss of lanthanum gas

from LaB_4 to a hexaboride product, and probably imply a congruently vaporizing hexaboride. The behavior of cerium is probably identical to that of lanthanum.

4. 1. 4. 3 Pr and Nd. The starting material in 1PrAM, Table 4. 1, was a mixture of PrB_6 and PrB_4. The final product after vaporization was PrB_6. Thus, PrB_4 loses metal to the gas to form a PrB_6 residue, which vaporizes congruently.

In the three Nd experiments of Table 4. 1 the initial and final product was hexaboride. This observation implies congruent vaporization of NdB_6. The observation reported in Table 4. 1 of the coexistence of ZrB_2, ZrB_{12}, NdB_6 and NdB_4 at the ZrB_2/NdB_6 interface would lead one to believe that NdB_6 reacts with ZrB_2 to form NdB_4 and ZrB_{12}. However, in Table 3, an unsuccessful attempt to cause reaction between NdB_6 and ZrB_2 in the arc-melter was reported. In view of this interaction test and the failure to observe ZrB_2 interaction in any other experiment, the observation in Table 4. 1 is not given much weight.

4. 1. 4. 4 Yb. The starting material in the ytterbium free evaporation study (3YbAMa) was a mixture of YbB_6 and YbB_{12}. The final product on the surface of the pellet was a mixture of YbB_6, YbB_{12} and YbB_{100}. This observation implies preferential loss of metal from YbB_6 and YbB_{12} to form a YbB_{100} residue.

The coexistence of three condensed phases in the product is difficult to interpret. No melting was observed. Microscopic examination of the pellet cross section did not define separate layers of YbB_6, YbB_{12} and YbB_{100} because of the infinitesimal thickness of the outer scale.

Certainly a kinetic explanation of the presence of three condensed phases must be involved.

One reasonable explanation can be found in the following scheme. Initially, the process in equation 1. 4 (loss of Yb(g) from YbB_6) occurred at the surface. As more ytterbium was required, the YbB_{12} layer increased until the surface activity of Yb was decreased to that in the process,

$$100/12\ YbB_{12}(s) = YbB_{100} + 88/12\ Yb(g)\ . \qquad (4)$$

At the YbB_{12} critical thickness, YbB_{12} decomposed to YbB_{100} at the surface. In the steady state, the outer layer was YbB_{100}. Just under this was a YbB_{12} layer, then the core of the cylinder, which contained YbB_6 in major amounts with smaller amounts of YbB_{12}. Material scraped from the surface of such a sample would show YbB_{100}, YbB_{12} and YbB_6 on X-ray analysis. Since the metal content of YbB_6 is high relative to YbB_{12} and YbB_{100}, its enhanced X-ray scattering would make the apparent YbB_6 content seem higher than it actually was. The critical thickness of YbB_{12} was probably quite small, explaining its low concentration in the layered structure.

4. 1. 4. 5 Gd, Tb, Dy and Y. Mixtures of hexaboride and tetraboride in samples 81GdAMa1 to a10, 15-50GdAM, 15-50GdAM2, 1TbAM2, 2TbAM, and 3DyAMa (cf. Table 4. 1) were the starting materials in all these experiments. In every case the residue was tetraboride, indicating preferential loss of boron gas from the hexaboride and probable congruent tetraboride vaporization. In samples 80GdAM1, 80GdAM2 and 741TbAM the initial and final products both were tetraborides, confirming congruence of tetraboride vaporization.

Experiment 770GdAM was an attempt to approach GdB_4 by vaporization of excess metal from a metal-rich starting material. The temperature

of the experiment exceeded the gadolinium melting point. At this relatively low temperature, vaporization was not appreciable. On exposure to the atmosphere, the metal reacted partially with oxygen to form Gd_2O_3. The experiment demonstrated that GdB_2 does not exist at these temperatures.

Sample IYAM contained a mixture of YB_4, YB_6 and YB_{12} initially and a final product of YB_4 and YB_6 with the concentration of YB_4 much higher than in the starting mixture. No YB_{12} was observed in the product. These observations imply preferential loss of boron gas from YB_{12} and YB_6 to YB_4, which probably vaporizes congruently.

4. 1. 4. 6 General Conclusions. With the assumption of the absence of gaseous molecules (cf. Chapter 5), the conclusions reached from this free evaporation survey are these: First, La, Ce, Pr and Nd borides vaporize according to the processes defined in equations 1. 1 (loss of Ln(g) from LnB_4) and 1. 5 (congruency of LnB_6). Second, Gd, Tb, Dy and Y borides vaporize according to the processes of equations 1. 2 (congruency of LnB_4) and 1. 6 (loss of B(g) from LnB_6). Finally, ytterbium probably exhibits the behavior of equations 1. 1 (loss of Ln(g) from LnB_4), 1. 4 (loss of Ln(g) from LnB_6) and 4 (loss of Ln(g) from LnB_{12}) with the hectoboride vaporizing congruently.

4. 2 Knudsen Evaporation Experiments

4. 2. 1 Scope of the Experiments

In order to confirm the validity of the conclusions of the free evaporation experiments, Knudsen evaporation experiments (cf. Chapter 8. 2) in ZrB_2 crucibles were performed on selected portions of the boride residues

of the free evaporation studies. Hexaborides of lanthanum, cerium and gadolinium and hexaboride/tetraboride mixtures of praseodymium and neodymium were vaporized. GdB_4 was investigated in many Knudsen experiments.

4. 2. 2 Experimental

Lanthanum, cerium, praseodymium and neodymium hexaboride-containing samples were obtained from the outer surfaces of the pellets resulting from the free evaporation experiments of Table 4. 1. The GdB_4 samples were portions of the residue of 81GdAMa10 in Table 4. 1. Gadolinium hexaboride, 83GdAM, was prepared according to the technique described in Chapter 2. 2. 2.

The boride powders were placed into a 5/8" diameter, outgassed, tared, ZrB_2 crucible fitted with a tared ZrB_2 lid, in which a 1mm. cylindrical orifice had been drilled. This crucible (cf. Figure 8. 4) was enclosed in a graphite outer crucible, mounted on a tantalum tripod on a quartz semi-kinematic table, surrounded by a tantalum heat shield and encased in a glass vacuum assembly similar to Figure 8. 3 and capable of evacuation to a pressure of 5×10^{-7}mm. The crucible was heated by induction and the temperature determined from a calibrated optical pyrometric sighting of a black-body hole in the bottom of the graphite crucible. The lid was a few degrees cooler than the base of the crucible. Thus, lid deposits could be examined. After appreciable material was thought to have vaporized, the apparatus was disassembled and the deposits on the ZrB_2 lid and the residues were analyzed by X-ray diffraction and microscopy for the phases present. Melting of the crucible or contents was not observed in any of these experiments.

These experiments are summarized in Table 4. 2. The columns in Table 4. 2 are self-explanatory except for columns four and seven. Column four lists the initial total weight in milligrams of the sample in the crucible of column three. Column seven contains the sample weight loss in milligrams. The difference in the weight of the ZrB_2 crucible base with its contents before and after the experiment was corrected for the weight loss on vaporization of the ZrB_2 base during the experiment, which was obtained by the difference in initial and final empty crucible weights. Thus, the weight loss of column seven represents the weight of lanthanide boride lost from the base of the ZrB_2 crucible to the ZrB_2 lid, the graphite outer crucible, or the vacuum apparatus during the heating period.

4. 2. 3. Results

None of the kinetic problems noted in Chapter 4. 1 was observed in these experiments. No layered structures were observed on the sample granules after appreciable vaporization had occurred. In addition, no lattice parameter variation was observed for any of the borides involved, implying univariant vaporization conditions.

Initial samples of LaB_6, CeB_6 and PrB_6 did not change solid composition while producing appreciable lid deposits of hexaboride. The NdB_4/NdB_6-mixture heating was inconclusive because of insufficient material transport. In many experiments, GdB_4 was observed to vaporize congruently with very large weight losses. Experiment 769GdAM demonstrated that GdB_6 lost boron to the gas phase preferentially on heating, leaving a GdB_4 residue.

No interaction of these samples with the ZrB_2 crucibles was observed. In the lanthanum hexaboride heating, a deposit of LaB_6 was ob-

TABLE 4. 2

Knudsen Evaporation Experiments in ZrB_2 Crucibles

Sample	Initial Phase Content	Crucible	Initial Weight (g.)	Temp. (°C.)	Time (min.)	Weight Loss (g.)	Residue Phases	Film	Lid Deposit	Film
6LaAM2	LaB_6 (6LaAM)	ZrB_2-4	0.17990	2070	63	0.05723	LaB_6 only	D-1913	LaB_6 only	C-3115
863CeAM	CeB_6 (1CeAM)	ZrB_2-4	0.10178	2000	80	0.01848	CeB_6 only	C-3119	CeB_6 only	C-3112
1PrAMb	PrB_6, mjr. PrB_4, tr. (1PrAM)	ZrB_2-1	0.03790	2080	16	0.01553	PrB_6 only	C-3014	PrB_6, mjr. ZrB_2, mnr. PrB_4, tr.	C-3012
7NdAMb	NdB_6, mjr. NdB_4, tr. (7NdAMa)	ZrB_2-1	0.05030	> 1850	15	0.00121	NdB_6, mjr. NdB_4, tr.	C-2939	no identification	
835GdAM	GdB_4 (81GdAMa10)	ZrB_2-4		1720	27		GdB_4 only	visual	GdB_4 only	visual
843GdAM	GdB_4 (81GdAMa10)	ZrB_2-4		1820	283		GdB_4 only	visual	GdB_4 only	visual
923GdAM	GdB_4 (81GdAMa10)	ZrB_2-2	0.59295	1700-2200	hours	0.48472	GdB_4 only	visual	GdB_4 and ZrB_2	C-3211 C-3215 C-3215a
Knudsen effusion sample										
937GdAM	GdB_4 (81GdAMa10)	ZrB_2-4	1.41175	1700-2200	hours	0.66547	GdB_4 only	visual	GdB_4 only	C-3214
Knudsen effusion sample										

TABLE 4. 2, continued

Sample	Initial Phase Content	Crucible	Initial Weight (g.)	Temp. (°C.)	Time (min.)	Weight Loss (g.)	Residue Phases	Film	Lid Deposit	Film
759GdAM	GdB_6 (83GdAM)	ZrB_2-1	0.24657	1600	70		GdB_6 and GdB_4	C-2863	no identification	

served on the bottom of the graphite lid of the outer crucible at the periphery of its orifice. Apparently, the solubility limit of carbon in LaB_6 was not exceeded under these conditions; otherwise LaB_2C_2 would have been observed (cf. Figure 3. 2, Part I). On the other hand, a similar deposit of GdB_4 on the graphite outer crucible resulted in GdB_2C_2, as expected (cf. Part I).

4. 2. 4 Confirmation of Free Evaporation Observations

All of these equilibrium observations confirm the interpretation of the Langmuir free evaporation heatings above. Because of the square root dependence on the molecular weight in a vaporization experiment (cf. Chapter 6. 3), the rate of escape of boron atoms into the gas is much faster than that of the much heavier metal atoms. It is possible that the boron loss is so highly preferred that a solid phase, which would vaporize congruently under equilibrium conditions, might show a preferential loss of boron to the gas and force the appearance of the next lower solid boride. Further, a solid, which would normally lose metal to the gas preferentially, might be constrained to vaporize congruently. These Knudsen experiments deny that the component activities in the free evaporation experiments have changed sufficiently from equilibrium values for the systems to vaporize by processes different from the equilibrium process.

4. 2. 5 Previously Observed Vaporization Behaviors

The literature contains evidence for the vaporization behavior of these and other lanthanide borides. Eick, in a communication to Leitnaker (133), stated that LaB_6 vaporizes congruently. This behavior is contrary

to the observation by Lafferty (103), who found that LaB_6 loses lanthanum gas preferentially. However, Lafferty's experiments involved vaporization from reactive graphite, tantalum and tantalum carbide substrates, which abstracted boron and released metal gas (133).

Galloway and Eick (117) have studied the vaporization of samarium borides in various Knudsen cells. They concluded that SmB_4, which is difficult to prepare, vaporizes to lose samarium gas and form SmB_6 solid. They further concluded that SmB_6 vaporizes congruently.

As noted above in Chapter 2. 1. 4, EuB_4 apparently cannot be made. Efforts to prepare EuB_4 result in EuB_6, indicating the decomposition of EuB_4 to EuB_6 solid and europium gas in vacuum.

Eick and Gilles (02), on attempting YbB_4 preparation, found only ytterbium and YbB_6. Post, et al. (113), noted difficulty in preparing single-phase YbB_4. This research could not produce YbB_4 without YbB_6 present. These observations indicate that YbB_4 also decomposes to ytterbium gas and YbB_6 solid in vacuum.

Eick and Gilles (139) prepared holmium and erbium borides in molybdenum and tungsten crucibles. They presented evidence for the preferential loss of boron to the gas phase from DyB_6, HoB_6 and "ErB_6." Further, an ErB_4 preparation in this work produced a two-phase mixture of ErB_4 and ErB_{12}, not ErB_4 and ErB_6. Eick and Gilles (02) could not prepare ErB_6 in any manner. Sturgeon and Eick have noted difficulty in preparing ErB_6 (101). These observations indicate that ErB_6 is unstable with respect to ErB_{12} and ErB_4 solids. ErB_{12} probably loses boron to ErB_4 solid.

The uranium-boron system is similar to the erbium-boron system. The phase, UB_6, has not been prepared. Brewer, Sawyer, Templeton and

Dauben (74), Bertaut and Blum (109) and Andrieux and Blum (110) reported that UB_{12} decomposes to UB_4 because of the high boron pressure over UB_{12} above 1500°C.

Magnesium, which has a metal volatility a little higher than that of ytterbium, is lost preferentially from MgB_2 and MgB_6 leaving a final product of MgB_{12} according to Markovsky, Kondrashev and Kaputovskaya (140) and Wright and Walsh.

4. 2. 6 Summary

In summary, the free evaporation experiments, the Knudsen evaporation experiments and the boride preparation experiments indicate congruent vaporization of LnB_6 and preferential loss of metal from the tetraborides for the five lanthanide metals, La, Ce, Pr, Nd and Sm. For four of the metals, Gd, Tb, Dy and Y, the opposite behavior, i. e., loss of boron gas from the hexaboride, is exhibited. The tetraboride, EuB_4, loses europium and has either a congruently vaporizing hexaboride or a hexaboride which loses metal preferentially. The phases HoB_6 and ErB_{12} appear to lose boron gas to tetraboride residues. Their tetraborides probably vaporize congruently. The tetraboride of ytterbium vaporizes with loss of metal gas to YbB_6; and, also, YbB_6 loses ytterbium preferentially to form a YbB_{12} residue. YbB_{12}, in turn, appears to lose ytterbium to YbB_{100}, which either vaporizes congruently or loses ytterbium to elemental boron. These vaporization processes are summarized in Figure 4.

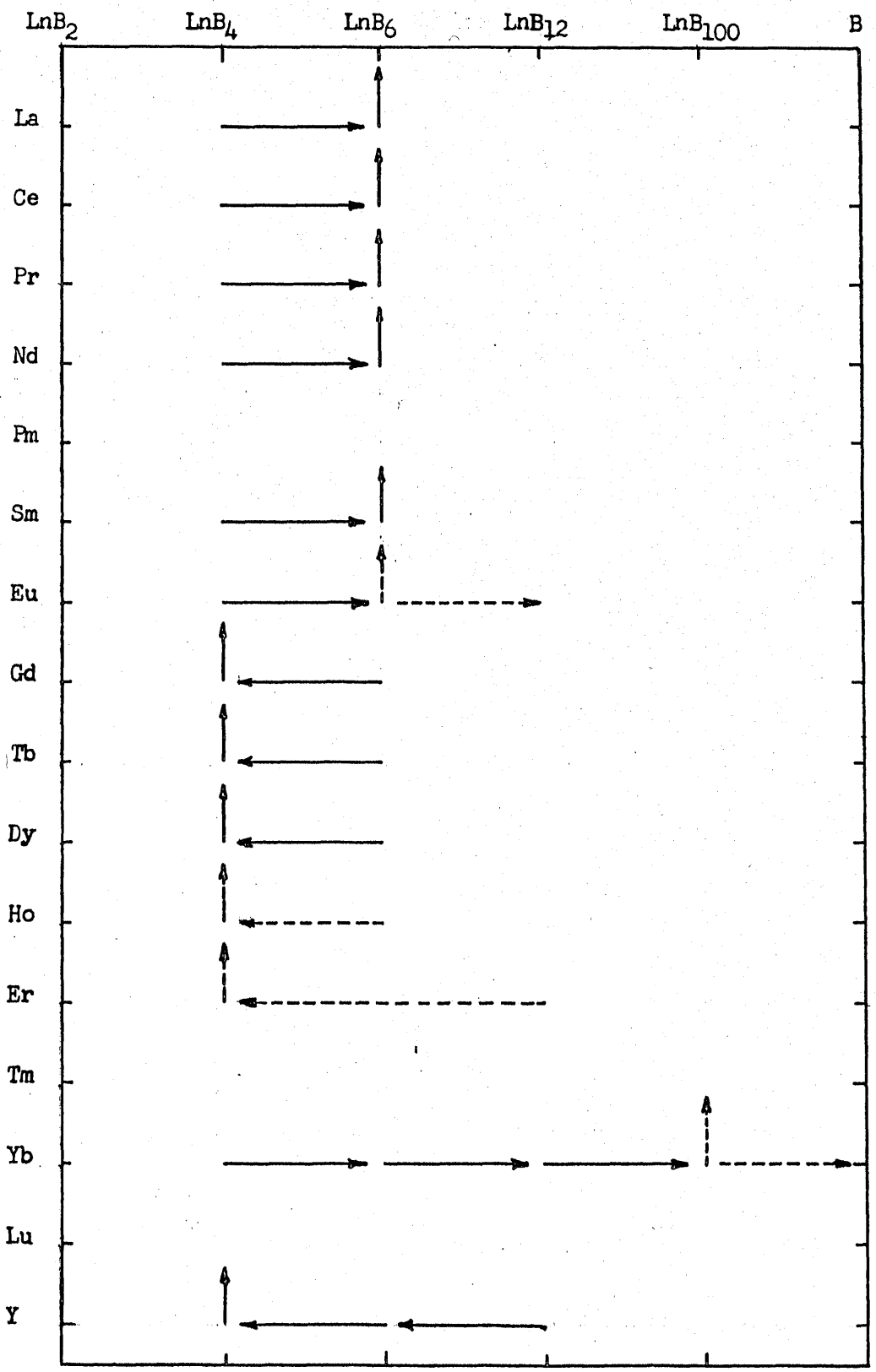

VAPORIZATION PROCESSES OF LANTHANIDE BORIDES

FIGURE 4

CHAPTER 5

GASEOUS SPECIES

5. 1 Background on Gaseous Species Identification

After establishing the vapor and solid composition changes on vaporization of these borides, it is then necessary to identify the gaseous species in order to establish the vaporization reaction. Molecular gas species strongly influence the way that a system vaporizes. Equilibrium pressure measurements cannot be interpreted unless the species exhibiting the pressure are known. For instance, GdB_4 may vaporize congruently in many ways:

$$GdB_4(s) = Gd(g) + 4B(g) \qquad (5.1)$$

$$GdB_4(s) = GdB_2(g) + 2B(g) \qquad (5.2)$$

$$GdB_4(s) = GdB(g) + 3B(g) \qquad (5.3)$$

$$GdB_4(s) = GdB_4(g) \qquad (5.4)$$

$$GdB_4(s) = GdB(g) + 3/2\ B_2(g) \qquad (5.5)$$

$$GdB_4(s) = 1/2\ Gd_2B_2(g) + 3B(g) \qquad (5.6)$$

Which of these processes is most important?

Many indirect methods available for establishing the vapor species are discussed by Gilles (142). Among these methods are the coupling of the pressures measued by transpiration, torsion effusion or Knudsen effusion techniques on the same system to define the average molecular weight

of the gas. Enthalpy changes for each of the possible processes may be estimated and pressures predicted. If the predicted pressures differ widely from the observed pressures, the process suspected may be ruled out. Discrepancy between a Third and a Second Law treatment of pressure data and any unreasonable thermodynamic quantities might imply an erroneously assigned process. Further, emission spectrographic analysis might indicate molecular species. There are, of course, many more methods. But the most direct method to identify gaseous species is with mass spectrometry.

No metal boride gaseous molecule has yet been discovered. The molecule, B_2, was reported by Chupka (143), but is not very important with respect to monatomic boron gas over solid boron at 2500°K. Also, Ln_2 gas is unimportant over lanthanide metal (144, 49). In order to confirm that atomic species alone exist in the gas phase, samples of terbium and gadolinium borides were vaporized in a mass spectrometer and the principal ion currents were determined.

5. 2 Experimental

The mass spectrometer employed in this study was a 12" radius, magnetic, 60° sector, first-order, direction-focusing instrument of the Inghram design (145-6) and was custom built by Nuclide Analysis Associates, State College, Pa. Mixtures of TbB_4 and TbB_6 and of GdB_4 and GdB_6 were vaporized in tungsten effusion cells heated by electron bombardment. Samples of GdB_4 were vaporized from a ZrB_2/C crucible (cf. Figure 8. 4). Temperature was determined by a pyrometric sighting on a black-body hole in the side or base of the crucible. By moving a shutter between the orifice of

the crucible and the ionization region, any mass escaping from the crucible can be distinguished from background at that mass. This procedure is called a shutter check. The temperature range investigated was 1300 to 2200°C.

5. 3 Results

Shutter checks of B_2^+, Tb_2^+, Gd_2^+, TbB^+, GdB^+, TbB_2^+, GdB_2^+, GdB_3^+, GdB_4^+, GdB_6^+, $Tb_2B_2^+$, $Gd_2B_2^+$, Gd_3^+, Tb_2B^+ and Gd_2B^+ were all negative. Excellent positive shutter checks on Tb^+, Gd^+, B^+, Tb^{++} and Gd^{++} were obtained. No other appreciable ion currents were observed except those which represent the normal background in a typical mass spectrum. The limit of detection with the electron multiplier and low background was about 1/1000 of the principal sample peak intensity. Therefore, the lanthanide borides vaporize according to net processes involving gaseous atomic species only.

CHAPTER 6

THEORETICAL BACKGROUND FOR MEASUREMENT AND TREATMENT OF PRESSURES

6. 1 Phase Rule

When the numbers of phases and components present fix the variance of the system at one, at each temperature there will be a unique pressure and composition. For example, univariant conditions exist for the loss of boron from GdB_6 to form GdB_4. There are three phases and two components. Thus, there is only one degree of freedom for the system. Then the boron pressure is fixed when the temperature is fixed. In the case of congruent vaporization, the vapor composition and the solid composition are the same. Thus, even though there are only two phases and two components, the additional composition restraint still establishes unit variance. Consequently, pressure is a function of temperature only. Measurement of the pressure as a function of temperature under univariant conditions will provide thermodynamic information about the equilibrium studied (cf. Chapter 6. 4).

6. 2 Temperature Measurement

By matching the brightness of a filament in a temperature-calibrated potentiometer circuit with the brightness of a black-body hole drilled into the crucible, a precise temperature may be ascertained. Temperatures in these experiments were determined by Leeds and Northrup

vanishing-filament optical pyrometer, P-3, serial number 1157029. The background principles in optical pyrometry are discussed by Kostkowski and Lee (147).

The pyrometer used in these experiments was calibrated by the National Bureau of Standards, test no. G-24953b, and also calibrated against another NBS-calibrated pyrometer (ser. no. 723042, test no. G-26364) by the observation of the brightness of a tungsten band lamp with both pyrometers. The calibration temperature range was 900 to 2200°C. The differences in the two calibrations were usually less than three degrees and never more than six degrees.

When a sighting was made through a prism and window in the vacuum assembly, a correction for the brightness attenuation may be made with the relation,

$$1/T_o - 1/T_t = 1/C, \qquad (6.1)$$

where T_o is the true temperature in the black-body hole, T_t is the apparent temperature on the pyrometer scale, and C is a constant determined experimentally by sighting on a tungsten band lamp with and without optics at several temperatures.

It is believed that the error in pyrometer calibration, compounded by the error in calibration of optics and the error in the actual experimental observations, would not exceed a total temperature error of about ten degrees. While temperature observations were taken often and were reproducible to two or three degrees during the vaporization experiments, drifts in the power output of the induction furnace caused a slow

temperature drop with time, which was corrected after an average three degree drop by increasing the power output of the induction heater.

6. 3 Pressure Measurement

Pressure measurement in the range 10^{-11} to 10^{-3}mm. is discussed briefly by Bockris, White and Mackenzie (148). The techniques employed in this work all depend on the measurement of a kinetic property of ideal gas flow, which can be interpreted in terms of equilibrium pressures in equilibrium systems. The three experimental methods employed to measure pressures in this work are the Langmuir effusion, the mass spectrometric and the Knudsen effusion techniques.

6. 3. 1 Langmuir

The Langmuir technique (149) involves the measurement of the rate of evaporation into a vacuum and uses the expression,

$$p_L = W\, T^{1/2} / \alpha\, 44.33\, a\, t\, M^{1/2}, \qquad (6.\ 2)$$

where W is the weight loss from the sample in grams, M is the molecular weight of the effusing species, a is the total surface area of the sample in cm^2., t is the total time in seconds, T is the absolute temperature of the experiment, p_L is the pressure in atmospheres and α is the evaporation coefficient.

The evaporation coefficient is defined as the ratio of the actual evaporation rate to the absolute evaporation rate characteristic of the material under equilibrium conditions. It is normally assumed that this coefficient is unity and the rate limiting step on vaporization is deter-

mined by the simple desorption from the solid surface of activated potential gaseous species into the vacuum. Since the sample is not enclosed in a crucible in Langmuir experiments and since vaporization occurs into a vacuum, it is possible for other processes to be rate limiting, as in Chapter 4. 1. 4. Then this coefficient is not unity and usually is not known. Further, the temperature dependence of α is not known. Therefore, neither Second Law nor Third Law treatments (cf. Chapter 7. 4) can be applied to the measured evaporation rate if α is not unity.

The definition of the temperature in equation 6. 2 is difficult. The temperature required is the surface temperature. Without a knowledge of the characteristic emissivity for the sample, temperature must be observed from a black-body hole below the surface. This temperature may be quite different from the surface temperature. Further, the energy exchange on interaction of gases with condensed surfaces has led Knudsen (150-1) to postulate a thermal accommodation coefficient, which accounts for a temperature difference between the condensed surface and the gas.

A definition of surface area strictly is not composed simply of the flat area calculated from the gross dimensions of the sample. The evaporating area is composed of all the microscopic topographic area.

Congruent evaporation in a Langmuir experiment requires that the composition of the escaping gas be the same as the condensed phase composition. Since the rate of escape of a particular species varies inversely with $M^{1/2}$, the pressure (calculated from equation 6. 2) of metal and of boron will not be in the same ratio as the evaporating condensed phase, but will exhibit a ratio adjusted by their $M^{1/2}$ values.

In the weight loss measurements on GdB_4 in Chapter 9 the Langmuir equation 6. 2 was used with the assumption of unity for the evaporation coefficient. To interpret weight loss data in terms of gadolinium and boron pressures, the following relations are derived on the basis of the congruent vaporization of one mole of GdB_4.

$$W_{Gd} = \left[M_{Gd}/(M_{Gd} + 4.00M_B)\right] W , \qquad (6. 3)$$

and

$$W_B = \left[4.00M_B/(M_{Gd} + 4.00M_B)\right] W_T. \qquad (6. 4)$$

Substitution of equations 6. 3 and 6. 4 into 6. 2 produces the relations,

$$p_{Gd} = M_{Gd}^{1/2}\, T^{1/2}\, W_T/\, 44.33\ a\ t\ (M_{Gd} + 4.00M_B) \qquad (6. 5)$$

and

$$p_B = 4.00M_B^{1/2}\, T^{1/2}\, W_T/\, 44.33\ a\ t\ (M_{Gd} + 4.00M_B). \qquad (6. 6)$$

The solution of equations 6. 5 and 6. 6 for p_B reveals the relation between p_B and p_{Gd} for this process:

$$p_B = 4.00p_{Gd}\ (M_B/M_{Gd})^{1/2}. \qquad (6. 7)$$

If the evaporation coefficient, α, is not unity, the boron and gadolinium pressures calculated from this treatment will be lower than the equilibrium pressures. A non-unity evaporation coefficient was indeed observed in this work (cf. Figure 13).

6. 3. 2. Mass Spectrometer

Mass spectrometry provides a tool for analyzing the vapor from a Knudsen cell for both its mass and intensity distributions. One asks the question, "What is the relation between the ion current produced at a mass spectrometer detector and the equilibrium pressure of a species in a Knudsen cell below the mass analyzer?" From electron impact and kinetic principles, $I_i^+ \propto c_i t_i \sigma_i$ at constant ionizing electron energy. The ion current for the ith species is given by I_i^+; c_i is the number of i molecules passing through the ionizing region per unit time per unit area; t_i is the average residence time of the molecules in the ionizing region; and σ_i is the fraction ionized. The residence time is given by $t_i = \frac{l}{v_i}$, where v_i is the velocity of the neutral molecules and l is the length of the ionizing region. Kinetic energy is given by $1/2 m_i v_i^2 = A\ k\ T$, for thermal energies. Thus, $v_i \propto (\frac{T}{m_i})^{\frac{1}{2}}$. Hence, $I_i^+ \propto c_i\ (\frac{m_i}{T})^{\frac{1}{2}}$, where m_i is the mass of an i molecule. Now from the Knudsen theory, the rate of escape of species i from a Knudsen crucible is given by $c_i' = p_i/(2\pi m_i kT)^{\frac{1}{2}} \propto p_i/(m_i T)^{\frac{1}{2}}$, where c_i' is the number of i molecules leaving the crucible per unit time per unit orifice area; p_i is the equilibrium pressure over the condensed phase in the crucible; and m_i is the mass of an i molecule. The fraction of effusate passing through the ionizing region is defined by the geometry of the system and is a constant. Hence, $c_i \propto c_i'$. Therefore, $I_i^+ \propto \sigma_i\ p_i/(m_i T)^{\frac{1}{2}} \cdot (m_i/T)^{\frac{1}{2}} \propto \sigma_i\ p_i\ /T$. Finally, $p_i = k'\ \sigma_i^{-1}\ I_i^+\ T$, defines the desired relation between ion current and Knudsen pressure. Similar derivations are presented by Inghram and Drowart (152), by Chupka and Inghram (153) and by Drowart and Goldfinger (154).

This relation is described in its more usual form in equation 6. 8.

$$p_i = K I_i^+ T_i / \sigma_i \gamma_i n_i. \qquad (6.\ 8)$$

The quantity, I_i^+, is the measured ion current for the ith species; T is the absolute temperature of the sample; σ_i, the cross section, is the fraction of vapor species, i, ionized from a particular charged state or a neutral state to another particular charge on passing across the electron gun; γ_i, the multiplier efficiency, is the number of secondary electrons formed on the first dynode stage of the electron multiplier on impact of each ith species ion at a particular accelerating potential; n_i is the fractional abundance of the particular isotope to all isotopes of the ith species; p_i is the pressure of the ith species; and K is a machine constant characteristic of the magnet radius, source and collector defining slit widths, Clausing and distribution corrections on the effusion from the Knudsen crucible, Knudsen cell orientation with respect to the source slit and other geometric considerations.

Absolute values for σ_i have not been determined, but relative values are available or can be estimated from the data of Otvos and Stevenson (155). Since there is no theoretical or experimental determination of absolute cross sections, unknown pressures must be determined by comparing intensity measurements on the ith species to the intensity of a species, s, of known pressure, for which relative values of σ_i and σ_s are known. Thus,

$$p_s = K I_s^+ T_s / \sigma_s \gamma_s n_s. \qquad (6.\ 9)$$

Dividing equation 6. 8 by equation 6. 9 and rearranging, one derives the relation,

$$p_i = p_s \, (I_i^+/I_s^+) \, (T_i/T_s) \, (\sigma_s/\sigma_i) \, (\gamma_s/\gamma_i) \, (n_s/n_i) \quad . \qquad (6.10)$$

Implicit in equation 6.10 is the assumption that the ionizing potential, machine constant, electron gun current, ionization region temperature, focusing voltages and multiplier characteristics are constant for both sets of measurements. For observations at different electron gun voltages, a correction must be made on p_i according to the expression,

$$p_i = p_s(I_i^+/I_s^+) \, (T_i/T_s) \, (\sigma_s/\sigma_i) \, (\gamma_s/\gamma_i) \, (n_s/n_i) \, (\overline{E_i - A_i}/\overline{E_s - A_s}), \quad (6.11)$$

where E is the electron gun voltage and A is the extrapolated-slope appearance potential determined from a plot of ion current versus electron gun voltage. Changes in the intensities are linear with the regulated electron gun current and can easily be corrected to the same gun current.

If one defines an effective sensitivity constant, which represents the collected charge per effused neutral particle, as

$$S_s^* = I_s^+ \, T_s / \, p_s, \qquad (6.12)$$

equation 6.11 may be simplified to

$$p = \frac{I_i^* \quad T_i}{S_s^*} \quad \frac{(\sigma \gamma n)_s}{(\sigma \gamma n)_i} \quad \frac{(E-A)_i}{(E-A)_s} \qquad (6.13)$$

The quantity, S_s^*, is determined experimentally from any convenient well known pressure-temperature relationship, e. g., the vaporization of silver. The ratio, γ_s/γ_i, may be determined experimentally as the ratio of mul-

tiplier gains for the sth and ith species at constant accelerating potential and multiplier characteristics.

Another calibrating procedure, which has the advantage of not requiring an estimate of the relative ionization cross sections and the multiplier efficiency, arises from the relation (156),

$$S_i = I_i^+/p_i = S_i^*/T, \tag{6.14}$$

and the Knudsen expression for pressure of equation 6.17.

$$S_i = \frac{a\, M_i^{\frac{1}{2}} 0.0585}{W_i} \int_0^t \frac{I_i^+}{T^{\frac{1}{2}}}\, dt, \tag{6.15}$$

and

$$S_i \backsim \frac{a\, M_i^{\frac{1}{2}}\, 0.0585}{W_i} \sum_{k=1}^{\infty} \frac{I_i^+}{T^{\frac{1}{2}}}\, (t_k - t_{k-1}). \tag{6.16}$$

The quantity, S_i, is the sensitivity of the machine in amperes per atmosphere for the species, i. In practice, S_i is determined by vaporizing to dryness a known weight, W_i, of solid, i, through a Knudsen orifice of area, a. During the total evaporation the temperature may be varied, but the intensity and length of time during which a particular temperature was held are measured. If for some reason it is difficult to determine the total weight vaporized of the species whose pressure is to be measured, S_s for some standard such as silver might be determined as in equation 6.16. However, a knowledge of the relative cross sections of species, s and i, would then be required. One must be careful to include Clausing and effusion-distribution geometric corrections in equations 6.15 and 6.16, if vaporization occurs through a non-ideal orifice. The simultaneous meas-

urement of the temperature coefficient on the sample species while determining the ion current-time-temperature sensitivity relationship is another advantage of the calibration procedure of equation 6.16. Thus, Third Law as well as Second Law treatment of the pressure data can be performed (cf. Chapter 6. 4).

The advantages mass spectrometry affords include direct measurement of the vapor composition, continuous partial pressure measurement, very high sensitivity, ionization potential determination, appearance potential and dissociation energy measurement, wide range of pressure, temperature and mass applicability, an understanding of the effect of background gases and crucible materials on mass transport, rapid discovery of net vaporization process, discovery of solid solution effects and recognition of equilibrium conditions.

The principal difficulty in the use of a mass spectrometer for thermodynamic measurements lies in relating the observed ion currents to the partial pressures. Aside from the problem of determining the ionization cross section for a particular species, parent and fragment ions must be recognized and the source of the observed ions characterized. Further, with the electron bombardment heating technique used in most high temperature mass spectrometers (cf. Chapter 8. 3), temperature gradients are quite large and temperature measurement is difficult.

6. 3. 3 Knudsen

From the kinetic theory of ideal gases, Knudsen (150-1, 157-8) derived the following expression relating the rate of effusion of gaseous

species through a small area knife-edge orifice in a crucible to the equilibrium pressure inside the crucible.

$$p_K = W\, T^{1/2} / 44.33\, a\, t\, M^{1/2}. \qquad (6.17)$$

The quantities, p_K, t, W, T and M have the same significance and dimensions as in the Langmuir expression (cf. Chapter 6. 3. 1). However, a is the area of the orifice and not the sample area.

For orifices which are not knife-edged, a geometric correction to p_K must be made because of channeling of the effusate. This correction is called the Clausing correction, W_o (159-60). Further, if the orifice is so large compared to the sample area that the condensed sample cannot vaporize as fast as the vapor leaves the orifice, rate measurements will not indicate the equilibrium pressures. Thus, under these conditions a correction, called the condensation coefficient, must be made on the observed pressures. The form of this correction has been discussed by Motzfeldt (161) and by Carlson, Gilles and Thorn (162).

If one is collecting the effusate on a target rather than determining the weight loss of the sample, a correction must be made which relates the fraction of the total effusate intercepted by the target to the total flux of effusate from the orifice (148). This correction was applied in the Knudsen data and is discussed in Chapter 11. 3 and in Chapter 12. 7. The theoretical significance of the condensation coefficient and of the evaporation and accommodation coefficient is discussed by Knacke and Stranski (163) and by Hirth and Pound (164).

Congruent evaporation in a Knudsen experiment requires that the rate of escape of the components through the crucible orifice be in the

same ratio as that in the condensed phase in the crucible. Necessarily, then, the equilibrium partial pressures in the Knudsen crucible will not be in this ratio, but will deviate by the ratio of $M^{1/2}$ of the species (cf. Chapter 6. 3. 1). In particular, the ratio of the boron pressure to the gadolinium pressure over congruently vaporizing $GdB_{4.00}$ in a Knudsen cell will not be four but 4/3.8.

6. 4 Thermodynamics

6. 4. 1 Second Law

For a system containing a condensed substance and its vapor at equilibrium with each other, the standard Gibbs free energy change is given by

$$\Delta F^{\circ} = -RT \ln K = \Delta H^{\circ} - T \Delta S^{\circ}. \tag{6.18}$$

Rearrangement of equation 6.18 leads to

$$\ln K = -\Delta H^{\circ}/RT + \Delta S^{\circ}/R. \tag{6.19}$$

In the process,

$$GdB_4(s) = Gd(g) + 4\ B(g), \tag{6.20}$$

$$K = a_{Gd(g)} a^4_{B(g)} / a_{GdB_4(s)}. \tag{6.21}$$

Further,

$$K = p_{Gd} p_B^4 \tag{6.22}$$

for pure $GdB_4(s)$ and ideal gases.

Substituting equation 6. 7 into equation 6.22, one derives the relation,

$$K = (4.00)^4 \, (M_B/M_{Gd})^2 p_{Gd}^5 \qquad (6.23)$$

Substitution of equation 6.23 into equation 6.19 yields the relation,

$$\ln p_{Gd} = -\Delta H^\circ/5RT + \Delta S^\circ/5R - \ln (4.00)^{4/5}(M_B/M_{Gd})^{2/5}. \qquad (6.24)$$

It is apparent that a plot of $\ln p_{Gd}$ versus $1/T$ will produce a straight line, if ΔC_p° for the process is zero in the temperature range of interest. The slope of such a curve is proportional to the standard heat of vaporization of $GdB_4(s)$, and the ordinate intercept is proportional to the standard entropy change for the process, both in the temperature range studied. From a knowledge of heat capacity as a function of temperature, these thermodynamic quantities may be obtained at other temperatures. This method of reducing observed temperature coefficient data to thermodynamic entities is called the Second Law Method.

6. 4. 2. Third Law

By definition,

$$F_T^\circ \equiv H_T^\circ - TS_T^\circ. \qquad (6.25)$$

By subtracting a standard enthalpy at some reference temperature, θ, from both sides of equation 6.25 and dividing by the absolute temperature, the relation,

$$\left[(F_T^\circ - H_\theta^\circ)/T\right]_i = \left[(H_T^\circ - H_\theta)/T\right]_i - (S_T^\circ)_i \equiv (\mathrm{fef}_\theta^\circ)_i \ , \qquad (6.26)$$

is established. This relation defines the free-energy-function for a

reactant or product. The coupling of the sum of the free-energy-function for reactants and products produces the relation,

$$(\Delta F_T^\circ - \Delta H_\theta^\circ)/T = \sum_{\substack{\text{prod.} \\ i}} (fef_\theta^\circ)_j - \sum_{\substack{\text{react.} \\ i}} (fef_\theta^\circ)_i = \Delta fef^\circ. \qquad (6.27)$$

Substitution of equation 6.18 into equation 6.27 and rearrangement produces equation 6.28.

$$\Delta H_\theta^\circ = T\,(-R \ln K - \Delta fef^\circ). \qquad (6.28)$$

Substitution for K in terms of the gadolinium pressure produces the relation,

$$\Delta H_\theta^\circ = T\,[-R \ln (4.00)^4 (M_B/M_{Gd})^2 P_{Gd}^5 - \Delta fef^\circ]. \qquad (6.29)$$

The quantity calculated from the measured pressures in the vaporization experiments is the standard free energy change for the vaporization at the temperature of the experiment, as indicated by equation 6.18. If data are available for calculating or estimating absolute entropies for all reactants and products in the process at the temperature of the measurement, then the standard heat of vaporization may be calculated at the temperature of the experiment by equation 6.18. If standard free-energy-functions for the reactants and products may be determined from standard heat capacity and entropy data or from statistical mechanical methods, then the standard enthalphy change for the vaporization may be determined at some reference temperature for each experimental pressure-temperature measurement, as is indicated by equation 6.29. This treatment of experimental data is called the Third Law Method.

These methods and their reliabilities are discussed by Lewis and Randall (70), by Carlson, Gilles and Thorn (162), by Brewer (165) and by Ackermann and Thorn (166). Generally the Third Law treatment is preferred because of the inherent temperature-dependent errors of the Second Law method. Estimates of entropies are often quite good and the free-energy-function lends itself to extrapolation without serious error into temperature regions where heat capacity data are unavailable. Comparison of Second and Third Law enthalpies and entropies and variations of Third Law enthalpies with temperature will provide insight into the errors involved in the experimental measurements.

CHAPTER 7

GdB_4 AND GdB_6 CHEMICAL ANALYSES

Chemical analyses of gadolinium boride samples for both boron and gadolinium were performed on GdB_4 (81GdAM) and GdB_6 (83GdAM) samples after arc melter preparation (cf. Chapters 2. 2. 1 and 2. 2. 2), on the Langmuir GdB_4 residue (81GdAMa10), and on the mass spectrometric GdB_4 residue (81GdAMa11). These analyses were intended to confirm the stoichiometry of these borides, to establish solid solution effects, to confirm the constancy of the vaporizing GdB_4 composition, and to reveal serious reaction, if any, with background gases or crucible.

The analytical technique employed in analysis of the vaporization residues is described in Part I, Chapter 4. 2. The theoretical $GdB_{4.00}$ analysis should be 21.58% B and 78.42% Gd and for $GdB_{6.00}$ should be 71.10% Gd and 28.90% boron. Analyses of the gadolinium boride materials employed in this work are summarized in Table 7. Column one denotes the samples with its analysis number. The digit before the decimal indicates the 100 ml. solution containing the dissolved weight of sample of column two. The digit after the decimal indicates the analysis performed on different aliquots taken from this particular dissolved sample. Lower case letters after this digit indicate multiple boron analyses on the filtrate after precipitating gadolinium from a particular aliquot. Columns three and four contain the weight percent of gadolinium and boron, respec-

TABLE 7

GdB_4 and GdB_6 Chemical Analysis

Sample	Weight (g.)	% Gd	% B	% Total	Composition
Initial GdB_4 Products					
81GdAM-1.2	0.46097	75.24	17.75	92.99	$GdB_{3.43}$
-2.1	.82034	77.92	17.23	95.15	$GdB_{3.22}$
-2.2	.82034	76.46	17.30	93.76	$GdB_{3.29}$
-1.1	.46097	77.14			
		76.69 ± 1.20	17.43 ± 0.20		$GdB_{3.31}$ ± 0.07
Initial GdB_6 Product					
83GdAM-1.1	.39960	69.11	28.00	97.11	$GdB_{5.90}$
-1.2	.39960	70.42	28.72	98.14	$GdB_{5.94}$
-2.1	.36285	70.23	28.97	99.20	$GdB_{6.00}$
-2.2	.36285	68.20	29.18	97.38	$GdB_{6.23}$
		69.49 ± 0.90	28.72 ± 0.44		$GdB_{6.02}$ ± 0.13
Final Langmuir GdB_4 Residue					
81GdAMal0-1.1a	.62608	77.36	18.16	95.52	$GdB_{3.42}$
-1.2a	.62608	78.12	18.30	96.42	$GdB_{3.41}$
-2.1a	.64562	78.33	18.30	96.63	$GdB_{3.40}$
-2.2a	.64562	78.25	18.31	96.56	$GdB_{3.40}$
-1.1b	.62608	77.36			
-1.2b	.62608	78.12	18.08	96.20	$GdB_{3.37}$
-2.1b	.64562	78.33	18.06	96.39	$GdB_{3.35}$
-2.2b	.64562	78.25	18.89	97.14	$GdB_{3.51}$
-1.2	.62608	78.37			
		78.05 ± 0.26	18.30 ± 0.26		$GdB_{3.41}$ ± 0.05
Final Mass Spectrometer GdB_4 Residue					
81GdAMall-2.1	.10625	85.98	26.50	112.48	$GdB_{4.48}$
-2.2	.10625	83.15	29.16	112.31	$GdB_{5.10}$
-2.1a	.10625		33.17		
-2.2a	.10625		32.01		
-3.1	.21104	82.04	25.28	107.32	$GdB_{4.48}$
-3.2	.21104	81.30	24.10	105.40	$GdB_{4.31}$
-3.1a	.21104		31.07		
-3.2a	.21104		32.04		

TABLE 7, continued

Sample	Weight (g.)	% Gd	% B	% Total	Composition
81GdAMall-4.1	0.23200	81.46	23.56	105.02	$GdB_{4.21}$
-4.2	.23200	79.27	24.45	103.72	$GdB_{4.49}$
-4.1a	.23200		31.44		
-4.2a	.23200		31.35		
		82.20 ± 1.90	25.51 ± 1.77*		$GdB_{4.51 \pm 0.29}$
99.5% Amorphous Boron.					
Boron-1.1			94.9		
-1.2			97.9		
-1.3			86.3		
-1.4			89.8		
-1.5			96.4		
-1.6			95.3		
-1.7			92.9		
-1.8			95.7		
-2.1			98.2		
-2.2			98.5		
			94.6 ± 2.5		

*Low analyses (< 30%) only.

tively, with their standard deviations. The total sample accounted for is listed in column five. The atomic composition is contained in column six. These atomic fractions were calculated from the metal and boron weight percents on the same row of the table.

It is obvious from the analyses of the GdB_4 sample before the free evaporation experiment (81GdAM) and after the free evaporation studies (81GdAMal0) that the sample did not change in composition during the ten Langmuir heatings and a 23% weight loss. This constancy of composition supports congruence of GdB_4 vaporization.

One should wonder why the analyses for the 81GdAM and 81GdAMal0 samples display apparent non-stoichiometry? Further, does a total gadolinium and boron content on only 96 to 97% of the samples in 81GdAM and 81GdAMal0 imply a 3 or 4% impurity content? These discrepancies are resolved by low boron analyses. Evidence for the low boron analysis was indicated by analyses performed on the amorphous boron reagent with a manufacturer's assay of 99.5% boron shown in Table 7.

While the average percent return on the boron analyses was 94.6%, analyses as low as 14% were noted. Hence, while the boride analyses were of good precision, the boron weight percent was low. The sum of the average gadolinium and boron weight percents in 81GdAMal0 was 96.35%. This leaves 3.65% of the sample weight unaccounted for. If this deficiency were boron, the atomic ratio of gadolinium to boron would be $GdB_{4.0}$ rather than $GdB_{3.4}$. Hence, the tetraborides in these experiments were assumed pure and stoichiometric.

An analysis of the GdB_4 mass spectrometer residue, 81GdAMal1, is illustrated in Table 7. These analyses were prolonged over a period of

thirty or forty days, during which time the standard NaOH solution and sample solutions were allowed to stand. Obviously, the boron analyses, which vary from 23 to 29%, were too high. More than 100% of the sample was accounted for. These apparently large boron contents arose from the decrease in the NaOH normality because of CO_2 absorption and because of CO_2 entering the sample filtrates after gadolinium removal. However, the gadolinium analyses are thought to be accurate to $\pm$2% in these particular analyses. The generally high gadolinium contents could indicate Gd_2O_3 content before analysis. Gd_2O_3 was observed in trace amounts in this particular mass spectrometer residue. In consideration of the errors in the titrating solution standardization and the Gd_2O_3 content, the composition of the boride really had not changed significantly from the initial composition of the 81GdAMa10 sample used in the mass spectrometric studies. Hence, congruence is again suspected.

While considerable effort was made to establish the variables in the analytical procedure, especially the influence of CO_2, the effect of gadolinium ion on the boron analysis, and the effect of varying the analyst, the boron analyses could not be improved beyond a precision of 0.25% and an accuracy of about $\pm$1% for boron in the boride. The gadolinium analysis was precise and accurate to $\pm$0.5% for gadolinium in the boride. Allowing for the inherent boron deficiency in the tetraboride and in the elemental boron analyses, one concludes that there was no evidence of non-stoichiometry for GdB_4. Therefore, in writing the net process occurring on vaporization, stoichiometry was assumed.

A sample of GdB_6 from an arc melter preparation (83GdAM) was analyzed for gadolinium and boron with the results of Table 7. No vacuum

distillation of oxide materials was performed with this material. The analytical technique was varied somewhat, in that the end-point of the borate-mannitol complex titration with NaOH was determined potentiometrically, rather than with a phenophthalein indicator. Therefore, the higher pH end-point required more standard base and eliminated the necessity to perform a control analysis on a pure boron sample, as was required in the tetraboride analyses. The arc melter preparation showed stoichiometric GdB_6 within the analytical errors with 97 to 99% of the sample accounted for.

The GdB_6 (83GdAM) analyses and GdB_4 (81GdAM) analyses established the ability of the arc melter preparative techniques to prepare pure single-phase boride materials with the X-ray diffraction analysis as the indicating control on the preparation. Further, all these analyses supported the assumption of stoichiometry in gadolinium tetra- and hexaborides and the assumption of fairly narrow solid solution limits.

CHAPTER 8

HEATING APPARATUS

8. 1 Langmuir

Vacuum line number 14, employed in the experiments of Chapter 4. 1 and in the Langmuir pressure measurements on GdB_4 of Chapter 9, is shown in Figure 8. 1. The vacuum train consisted of a liquid nitrogen cold trap below the furnace chamber, behind which was a three stage mercury diffusion pump (GHG-15, Consolidated Electrodynamics Corporation). Backing the diffusion pump was a Welch, Duo-Seal, model 114B, mechanical pump. Low pressure was monitored with a cold cathode ionization gauge (control circuit 3) just above the trap, and forepressure was measured behind the diffusion pump with a thermocouple gauge.

Water-cooled current concentrators, described by Northrop (167) and by Babat and Losinsky (168), are devices to increase the coupling between the sample and the rf work coils, which are outside the vacuum housing. The particular designs used here are adaptations of a design used at the Los Alamos Scientific Laboratory, Los Alamos, New Mexico. Depending on the dimensions of the cylindrical specimen to be heated, concentrators were designed with different bore diameters and heights to heat the specimen as uniformly as possible. A cutaway drawing of a typical current concentrator is shown in Figure 8. 2.

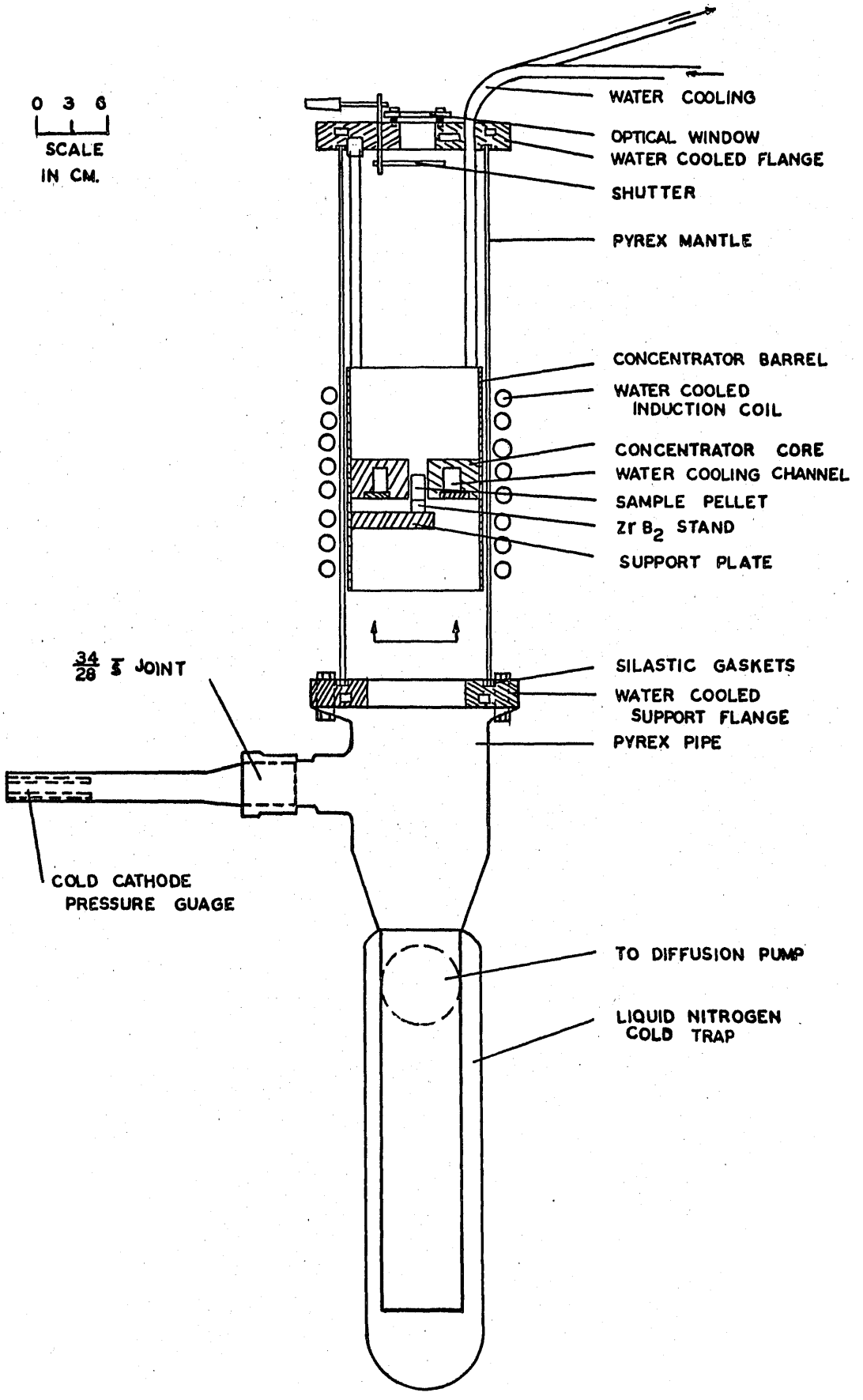

CURRENT CONCENTRATOR APPARATUS

VACUUM SYSTEM #14

FIGURE 8. 1

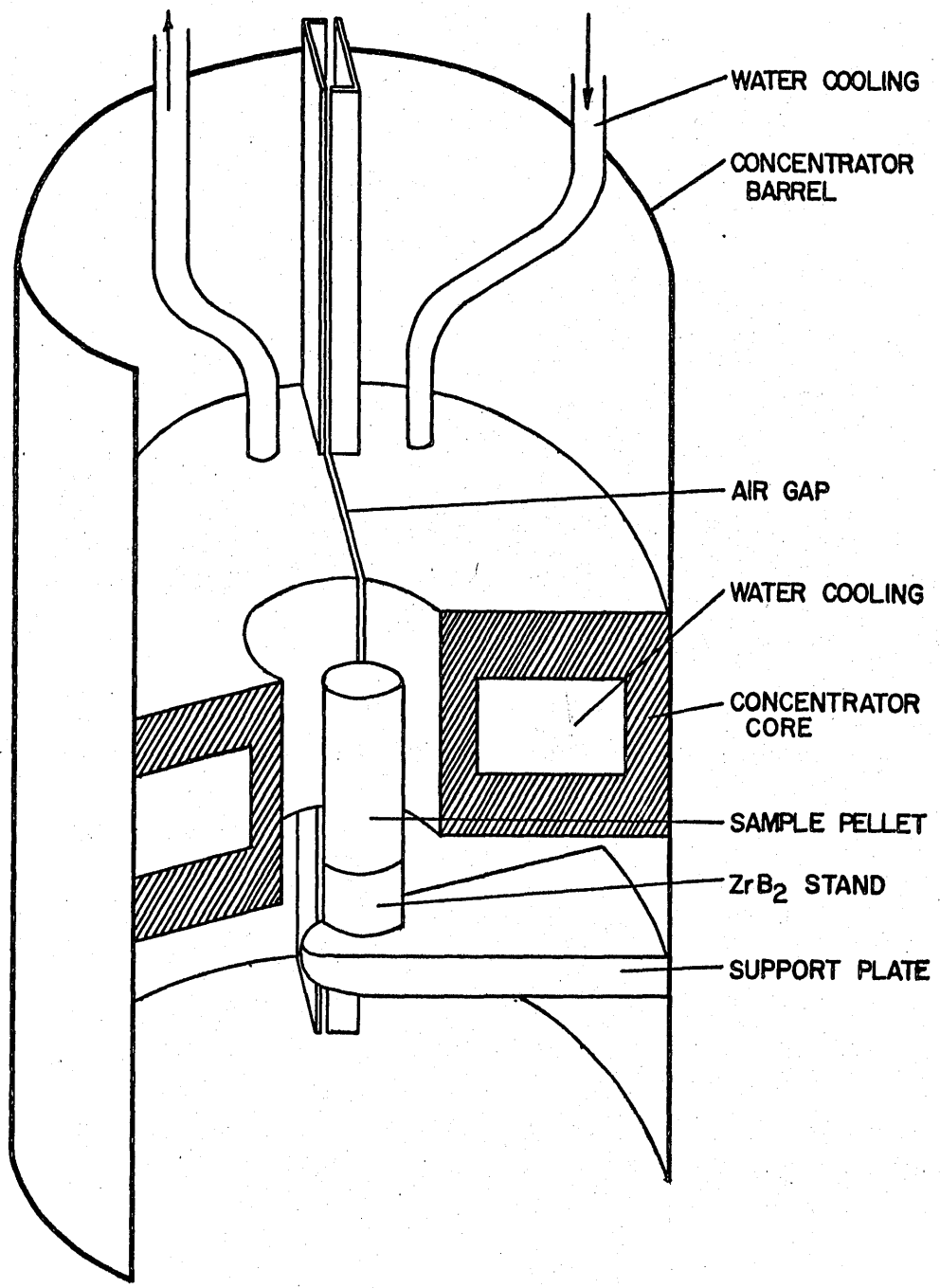

CURRENT CONCENTRATOR FURNACE CORE

FIGURE 8. 2

After the pellet had been positioned on the copper support plate under the concentrator bore, the concentrator was lowered into the Pyrex sheath. This glass envelope was ground at both ends and sat against 1/8" Silastic gaskets (Silastic 50, fully cured, Dow Corning Corporation) in gasket slots in the base plate and in the current concentrator upper flange. Before the assembly operation, Lubriseal Improved Formula grease was applied to the gaskets and the ground ends of the glass to effect a vacuum seal. With this procedure the apparatus could be routinely evacuated to pressures of 10^{-6}mm.

Power was delivered from a 7.5 kw., 400kc., Scientific Electric Company, thyratron-controlled, rf generator to the 4-1/2" diameter, seven-turn work coil, fabricated from $\frac{1}{4}$" copper tubing and surrounding the glass sheath opposite the sample. Temperature was measured by observing with the calibrated optical pyrometer a black-body hole in the sample through a calibrated optical window and prism above the concentrator. A shutter, operable from outside the vacuum assembly, prevented vapor deposit from covering the window between temperature measurements. Temperatures up to 2500°C. could be achieved and regulated manually to within 15°C.

8. 2 Knudsen

Knudsen vapor collection experiments were made on the vapor over GdB_4 in ZrB_2 crucibles with the apparatus of Figure 8. 3, line 11. The Knudsen experiments of Chapter 4. 2 were also performed in this vacuum assembly.

Vacuum was achieved by pumping through a liquid-nitrogen cold trap with a single-stage, divergent-nozzle, mercury diffusion pump of the

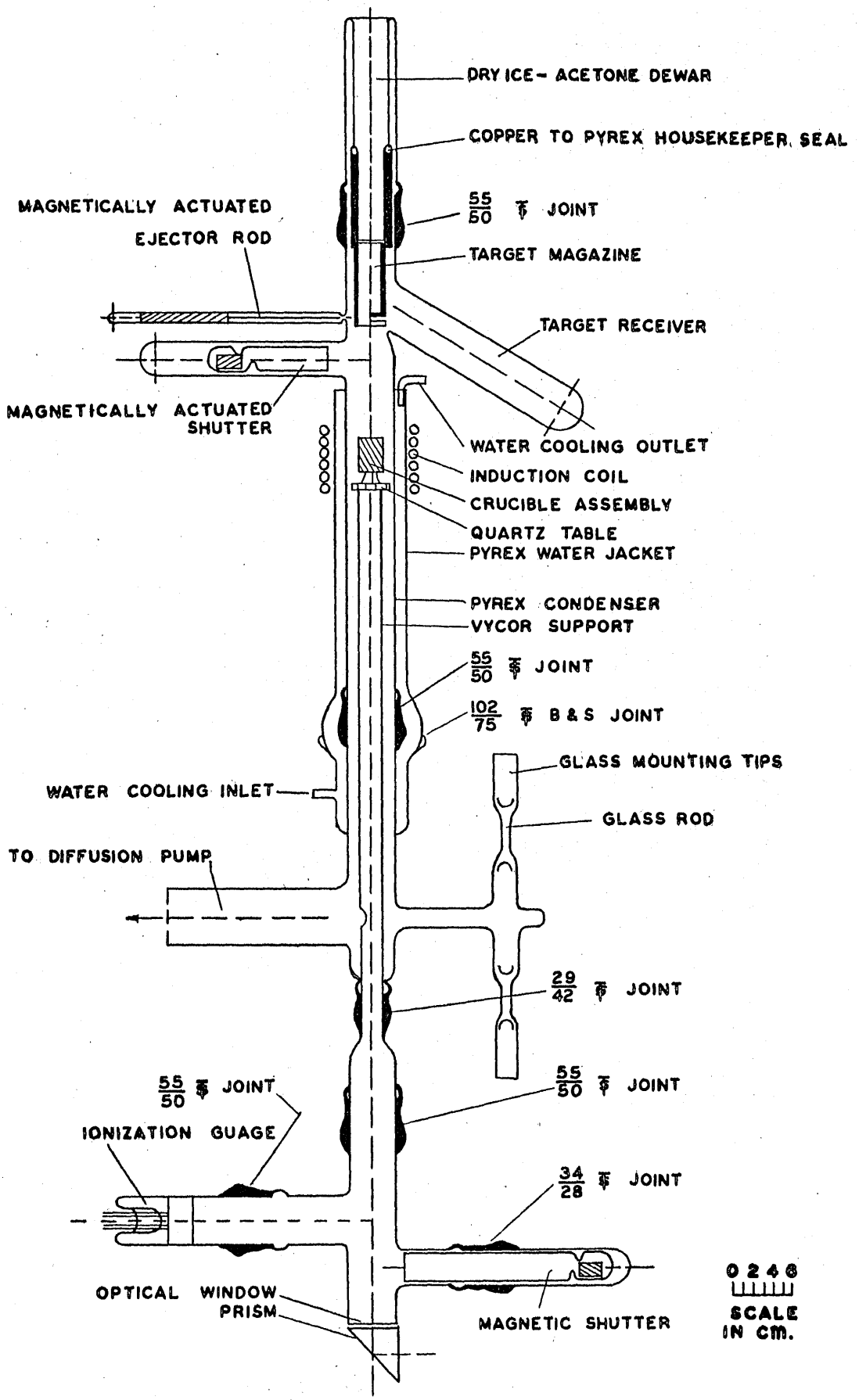

Vacuum Effusion Apparatus

FIGURE 8. 3

"Phipps" type. The system was designed by Dr. P. G. Wahlbeck in this Laboratory. The diffusion pump was backed by a Cenco Megavac forepump. Foreline pressure was measured with a McLeod gauge, and a hot cathode VG-1A ionization gauge in conjunction with circuit DPA-38 was used for measuring high vacuum. With ten hours pumping a pressure of 2×10^{-7}mm. could be attained.

The crucible assembly, illustrated in Figure 8. 4, was employed in all the Knudsen experiments in this work. The characterization of the ZrB_2 material appeared in Chapter 3. 3. 4. Because of the low electrical conductivity of ZrB_2, the power that could be introduced into the ZrB_2 crucible from the induction heater was insufficient to achieve temperatures over 800°C. Hence, a graphite outer crucible was needed to increase the coupling to the induction coil and allow temperatures up to 2100°C. to be achieved. Nowotny, Rudy and Benesovsky (08) have demonstrated that graphite and ZrB_2 will not react with each other. The graphite crucible was machined from 3/4" graphite rod, grade UF-4-S, United Carbon Products Company. The tungsten radiation shield helped decrease the temperature difference between the ZrB_2 orifice and the black-body hole in the graphite base. A tantalum radiation shield enveloping the crucible assembly allowed temperatures up to 2400°C. and improved temperature uniformity in the crucible.

The crucible assembly was placed on a tantalum tripod, surrounded by a tantalum radiation shield and the entire assembly mounted on a quartz semi-kinematic table supported by Vycor glass tubing. Above the crucible was a copper target magazine previously used by Robson (178), cooled by dry ice and acetone, and containing eight to twelve aluminum target disks.

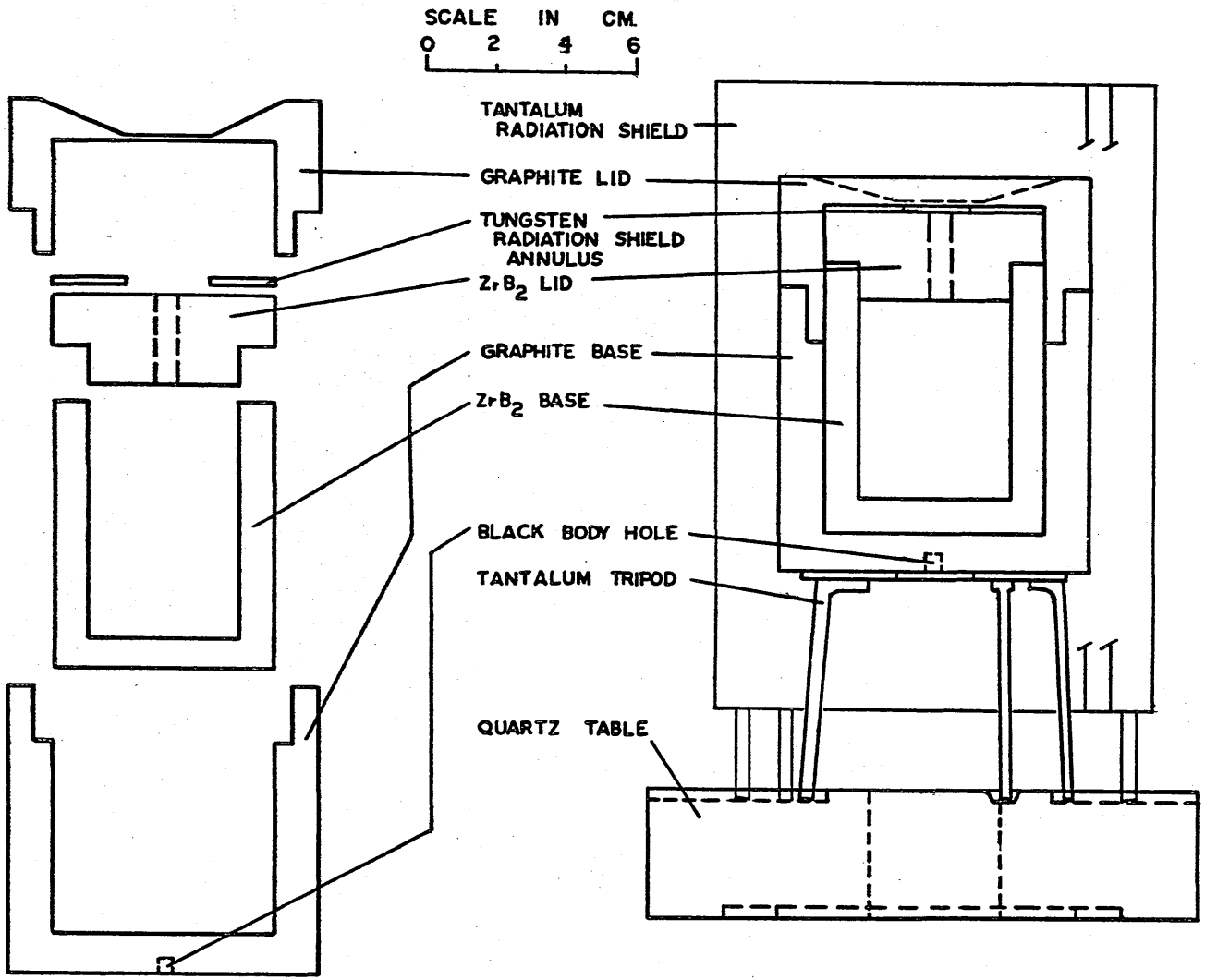

CRUCIBLE ASSEMBLY

FIGURE 8. 4

A magetically-actuated rod ejected exposed targets from the magazine and into a glass target receiver, exposing a fresh target. Effusate was blocked from the target with a magnetically-actuated shutter. All 55/50 joints in Figure 8. 3 were sealed with black wax except that joining the condenser to the base of the vacuum line. This joint, the 102/75 joint and the 29/42 joint were sealed with Lubriseal High Vacuum formula grease. During the heatings, an air stream, directed through a circle of perforated copper tubing, was passed over the joint over the target magazine to prevent black wax from receding from the warm joint. Temperature was observed through a calibrated optical window and prism with the calibrated pyrometer sighted on a black-body hole in the base of the graphite outer crucible.

Surrounding the Pyrex condenser was a Pyrex water jacket through which cooling water flowed upward; surrounding this was a work coil of thirteen turns, three inches in diameter and four inches long and made of $\frac{1}{4}$" copper tubing. Rf power was delivered to the coil from a General Electric Company, thyratron-controlled, 450 kc., 20 kw. generator. The crucible was heated by induction to temperatures up to 2400°C. with manual control always within ten degrees.

8. 3 Mass Spectrometer

In the study of the gas phase over GdB_4, the same graphite-ZrB_2 crucible arrangement as used for the Knudsen experiments was employed (cf. Figure 8. 4). The Nuclide Analysis Associates mass spectrometer, described in Chapter 5. 2, was employed. After the crucible had been mounted onto three tungsten support rods, two 0.003 x 0.030" tungsten filaments were

spot welded through tantalum onto tungsten rods in such a position as to be concentric with the crucible and positioned at one-third and two-thirds the heighth of the crucible. A stack of five concentric tantalum radiation shield cans enclosed the crucible and its heating filaments.

With the use of an alignment jig, the crucible orifice and the hole in the shield cans were aligned with respect to the axis of the mass spectrometer. When this Knudsen assembly had been bolted and sealed through gold gaskets to the mass spectrometer and the system evacuated, AC power (up to 18 amp. at 25 volts) was applied to the tungsten filaments. By radiation alone the crucible could be heated to 1100°C. Temperatures up to 2300°C. could be achieved by applying a positive DC voltage up to 1000 volts to the crucible and heating by electron bombardment. Temperature was measured with the calibrated optical pyrometer by sighting through a shutterable, calibrated, optical glass window below the crucible onto a black-body hole drilled into the bottom of the crucible. By varying the filament power or crucible voltage, temperature could be regulated to within 10°C.

After leaving the furnace region, the molecular beam passed through the jaws of a variable width shutter, through collimating slits and high positive potential fields into the ionization region. Bombardment by electrons with energies up to 70 ev., moving perpendicularly to the molecular beam path, produced ions which were expelled from the ionization region by small positive repeller voltages below the ionization region and by slightly negative drawing out potentials above the ionization region. The ion beam was accelerated through 4500 volts, collimated, and focused before passing through a 0.008" source slit into the magnetic mass ana-

lyzer. After the ion beam passed through the 0.010" collector slit, ion current was detected with either a Faraday cup collector or a sixteen stage Be-Cu electron multiplier. Both currents were amplified with Cary vibrating-reed electrometers whose output was traced on a recorder. Different masses could be observed by changing the magnet current or the accelerating potential.

CHAPTER 9

LANGMUIR PRESSURE MEASUREMENTS ON GdB_4

9. 1 Introduction and Scope of the Experiment

While observations of the principal vaporization processes exhibited by the lanthanide borides provide insight into the relative stabilities of the lanthanide borides with respect to gaseous atoms, it is of interest to determine the actual volatilities of these borides. To simplify this prodigious task the volatility of only one particular boride need be measured.

The heats of vaporization and entropies of the lanthanide metals and of boron are available or can be estimated. A systematic variation in the heats of formation and entropies of corresponding lanthanide borides may be assumed. Hence, a measurement of ΔF^{o} for vaporization of the reference boride to gaseous atoms (volatility) will allow one to determine the absolute stabilities of other corresponding lanthanide borides. The observed principal vaporization processes exhibited by different lanthanide borides, then, provide insight into the absolute stabilities of non-corresponding borides and define the nature of the systematic variation in the heats of formation of the lanthanide borides. These considerations are discussed in detail in Chapter 15.

The compound, GdB_4, was selected for decomposition pressure measurements for four principal reasons. First, it was shown in Chapters 4 and 7 that GdB_4 vaporizes congruently. All lanthanide tetraborides of the lighter lanthanides decompose with preferential loss of metal gas rather than vaporizing congruently. Hence, the vaporization behavior exhibited by GdB_4 represents the point in the lanthanide series where transition to congruence of tetraboride vaporization occurs. Therefore, if one assumes a systematic variation of LnB_4 heat of formation with atomic number, the free energy measured for the congruent process (equation 1. 2) should not be much smaller than that for preferential loss of Gd(g) from GdB_4(s) (equation 1. 1). Thus, the decomposition pressure of GdB_4 to form GdB_6(s) can also be fairly well defined.

Second, the volatility of gadolinium metal represents an intermediate value for lanthanide metals. Third, the metal pressure over the tetraboride is greater than over the hexaboride, providing a higher rate of metal transport on vaporization. Pressure measurement techniques, which monitor the rate of metal transport, are, therefore, more sensitive for tetraboride congruent vaporization than for hexaboride vaporization. Finally, a tetraboride was chosen because of the absence of a complicating solid solution effect. In Chapter 2 it was stated that hexaborides were believed by some authors to show some range of solid solution, whereas tetraboride solid solution was not detectable.

In order to ascertain the volatility of a lanthanide boride, it is necessary to determine the equilibrium metal and boron pressures as functions of temperature under the univariant condition of congruent vaporization (cf. Chapter 6. 1). The methods for determining these pressures

used in this work are the Langmuir effusion technique, the mass spectrometric technique, and the Knudsen effusion technique (cf. Chapter 6. 3).

This chapter describes the measurement of gadolinium pressures over GdB_4(s) by Langmuir weight loss experiments. The gadolinium temperature-coefficient calculation, the equilibrium constants measured and a Third Law treatment of the gadolinium pressure data (cf. Chapter 6. 4) define the standard enthalpy and free energy changes for the congruent vaporization of GdB_4.

9. 2 Experimental

A compacted pellet of GdB_4 (81GdAM), 1/2" diameter by 3/4" high, was mounted on a ZrB_2 stand, 1/2" diameter by 1/4" high, and heated in a 5/8" diameter current concentrator, described in Chapter 8. 1 and shown in Figures 8. 1 and 8. 2, for one-half hour at 2100 to 2200°C. to purge the boride of oxides, borates and hexaboride that might be present in trace amounts. The analysis of this material is discussed in Chapter 7. The resulting gray pellet was sintered, very hard and, although it had shrunk, retained its right-cylinder geometry. Weight loss experiments on this tared pellet, weighing 7.39221 g. initially, were performed, the time, temperature, weight and dimensions of the pellet being recorded before and after each heating. A total weight loss of 23% to a final weight of 5.68549 g. was observed. Temperature was determined by sighting on a 1/16" blackbody hole drilled into the top of the pellet. The vaporizing area was taken as the cylinder area, excluding that lower surface in contact with the ZrB_2 stand. Time was recorded with precision Time-It second meter (Precision Scientific Company, Chicago, Illinois). Timing began when the

power was increased from that power which achieved 1400 to 1500°C. to an arbitrary level at which the experiment was conducted. The time required to achieve the experimental value from a warm-up level was one minute or less. Weight of the GdB_4 pellet was determined with a Mettler Gram-Atic balance (Fisher Scientific Co.) to a precision of 50 micrograms.

9. 3 Results

Assumed in these experiments were the following: First, the vaporization coefficient was unity; second, the black-body temperature was the surface temperature and the thermal accommodation coefficient was unity; third, the vaporizing area was the smooth cylinder area; finally, the vaporizing composition was $GdB_{4.00}$. The actual analyses of the initial and final material in these experiments were identical and not distinguishable from $GdB_{4.00}$ within the experimental accuracy of the analysis. These analyses are shown in Chapter 7, Table 7.

Table 9 contains a summary of the observations in these experiments. Column one identifies the individual successive weight loss determinations on sample 81GdAMa, with the order of the experiments indicated by the final number in the sample designation. Experiment 81GdAMa1 was a sintering to remove residual oxides and shrink the pellet. Experiment 81GdAMa3 was omitted because of poor temperature control. The vaporizing area in all experiments was 2.60 $cm.^2$ except for 81GdAMa2, for which the area was 3.80 $cm.^2$ Column four lists the black-body hole temperatures corrected for pyrometer calibration and transmission of the optics. Sample weight loss data and the time at the experimental temperature are contained in column two and three, respectively.

TABLE 9

Langmuir Effusion Data and Thermodynamic Quantities for GdB_4 Vaporization

Sample	Wt. Loss (mg.)	Time (sec.)	Temp. (°K.)	P_{Gd} (10^{-7}atm.)	-RlnK (eu.)	ΔF_T° (kcal./ 1/5mole)	ΔS_T° 1/5(eu.)	ΔH_T° (kcal./ 1/5mole)	$-\Delta fef^\circ$ 1/5(eu.)	ΔH_{298}° (kcal./ 1/5mole)
81GdAMa4	52.57	8856	2112	1.480	156.65	66.17	32.48	134.77	33.93	137.85
81GdAMa7	30.48	3000	2135	2.547	151.25	64.58	32.45	133.85	33.92	137.02
81GdAMa8	76.81	3244	2233	6.070	142.62	63.69	32.33	135.86	33.84	139.26
81GdAMa10	54.76	3300	2234	4.255	146.15	65.30	32.32	137.50	33.85	140.91
81GdAMa6	106.55	3000	2240	9.119	138.58	62.08	32.31	134.45	33.86	137.37
81GdAMa9	88.86	2180	2300	10.60	137.08	63.06	30.63	133.59	33.81	140.83
81GdAMa5	203.56	1415	2349	37.84	124.44	58.46	30.60	130.25	33.76	137.75
81GdAMa2	375.16	1653	2403	41.30	123.57	59.39	30.56	132.84	33.66	140.28
								avr. 134.2 ± 1.5		avr. 138.9 ± 1.6

$\Delta H^\circ_{2250°K.}$ (Second Law) = 116.4 ± 8.3 kcal./1/5mole

$\Delta S^\circ_{2250°K.}$ (Second Law) = 23.9 ± 3.7 eu.

$$-RlnK = 1.987 \ln\left[(4.00)^4 \left(\frac{M_B}{M_{Gd}}\right)^2 P_{Gd}^5\right]$$

Area = 2.60 cm.^{2} for 81GdAMa4-10

Area = 3.80 cm.^{2} for 81GdAMa2

The gadolinium pressures were calculated according to equation 6. 5 and are listed in Table 9, column five. These data were fitted to a two-parameter least squares reduction process, according to the Second Law discussion in Chapter 6. 4. 1, with an IBM 1620 computer. From the slope of this curve, the Second Law standard heat of vaporization to form one total mole of gaseous atoms according to the process in equation 1. 2 is 116.4 ± 8.3 kcal. at 2250°K. The Second Law temperature coefficient of the gadolinium pressure is graphed in Figure 9. From the ordinate intercept $\Delta S^{\circ}_{2250°K.}$ for the vaporization of 1/5 mole of GdB_4 to the gaseous elements is 23.9 ± 3.7 eu.

Columns six and seven of Table 9 contain -RlnK and ΔF°_{T} calculated from the gadolinium pressures of column five. In view of the absence of heat capacity and entropy data for $GdB_4(s)$, the standard entropy of formation of $GdB_4(s)$ is taken to be zero at the temperatures of the experiments. Using entropies taken from interpolations of the values given in JANAF (69) for B(s) and B(g) and in Stull and Sinke (65) for Gd(l) and Gd(g), and listed in column eight of Table 9, one calculates the heat of vaporization values listed in column nine from the Third Law treatment described in equation 6.18. The average of these values produces a value for the standard heat of vaporization of 1/5 mole of GdB_4 at 2250°K. of 134.2 ± 1.5 kcal.

A Third Law treatment of these data, according to equation 6.29, results in a value of 138.9 ± 1.6 kcal. for $\Delta H^{\circ}_{298°K.}$ (column ten). This value assumes that $\Delta S^{\circ}_{298°K.}$ and ΔC°_{p} at all temperatures for formation of GdB_4 are zero. The standard free-energy-functions for the elements

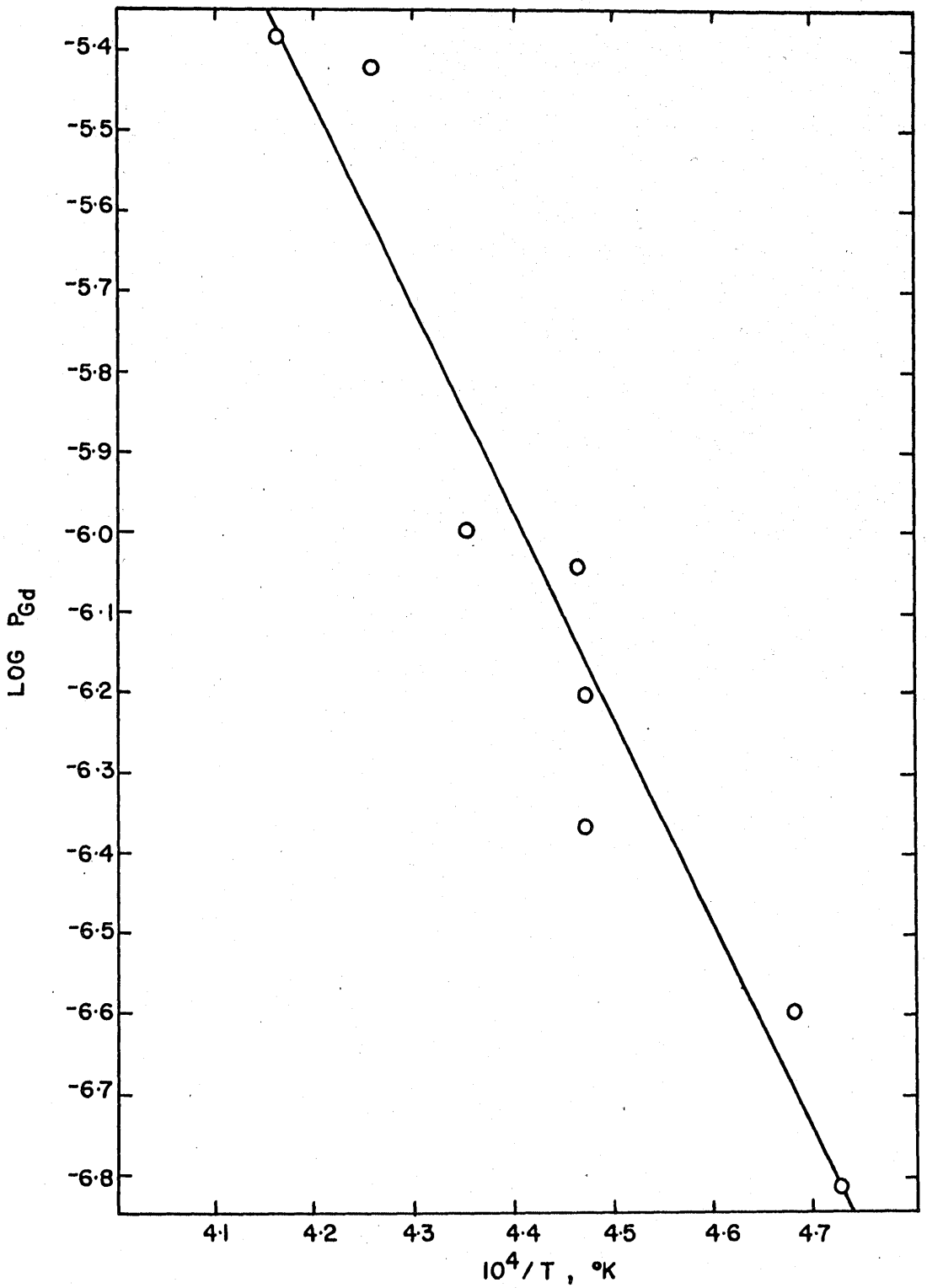

PLOT OF LOG P_{Gd} VERSUS 1/T ; LANGMUIR

FIGURE 9

were interpolated from graphs of the data in JANAF (69) and in Stull and Sinke (65).

CHAPTER 10

MASS SPECTROMETRIC INVESTIGATION OF GdB_4

10. 1 Scope of the Experiments

The mass spectrometric investigation of the vaporization of GdB_4 was performed for several reasons. First, the previous assumption that only atomic species exist in the gas phase over GdB_4 must be confirmed (cf. Chapter 5). Second, the stoichiometry of the gas and the invariance of the vaporization process must be confirmed. Third, the influence on sample transport because of reactive background gases and crucible interference should be ascertained. Finally, the volatility of GdB_4 can be determined from either gadolinium or boron ion current-temperature coefficient data. Gadolinium or boron pressures also can be determined from a calibration of the mass spectrometer (cf. Chapter 6. 3. 2).

It should be emphasized at the outset of this chapter that the work contained herein was performed only to survey the chemical behavior during GdB_4 evaporation in order to confirm the treatment and interpretation of the results of the Knudsen and Langmuir experiments on GdB_4. Hence, only the results pertaining to the first three of the above reasons are useful. The temperature coefficient of the ion current for gadolinium and the gadolinium pressures, estimated from a rough silver calibration of the mass spectrometer, were determined. However, these data were not

intended to be precise, but were intended only as guide lines to reveal the nature of the vaporization process.

Shutter profiles, anomalous peak characteristics, fragmentation patterns and appearance potentials were determined to define the source of the observed masses in the mass spectrum of the vapor over GdB_4(s) in a ZrB_2/C crucible. The influence of high background pressures on the transport of sample was partially characterized. Finally, rough gadolinium pressure data were collected, from which the volatility and free energies of vaporization of GdB_4 to gaseous elements were computed. The boron and zirconium temperature coefficients over the ZrB_2 crucible were determined.

10. 2 Materials, Crucible and Apparatus

The GdB_4 product (81GdAMa10) from the Langmuir experiments described in Chapter 9 was crushed and ground to a 325 mesh powder. A total of two grams of this sample was employed in this mass spectrometric investigation. The results of chemical analysis of this material and a Gd_2O_3 contaminated residue (81GdAMa11) from one of the high background pressure mass spectrometer experiments are shown in Table 7 and discussed in Chapter 7. Within the analytical accuracy, deviation from the stoichiometric composition, $GdB_{4.0}$, was not detectable.

Granular silver (99.9+%), filed from silver rod and freed from the iron filings with a magnet, was added to the crucible for calibration of the mass spectrometer.

The crucible in all the experiments in the mass spectrometric study of GdB_4 was ZrB_2/C-2. The tapered orifice channel through the ZrB_2 lid was 0.0851 cm. in diameter at the under-surface of the lid and

0.0672 cm. in diameter at the topside of the lid. The channel length was 0.658 cm. Chapter 3. 3. 4 characterizes the ZrB_2 crucible for use in vaporization experiments with GdB_4, and Figure 8. 4 shows the crucible assembly discussed in Chapter 8. 2. The mounting and geometrical arrangement of the crucible in the mass spectrometer are described in Chapter 8. 3.

The principles, apparatus, and procedures are discussed in Chapters 6. 3. 2 and 8. 3. Temperatures were measured with the calibrated optical pyrometer, P-3. The heating arrangement described in Chapter 8. 3 necessarily allows severe crucible temperature gradients, particularly at temperatures below 1500°C. When electron emission from the heated shield cans becomes comparable to the emission from the heating filaments, temperature gradients are not so severe. Temperatures in these experiments were above 1500°C. and shield emission current was greater than filament emission current. Further, the absence of vapor deposits at cold spots inside the crucible implied small gradients. Temperature errors, liberally estimated, are discussed in Chapter 12. 5.

10. 3 Shutter Profiles

By moving a 0.025" shutter slit, located between the crucible and the ionization region, across the molecular beam path and determining the variation in ion current as a function of shutter position for a particular mass, a shutter profile is generated. The shape of this curve reveals the crucible orientation and distinguishes between crucible gases and background gases or anomalous masses. The use of the shutter profile in defining the origin of the ion current is discussed by Drowart (152).

Figure 10. 1 illustrates the shutter profiles of Ag^+, Gd^+, GdO^+, GdO_2^+ and B^+ for a properly aligned crucible. If the molecular beam was emanating directly from the crucible orifice through the shield can orifice and into the mass analyzer, its shutter profile should peak sharply and symmetrically with a half-height peak width of about 0.025", as Figure 10. 1 indicates. A small wing on the left side of the Gd^+, Ag^+, GdO^+ and GdO_2^+ profiles was noticed in Figure 10. 1. This wing intensity resulted from background gas at that mass inside the radiation shield can. The presence of such a wing indicated that the crucible orifice, on projection along the axis of the mass spectrometer onto the shield can orifice, was not concentric with the orifice in the shield cans, but was nearly tangent to the shield can orifice. Thus, wing formation resulted when the shutter was aligned with respect to the shield can orifice, but not aligned with respect to both the shield can orifice and the crucible orifice. When the shutter slit passed to the right in Figure 10. 1 through the molecular beam, the shutter position was not over the crucible orifice or the shield can orifice, thus blocking any molecular beam from the crucible region. It is readily seen, then, that one must take care to define the intensity of a particular mass coming from the crucible as that intensity difference between the shutter positioned at maximum intensity and the shutter positioned on the wing.

In each experiment in which temperature coefficient information was collected, only shutter profiles, such as those of Figure 10. 1, were demonstrated. In some cases the shutter position for maximum intensity was observed to shift downwards by about 0.020" with a 1000° temperature increase, probably because of crucible sagging.

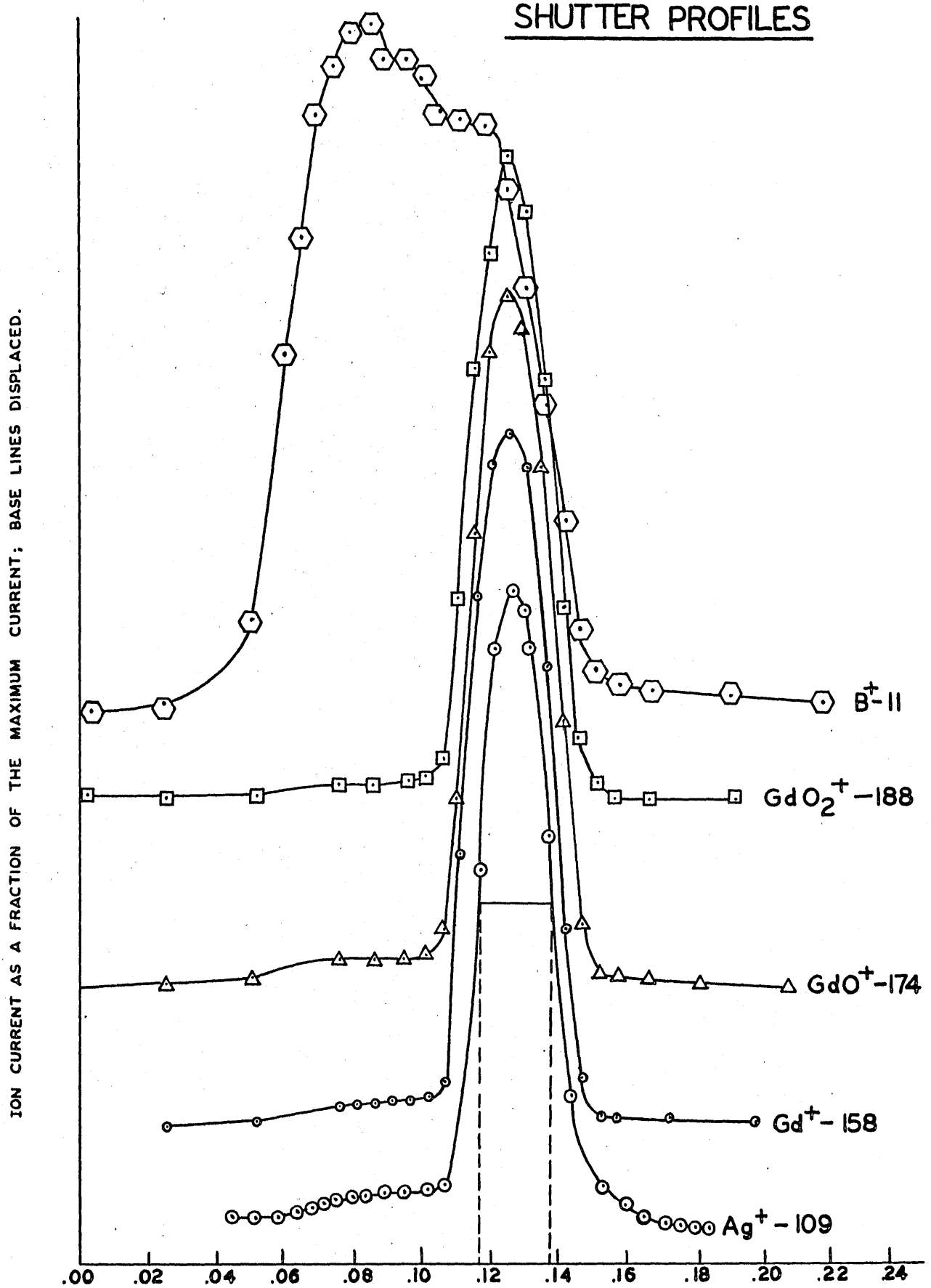
SHUTTER PROFILES
ION CURRENT AS A FRACTION OF THE MAXIMUM CURRENT; BASE LINES DISPLACED.
B+-11
GdO2+-188
GdO+-174
Gd+-158
Ag+-109
.00
.02
.04
.06
.08
.10
.12
.14
.16
.18
.20
.22
.24
SHUTTER POSITION, INCHES

FIGURE 10. 1

The wide B^+ shutter profile of Figure 10. 1 demonstrated boron emanating from two sources -- from the ZrB_2 crucible lid and through the orifice from the GdB_4 sample. Peaks from Zr^+, Zr^{++}, ZrO^+ and ZrO_2^+ were also observed in the mass spectrum with the order of relative intensities, 0.5, 0.1, 3.5 to 0.3 compared to relative intensities of boron and gadolinium of 3.0 and 0.4. Even though congruently vaporizing ZrB_2 develops a volatility ten to one-hundred times less than GdB_4 (cf. Chapter 3. 3. 1) at 2000°K., the ratio of the ZrB_2 lid area to the orifice area emphasized the boron vaporizing from the ZrB_2 crucible lid to the point where it was impossible to distinguish these sources of boron. Therefore, the boron pressure must be determined from the gadolinium pressure and the stoichiometry of the process.

10. 4 Anomalous Masses

Anomalous masses exhibiting behavior exactly as described by Hildenbrand and Theard (169) were observed for the species Gd^+, GdO^+, B^+, GdO_2^+, Gd^{++}, $GdB_2O_3^+$ and $(GdO)_2^+$, arranged in decreasing order of their intensities. Inghram (170) and Hildenbrand and Theard explained anomalous peaks by a "photo effect," wherein neutral gaseous species of low ionization potential in the furnace region are activated, proceed beyond the high positive potentials below the ionization region, strike the edge of or condense on a focusing or repeller plate, lose an electron into the lower Fermi levels of the plate material, reflect or desorb as positive ions and then continue in the ion beam with an accelerating potential greater than that of a normal ion by the voltage difference between the positive plate at which the anomalous ion was formed and that voltage of

the ionization region. The anomalous character of these ions was completely eliminated by setting the trap voltage to zero and setting the repeller and drawing out potentials as small as possible. After these voltages were adjusted, ion currents for $GdB_2O_3^+$ and $(GdO)_2^+$ disappeared.

Six additional low intensity anomalous or metastable masses were observed in the mass region 9 to 11 early in these mass spectrometric heatings, but disappeared with proper focusing conditions for normal masses. These masses were 9.18 (Chart No. 3017), 9.8 (Chart No. 3023), 10.0 (3023), 10.23 (3017), 10.8 (3023) and 11.0 (3023). The 9.18 and 10.23 masses could be metastable peaks arising from the decomposition of BH^+ into B^+ and H. The 9.8 and 10.8 masses probably arise from metastable decomposition of boron oxides.

10. 5 Fragmentation and Appearance Potentials

The normal masses emanating from the crucible that were detected were Gd^+, Gd^{++}, B^+, GdO^+ and GdO_2^+, in decreasing order of their importance depending on the temperature and background pressure. To about 1/10 percent of the gadolinium intensity, no other crucible species were detected (cf. Chapter 5. 3). Oxygen-bearing species were present as background gases in the mass spectrometer, and their influence on the gadolinium pressure is discussed later in this chapter.

Fragmentation effects must be characterized to be certain the gadolinium or boron ions observed were not being produced by the dissociation of some molecule by the high energy electron beam. This phenomenon is discussed by Inghram and Drowart (152). Plots of ion intensity versus

the energy of the ionizing electrons in electron volts for particular species are called ionization efficiency curves. Such curves for Gd^+, Gd^{++}, Ag^+, B^+, GdO^+ and GdO_2^+ are illustrated in Figure 10. 2. The abscissa in these graphs represents an electron voltage calibrated with a voltmeter for the emission current used in the efficiency curve determination. Any abrupt discontinuities in these curves would be indicative of a second process taking place. For instance, if on increasing the energy of the ionizing electrons a critical value is reached at which destruction of GdO^+ into Gd^+ and O occurs, the ionization efficiency curve for GdO^+ ought to deviate markedly from a smooth curve toward lower ion currents; and the Gd^+ curve ought to rise markedly at this electron voltage. No abrupt deviations from expected behavior were observed in Figure 10. 2 for any of the species.

Another test for fragmentation effects is the value of the appearance potential (152). By the method of linear extrapolation, the abscissa intercept of the linear portion of the ionization efficiency curve is called the "appearance potential." This energy is the sum of the adiabatic ionization potential of the species, the dissociation energy, the electron affinity, the kinetic energies, the electronic energies, the vibrational-rotational energies and the emitted photon energy. By far the two largest terms are the ionization potential and the dissociation energy. Should the graphically determined appearance potential be in good agreement with the known ionization potential, one can be fairly certain that the species originates from simple ionization of the neutral species, rather than from ionization and dissociation of a parent molecule.

IONIZATION EFFICIENCY CURVES

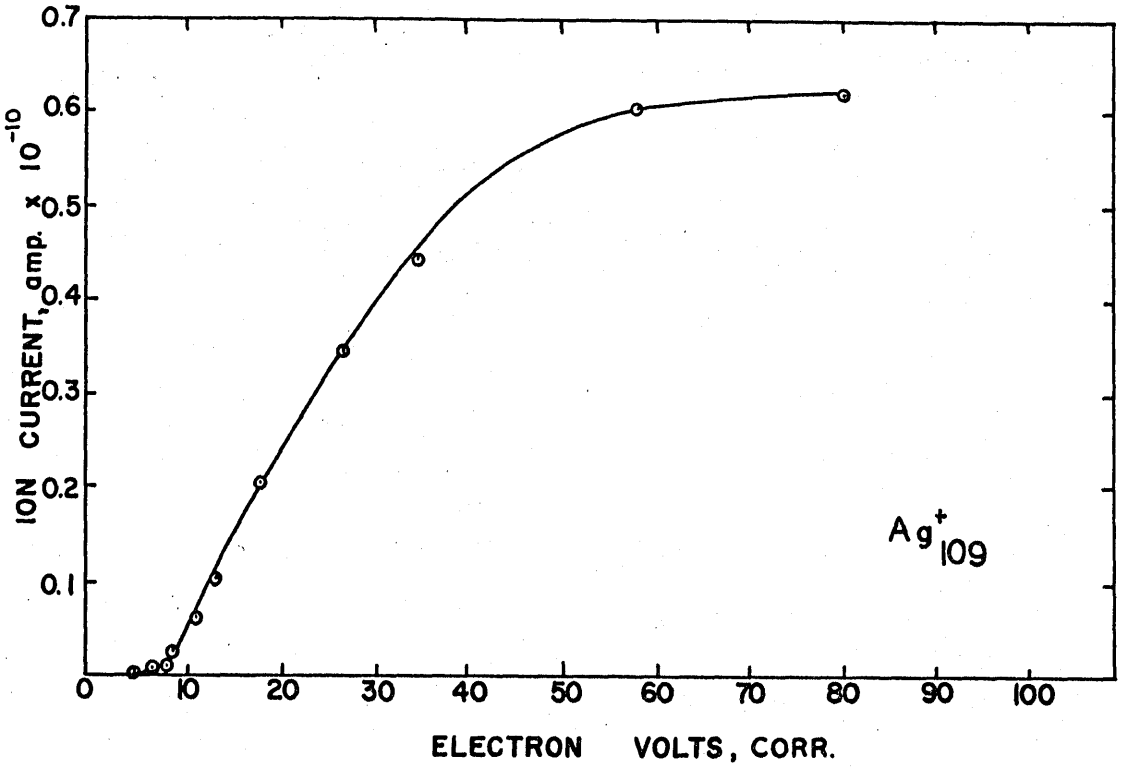

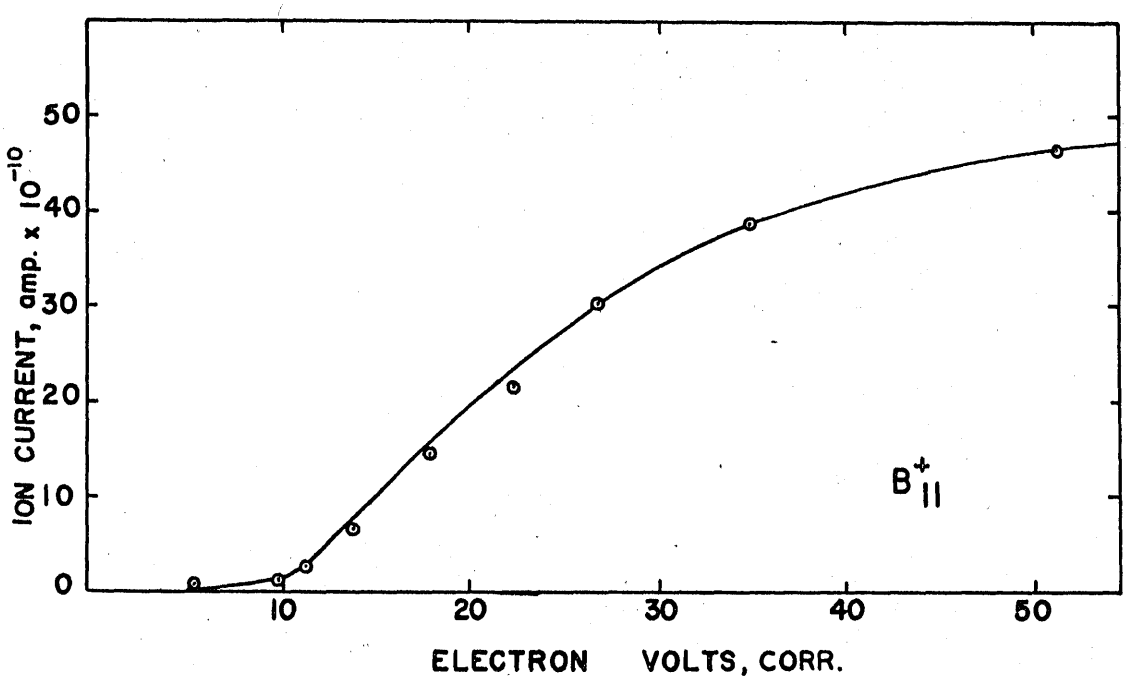

FIGURE 10. 2

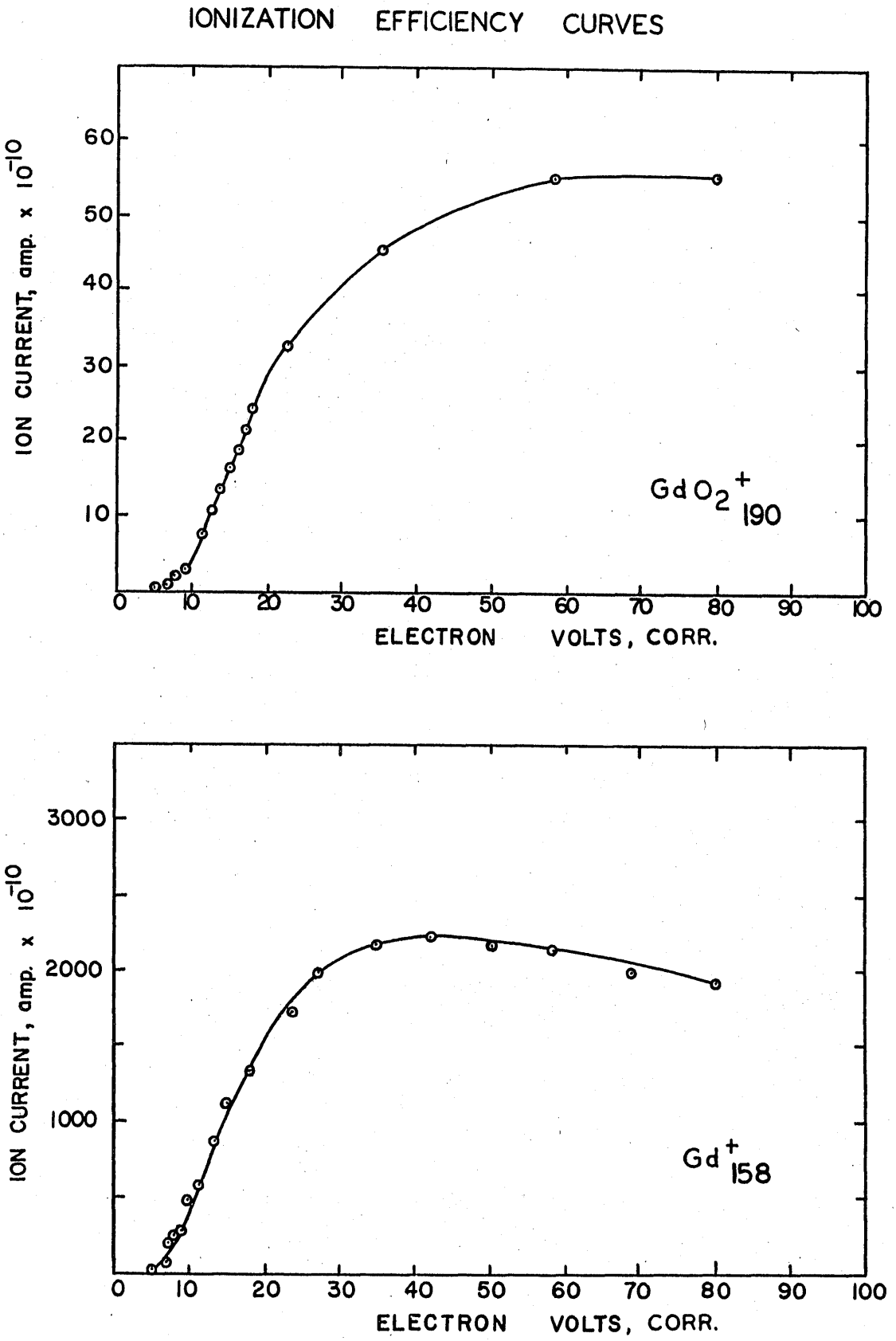
IONIZATION EFFICIENCY CURVES
ION CURRENT, amp. x 10^{-10}
60
50
40
30
20
10
0
10
20
30
40
50
60
70
80
90
100
ELECTRON VOLTS, CORR.
GdO_2^+ 190
ION CURRENT, amp. x 10^{-10}
3000
2000
1000
0
10
20
30
40
50
60
70
80
90
100
ELECTRON VOLTS, CORR.
Gd^+ 158

FIGURE 10. 2

IONIZATION EFFICIENCY CURVES

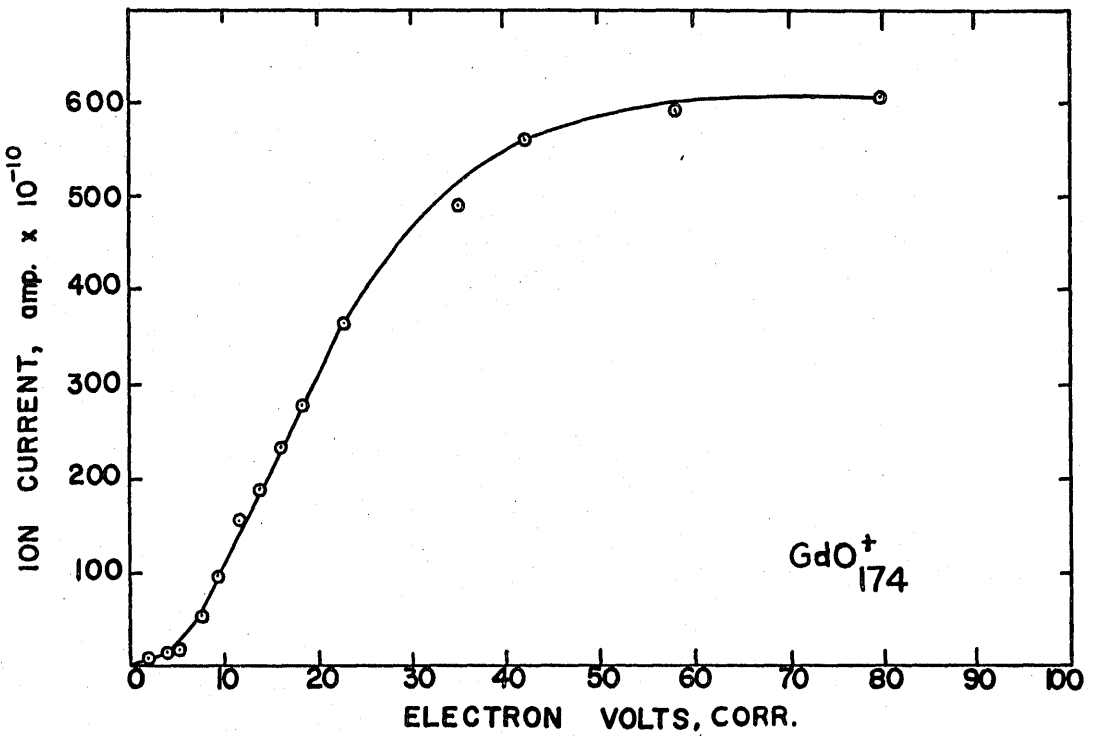

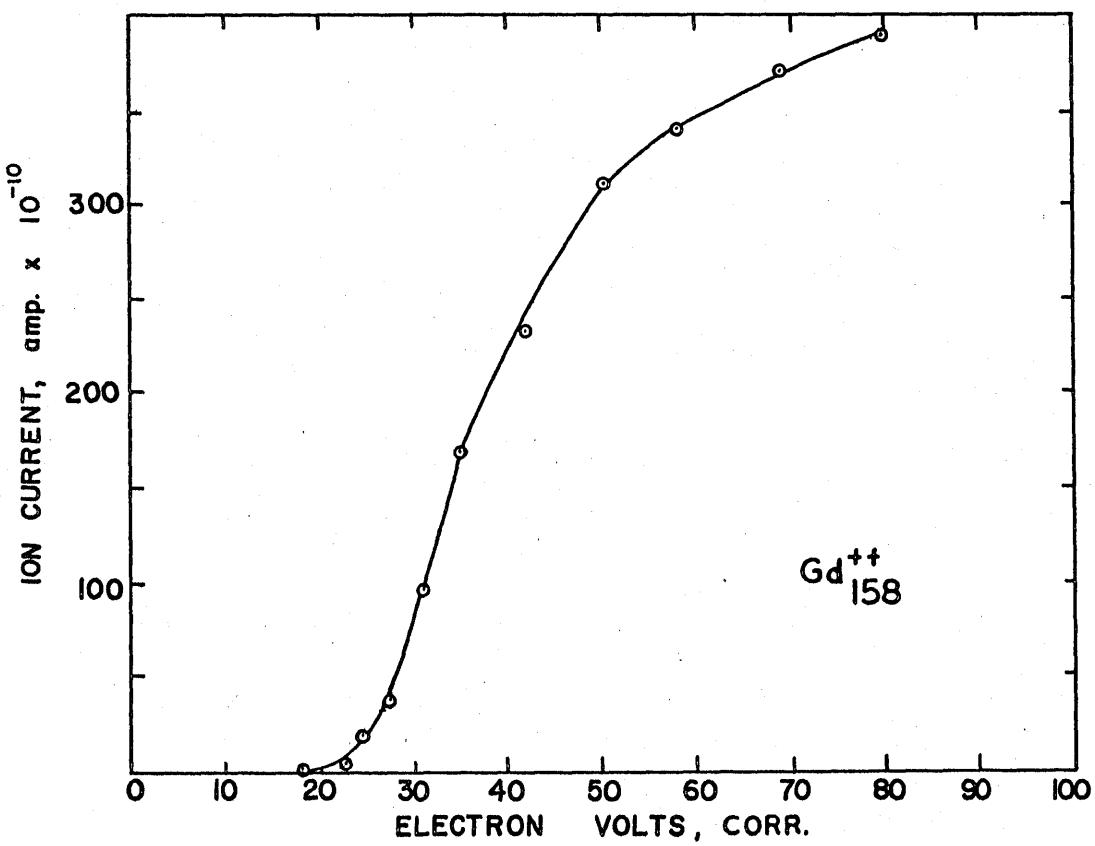

FIGURE 10. 2

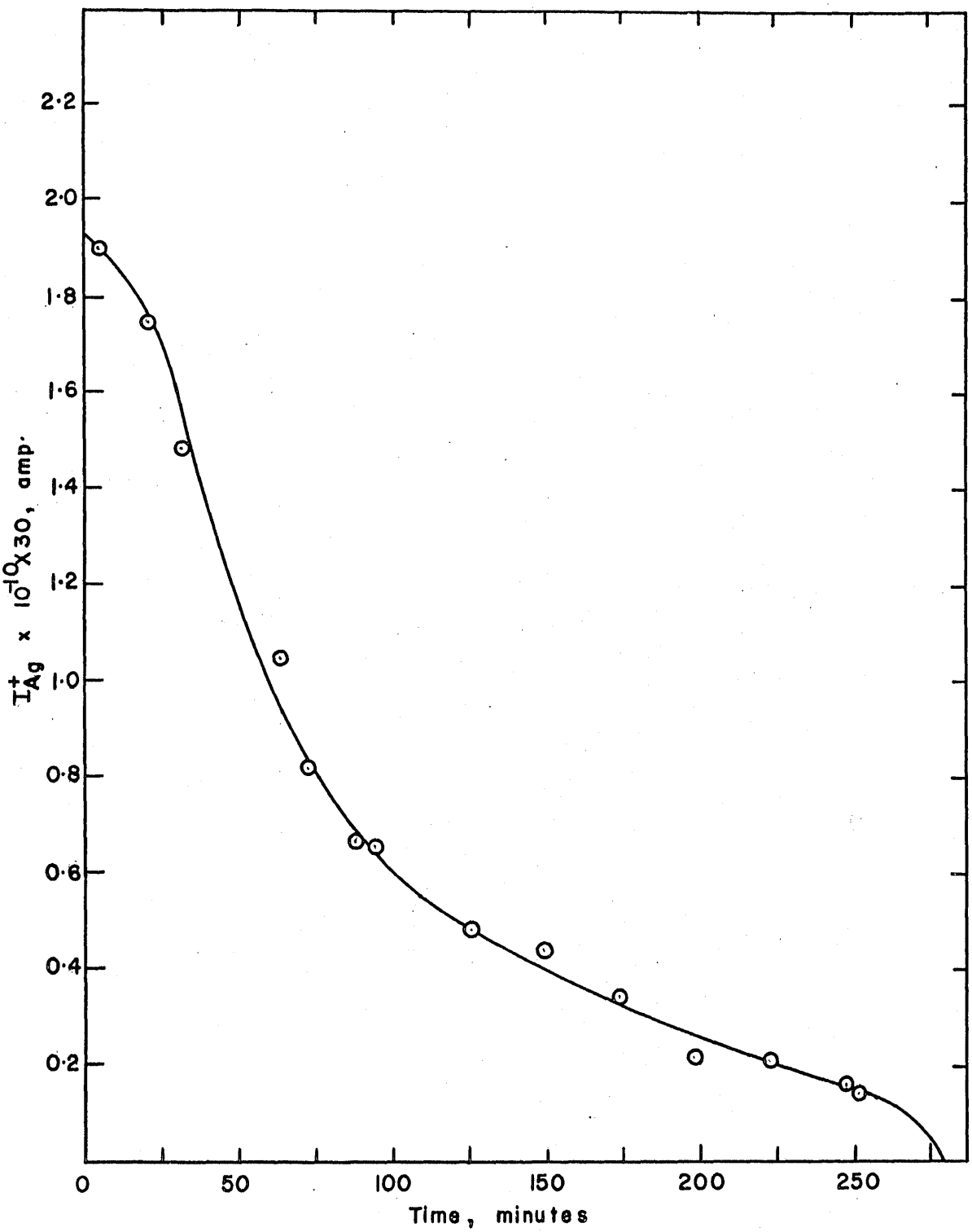

PLOT OF I^+_{Ag} VERSUS TIME AT 1026°C; MASS SPECTROMETER

FIGURE 10. 3

The appearance potentials determined in these experiments are given in Table 10. 1. The agreement between observed and literature values for Ag^+, Gd^+, Gd^{++} and B^+ was quite within the precision afforded by the scatter in the data used to define the ionization efficiency curves. No literature data for GdO^+ and GdO_2^+ were available; however, the shapes of the curves and the small appearance potential values indicated that GdO^+ and GdO_2^+ were parent molecules. It is concluded that all species in this work, arising from the crucible, were parent ions.

Since there were no fragmentation effects, in order to measure consistent intensities and to avoid corrections to the observed intensities of the form (E-A) (cf. equation 6.11), all data were taken with 56.0 ev. electrons. The electronic settings of the ionization and detection instruments were not varied for an experiment once calibration was performed. Temperature coefficients of pressure were determined by setting the accelerating voltage and magnet currents for a particular mass and determining intensities at the two shutter positions discussed above for each of several temperatures.

10. 6 Silver Calibration

In order to calculate absolute gadolinium pressures from measured gadolinium ion currents, the mass spectrometer must be calibrated with a material of known vapor pressure. The calibration of the mass spectrometer with silver according to equation 6.28 was not achieved. Figure 10. 3 is a plot of ion current versus time at a constant temperature of 1026°C. for the total vaporization of 1.75 mg. of silver metal. The very large decrease in intensity with time can only be explained by

TABLE 10. 1

Appearance Potentials Obtained from Linear Extrapolation

Species	Temp. (°C.)	Observed A. P. (ev.)	Literature A. P. (ev.)	Chart	Reference
Ag^+	967	7.7 ± 0.2	7.574	5/5/63	1036
Gd^+	1836	5.9 ± 0.5	6.16	5/1/63	1036
Gd^{++}	1841	24 ± 1	(21)	5/1/63	1036
B^+	1778	9 ± 2	8.3	4/5-6/63	1147
GdO^+	1844	5.0 ± 0.3		5/1/63	
GdO_2^+	1842	8.4 ± 0.5		5/1/63	

orifice plugging. This same problem arose on other occasions and at lower temperature. Therefore, the sensitivity of the instrument was determined from temperature coefficient of pressure data on silver ion.

Samples of silver metal were added to the crucible before each experiment and the sensitivity redetermined to detect any drift in the characteristics of the mass spectrometer. The particular silver-109 temperature coefficient data taken in the same experiment as the measurements on Gd^+ over GdB_4 are shown in Table 10. 2 (MS - 5/7/63). Columns one and two contain the measured temperature and Ag^+_{109} ion currents. Column three lists -log (I^+T) values. Pressures in atmospheres, listed in column four, were taken from Stull and Sinke (65). Column five contains the machine sensitivities in amp./atm. determined from these data by dividing the values in column two by those in column four to define the sensitivity in column five. By dividing the product of the values in columns one and two by the data of column four, one determines the sensitivities in column six. These latter sensitivity data represent the collected charge per effused neutral particle and should be constant with varying temperature (cf. Chapter 6. 3. 2).

The values of $S_{Ag^+_{109}}$ were calculated from equation 6.14. A plot of $S_{Ag^+_{109}}$ versus 1/T was fitted visually with the curve of Figure 10. 4. From this graph an $S_{Ag^+_{109}}$ value was taken as 7.35×10^{-4} amp./atm., when $I^+_{Ag_{109}} = 5.71 \times 10^{-10}$ amp. at 1176°K. and a silver pressure of 7.76×10^{-7} atm., and with 56.0 ev. electron energy and 0.3 ma. electron emission current. These calibration specifications were used in all the gadolinium pressure calculations in conjunction with equation 6.10.

TABLE 10. 2

Mass Spectrometer Sensitivity Determination with Silver

Chart MS - 5/7/63

Temp. (°K.)	$I^+_{Ag_{109}}$ (10^{-10}amp.)	$-\log(I^+_{Ag_{109}}T)$	P_{Ag} (10^{-7}atm.)	$S_{Ag^+_{109}}$ (10^{-4}amp./atm.)	$S^*_{Ag^+_{109}}$ (amp.deg./atm.)
1143	2.72	6.5080	3.483	7.81	.893
1176	5.70	6.1737	7.763	7.34	.863
1209	11.79	5.8460	17.70	6.66	.805
1247	22.89	5.5498	41.50	5.52	.688
1262	39.0	5.3078	56.75	6.87	.867
1266	34.7	5.3572	60.53	5.73	.726
1272	42.92	5.2605	68.87	6.23	.793
1292[a]	55.1	4.7935	128.8	4.28	1.25
1334[a]	61.8	5.0839	216.8	2.85	.380
1337[a]	81.8	4.9613	229.1	3.57	.477

P_{Ag} from 1045

$S_{Ag^+_{109}} = I^+_{Ag_{109}}/P_{Ag}$; equation 6.26

$$S^*_{Ag^+_{109}} = \frac{I^+_{Ag_{109}}T}{P_{Ag}} = \text{constant; equation 6.24}$$

a, Data taken much later in time

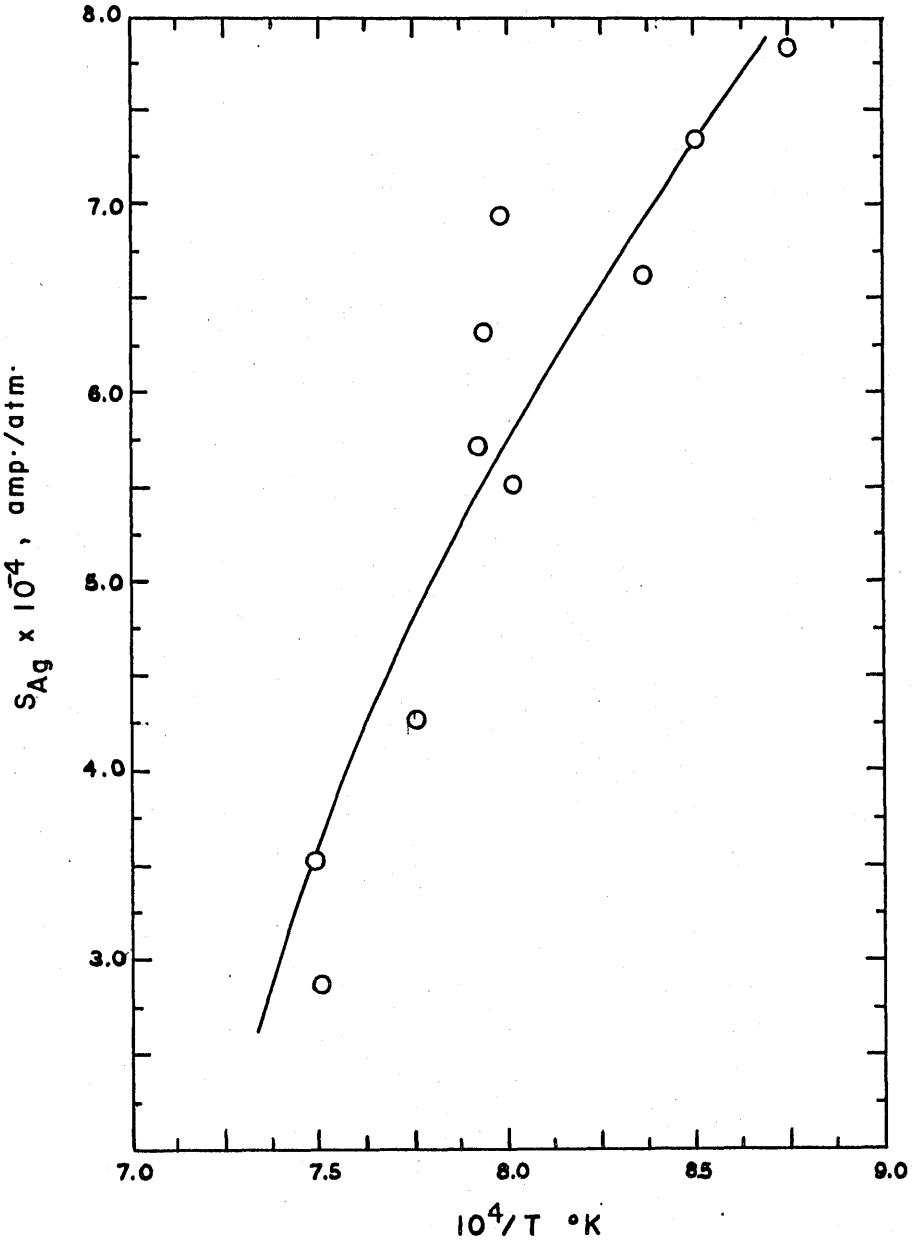

PLOT OF S_{Ag} VERSUS $1/T$;
MASS SPECTROMETER CALIBRATION

FIGURE 10. 4

A Second Law (Chapter 6. 4. 1) treatment of the Ag^{+}_{109} temperature coefficient data of Table 10. 2 is graphed in Figure 10. 5. From the slope and intercept, $\Delta H^{o}_{1250^{o}K.}$ for liquid silver vaporization is 58.1 ± 4.2 kcal/g-at.to be compared to values of 60 to 68 kcal./g-at. determined from Second Law mass spectrometer data taken by Büchler and Berkowitz-Mattuck (171) and a Third Law value of 67.0 ± 0.2 kcal./g-at. found by Knudsen effusion by Panish (172). In view of the few experimental points and the variance in the last three highest-temperature experimental points, this agreement is acceptable.

10. 7 Cross Section and Multiplier Efficiency

In order to use equation 6.10 to calculate the pressure of gadolinium, a knowledge of $\sigma_{Ag^+}/\sigma_{Gd^+}$ and $\gamma_{Ag^+}/\gamma_{Gd^+}$ is needed. The relative ionization cross section for silver was taken from Otvos and Stevenson (155) as 34.8 and estimated for gadolinium from Otvos and Stevenson's data as 71. The ratio of the secondary electron yields was determined experimentally from a ratio of electron multiplier gains as 1.5 ± 0.5 and estimated from an assumed inverse square root mass dependence, specified by Inghram(173), as 1.2. The value 1.3 ± 0.3 was chosen for the calculations.

10. 8 Results

10. 8. 1 Gadolinium Pressures

As demonstrated in Chapter 5 and in this chapter, only atomic gadolinium and boron were found in the vapor over $GdB_4(s)$. Temperature-coefficient data collected on Gd^{+}_{158} over $GdB_4(s)$ from experiments

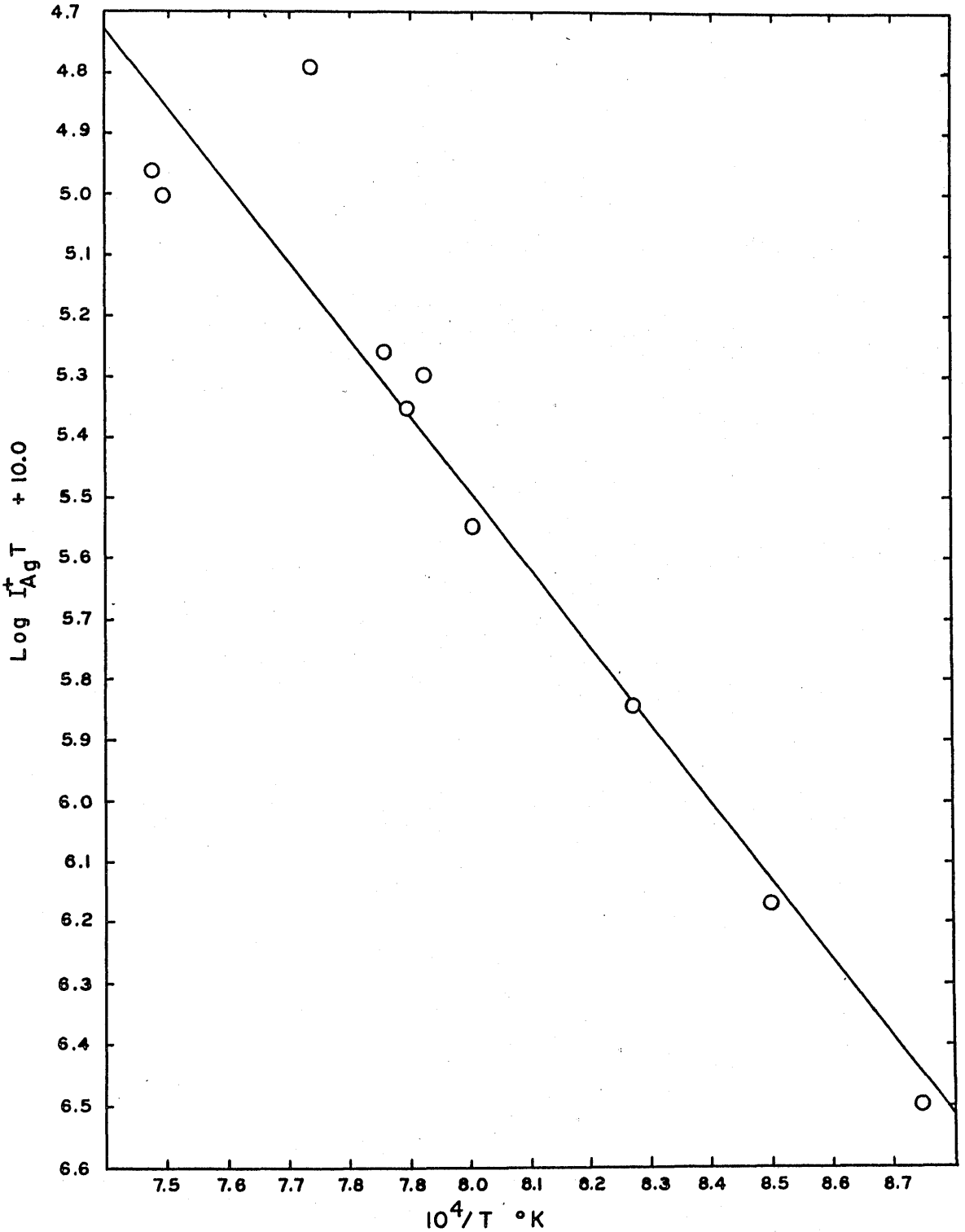

PLOT OF LOG $I^+_{Ag}T$ VERSUS 1/T; MASS SPECTROMETER

FIGURE 10. 5

MS-5/6-9/63 and MS-5/10/63 are summarized in Table 10. 3. While the measured ion currents of column three are listed in the order of the temperatures of column two, the order in which each datum was taken is indicated in column one. Thus, any hysteresis effect on going up and down in temperature or drifts in the machine characteristics may be revealed (cf. Figure 10. 6). Column four contains the gadolinium pressures calculated from equation 6.10 with the calibration data in the above section. Column five contains $-\log P_{Gd}$ values for temperature-coefficient determination.

The Third Law values for $\Delta H^{o}_{298^{o}K.}$ for the congruent vaporization of one mole of $GdB_4(s)$ are listed in column six. These enthalpies were calculated with the assumption that $\Delta S^{o}_{298^{o}K.}$ and $\Delta C_p{}^{o}$ at all temperatures for formation of $GdB_4(s)$ from the condensed elements were both zero. Free-energy-functions for elemental boron were taken from JANAF (69) and for elemental gadolinium were taken from Stull and Sinke (65).

Graphs of $\log p_{Gd}$ vs.$1/T$ and of $\Delta H^{o}_{298^{o}K.}$ vs. T in Figures 10. 6 and 10. 7, respectively, reveal a fairly abrupt decrease in slope for the Second Law temperature coefficient graph and an abrupt increase in $\Delta H^{o}_{298^{o}K.}$ above $1800^{o}K$. The deviation from a linear temperature-coefficient slope and the change from a constant value of $\Delta H^{o}_{298^{o}K.}$ with temperature to a value increasing with temperature indicate a second chemical process becoming important.

10. 8. 2 Influence of Background Gases

The relative decrease in the gadolinium pressure above $1800^{o}K$. can be explained by reaction with the background gases, CO and H_2O, in the

TABLE 10. 3

Collected Data, Pressures, and $\Delta H^{o}_{298^{o}K.}$ from Mass Spectrometric Measurements on Gd^{+}_{158} over GdB_4

Charts MS - 5/6-9/63 and MS - 5/10/63

Chronology of Data	Temp. ($^{o}K.$)	$I^{+}_{Gd_{158}}$ (10^{-10} amp.)	P_{Gd} (10^{-7} atm.)	$-\log P_{Gd}$	$\Delta H^{o}_{298^{o}K.}$ (kcal./mole)
41	1599	.092	.0555	9.744	578
40	1643	.188	.117	8.068	581
42	1650	.218	.136	8.1335	581
23	1666	.411	.259	8.413	576
43	1702	.505	.324	8.5100	584
39	1713	.970	.627	8.797	576
46	1745	3.11	2.05	7.3115	567
22	1760	2.10	1.39	7.143	579
38	1761	1.65	1.10	7.0413	583
45	1797	2.15	1.46	7.1642	589
10	1807	2.16	1.47	7.167	593
24	1811	4.38	3.00	7.477	581
37	1818	2.71	1.86	7.2695	592
44	1839	3.42	2.37	7.3745	594
21	1854	7.26	5.07	7.705	585
36	1868	3.86	2.71	7.4330	600
25	1869	6.94	4.90	7.690	590
20	1888	10.92	7.78	7.891	588
48	1904	3.74	2.69	7.4295	612

TABLE 10. 3, continued

Chronology of Data	Temp. (°K.)	$I^{+}_{Gd}{}_{158}$ (10^{-10} amp.)	P_{Gd} (10^{-7} atm.)	$-\log P_{Gd}$	$\Delta H^{0}_{298°K.}$ (kcal./mole)
35	1914	4.98	3.60	7.5560	610
26	1916	8.19	5.91	7.7715	601
47	1936	5.13	3.75	7.574	616
9	1942	3.20	2.34	7.369	628
49	1945	4.54	3.34	7.5235	621
34	1955	6.45	4.76	7.6775	618
12	1963	5.21	3.87	7.5875	624
27	1970	9.81	7.30	7.8632	614
50	1984	5.30	3.96	7.5976	630
51	1984	5.47	4.08	7.6105	629
33	1995	7.98	6.01	7.779	625
7	1996	6.72	5.07	7.705	629
8	2013	5.03	3.82	7.582	640
11	2017	4.66	3.56	7.5515	643
52	2021	6.41	4.88	7.6884	638
28	2023	11.82	9.03	7.9558	626
32	2027	9.42	7.21	7.858	632
13	2028	6.60	5.04	7.7025	639
6	2040	9.45	7.29	7.865	635
29	2062	13.92	10.8	6.0335	633
14	2066	7.80	6.08	7.784	646
31	2075	12.84	10.1	6.0042	639

TABLE 10. 3, continued

Chronology of Data	Temp. (°K.)	$I^{+}_{Gd_{158}}$ (10^{-10} amp.)	P_{Gd} (10^{-7} atm.)	$-\log P_{Gd}$	$\Delta H^{o}_{298°K.}$ (kcal./mole)
5	2097	13.80	10.9	6.0373	644
1	2097	11.43	9.03	7.9558	648
4	2108	15.45	12.3	6.0900	645
15	2113	9.09	7.25	7.8605	658
30	2122	16.95	13.6	6.1337	647
2	2128	14.22	11.4	6.0567	652
16	2141	11.76	9.49	7.977	660
3	2148	16.11	13.1	6.1173	655
17	2187	18.33	15.1	6.179	663
18	2200	21.15	17.6	6.2455	663
19	2200	22.26	18.5	6.2670	663

$S^{+}_{Ag_{109}} = 7.35 \times 10^{-4}$ amp./atm.

$I^{+}_{Ag_{109}} = 5.706 \times 10^{-10}$ amp.

$P_{Ag} = 7.763 \times 10^{-7}$ atm.

$T_{Ag^{+}_{109}} = 1176°K.$

P_{Gd} calculated from equation 6.10

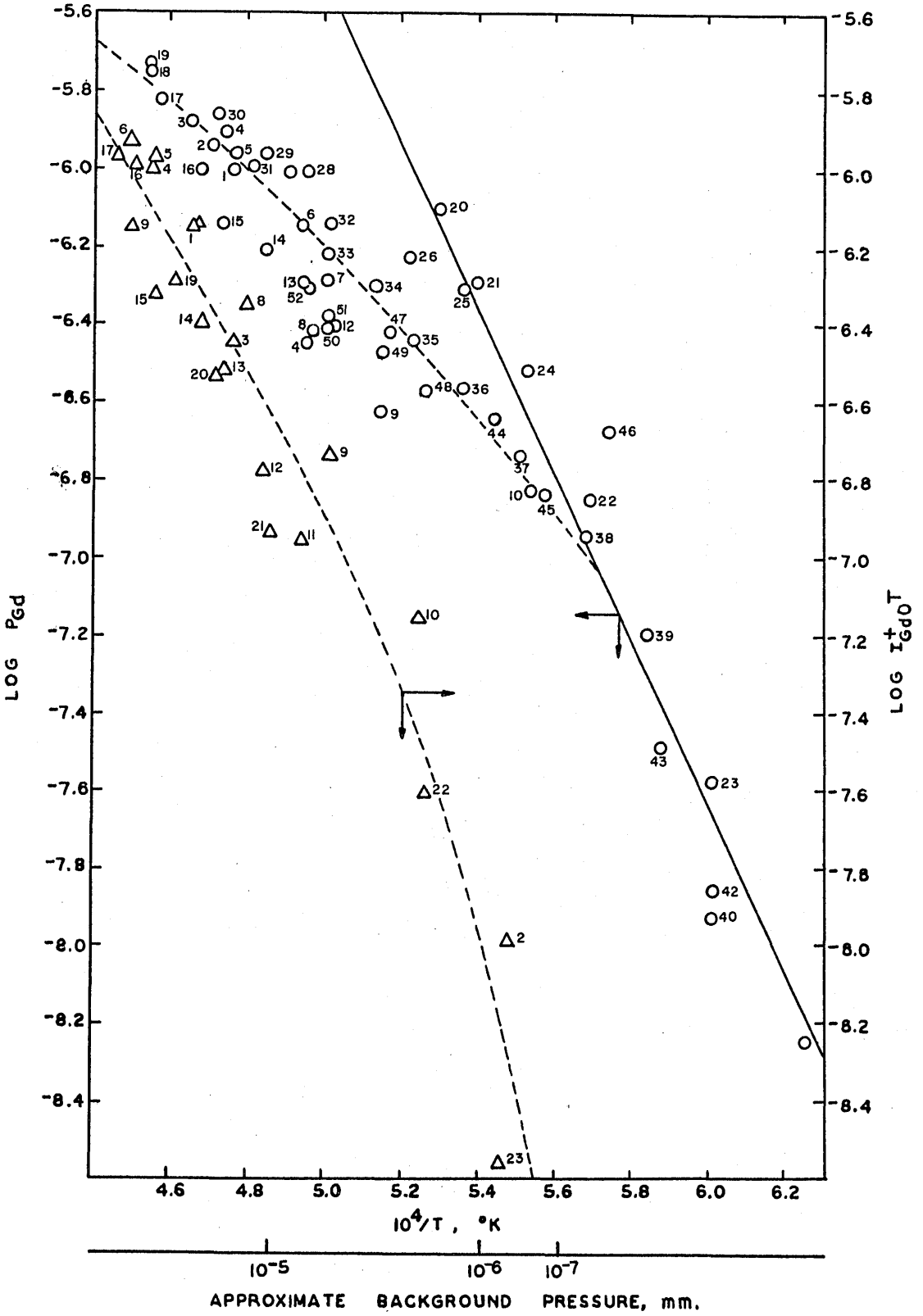

LOG P_{Gd} AND LOG $I^{+}_{GdO}T$ VERSUS 1/T ; MASS SPECTROMETER

FIGURE 10. 6

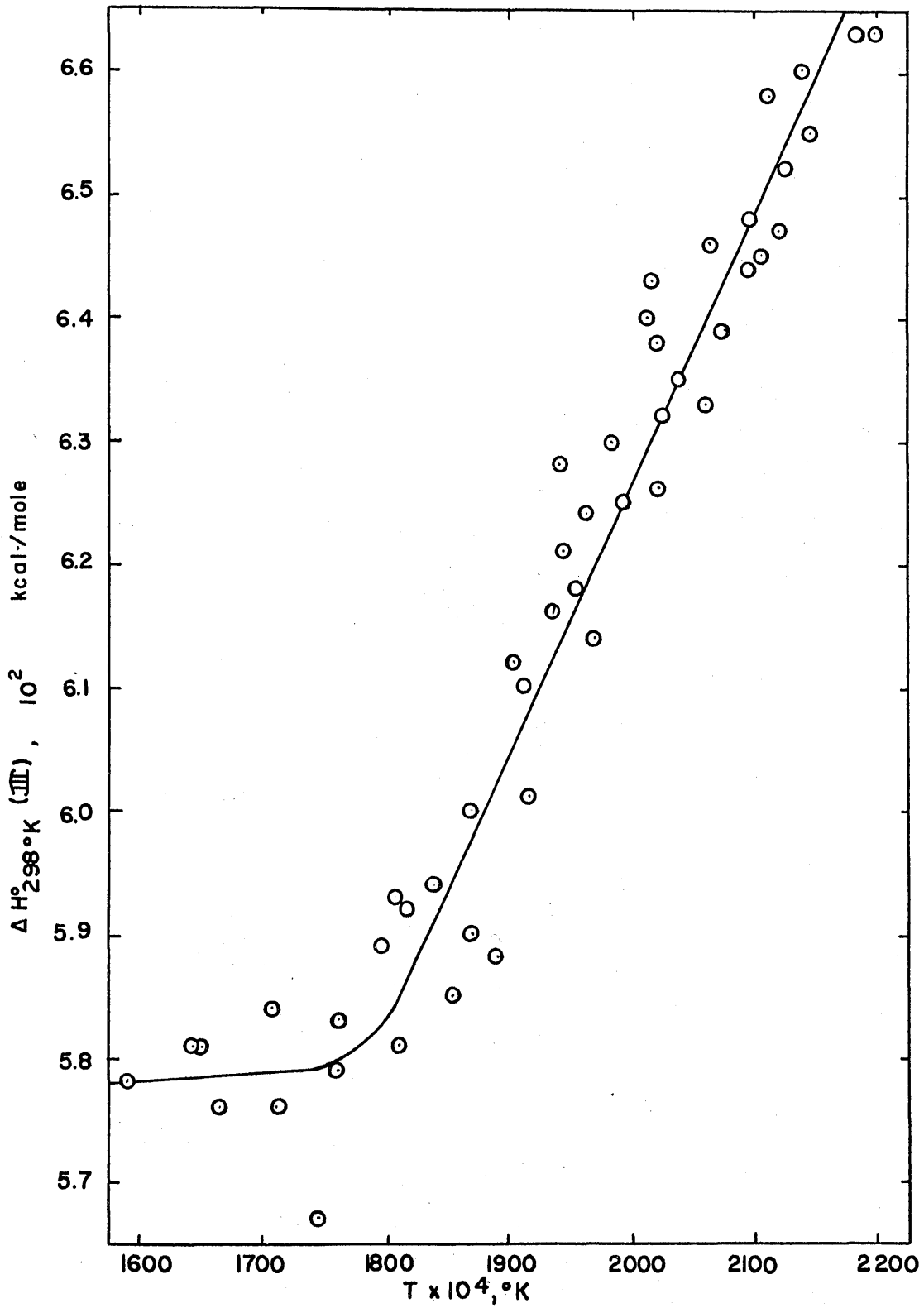

$\Delta H^{\circ}_{298^{\circ}K}$ (III) vs. T; MASS SPECTROMETER

FIGURE 10. 7

mass spectrometer, which become more abundant with increasing temperature of the apparatus. Considerable GdO and some GdO_2 were observed in increasing importance relative to atomic gadolinium as the temperature was raised (cf. Figures 10. 6 and 10. 8). The source of "oxygen" apparently arises from the increasing rate of desorption of water, CO or CO_2 from the large area metal walls of the vacuum assembly as these walls were heated by radiation from the crucible. Carbon monoxide was by far the most important species above 1800°K. in the mass spectrum except for mercury (cf. Table 10. 6). Water and CO_2 were the second most important gases in the background. It is probable that the CO(g) arises from reaction of $H_2O(g)$ with the graphite outer crucible of the crucible assembly.

After the experiment, the water cooling the vacuum housing was found to be blocked, accounting for the warming of the walls of the apparatus. Generally, the background pressure in the mass spectrometer furnace when cold was of the order of 10^{-7} to 10^{-8} mm., as indicated by an ionization gauge above a liquid nitrogen trap located about two feet from the crucible. The conductance of the vacuum line from the crucible to the diffusion pump was quite low because of the shield cans, support apparatus and slits through which the pumped gases must flow. At crucible temperatures of the order of 1590°K., the pressure indicated by the ionization gauge was 2.8×10^{-7} mm.; while at crucible temperatures of 2170°K., the background gas pressure had risen to 7×10^{-5} mm. at the gauge. Clearly, the background gas pressure depended on the temperature of the apparatus. The crucible had been outgassed to 5×10^{-5} mm. at 2470°K. The pressure inside the furnace region may have been as much

as two orders of magnitude larger than that indicated at the gauge, or 10^{-3} mm. in the furnace region.

From a magnetic scan across the Gd^+ and GdO^+ peaks at several temperatures and background pressures, the effect of increasing temperature and increasing background pressure could be noted. These data are listed in Table 10. 4. The Gd-158 and GdO-174 ion currents listed in columns three and four were measured in experiments MS-5/1/63, MS-5/6-9/63 and MS-5/10/63, at the temperatures indicated in column one and the ionization gauge background pressures in column two. All ion current data were taken with 56.0 ev. ionizing electrons at 0.3 ma. emission current and with all other electrical parameters identical in each experiment. Midway through experiment MS-5/10/63, the liquid nitrogen cold traps were replenished with additional liquid. However, no appreciable effect on the background gas pressure was noted. Columns five and six contain $-\log I^+T$ data for Gd-158 and GdO-174, respectively. Column seven lists values for the log of the Gd-158 to GdO-174 ion current ratio.

Figure 10. 8 graphs $\log [I^+_{Gd+}/I^+_{GdO+}]$ as a function of 1/T. Figure 10. 8 also shows the change in $\log [I^+_{Gd+}/I^+_{GdO+}]$ as a function of background pressure indicated by the ionization gauge. Clearly, the pressure of Gd and of GdO were dependent on both the crucible temperature and the background pressure, as well as on each other. From Table 10. 4 at 2200°K. a rather dramatic demonstration of the influence of background "oxygen" was observed when a five or ten degree temperature increase produced a sharp decrease in the Gd^+ ion current with a simultaneous increase in I^+_{GdO}.

TABLE 10. 4

Variation of I^+_{Gd} and I^+_{GdO} over GdB_4 with Background Pressure and Crucible Temperature

Mass Spectrometer Charts MS - 5/1/63, MS - 5/6-9/63, MS - 5/10/63

Temp. (°K.)	Knudsen Region Gauge Pressure (10^{-6} mm.)	$I^+_{Gd_{158}}$ (10^{-10} amp.)	$I^+_{GdO_{174}}$ (10^{-10} amp.)	$-\log(I^+_{Gd_{158}}{}^T)$	$-\log(I^+_{GdO_{174}}{}^T)$	$\log \frac{I^+_{Gd_{158}}}{I^+_{GdO_{174}}}$
MS - 5/1/63						
1830	.70	1.335	.055	6.61208	7.9970	1.3851
2150	24.	9.54	3.13	5.68803	6.1720	.4843
MS - 5/6-9/63						
1912	3.0	6.03	.360	5.93817	7.1625	1.2240
2000	7.3	9.66	.900	5.71399	6.7448	1.0306
2088	20	15.87	2.13	5.47965	6.3520	.8722
2096	40	5.64	1.695	5.92738	6.4494	.5224
2146	37	21.06	3.36	5.34496	6.1420	.7973
2200	70	8.97	4.32	5.70487	6.0310	.3263
2200	70	11.49	4.83	5.59422	5.9737	.3766
2229	88	9.84	5.19	5.65896	5.9368	.2788
MS - 5/10/63						
2029	4.4	2.12	.530	6.36643	6.9685	.6021
2070	8.5	2.73	.790	6.24787	6.7865	.5391
2113	16	3.43	1.43	6.13978	6.5198	.3802
2142	24	4.52	1.83	6.01403	6.4070	.3927
2196	46	8.25	3.45	5.74184	6.1210	.3784
2221	67	8.12	4.20	5.74400	6.0305	.2856
2245	94	7.00	4.73	5.80369	5.9740	.1703

TABLE 10. 4, continued

Temp. (°K.)	Knudsen Region Gauge Pressure (10^{-6} mm.)	$I^+_{Gd_{158}}$ (10^{-10} amp.)	$I^+_{GdO_{174}}$ (10^{-10} amp.)	$-\log(I^+_{Gd_{158}} T)$	$-\log(I^+_{GdO_{174}} T)$	$\log \frac{I^+_{Gd_{158}}}{I^+_{GdO_{174}}}$
		- liquid nitrogen traps filled -				
1834	.67	1.291	.015	6.62562	8.5590	1.9355
1906	1.6	2.583	.129	6.30777	7.6110	1.3015
2061	11	4.78	.880	6.00648	6.7418	.7348
2120	19	7.18	1.37	5.81759	6.5360	.7193
2171	23	7.55	2.34	5.78542	6.2940	.5092
2226	66	9.33	3.15	5.68256	6.1542	.4713

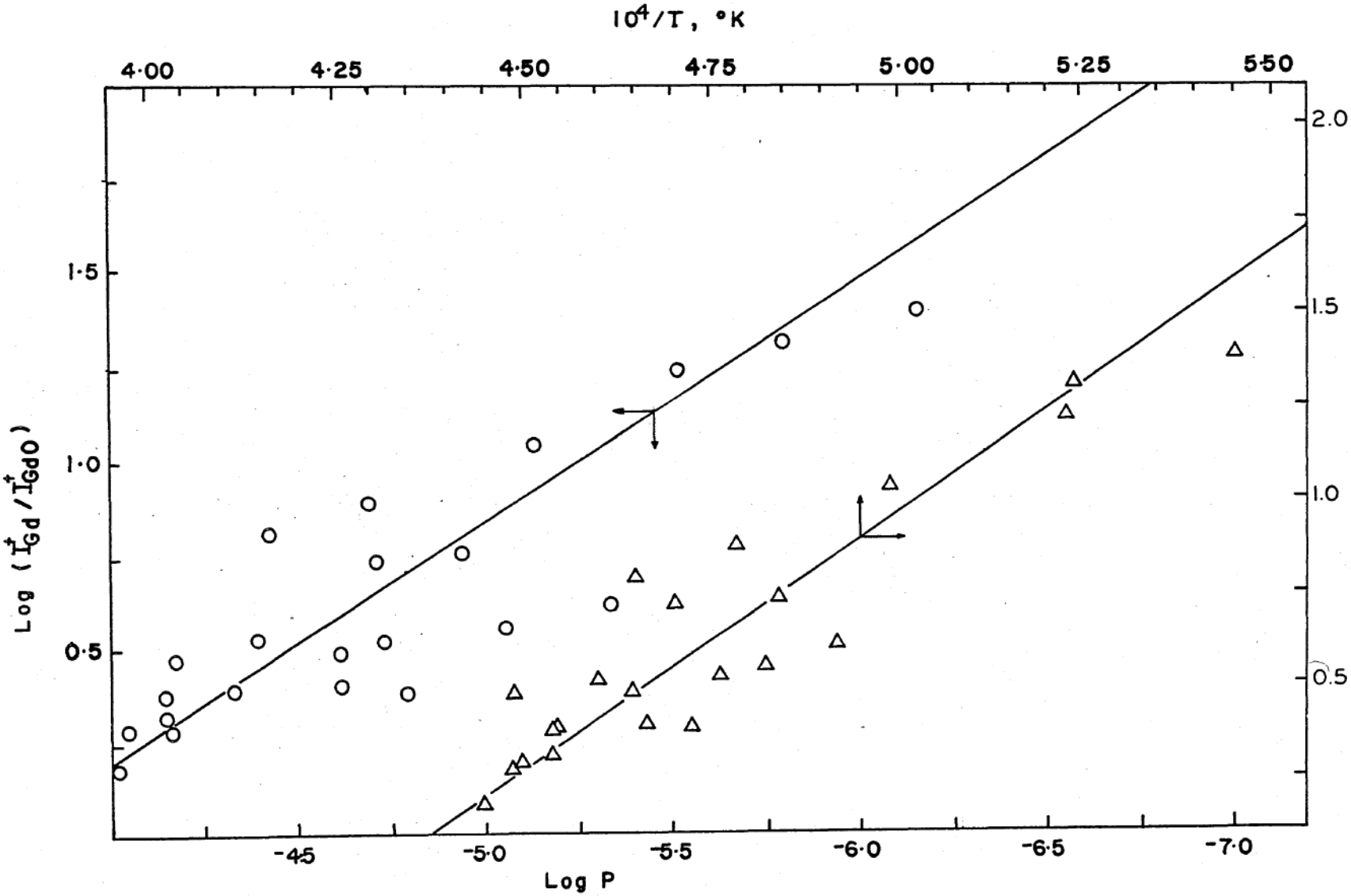

PLOT OF LOG(I^+_{Gd}/I^+_{GdO}) VERSUS 1/T AND VERSUS LOG BACKGROUND GUAGE PRESSURE

FIGURE 10. 8

No shutterable oxygen-containing masses corresponding to O^+, O_2^+, CO^+, CO_2^+, H_2O^+, BO^+, HBO^+, $(BO)_2^+$, HBO_2^+, $B_2O_3^+$, $H_3BO_3^+$ or OH^+ were observed. The conclusion that oxygen in some form was entering the crucible is supported by the shutterable GdO^+ and GdO_2^+ species and by the observation of trace amounts of Gd_2O_3 (from X-ray diffraction analysis) in the GdB_4 residue obtained after shutting off the power to the furnace with the crucible at 2200°K. and with a high background pressure.

Table 10. 5 is an ordered listing of the intensity of the principal background molecule ions and unknown masses under two widely different temperatures and background pressures. Column three contains ion currents as a percent of the 10V VRE scale at 1935°C. and 1.2×10^{-4} mm. background pressure (MS-5/9/63). Similar data are listed in column four at 1740°C. and 5×10^{-5} mm. background pressure (MS-5/10/63). Column one lists the mass and column two defines the molecular species at this mass. Shutter checks performed on the unassigned masses were absent, indicating that these masses did not originate from the crucible.

From experience the H_2O^+-18 and OH^+-17 ion intensities always greatly exceed O^+-16, O_2^+-32 and CO_2^+-44 intensities in a typical mass spectral background scan. Water intensity is always difficult to remove even with long pumping times. But in Table 10. 5 ion currents of CO^+ and CO_2^+ were much more important than water at the higher temperature and background pressure. The H_2O^+-18 intensity was more important than CO_2^+ at the lower background pressure. The high CO and CO_2 pressures possibly arose from H_2O interaction with the graphite crucible (cf. Chapter 12. 2).

While various processes for the reaction of water or CO_2 or oxygen with GdB_4 may be tested by predicting oxygen intensities or B_2O_2

TABLE 10. 5

Principal Background Masses and Relative Intensities of Effusing Species in Mass Spectrometric Study of GdB_4 Vaporization

Mass	Species	MS-5/9/63 % Scale	MS-5/10/63 % Scale	
28	CO^+, N_2^+	600	400	
44	CO_2^+	180	110	MS-5/9/63
29		150	208	1935°C., 10V scale, .3ma. emis-
158	Gd^+	100	0.5	sion, 56ev., 1.2 x 10^{-4}mm. line
18	H_2O^+	96	180	pressure, multiplier gain =
43		61	20	7 x 10^5
16	O^+	57	51	
174	GdO^+	47	n.d.	
69		35.5	9.0	MS-5/10/63
17	OH^+	31	110	1740°C., 10V scale, .3ma. emis-
27		24	13.5	mission, 56ev., 5 x 10^{-5}mm. line
79	Gd^{++}	24	n.d.	pressure, multiplier gain =
70		18	5.0	7 x 10^5
68		11	3.0	
53		10.5	2.5	
54		10	2.5	
32	O_2^+	10	27	
26		8.4	6.5	
52		5.5	0.5	
190	GdO_2^+	4.0	n.d.	
11	B^+	4	n.d.	
61		1.0	0.5	
62		1.0	0.25	

intensities from a properly plotted function of the logarithms of the Gd and GdO ion currents versus 1/T, the variance in the data and the lack of thermochemical information preclude the significance of this effort. Log ($I^+_{GdO}T$) versus 1/T from Table 10. 4 is graphed in Figure 10. 6 for comparison with the gadolinium temperature coefficient. It is sufficient to note that oxygen interaction is important at temperatures above 1800°K. and when the background pressure at the ionization gauge exceeds 1 x 10^{-6}mm.

10. 8. 3 $GdO_2(g)$

The possibility of GdO_2 molecule is interesting. The mass spectrometer had been used to study sulfides prior to this investigation. Since GdO_2^+ and GdS^+ would appear at the same masses and have the same metal isotope distribution, the possibility that GdO_2 is really GdS must be considered. However, below the magnet the mass spectrometer was entirely cleaned of past deposits prior to these studies. Further, the $I^+_{Gd+}/I^+_{GdO_2+}$ ratio showed the same dependence on background pressure and temperature of the apparatus as did I^+_{Gd+}/I^+_{GdO+} and could be reproduced with the same intensity ratios between experiments. Thus, this mass has been assigned as GdO_2.

No GdO_2^+ or TbO_2^+ was observed when $TbB_{4,6}$ and $GdB_{4,6}$ were vaporized in the mass spectrometer from tungsten cells with low background pressure in the mass spectrometer. White, Walsh, Ames and Goldstein (52) looked at the vaporization of lanthanide sesquioxides mass spectrometrically in tungsten crucibles without finding $LnO_2(g)$. White did observe $CeO_2(g)$ over $CeO_2(s)$, $PrO_2(g)$ over $Pr_6O_{11}(s)$ and

$TbO_2(g)$ over $Tb_4O_7(s)$. Perhaps the reducing condition in the presence of tungsten prevents $LnO_2(g)$ formation in those cases where the molecule was not observed. Certainly the ZrB_2 crucible in this work is less reducing than tungsten.

10. 8. 4 Boron and Zirconium Temperature Coefficients

Zirconium, coming from the crucible lid, was observed in the mass spectrum. A Second Law treatment of the zirconium ion current is graphed in the range 2048 to 2268°K. in Figure 10. 9. From the slope, a value of 117.6 ± 1.2 kcal. for the heat of vaporization of 1/2.91 $ZrB_{1.91}(s)$ in the process established by Leitnaker (131), $ZrB_{1.91}(s) = Zr(g) + 1.91B(g)$, was obtained. A similar Second Law slope from the B_{11}^+ intensities in the range 2021 to 2199°K. is shown in the same figure. From the boron slope, a value of 118.9 ± 6.7 kcal./g-at. boron was obtained for the vaporization of boron from the crucible region.

The heat of congruent vaporization of GdB_4 at 2100°K. was estimated at 133 kcal./total gas atom, which is larger than the boron temperature-coefficient value above. However, the Second Law values for boron and zirconium are in excellent agreement. This observation further indicates that the large vaporizing area of the ZrB_2 crucible lid is the principal source of boron and prevents a determination of the boron pressures over $GdB_4(s)$. While these enthalpy values for zirconium and boron are lower than the Third Law heat of vaporization of 1/3 $ZrB_2(s)$ determined by Leitnaker (131) as 150 kcal., they do overlap the error (127 ± 6 kcal.) in one series of Second Law experiments performed by Leitnaker.

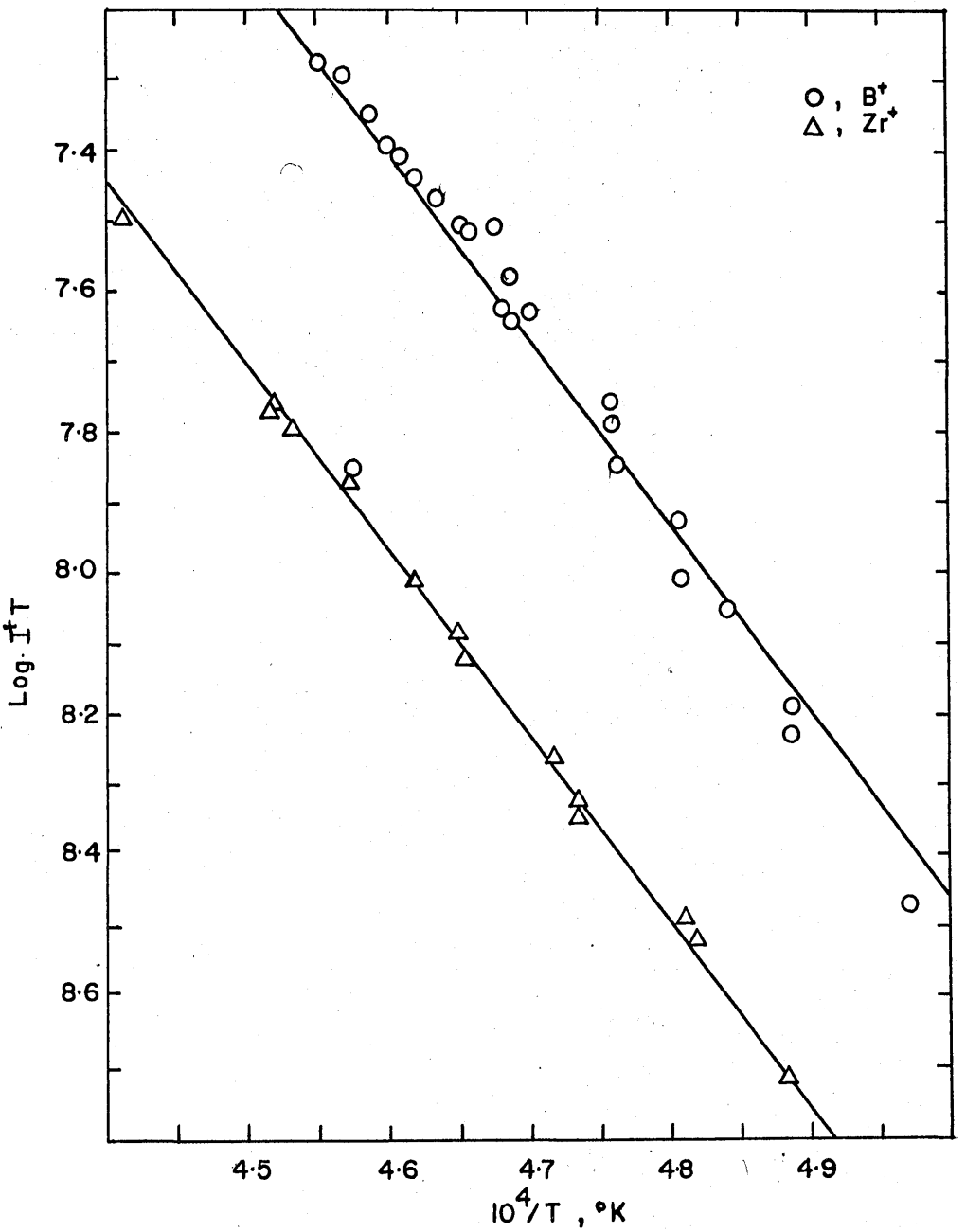

PLOT OF LOG I⁺T VERSUS 1/T FOR B AND Zr; MASS SPECTROMETER

FIGURE 10. 9

During the course of the mass spectrometer experiments, the upper side of the ZrB_2 lid became coated with a pale blue material which had no structure lines on X-ray diffraction analysis. No Zr^+, ZrO^+ or ZrO_2^+ was observed in the mass spectra after the coating appeared. Further, the boron intensities were considerably lower after the lid became coated. This coating may have consisted of Ta borides.

10. 8. 5 Thermodynamic Values

In view of the transport of gadolinium from GdB_4 as GdO and GdO_2 at high background pressures, only the low background pressure data below 1890°K. of Table 10. 3 were used in the thermochemical calculations for the congruent vaporization of GdB_4 to the gaseous elements. Under these conditions the GdO^+ ion current was less than 5% of the gadolinium ion current. These gadolinium pressures are listed with increasing temperature in Table 10. 6, columns two and one, respectively. Column three contains values of -RlnK per mole of GdB_4(s). Column four lists the measured free energies of vaporization per one mole of gas formed. The values of ΔH_T^o and $\Delta H_{298°K.}^o$ calculated by the Third Law for formation of one mole of gas are listed in columns six and eight, using ΔS_T^o and Δfef^o values of columns five and seven.

Log p_{Gd} in the range 1599 to 1888°K. is graphed in Figure 10. 6. A least squares treatment of these data defines $\Delta H_{1750°K.}^o$ as 99.1± 5.8 kcal. for the vaporization of 1/5 mole of GdB_4 to the gaseous elements. The value of $\Delta S_{1750°K.}^o$ from the ordinate intercept is 24.4± 3.4 eu.

TABLE 10. 6

Calculated Thermodynamic Quantities from Low Background Pressure Data of Mass Spectrometric Measurements on Gd(g) over GdB_4.

Temp. (°K.)	P_{Gd} (10^{-7} atm.)	-RlnK (eu.)	ΔF_T° (kcal./$\frac{1}{5}$ mole)	ΔS_T° (1/5 eu.)	ΔH_T° (kcal./$\frac{1}{5}$ mole)	$-\Delta fef^\circ$ (1/5 eu.)	$\Delta H^\circ_{298°K.}$ (kcal./$\frac{1}{5}$ mole)
1599	0.0555	188.50	60.28	33.03	113.09	34.32	115.16
1643	0.117	181.13	59.50	32.99	113.70	34.27	115.83
1650	0.136	179.61	59.27	32.98	113.69	34.27	115.81
1666	0.259	173.18	57.70	32.96	112.61	34.28	114.82
1702	0.327	170.96	58.19	32.91	114.20	34.24	116.47
1713	0.627	164.41	56.33	32.90	112.69	34.24	114.98
1745	2.05	152.66	53.28	32.87	110.64	34.21	112.97
1760	1.39	156.47	55.08	32.86	112.91	34.20	115.26
1761	1.10	158.86	55.95	32.85	113.80	34.20	116.17
1797	1.46	156.03	56.08	32.74	114.91	34.16	117.47
1807	1.47	155.93	56.35	32.79	115.60	34.17	118.11
1811	3.00	148.85	53.91	32.79	113.29	34.17	115.80

TABLE 10. 6, continued

Temp. (°K.)	P_{Gd} (10^{-7} atm.)	-RlnK (eu.)	ΔF_T^o (kcal./$\frac{1}{5}$ mole)	ΔS_T^o (1/5 eu.)	ΔH_T^o (kcal./$\frac{1}{5}$ mole)	$-\Delta fef^o$ (1/5 eu.)	$\Delta H^o_{298°K.}$ (kcal./$\frac{1}{5}$ mole)
1818	1.86	153.61	55.85	32.78	115.44	34.15	117.93
1839	2.37	151.17	55.60	32.67	115.68	34.13	118.36
1854	5.07	143.63	53.26	32.73	113.94	34.13	116.54
1868	2.71	149.85	55.98	32.73	117.12	34.12	119.72
1869	4.90	143.98	53.82	32.73	114.99	34.12	117.60
1888	7.78	139.37	52.63	32.70	114.37	34.10	117.00
					avr. 114.0 ± 1.4		avr. 116.4 ± 1.5

$\Delta H^o_{1750°K.}$ (Second Law) = 99.1 ± 5.8 kcal./$\frac{1}{5}$ mole

$\Delta S^o_{1750°K.}$ (Second Law) = 24.4 ± 3.4 eu.

$$-RlnK = 1.987 \ln \left[(4.00)^4 \left(\frac{M_B}{M_{Gd}} \right)^2 P_{Gd}^5 \right]$$

With the use of equation 6.18 ΔH_T^o was calculated for each measurement in Table 10. 6 by the Third Law. The average $\Delta H^o_{1750^oK.}$ is 114.0± 1.5 kcal. for the vaporization of 1/5 mole of $GdB_4(s)$. The Third Law treatment assumes that ΔS_T^o for formation of $GdB_4(s)$ from the condensed elements is zero. From equation 6.29 and the further assumption that $\Delta C_p^o = 0$ for formation of $GdB_4(s)$ at all temperatures, the average $\Delta H^o_{298^oK.}$ was found to be 116.4± 1.5 kcal. per one total mole of gas formed. Entropy and free-energy-function data for B(s) and B(g) were taken from JANAF (69) and for Gd(1) and Gd(g) from Stull and Sinke (65).

CHAPTER 11

KNUDSEN PRESSURE MEASUREMENTS ON GdB_4

11. 1 Scope of the Experiment

Pressure measurement by the Langmuir method suffers from indefinite specification of temperature and surface area as well as possible kinetic effects which retard the rate of vaporization and, thus, predict lower pressures than the vapor saturation pressures. While the mass spectrometric investigation of GdB_4 demonstrated atomic gaseous species and described the tolerable levels of background pressure, the pressure data taken from the mass spectrometer are subject to large errors arising from calibration, temperature and background pressure problems. On the other hand, the Knudsen experiments in this chapter were performed with better definitions of the factors entering into the pressure determinations than in the Langmuir and mass spectrometric studies. Of the three methods used to determine GdB_4 volatility the Knudsen experiments were intended and expected to provide the most reliable gadolinium pressure data, and they did.

In the experiments of this chapter, gadolinium pressures were determined by measuring the rate of collection of gadolinium on a target over the ZrB_2/C crucible as a portion of the vapor in equilibrium with GdB_4(s) effused through the crucible orifice. Second and Third Law

treatment of these fourteen pressure measurements in the 2047 to 2362°K. temperature range defined the volatility of GdB_4(s).

11. 2 Experimental

The Knudsen effusion experiments were performed in three series. Series 1 was performed with 500 mg. of the 325 mesh GdB_4 sample (81GdAMa10) remaining from the Langmuir measurements and analyzed for boron and gadolinium in Chapter 7. Crucible ZrB_2/C -4 with a tapered orifice, 0.1273 cm. in diameter at the top of the ZrB_2 lid, 0.1503 cm. diameter at the under-surface of the ZrB_2 lid, and a channel length of 0.689 cm., was used. Series 2 experiments were performed in crucible ZrB_2/C-2, the same crucible used and described in the mass spectrometer experiments, with another 500 mg. portion of the GdB_4 sample, 81GdAMa10. This crucible contained 100 mg. of a GdB_4 deposit on the side of the ZrB_2 base, deposited during the mass spectrometer experiments of Chapter 10. With the use of crucible ZrB_2/C-4 again and 1.41175g. of the GdB_4 sample (81GdAMa10), Series 3 experiments were performed.

In these experiments no attempt was made to correct the orifice area for the expansion of ZrB_2 as a function of temperature, in view of the small correction (5.5×10^{-6}/°C., (136)) and the precision of the experiment. The apparatus described in Figure 8. 3 and in Figure 8. 4 was used for all experiments.

Aluminum disks, 1-1/8" in diameter and cleaned with dilute nitric acid and distilled water, were stacked in the target holder in individual spring-loaded mounting rings. The condensation coefficient for the

gadolinium component of the effusate was assumed unity. Distances between the upper surface of the ZrB_2 lid and the target were measured with a cathetometer (Gaertner Scientific Corp.).

There was some inherent temperature gradient in the design of this crucible arrangement, as evidenced by the transport of significant quantities of GdB_4 to the underside of the lid during long heatings. However, the orifice channel was never blocked. All temperatures were observed by sighting onto a black-body hole in the base of the crucible with the calibrated optical pyrometer, P-3. The black-body hole had been calibrated in terms of the temperature observed through the orifice and for the optics in the apparatus. The orifice-black body hole temperature differences are graphed in Figure 11. 1. These differences were generally less than 40^{o} and narrowed to 10^{o} at $2300^{o}K$.

Background pressures during target exposures generally were less than 5×10^{-5} mm., as indicated by the ionization gauge. Because of the conductance of the vacuum system, the glass construction rather than metal, and the high pumping speed compared to the mass spectrometer, it was believed that the oxygen-bearing components in the background gas were less a problem than they were in the mass spectrometer experiments. Significant sample transport by interaction with the background gases was discounted by the absence of variation of the Third Law enthalpy changes with temperature.

After initial outgassing of the sample at $2400-2500^{o}K$. for about sixty minutes, the power was adjusted to a lower temperature. When several successive temperature observations at one-minute-intervals were constant within two degrees of each other, the target was exposed and

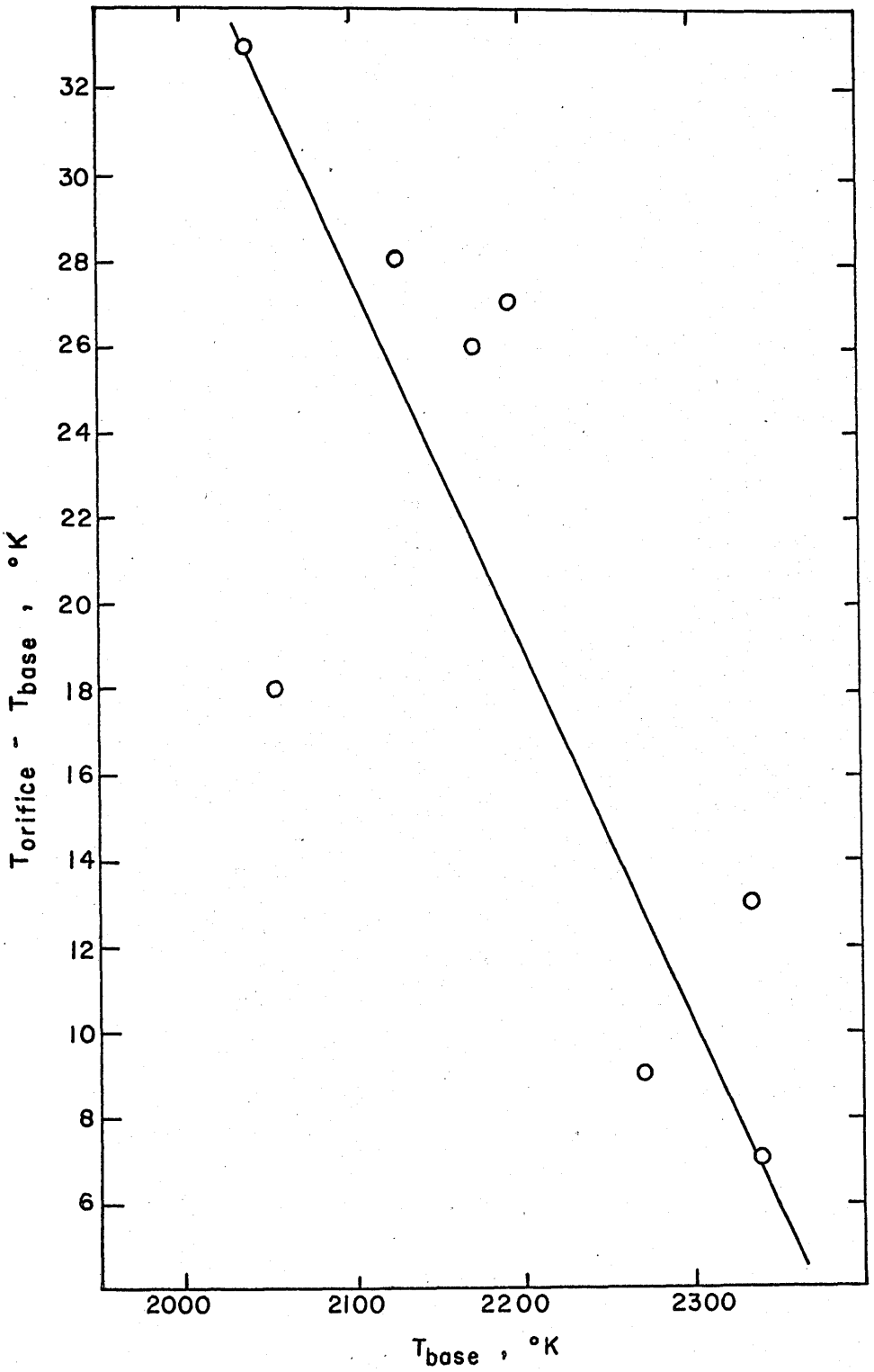

$T_{orifice} - T_{base}$ VERSUS T_{base} IN KNUDSEN EXPERIMENTS

FIGURE II. I

timing begun. Temperature was measured every five minutes and the power adjusted to maintain constant temperature. Generally, the experiments were isothermal within five degrees. The shadow on the apparatus, cast by the effusing beam intercepting the radiation shield and shutter, indicated material coming only from the orifice and gave no indication of re-evaporation from the glass condenser walls towards the cold target.

11. 3 Target Analysis

The aluminum disks were colored from yellow through reds and blues to nearly black depending on the thickness of the sublimate. These targets were analyzed for the weight of gadolinium in a defined area by X-ray spectrographic analysis (X-ray Spectrograph Attachment, type number 52260, Philips Electronics, Inc.). Tungsten radiation stimulated L_α emission from the gadolinium on the target disks, which, on separation from other characteristic radiation by a LiF analyzing crystal, appeared at a goniometer setting of 61.05°. Counting was performed with a P-10/He flow proportional counter at 1650 V. The counter was coupled to a Philips binary scaler and rate meter, operating at a time constant of 2 sec. and a multiplier setting of 1.0. The number of seconds for 1000 counts was the experimentally measured quantity.

Because of the geometry of the tungsten X-ray tube with respect to the sample, the intensity of the incident radiation was not uniform in the trapezoidal area covered by the incident radiation on the target disk. It was necessary to optimize the fluorescent intensity and then to reproduce the same position in the incident beam for every target.

This was accomplished by overlapping the target with a 1/32" thick aluminum disk with a 0.550 cm. center hole positioned over the sublimate on the sample target and in the optimum position with respect to the incident X-ray beam. The positions of these two disks were reproduced between analyses by defining the optimum position with paraffin wax slots on the sample mounting plate. Repeated analyses and target rotation demonstrated a precision well within that of the standard sample preparation.

A goniometer scan of blank targets indicated no other elements were present near the 61.05°, $L\alpha$, line of gadolinium with the sensitivity used for the gadolinium analysis. A blank target covering a target on which appreciable gadolinium had been deposited prevented any gadolinium emission detection. Hence, the area investigated for gadolinium was indeed that within the 0.550 cm. radius hole in the target overlay disk.

A calibration curve was determined from several standard aluminum targets. These standard samples were prepared from a standard solution of Gd_2O_3 in dilute HCl. This standard solution was prepared in desired concentrations of gadolinium such that one to two hundred micrograms of gadolinium could be delivered from a 1.00 cc. tuberculin syringe onto the cleaned aluminum target within an area of 0.550 cm. While the white Gd_2O_3 crust left on evaporation was not uniform, several standards of the same concentration produced the same fluorescent intensity within the five percent precision of the delivered volume. Targets and standards were not analyzed until the electronics had warmed for two hours. All standards and samples were analyzed in the same experiment.

Generally, the intensity in counts per second is proportional to the concentration, or the product of concentration and seconds per fixed count is a constant. Therefore, to develop a nearly linear calibration curve, a plot of log W_{Gd} versus log t/1000 counts was used for the calibration. Figures 11. 2 and 11. 3 illustrate this calibration curve and its non-logarithmic analog. The deviation from linearity at low concentrations is inherent in the counting circuits at low counting rates.

11. 4 Clausing and Distribution Correction

The gadolinium pressures were determined from equation 6.17 with a Clausing factor and cosine correction specified by Freeman and Searcy (174) of the form,

$$n = \sin^2\theta - [\ 0.0815\ (L/r)(\sin 2\theta - 2\theta \cos 2\theta)\ ]\ , \qquad (11.\ 1)$$

where n is the correction to the pressure. More specifically, n is the fraction of molecules striking the target compared to the total number entering the cylindrical orifice. The angle, θ, is the angle in radians between the normal from the target to the orifice and the side of the cone whose apex is at the top of the orifice and whose base is the 0.550 cm. collector radius. The length of a ZrB_2 cylindrical orifice in centimeters is denoted by L, and r is the radius of the orifice in centimeters. The r value used in these experiments was the average of the top and bottom radii of the tapered channels in the ZrB_2 lids.

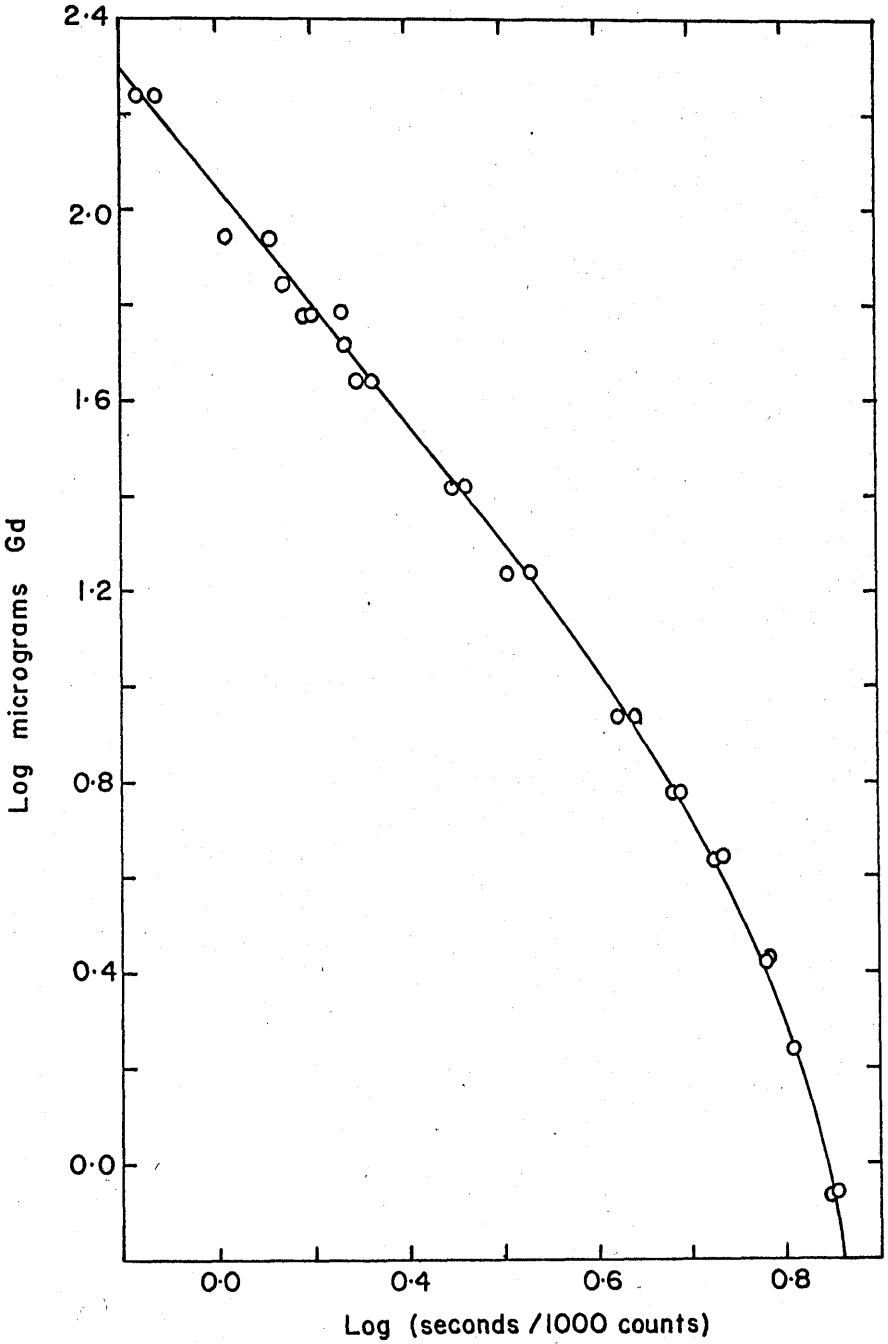

Gd TARGET ANALYSIS CALIBRATION CURVE; LOG-LOG

FIGURE II. 2

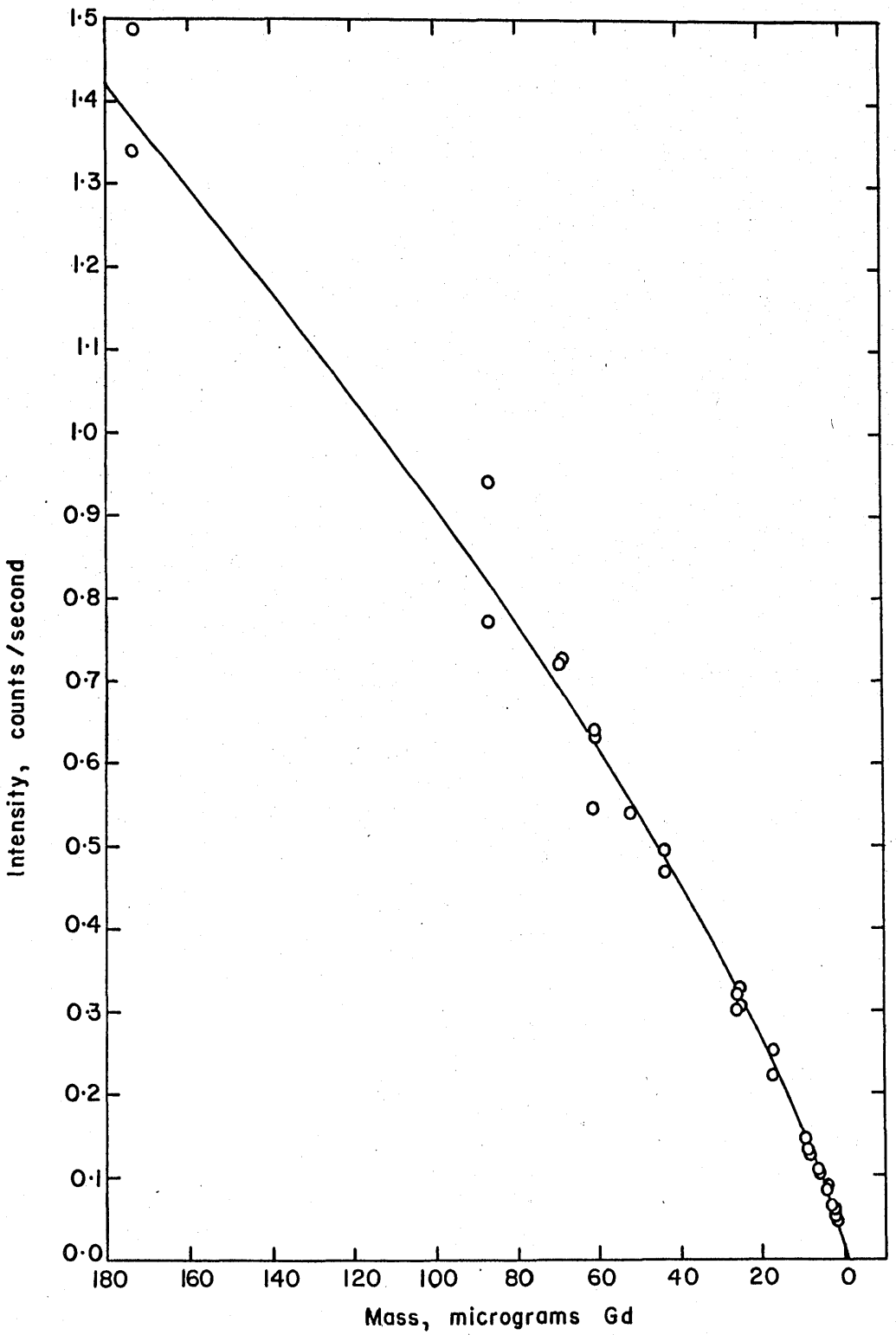

Gd TARGET ANALYSIS CALIBRATION CURVE

FIGURE II. 3

For crucibles ZrB_2/C-2 and ZrB_2/C-4, the average r values were 0.0694 and 0.0381 cm., respectively. The channel lengths were 0.689 and 0.658 cm., respectively. Target distances for Series 1, Series 2 and Series 3 experiments were 13.99, 13.27 and 13.45 cm., respectively. In all experiments, the target radius was fixed on target analysis as 0.550 cm. The collection angles, θ, were calculated as 0.0393, 0.0414 and 0.0409 radians for the three series. From these measurements the Clausing-distribution corrections were calculated as 1.41, 1.45 and 1.52 x 10^{-3}, respectively.

11. 5 Results

Table 11 contains the collected Knudsen data and the calculated thermodynamic quantities in order of increasing temperature. Column one lists the series and target designation. The first number defines the series and the second number designates the chronology of the measurements over the three series. Columns two, three and four list the exposure time, weight of gadolinium on the target and temperature for each Knudsen measurement. The computed gadolinium pressures defined by equation 6.17 and including the correction factors of Chapter 11. 4 are listed in column five. Column six contains values of -RlnK per mole of GdB_4(s). The measured free energy change on formation of one total mole of gas at each temperature is listed in column seven. Third Law values of ΔH^o_T and $\Delta H^o_{298^oK.}$ per mole of gas were calculated from equations 6.18 and 6.29 and are listed in columns nine and eleven. Columns eight and ten contain the values of ΔS^o_T and Δfef^o in eu./1/5 mole GdB_4 used

TABLE 11

Calculated Thermodynamic Quantities for GdB_4 Vaporization from Knudsen Effusion Data *

Series and Target	Time (sec.)	Gd on Target (g.)	Temp. (°K.)	P_{Gd} (10^{-7}atm.)	-RlnK (eu.)	ΔF_T° (kcal./$\frac{1}{5}$mole)	ΔS_T° ($\frac{1}{5}$eu.)	ΔH_T° (kcal./$\frac{1}{5}$mole)	$-\Delta fef^\circ$ ($\frac{1}{5}$eu.)	$\Delta H^\circ_{298°K.}$ (kcal./$\frac{1}{5}$mole)
1-2S	9426	2.09	2047	8.28	138.76	56.81	32.56	123.45	33.98	126.36
1-1S	7074	1.91	2128	10.02	140.76	59.91	32.45	128.96	33.93	132.11
2-"3"	13122	1.377	2169	13.2	138.01	59.87	32.60	130.58	33.91	133.42
3-13S	2276	4.074	2169	97.9	114.21	49.54	32.60	120.25	33.91	123.09
3-7S	9575	15.17	2182	86.9	115.41	50.36	32.38	121.01	33.89	124.31
3-12S	4329	15.10	2216	192.9	107.46	47.62	32.34	119.29	33.89	122.72
3-8S	9048	30.41	2237	186.7	107.81	48.23	32.33	120.55	33.86	123.97
3-11S	3000	20.28	2242	376.0	100.81	45.20	32.31	117.64	33.85	121.09
2-3S	6854	7.603	2258	142.7	110.46	49.88	32.30	122.82	33.85	126.31
3-9S	9477	51.76	2264	305.2	102.91	46.60	32.28	119.67	33.83	123.18
3-10S	2156	10.64	2299	277.9	103.86	47.75	32.64	122.75	33.81	125.48
2-5S	12741	19.68	2318	201.3	107.06	49.63	30.65	120.68	33.79	127.95
2-4S	7790	27.80	2355	468.9	98.66	46.49	30.62	118.59	33.74	125.92

TABLE 11, continued

Series and Target	Time (sec.)	Gd on Target (g.)	Temp. (°K.)	P_{Gd} (10^{-7}atm.)	-RlnK (eu)	ΔF_T° (kcal./$\frac{1}{5}$mole)	ΔS_T° ($\frac{1}{5}$eu.)	ΔH_T° (kcal./$\frac{1}{5}$mole)	$-\Delta fef^\circ$ ($\frac{1}{5}$eu.)	$\Delta H^\circ_{298°K.}$ (kcal./$\frac{1}{5}$mole)
2-6S	7428	7.709	2362	136.7	110.86	52.37	30.60	124.64	33.74	132.06
								avr. 122.2 ± 3.6		avr. 126.3 ± 3.7

$\Delta H^\circ_{2200°K.}$ (Second Law) = 121.2 ± 16.6 kcal./$\frac{1}{5}$ mole

$\Delta S^\circ_{2200°K.}$ (Second Law) = 31.6 ± 7.4 eu.

$$-RlnK = 1.987 \ln\left[(4.00)^4 \left(\frac{M_B}{M_{Gd}}\right)^2 P_{Gd}^5\right]$$

* Crucibles ZrB_2/C-2 for Series 2 and ZrB_2/C-4 for Series 1 and Series 3 had upper orifice diameters of 0.0672 and 0.01273 cm., respectively; lower orifice diameters, 0.0851 and 0.1503 cm., respectively; and channel lengths of 0.658 and 0.689 cm., respectively. The target distance was 13.99, 13.27 and 13.45 cm. for Series 1, Series 2 and Series 3, respectively. The target diameter was 0.550 cm. in all experiments.

in calculating ΔH^{o}_{T} and $\Delta H^{o}_{298^{o}K.}$, respectively.

A two-parameter least squares treatment of these data, prescribed by the Second Law technique of Chapter 6. 4. 1, was performed with the IBM 1620 computer. From the slope $\Delta H^{o}_{2200^{o}K.}$ is 121.2 $\pm$ 16.6 kcal. for the vaporization of 1/5 mole of GdB_4 to the gaseous elements. The value of $\Delta S^{o}_{2200^{o}K.}$ from the intercept is 31.6 $\pm$ 7.4 eu. for the same process. Figure 11. 4 is a graph of log p_{Gd} versus 1/T.

With the same assumptions regarding the use of the Third Law as were used in the Langmuir experiments (cf. Chapter 9. 3) and the employment of entropy data on elemental boron and gadolinium taken from JANAF (69) and Stull and Sinke (65), respectively, the average Third Law standard heat of vaporization at 2200°K. is 122.2 $\pm$ 3.6 kcal. for 1/5 mole of GdB_4. The average $\Delta H^{o}_{298^{o}K.}$ was calculated as 126.3 $\pm$ 3.7 kcal. for the same vaporization process.

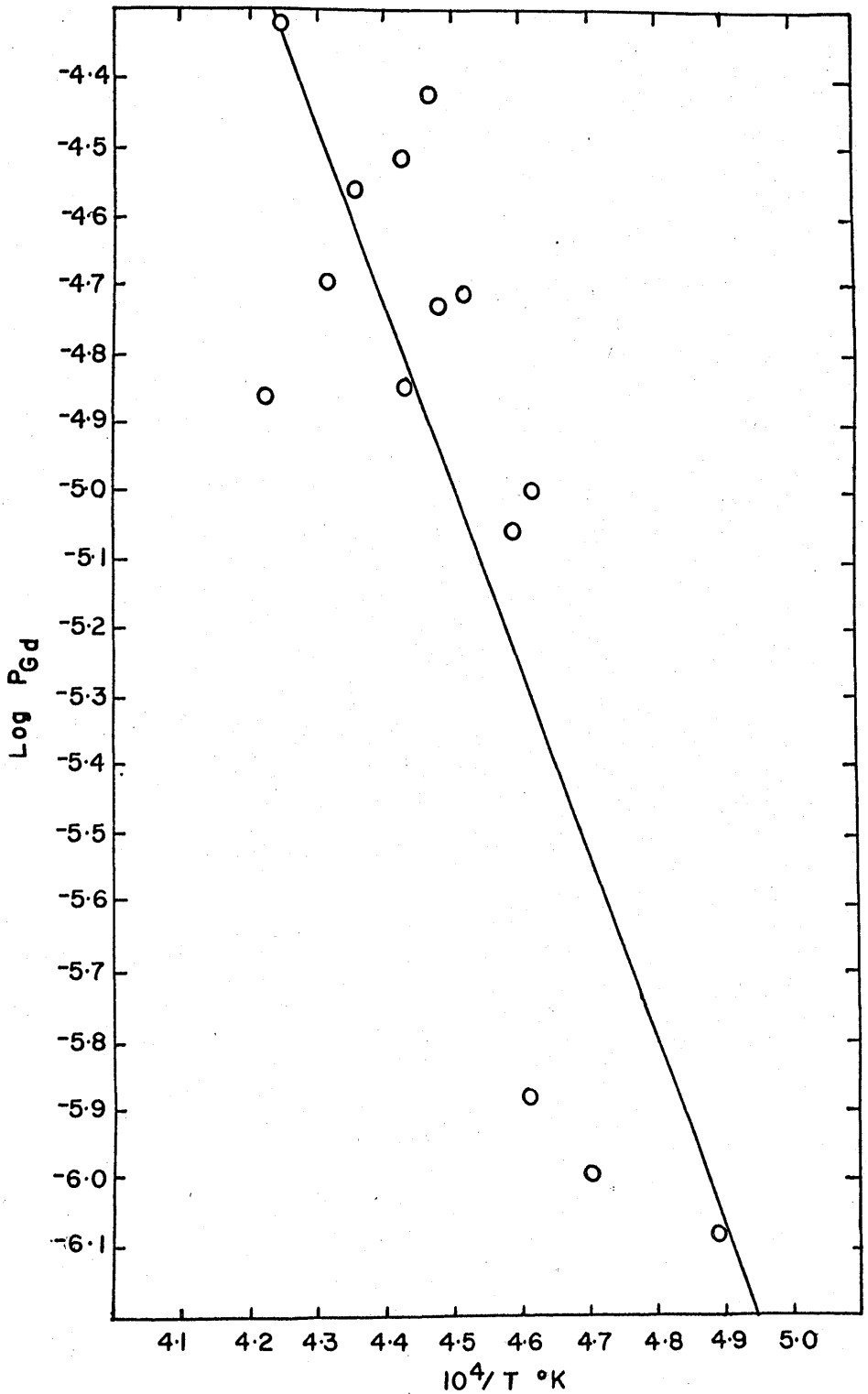

PLOT OF LOG P_{Gd} VERSUS 1 / T ; KNUDSEN

FIGURE II. 4

CHAPTER 12

ERRORS IN PRESSURE MEASUREMENTS ON GdB_4

12. 1 Kinds of Errors

Any discussion of the influence of errors on the heat of vaporization of $GdB_4(s)$ would include the following factors:

1. The influence of oxygen, water, carbon monoxide and carbon dioxide in the background on the transport of gadolinium and boron.

2. The errors in the entropies and free-energy-functions used in the Third Law treatments.

3. The stoichiometry error of the process.

4. The error in the temperature.

5. The cross section and multiplier efficiency errors and the silver calibration error in the mass spectrometric data.

6. The influence of orifice and sample areas, the Clausing-distribution correction and the possibility of non-unity condensation or evaporation coefficients.

7. Target analysis in the Knudsen experiments.

8. Equilibration with ZrB_2, contamination, sample history and mechanical measurements.

9. The sparsity of experimental points.

12. 2 Influence of Background Pressure

Perhaps the best method of demonstrating the importance of background gases is to study the rate of transport of gadolinium from the crucible as a function of the background pressure of H_2O, O_2 and CO_2 on being admitted from a controlled leak. In essence, this was the case with the mass spectrometer experiments. In Figure 10. 6 it was clear that p_{Gd} fell off from the linear temperature-coefficient slope as the background gauge pressure exceeded a pressure of 10^{-6}mm. However, because of the location of the pressure gauge and the problem of determining the conductance of the vacuum system, no reliable determination of the background pressure in the furnace itself was available.

It was noted in the mass spectrometer experiments that the Second and Third Law heats began to vary from constancy at background pressures at the ionization gauge exceeding 1×10^{-6}mm. It was further noted that the pressure in the furnace region could have been two orders of magnitude higher than the pressure at the ionization gauge. From the relative ion currents, CO^+-28 was by far the most important background gas. Historically, when non-graphitic crucibles were used in the mass spectrometer, water was by far the most important gas. Water can be absorbed quite easily on cold metal surfaces in large concentrations and with great tenacity. A plausible hypothesis, then, is the desorption of water from the apparatus walls as they are warmed and the reaction of water vapor with the graphite outer crucible to form CO(g) and hydrogen. While this reaction is not favored at room temperature, at the high crucible temperatures of the experiment the $T\Delta S$ factor becomes

quite large, and the reaction is favored.

In the glass vacuum apparatus of the Langmuir and Knudsen experiments a graphitic crucible effect similar to that of the mass spectrometer was noticed. Metal crucibles could be heated at high temperatures with background pressures two orders of magnitude below that achieved when graphite crucibles were heated to high temperature. Carbon monoxide or gaseous species absorbed by the graphite probably were the principal contributors to the background pressure.

However, within the limits of experimental error there was no pronounced deviation from constant values of the Third Law enthalpies of vaporization for either the Knudsen or the Langmuir experiments. These experiments were performed with background gauge pressures below 5×10^{-5} mm. Further, $\Delta S^{o}_{2200^{o}K.}$ from the Second Law Knudsen data is 31.6 ± 7.4 eu., which compares favorably with an estimated value of 32.4 eu. for the vaporization process to form one mole of gaseous species (cf. Chapter 13).

Further, still, the Second and Third Law enthalpies of the Knudsen study are in good agreement, which would indicate confirmation of the congruent vaporization process used to calculate the Third Law values. Thus, GdO(g) is not considered important within the limits of error in the Knudsen or Langmuir experiments.

In order to estimate the extent of reaction of CO, H_2O or O_2 with GdB_4 at high temperatures, one should examine suitable interaction processes. Consider the reactions of CO(g) with GdB_4.

$$2CO(g) + 8GdB_4(s) = 2GdO(g) + 5GdB_6(s) + GdB_2C_2(s) \qquad (12.\ 1)$$

White, Walsh, Ames and Goldstein estimate $D_o^o(GdO)$ at -160 kcal./mole and $S^o_{2200^oK.}$ for GdO at 75.9 eu. (52). JANAF (69) gives ΔH^o_f for formation of and $S^o_{2200^oK.}$ for CO(g) and O(g). The heats of formation of GdB_4, GdB_6, and GdB_2C_2 were estimated as -45, -50 and -50 kcal./mole, respectively. The entropy for the solids was estimated from $\Delta S^o_f = 0$. Then, for a CO(g) pressure of 5×10^{-8} atm., the GdO(g) pressure is about 5×10^{-14} atm. at 2200°K. Hence, CO(g) will not appreciably react with GdB_4 in this process.

Carbon monoxide may react with GdB_4 by process (12. 2):

$$GdB_4(s) + 2CO(g) = GdB_2C_2(s) + B_2O_2(g) \qquad (12.\ 2)$$

With ΔH^o_f and $S^o_{2200^oK.}$ data for GdB_4, CO and GdB_2C_2 indicated above, ΔH^o_f of $B_2O_2(g)$ at 2200°K. -116 kcal./mole and $S^o_{2200^oK.}$ for $B_2O_2(g)$ 92.1 eu., according to JANAF (69), the equilibrium constant for reaction 12. 2 can be estimated. Again assuming p_{CO} to be 5×10^{-8} atm., one calculates a corresponding B_2O_2 pressure of 3×10^{-16} atm. Hence, CO(g) does not transport GdB_4 in any way. The possibility of sample transport by $CO_2(g)$ is even more remote.

Consider now the process,

$$5/2\ O_2(g) + GdB_4(s) = GdO(g) + 2B_2O_2(g). \qquad (12.\ 3)$$

With background oxygen pressures of 10^{-8} atm., it is estimated that the GdO(g) pressure would be nearly atmospheric. Hence, $Gd_2O_3(s)$ and $B_2O_3(l)$ or possibly borates will be the products at this pressure of oxygen.

This observation implies that every oxygen molecule which enters the crucible will react to transport gadolinium and boron as gaseous oxides. However, at this oxygen pressure, the rate of entrance of oxygen through the orifice is small compared to the rate of congruent vaporization of $GdB_4(s)$ through the orifice. Evidence for the negligible influence of oxygen is the relatively low ion current of the M-32 and M-16 peaks in the mass spectrometer, their constancy with I^+_{Gd+} variation, and the inability to detect $B_2O_2(g)$ or BO(g) in the mass spectrometer. Therefore, this process is not thought important.

Assuming that water is the principal oxygen-containing absorbed molecule in the vacuum system, one must consider the following reaction:

$$9H_2O(g) + GdB_4(s) = 4HBO_2(g) + GdO(g) + 7H_2(g). \qquad (12.4)$$

While the poor thermochemical information available for GdO(g), $HBO_2(g)$ and $GdB_4(s)$ preclude a reasonable estimate of the pressures expected, the estimates by Leitnaker (136) on the reaction of water with $ZrB_2(s)$ and a realization that GdO is more stable than ZrO (52) and that GdB_4 per boron atom is much less stable than ZrB_2 per boron atom, it is obvious that water would be a serious problem at pressures over 10^{-8}atm. This interfering process was especially applicable in the mass spectrometer experiments, where the vacuum apparatus had a large metal surface area and where the line conductance was low. The water partial pressure should become noticeable with GdO(g) appearance in the mass spectrum as the walls of the apparatus became hot. The species, H_2O^+-18, was certainly the second most important species (next to CO(g)) at 1740°C. in

the mass spectrometer (cf. Table 10. 5); however, the water intensity was decreased relative to GdO^+ as the temperature was increased. At room temperature water was the most important oxygen-bearing species in the mass spectrum. Perhaps water was reacting with the sample to a greater extent at higher temperatures. Some HBO_2^+-44 and HBO_2^+-43 could have existed in the mass spectrum in view of the large ion currents at these masses. However, shutter checks were absent; and considerable background normally is found at these masses.

In conclusion, the principal background gas species was CO(g). The effect on transport of gadolinium and boron by CO(g) at the CO pressures of the Knudsen and Langmuir experiments was negligibly small. Oxygen would have been a serious contaminant, but its background pressure was too low compared to the rate of GdB_4 vaporization. Water was also a serious contaminant and probably accounts for the GdO(g) observed in the mass spectrometer. However, at the background water pressures in the experiments performed in the glass vacuum systems, the water or oxygen entered the crucible to react with GdB_4 at a rate less than that for congruent vaporization of GdB_4 by a factor of 100.

12. 3 Free-Energy-Function Errors

While the pressures, equilibrium constants,and free energy changes on vaporization of GdB_4(s) can be determined as precisely as experimental effort is warranted by interest, in order to determine the heat of vaporization from Third Law treatments of these measured pressures, entropies and free-energy-functions for B(g), Gd(g) and GdB_4(s)

are needed up to 2500°K. Such data for GdB_4(s) are disappointingly absent, necessitating approximations and thereby introducing errors. While entropy and free-energy-function data have been measured for B(g), data for Gd(g) have not been collected at these temperatures; however, reasonable estimates do exist. The magnitude of the collective errors in these quantities is discussed in this section.

The free-energy-functions and enthalpy functions for boron (s), boron (g), gadolinium (s,1) and gadolinium (g) are tabulated at 100° intervals in the temperature range of interest in Table 12. 1. For B(s,1) and B(g) the first two data columns are taken from Stull and Sinke (65), while the last two columns are taken from the JANAF Tables (69). The data for gadolinium (s,1) and gadolinium (g) were taken from Stull and Sinke (65).

Boron

There is some difference in the two sets of data of Table 12. 1 for elemental boron. The values of JANAF (69) are those accepted in a recent critical review on the thermochemical data of boron by Schick (132). The data on boron were taken from JANAF throughout this work.

Gadolinium

The enthalpy, free-energy-functions and entropy data for monatomic, ideal, gadolinium gas are based on the spectroscopic data of Russell (175) in Stull and Sinke (65). Similar data for gadolinium, solid and liquid, were estimated by Stull and Sinke from measured entropy and heat capacity data below 355°K. and an estimated heat of fusion. These data were used throughout this work.

TABLE 12. 1

Enthalpy and Free-Energy-Function Data for Boron and Gadolinium

Temp. (°K.)	$H^{\circ}_T - H^{\circ}_{298°K.}$ (cal./g.-at.)	$-\frac{(F^{\circ}_T - H^{\circ}_{298°K.})}{T}$ (cal./deg./g.-at.)	$H^{\circ}_T - H^{\circ}_{298°K.}$ (cal./g.-at.)	$-\frac{(F^{\circ}_T - H^{\circ}_{298°K.})}{T}$ (cal./deg./g.-at)
	Stull and Sinke (65)		JANAF (69)	
Boron (s):				
1500	6409	4.88	6759	5.152
1600	7082	5.17	7454	5.448
1700	7765	5.44	8158	5.735
1800	8460	5.70	8870	6.013
1900	9165	5.96	9590	6.283
2000	9880	6.21	10315	6.544
2100	10605	6.45	11047	6.798
2200	11340	6.69	11783	7.045
2300	17380	6.92	17124	7.285
2400	18130	7.24	17874	7.602
2500	18880	7.55	18624	7.906
Boron (g):				
1500	5971	40.70	5972	40.696
1600	6468	40.96	6468	40.955
1700	6965	41.21	6965	41.202
1800	7462	41.44	7462	41.437
1900	7959	41.67	7959	41.662
2000	8455	41.89	8456	41.878
2100	8952	42.09	8953	42.085
2200	9449	42.29	9449	42.285
2300	9946	42.48	9946	42.476
2400	10443	42.66	10443	42.661
2500	10939	42.84	10940	42.839
	Stull and Sinke (65)		Stull and Sinke (69)	
Gadolinium (g):			Gadolinium (s):	
1500	7296	51.57	9480	21.91
1600	7885	51.89	14070	22.32
1700	8481	52.19	14870	22.86
1800	9087	52.48	15670	23.36
1900	9703	52.75	16470	23.83
2000	10330	53.01	17270	24.27
2100	10970	53.27	18070	24.69
2200	11622	53.51	18870	25.09
2300	12286	53.74	19670	25.47
2400	12963	53.97	20470	25.84
2500	13652	54.19	21270	26.18

$\underline{GdB_{4.00}(s)}$

In the absence of any heat capacity data at any temperature for $GdB_{4.00}(s)$, no experimental free-energy-functions could be calculated or extrapolated. A reasonable estimate of the heat capacity of a phase of the alloy type or of compounds with a coordination type structure can be made with the use of the Neumann-Kopp Rule. This correlation assumes that ΔC_p^o of formation of the phase from the elements is zero at all temperatures. In other words, the heat capacity and, therefore, the free-energy-function, entropy function and enthalpy function for $GdB_{4.00}(s)$ may be estimated by adding the heat capacities or appropriate functions of the elements. This assumption was employed in all calculations of the thermodynamic values for GdB_4 vaporization.

The second assumption used in the GdB_4 thermodynamic calculations was that $\Delta S^o_{298^oK.}$ for the formation of GdB_4 was zero. From this assumption and the assumption that ΔC_p^o of formation at all temperatures is zero, standard state free-energy-functions and entropies for $GdB_{4.00}(s)$ are given by the sum of the stoichiometric proportions of the elemental free-energy-functions or entropies in their standard states.

The error arising from these assumptions for $GdB_4(s)$ is difficult to evaluate. However, Swift and White (176) measured the heat capacity of $MgB_4(s)$ from 17.34 to 299.53°K. and estimated the heat capacity above that temperature. A comparison of the Swift and White data as interpreted by JANAF (69) with the above assumptions is made in Table 12. 2 at 298°K. (136).

TABLE 12. 2

Comparison of Measured Thermodynamic Data for Magnesium Boride and Lanthanum Hexaboride with Estimated Values at 298°K.

Substance	C_p^o (cal./mole)	S^o (eu)	$(H^o_{298}-H^o_o)/T$ (cal./deg./mole)	$-(F^o_{298}-H^o_o)/T$ (cal./deg./mole)
Mg	5.96	7.81	4.008	3.80
4B	10.52	5.60	3.918	1.68
MgB_4(calc.)	16.48	13.41	7.93	5.48
MgB_4(expt.)	16.858	12.410	7.63	4.78
La	6.65	13.64		
6B	15.78	8.34		
LaB_6(calc.)	22.45	21.98		
LaB_6(expt.)	23.17	19.88		8.700

Swift and White's chemical analysis for MgB_4 described the composition as $MgB_{3.86}$; however, the data they reported were for MgB_4. If the entropy and free-energy-functions of GdB_4 are related to the entropy of the component elements in the same fashion as for MgB_4, then the entropy or free-energy-function calculated from the elemental data for GdB_4 should be decreased by 12.8 percent at 298^oK.

With the assumption that this 12.8% variation exists at all temperatures, $\Delta H^o_{298^oK.}$ from the Third Law for 1/5 $GdB_4(s)$ vaporization will be increased by 2.6 kcal. over the value calculated from the assumption that ΔC^o_p and $\Delta S^o_{298^oK.}$ for formation of GdB_4 are zero. An error of 10% in the free-energy-function or entropy of gadolinium solid or gas would affect this heat of vaporization about one kcal. Any errors in the free-energy-functions of elemental boron are negligible compared to those for gadolinium. Therefore, the errors in the heat of vaporization of GdB_4 with the free-energy-functions used should not exceed 3.5 kcal. of which 2.6 kcal. is systematic error.

12. 4 Composition Error

Since no deviation from a stoichiometric tetraboride composition has been observed for the lanthanides, the actinides and MgB_4, the assumption of a stoichiometric vaporization process seems appropriate. However, in view of the quality of the boron analyses, the precise four to one ratio of boron to lanthanide cannot be verified (cf. Chapter 7). While in this work no error for deviation from a stoichiometric process was used in the error analysis, it is interesting to calculate what the error in the Third Law $\Delta H^o_{298^oK.}$ for the vaporization would be, if the boron to lanthanide ratio were 3.950. Consider the process:

$$GdB_{\nu}\ (s) = Gd(g) + \nu B(g). \qquad (12.\ 5)$$

$$K = p_{Gd}\ p_B^{\nu} \quad .$$

$$P_B = p_{Gd}\ \nu\ (\frac{M_B}{M_{Gd}})^{1/2} \quad \text{from equation 6. 7.}$$

From equation 6.29,

$$\Delta H^{o}_{298^{o}K.} = T \left[[-R\ln p_{Gd}^{(1+\nu)}\ \nu^{\nu}\ (\frac{M_B}{M_{Gd}})^{\nu/2}] - [fef^{o}_{Gd(g)} + \nu\, fef^{o}_{B(g)} - fef^{o}_{Gd(s)} - \nu\, fef^{o}_{B(s)}] \right] . \qquad (12.\ 6)$$

On differentiation with respect to ν ,

$$d(\Delta H^{o}_{298^{o}K.}/T) = -(R\ln p_{Gd})\ d\nu - (R\ln \nu)\ d\nu - R d\nu - [\frac{R}{2}\ln(\frac{M_B}{M_{Gd}})]\ d\nu - fef^{o}_{B(g)}\ d\nu + fef^{o}_{B(s)}\ d\nu \quad . \qquad (12.\ 7)$$

For $\nu = 4.00$ and $d\nu = 0.05$, $d(\Delta H^{o}_{298^{o}K.})$ will be 13.64 kcal./mole at $2182^{o}K.$, or an error of 2.7 kcal./one total gaseous atom.

12. 5 Temperature Error

12. 5. 1 Langmuir

The difficulty in estimating the error here lies in the question of surface temperature discussed in Chapter 6. 3. 1. Assuming that the black-body temperature was the same as the surface temperature, one can estimate the temperature error from the equations developed below.

From Chapter 6. 2 an error of ten degrees was considered reasonable in the use of the pyrometer and calibrations for the optics involved. What error in the Third Law ΔH_T^o will such a temperature error produce? Substitution of equation 6. 5 into equation 6.29 provides equation 12. 8.

$$\Delta H^o_{298^oK.}(III) = T \left(-R\ln 4^4 \left(\frac{M_B}{M_{Gd}}\right)^{1/2} \left(W_T \cdot \frac{M_{Gd}}{M_{Gd}+4M_B} \cdot \frac{1}{44.33at}\right)^5 - R\ln T^{5/2} - \Delta fef^o \right) . \qquad (12.\ 8)$$

Differentiation of equation 12. 8 with respect to temperature gives equation 12. 9.

$$\Delta[\ \Delta H^o_{298^oK.}(III)] = \left(-R\ln 4^4 \left(\frac{M_B}{M_{Gd}}\right)^{1/2} \left(W_T \cdot \frac{M_{Gd}}{M_{Gd}+4M_B} \cdot \frac{1}{44.33at}\right)^5 - R\ln T^{5/2} - \Delta fef^o \right) - 5/2\ R\Delta T. \qquad (12.\ 9)$$

Therefore, a 10^o temperature error produces an error of 0.6 kcal. in the Third Law value for the heat of vaporization of 1/5 mole of $GdB_4(s)$.

12. 5. 2 Mass Spectrometer

The temperature error in the mass spectrometer data was probably much larger than in the Knudsen or Langmuir cases. The heating arrangement with two tungsten electron bombardment ribbons around the crucible described earlier necessarily allows temperature gradients. It is estimated that the gradient at the temperatures of the gadolinium measurements

might be as much as 30°; and at the temperatures of the silver calibration, about 15°. Coupling equation 6.10 with equation 6.29, substituting $e^{-\Delta F^{o}_{Ag}/RT_{Ag^+}}$ for the pressure of silver, and arranging the temperature terms in an easily differentiable fashion, one derives the relation in equation 12.10.

$$\Delta H^{o}_{298^{o}K.}(III) = -5T_{Gd^+} R\ln T_{Gd^+} + 5RT_{Gd^+} \ln T_{Ag^+} + 5\Delta F^{o}_{Ag} \frac{T_{Gd^+}}{T_{Ag^+}}$$

$$- RT_{Gd^+} \ln B - \Delta fef^{o}\, T_{Gd^+} \quad . \qquad (12.10)$$

Differentiation with respect to temperature produces the result,

$$\Delta(\Delta H^{o}_{298^{o}K.}(III)) = \left(-5R - 5R\ln T_{Gd^+} + 5R\ln T_{Ag^+} + \frac{5\Delta F^{o}_{Ag}}{T_{Ag^+}} - R\ln B - \Delta fef^{o} \right) dT_{Gd^+}$$

$$+ \left(5R \frac{T_{Gd^+}}{T_{Ag^+}} - 5/2\ \Delta F^{o}_{Ag} \frac{T_{Gd^+}}{T^2_{Ag^+}} \right) dT_{Ag^+} \quad . \qquad (12.11)$$

With an error in T_{Gd^+} of 30° at 2000°K. and an error in T_{Ag^+} of 15° at 1200°K., an error of 2.2 kcal. in the Third Law $\Delta H^{o}_{298^{o}K.}$ for the vaporization of 1/5 $GdB_4(s)$ is calculated.

12. 5. 3 Knudsen

The temperature in the Knudsen experiments does not depend on the assumption that surface temperature and black-body hole temperature are the same, as in the Langmuir experiments. Thus, the temperature error is that derived for the Langmuir case in Chapter 12. 5. 1 without this

assumption. Hence, an error of at most 0.6 kcal. in the Third Law ΔH_T^o for vaporization of GdB_4 to a mole of gaseous elements is estimated.

12. 6 Mass Spectrometer Calibration Error

As discussed in Chapter 6. 3. 2, the most accurate calibration method in mass spectrometry is the total vaporization of a known weight of the species, whose pressure is to be measured as a function of temperature, under the same geometry and electrical conditions as in the vaporizing system whose pressures are unknown. Because of the inability to distinguish ion current arising from sample boron from that of crucible boron, such a calibration could not be carried out for boron. The gadolinium ion current could have been interpreted in terms of gadolinium pressure by vaporizing a known weight of gadolinium metal. However, the behavior of gadolinium in ZrB_2 was not well characterized.

Therefore, a calibration of the mass spectrometer with silver was performed in each experiment prior to the collection of data generating the gadolinium temperature coefficient. This procedure necessitated an estimation of the relative ion cross sections and the multiplier efficiencies for gadolinium to silver. The gadolinium to silver cross section ratio was estimated in Chapter 10. 7 at 71/34.8 with an error certainly less than a factor of 1.3. And the multiplier efficiencies were determined in the same chapter to an accuracy of a factor of 1.3. Therefore, the error introduced into the gadolinium pressures from these estimates is generously estimated at a factor of 1.6.

While the calibration prior to each experiment was done both by determining the silver temperature coefficient and by monitoring the ion current as a function of time for the total vaporization of a weighed quantity of silver, in the particular experiments where the gadolinium temperature coefficients were considered reliable the latter calibrating scheme gave too low a sensitivity because of orifice clogging (cf. Figure 10. 3). With the use of equation 6.16 and a Clausing factor of 0.09, as defined by Iczkowski, Margrave and Robinson (198), for the cylindrical orifice in crucible ZrB_2/C-2, the sensitivity of the mass spectrometer for silver from the total weight loss method was 1.4×10^{-4} amp./atm. at $1302^{\circ}K$. This value is too low by the fraction of the orifice plugged and the error in the Clausing factor.

The sensitivity determined by temperature coefficient measurements taken immediately prior to noticeable orifice clogging resulted in a silver sensitivity of 5.5×10^{-4} amp./atm. at $1248^{\circ}K$. This sensitivity is to be compared with temperature coefficient silver sensitivities of 4.8×10^{-4} amp./atm. at $1244^{\circ}K$. and 2.5×10^{-4} amp./atm. at $1248^{\circ}K$. from two earlier experiments. Therefore, it is believed that the reliability of the sensitivity is within a factor of 1.8.

An interesting method of roughly determining Clausing factors for poorly defined orifice geometries is available. The Clausing factor for the orifice would be the ratio of the sensitivity determined from the temperature coefficient data to that determined from equation 6.16.

The measured gadolinium pressures in the mass spectrometer, in view of the above considerations, would be correct within a factor of 2.5.

An error in the pressure of this magnitude would be manifested as an error of 1.1 kcal. in the Third Law heat of vaporization of 1/5 GdB_4 at 1761°K.

12. 7 Condensation and Evaporation Coefficients; Clausing Factors; Angular Distribution Errors

It is difficult to interpret whether or not the GdB_4 vaporization experiments suffered from low non-equilibrium pressure measurements, arising from non-ideal conditions for Knudsen or Langmuir vaporization. Usually, one studies the effect of varying orifice size on the pressures inside the crucible. In essence, this study was accomplished in this work by comparing measured pressures between the limits of a very small orifice in the Knudsen experiments and the infinitely large orifice of the Langmuir experiments. If the measured pressures in the Langmuir case were too low because of failure to achieve equilibrium, the Third Law enthalpy calculated from Langmuir data will be higher than that of the Knudsen experiments. Within the statistical errors reported above, the Langmuir Third Law enthalpy does exceed that of the Knudsen and mass spectrometric values by 10 to 15 kcal. However, in view of the unknown temperature error of the Langmuir experiments and the meager volume of data, the actual size of this discrepancy cannot be defined. Therefore, condensation coefficients cannot be realistically evaluated.

There were two orifices used in the Knudsen experiments, one about one-fourth the area of the other. If a saturated vapor did not exist with the larger orifice, lower pressures and higher Third-Law enthalpies should be observed on comparison to the data with the smaller

orifice. However, quite the opposite was observed. The smaller orifice produced slightly lower pressures. In view of the large area of the massive powdered sample, the small orifice used, and the above consideration, it is believed that a saturated vapor existed in the Knudsen crucible.

Having demonstrated that vapor saturation existed in the Knudsen crucible, one must now consider the effect of orifice and target geometry on the rate of escape and on the collection of gas effusing from the orifice, i.e., the Clausing and the molecular distribution factors. The L/r ratio for the ZrB_2 orifices in the Knudsen work were 10.0 for crucible ZrB_2/C-4 and 17.3 for crucible ZrB_2/C-2 (cf. Chapter 11). The conical angles, τ, of these orifices, were 0.0137 rad. ($0^{\circ}47'$) for crucible ZrB_2/C-2, and 0.0166 rad. ($0^{\circ}57'$) for crucible ZrB_2/C-4. The solid angle, θ, between the normal to the orifice from the target and the target perimeter was $2^{\circ}23'$, for the Series 1 experiments and very slightly greater for the Series 2 and 3 experiments.

Should the convergent orifice, i.e., the diameter of the cylinder orifice at the vacuum end less than that opening into the crucible, have a value of $\tau \geq \theta$ where τ is the angle between the normal through the orifice and the conical wall of the orifice channel, then, according to Edwards and Freeman (177), there is no Clausing factor but only a cosine correction for the angular distribution of the effusing gas. This restriction is apparent if one realizes that under these conditions only a molecule passing through the orifice without striking the walls of the orifice could strike the target.

The formula, $N_\theta = \mu \pi r^2 \sin^2\theta$, defines the number of particles passing through the solid angle, θ, per second. The quantity, μ, is the number of particles striking the orifice/unit area/sec. in the cell; and r is the smallest orifice radius.

$$\mu = \frac{P}{m} \left(\frac{M}{2\pi RT}\right)^{1/2} \text{ from kinetic theory.} \tag{12.12}$$

Hence,

$$N_\theta = \frac{P\pi r^2 \sin^2\theta}{m} \left(\frac{M}{2\pi RT}\right)^{1/2}. \tag{12.13}$$

$$mN_\theta = m_T = Pa \sin^2\theta \left(\frac{M}{2\pi RT}\right)^{1/2} = \text{mass/sec.} \tag{12.14}$$

collected by the target.

Then,

$$P = \frac{m_T}{a \sin^2\theta} \left(\frac{2\pi RT}{M}\right)^{1/2} \tag{12.15}$$

and

$$P = \frac{m_T}{a \left(\frac{r^2}{r^2+L^2}\right)} - \left(\frac{2\pi RT}{m}\right)^{1/2}. \tag{12.16}$$

However, the smallest θ in the three sets of Knudsen experiments performed was $2^\circ 23'$ which is greater than 7°. Therefore, some error would arise from the use of the simple cosine correction of equation (12.16) because of the enhanced channeling of effusate onto the target area from the nearly cylindrical orifice. The use of equation (12.16) would produce gadolinium pressures which are too high.

At the other extreme, with the assumption of a cylindrical orifice one observes that molecules striking the walls of the orifice could reach the target. The combined Clausing factor and fraction-of-effusate-collected correction on the pressure was given by equation 11. According to Freeman and Searcy (174), this expression holds within $\pm$ 1 percent for $0 \leq L/r \leq 2.0$ and for values of $0 \leq \theta \leq 0.35$ radians, where θ is the angle between the normal through the orifice and the sloped walls of the orifice. For $2.0 \leq L/r \leq 8.0$ and $0 \leq \theta \leq 0.18$ rad. the error is $\pm$ 5 percent. The values of θ in these experiments were less than 0.18 rad., but L/r was greater than 8.0. If one assumes the decrease in error for such a small θ balances the increased error for $L/r > 8.0$, the error in the use of this correction formula is $\pm$ 5 percent.

Table 12. 3 shows the corrections for the three series of Knudsen arrangements with the ideal cosine distribution only and with the Searcy-Freeman formula. The corrections agree with 15 percent. The best correction would be an intermediate correction. Therefore, since the Searcy-Freeman values were used here, the random error in the correction is 5 percent, but a systematic error of about 7 percent too small a correction is applicable. Hence, the apparent gadolinium pressures will be from 2 to 12 percent too high. This effect will produce errors in the heat of vaporization of 1/5 GdB_4 of 0.02 to 0.12 kcal. in the Knudsen determinations.

TABLE 12. 3

Knudsen Effusion Correction Constant for Clausing Factor, Angular Distribution and Fraction Collected on Target

Series	Cosine Law (10^{-3})	Searcy-Freeman (10^{-3})
1	1.54	1.41
2	1.72	1.45
3	1.67	1.52

12. 8 Target Analysis Error

By far the largest error in the quantitative analysis of gadolinium on the aluminum targets from the Knudsen vapor collection experiments was in the delivery of a precise volume of gadolinium containing solution from a one ml. syringe onto the standard gadolinium plates. This error varied from 4.5 percent at one microgram of gadolinium to 15 percent at 175 micrograms of gadolinium on the standard targets. The scatter in the standards at low concentrations arose solely from the 5 percent error in delivering an accurate volume from a microsyringe. At high concentrations the error arose from the inaccuracy of the syringe delivery and from the uneven and thick layers of Gd_2O_3 that resulted on evaporation of such concentrated solutions.

Data scattering due to target alignment or rotation in the spectrograph, detector variations and reflection or blocking of gadolinium emission by the edge of the aluminum target overlay was insignificant.

Since the target analyses were in the one to 50 microgram range, the error in the analysis is assumed to be about eight percent. This error in the pressure of gadolinium would be realized as an error of $\pm$ 0.06 kcal. in the Third Law heat of vaporization of 1/5 GdB_4 at 2200°K., an insignificant error compared to other sources of error.

12. 9 Miscellaneous Errors

Errors left to be dealt with might arise from failure of the sample to equilibrate with the ZrB_2 crucible, errors in the geometry measurements, non-unity condensation coefficient on the target in the Knudsen experiments, the influence of possible contaminants in the sample, sample history, timing accuracy and weight measurement. There was no indication that these errors were large compared to those discussed above. Contamination might have been a serious problem, but cannot be effectively evaluated. The area error in the Langmuir measurements is estimated liberally at 10 percent.

The sparsity of experimental points was a large source of error. These random errors were evaluated statistically by the computer and are given with the calculated values in the appropriate chapters.

12.10 Summary

12.10. 1 Langmuir

The total root mean square error in the equilibrium constants of the Langmuir experiments equals the square root of the sum of the mean square errors in the weight loss, in the pellet area, in $T^{1/2}$, in the

time and, further, in the stoichiometry and the condensation coefficient, each weighted by the partial derivative of K with respect to the variable. From the above discussion, then, the error in the equilibrium constant is 11 percent. This deviation produces an error of 0.1 kcal. at 2200°K. in 1/5 RlnK which is quite within the experimental standard deviation of 1.5 kcal. The random error in the entropy or free-energy-functions and the temperature and the error from random scatter of experimental data fix the total error at 2.6 kcal. in the Third Law heat of vaporization of 1/5 GdB_4 at 2250°K. This error assumes no stoichiometry error, a unit condensation coefficient, no competing transport process, and ΔC_p^o and $\Delta S^o_{298°K.}$ of formation of GdB_4 equal to zero. Therefore, $\Delta H^o_{2250°K.}$ is 134.2 ± 2.6 kcal. for 1/5 $GdB_{4.00}$. This value is probably low by 2.6 kcal. because of the systematic entropy error in GdB_4(s).

12.10. 2 Mass Spectrometer

Accumulation of the estimated errors in the mass spectrometer experiments gives $\Delta H^o_{1750°K.}$ from Third Law analysis a value of 114.0 ± 4.6 kcal./1/5 mole. Again the systematic 2.6 kcal. error in the heat of vaporization, arising from the systematic error in the entropy of GdB_4, would tend to raise this value by that amount. The assumptions here are vapor saturation, no competing process, ΔC_p^o and $\Delta S^o_{298°K.}$ of formation for GdB_4(s) are zero, no stoichiometry error, and no geometry change between the temperature of silver calibration and the highest experimental temperature.

12.10.3 Knudsen

The errors in the Third Law heat of vaporization at 2200°K. from the Knudsen experiments are those of the Langmuir case less the area error but adding the error arising from the correction for effusion geometry and adding the error in target analysis. However, these errors produce an error in the equilibrium constant considerably less than the experimental deviation in K. Therefore, $\Delta H^{o}_{2200^{o}K.}$ from the Third Law is 122.2 ± 3.6 kcal. for $1/5GdB_{4.00}$. Again, the systematic error of 2.6 kcal., arising from the error in the entropy, would increase this value for the heat and reduce the error accordingly. The assumptions here are unit target condensation coefficient, vapor saturation in the crucible, no stoichiometry error, no other competing transport process and ΔC^{o}_{p} and $\Delta S^{o}_{298^{o}K.}$ of formation for $GdB_4(s)$ are zero.

CHAPTER 13

SUMMARY OF THERMODYNAMIC DATA ON GdB_4

Table 13 contains a summary of the enthalpies and entropies calculated from the pressure measurements over $GdB_4(s)$ from Langmuir, mass spectrometric and Knudsen measurements. The errors in the Second Law data are the computed least squares errors. The errors in the Third Law values are those discussed in Chapter 12.

For comparison purposes, it is useful to estimate $\Delta H^{\circ}_{2200^{\circ}K.}$ for the vaporization of 1/5 mole of GdB_4. The heat of formation of GdB_4 lies between -27.7 and -88 kcal./mole (cf. Chapter 14). The heat of vaporization of boron at 2200°K. is 133.9 $\pm$ 0.7 kcal./g.-at., according to Robson and Gilles (178), and the heat of vaporization of gadolinium at 2200°K. given in Stull and Sinke (65) is 75.3 kcal./g.-at. Therefore, the estimated heat of vaporization of 1/5 mole of GdB_4 vaporizing to give atoms at 2200°K. is between 127.6 and 139.8 kcal. From the assumption that $\Delta S^{\circ}_{298^{\circ}K.}$ and ΔC°_{p} for formation of $GdB_4(s)$ are zero at all temperatures, $\Delta S^{\circ}_{2200^{\circ}K.}$ per 1/5 mole is estimated at 32.4 eu. The Third Law enthalpy change for the vaporization at 298°K. would be 3.8 kcal. larger than $\Delta H^{\circ}_{2200^{\circ}K.}$

From the low Second Law entropy and from the high Third Law heats determined in the Langmuir experiments, it is obvious that the gadolinium pressures were too low. Thus, one must postulate a non-unity evaporation

TABLE 13

Summary of Thermodynamic Values for GdB_4 Vaporization in Langmuir, Mass Spectrometric and Knudsen Experiments.

Quantity	Langmuir	Mass Spectrometer	Knudsen
Temp. range (^{o}K.)	2112-2403	1599-1888	2047-2362
Temp. at which thermo. quantity measured (^{o}K.)	2250	1750	2200
ΔH^{o}_{T}(Second Law, kcal./$\frac{1}{5}$ mole)	116.4 ± 8.3	99.1 ± 5.8	121.2 ± 16.6
ΔS^{o}_{T}(Second Law, eu. for $\frac{1}{5}$ mole)	23.9 ± 3.7	24.4 ± 3.4	31.6 ± 7.4
ΔH^{o}_{T}(Third Law, kcal./$\frac{1}{5}$ mole)	134.2 ± 2.6	114.0 ± 4.6	122.2 ± 3.6
$\Delta H^{o}_{298^{o}K.}$ (Third Law, kcal./$\frac{1}{5}$ mole)	138.9 ± 2.7	116.4 ± 4.7	126.3 ± 3.7

coefficient for free evaporation of GdB_4. If the evaporation coefficient is not strongly temperature dependent, some reliance may be placed on the Second Law enthalpy. The Second Law value at 2250°K. agrees with the estimated values for the process within the errors involved.

From a comparison of measured gadolinium pressures in Tables 9, 10. 6 and 11 (cf. Figure 13), it is clear that the mass spectrometer measurements demonstrated the highest pressures. This is reflected in the Third Law value for $\Delta H^{\circ}_{1750°K.}$ of Table 13, which is lower than the Langmuir and Knudsen counterparts and considerably lower than the estimated values. The temperature coefficient value for the heat of GdB_4 vaporization is less than the Third Law value in the mass spectrometric measurements. If a process other than congruent GdB_4 vaporization were accounting for the gadolinium transport, the Third Law calculations, which employ free-energy-functions for the congruent process, would suppress the effect on the Third Law enthalpy change. On the other hand, the enthalpy determined from a slope of log p_{Gd} versus 1/T would bear no relation to the congruent process. Therefore, the Third Law value would be expected to be different from the Second Law value, if some other process were accounting for gadolinium or boron transport.

Recall from Chapter 10 that trace amounts of Gd_2O_3 were found in the mass spectrometer sample after the vaporization experiment. From the discussion of Chapter 10 and Chapter 12. 2, the presence of Gd_2O_3 is expected at sufficiently high background pressures of $H_2O(g)$ or $O_2(g)$. One may suspect, then, that gadolinium is being transported by the process,

$$Gd_2O_3(s) = 2GdO(g) + O(g). \qquad (13)$$

Using the heats of formation and free-energy-functions for Gd_2O_3 and GdO estimated by White, Walsh, Ames and Goldstein (52) and similar data for O(g) from Stull and Sinke (65), one finds p_{GdO} at 2000°K. is of the order of 10^{-7} atm. when the background oxygen pressure is 5×10^{-8} atm. Further, White, et al. (52), indicated that GdO is much more important over $Gd_2O_3(s)$ than Gd(g). This GdO pressure compares with an observed Gd pressure of 5×10^{-7} atm. at 2200°K. Hence, gadolinium transport as GdO(g) is important when Gd_2O_3 is present.

Thus, in view of the influence of background gases on GdB_4 vaporization, the thermodynamic data determined from the mass spectrometric study are not very useful in fixing the heat of vaporization of GdB_4. The value of the mass spectrometric studies lies in the confirmation of the vapor species, in the insight derived regarding the influence of background gases on material transport, in the confirmation of the principal vaporization process and the demonstration of equilibrium, and in the discovery of the possibility of GdO_2 molecules existing under reducing conditions.

The Knudsen experiments provided the most consistent set of thermochemical data. An examination of the Third Law calculations in Table 11 reveals no systematic variation with temperature. Thus, within the limits of error, no competing process was important. The agreement between the temperature coefficient intercept value of $\Delta S^{\circ}_{2200°K.} = 31.6$ eu. and the estimated value of 32.4 eu. is quite good, implying that the pressures are of the correct magnitude. In view of the large error limits, the remarkable agreement between Knudsen Third Law and Second Law heats of vaporization is, perhaps, fortuitous, but quite satisfying. These enthalpy values are low compared to the estimated $\Delta H^{\circ}_{2200°K.}$ of 127.6 to 139.8 kcal. per

1/5 mole GdB_4. Some of the difference can be accounted for when the systematic error of 2.6 kcal., or the assumption that ΔS_f^o is zero for GdB_4 formation, is added to the Knudsen enthalpy values (cf. Chapter 12. 3).

The best value for the heat of vaporization of 1/5 mole of GdB_4 is taken as the Third Law value of the Knudsen experiments, on the basis of the assumptions listed below:

1.) The stoichiometry of the vaporization process is assumed that in equation 1. 2.

2.) The entropies and the free-energy-functions for boron solid, liquid and gas are those of JANAF (69).

3.) The entropies and the free-energy-functions for gadolinium solid, liquid and gas are those given in Stull and Sinke (65).

4.) The value of $\Delta S^o_{298^oK.}$ for formation of $GdB_{4.00}$ differs from zero by the same extent as does that for MgB_4, as discussed in Chapter 12. 3.

5.) The quantity, ΔC_p^o, is zero at all temperatures above 298°K. for the formation of $GdB_4(s)$.

With these assumptions $\Delta H^o_{2200^oK.}$ is 124.8 ± 3.6 kcal. for the vaporization of 1/5 mole of $GdB_4(s)$. For the same process, $\Delta H^o_{298^oK.}$ is 128.9 ± 3.7 kcal.; ΔS^o is 31.6 ± 7.4 eu., and the pressure of gadolinium over GdB_4 at 2200°K. from equation 6.24 is 3.2×10^{-6} atm. The value of $\Delta F^o_{2200^oK.}$ is 55.3 kcal.

Within the framework of the above assumptions, and assuming $\Delta H^o_{298^oK.}$ for the vaporization of boron is 135.0 kcal./g.-at., according to Robson and Gilles (178) and that $\Delta H^o_{298^oK.}$ for the vaporization of gadolinium is 82 kcal./g.-at. (cf. Table 1.2), one finds that the heat of

formation of $GdB_{4.00}$ at 298°K. is -22.5 kcal./mole or -5.6 kcal./g.-at. boron. While this value is slightly outside the limits established in Chapter 14, the difference could easily be accounted for in the assumption either that ΔC_p^o for formation of GdB_4 is zero at all temperatures or that errors in the heats of vaporization of the component elements exist.

If p_{Gd} over GdB_4 at 2200°K. is 3.2×10^{-6} atm., then in the Knudsen cell p_B should be 3.2×10^{-6} atm. (cf. equation 6. 7). The vapor pressure of boron at 2200°K., according to Robson and Gilles (178), is 3.4×10^{-6} atm. The vapor pressure of gadolinium is 1.04×10^{-2} atm. at 2200°K. (65). If the boron pressure over $GdB_4(s)$ were, indeed, nearly equal to the boron vapor pressure, then the stabilities of GdB_6 and GdB_{100} are very severely restricted. In order for GdB_6 and GdB_{100} to exist, the boron pressures over both GdB_6 and GdB_{100} must be between 3.2 and 3.4×10^{-6} atm. with p_B over GdB_6 less than p_B over GdB_{100}.

This extremely restrictive stability requirement for GdB_6 and GdB_{100}, the low heat of formation of GdB_4, the low heat of congruent evaporation compared to estimated values, and the proximity of the boron pressure over GdB_4 to that over B(s), all indicate too high a gadolinium pressure in the Knudsen experiments on GdB_4. This apparent anomaly can best be shown in the composite log p_{Gd} versus 1/T graph of Figure 13. Clearly the Knudsen gadolinium pressures are a factor of ten greater than the Langmuir pressures. The Knudsen gadolinium pressures also represent the corresponding boron pressures in the Knudsen cell. The vapor pressure of boron versus 1/T is indicated on the graph, showing that at sufficiently low temperatures p_B over GdB_4 actually is greater than p_B over B(s). This apparent result, of course, cannot be correct.

Another inconsistency is found in the comparison of p_B over GdB_4 to p_B over B_4C. From the ternary Gd-B-C studies of Part I, it was established that GdB_4 will react with B_4C to form GdB_6 and graphite. Hence, p_B over the GdB_4-GdB_6 pair must be less than p_B over the B_4C-C pair. Then it follows that p_B over GdB_4 must be less than p_B over the B_4C-C mixture. The boron pressures over B_4C-C were measured by Robson and Gilles (178) and are shown in Figure 13. Clearly, the boron pressures over GdB_4 corresponding to the measured gadolinium pressures are greater than the boron pressure over B_4C, in violation of the Gd-B-C equilibria observed in Part I.

While the error analysis on the Knudsen experiments and the spread in the experimental data allow an error of a factor of two in p_{Gd} and, hence, in p_B, the decrease of a factor of ten in p_{Gd} needed to satisfy the above inconsistencies cannot be explained by errors in the Knudsen experiments. A chemical phenomenon must explain the apparent high gadolinium and boron pressures.

A very plausible explanation is available. Leitnaker (136) reported that $ZrB_{1.96}$ vaporizes congruently with a boron partial pressure of 1.5×10^{-8} atm. at 2200°K. Hence, the boron pressure at the outer surface of the ZrB_2 cell is two decades lower than the boron pressure inside the cell estimated from the measured gadolinium pressures. This activity gradient of boron through the crucible walls invites boron to move from inside the cell to the large vaporizing area of the ZrB_2 outer surface. The amount of boron transport through the crucible, compared to the amount of boron leaving the cell through the orifice, depends on the diffusion constant for boron in ZrB_2. Certainly the boron pressure inside the

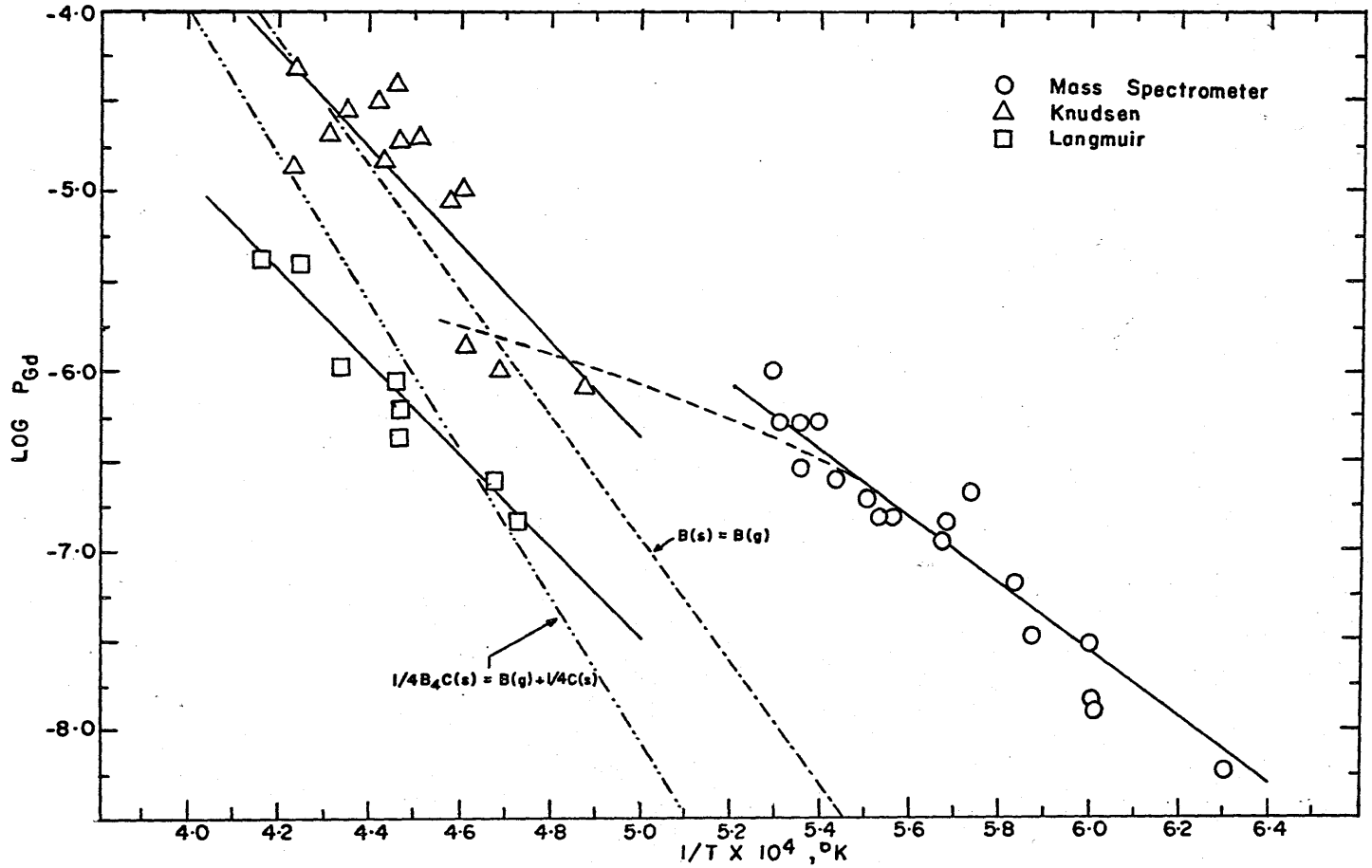

COMPOSITE PLOT OF LOG P_{Gd} VERSUS 1/T

FIGURE 13

crucible will be lower than p_B calculated from p_{Gd} for an inert Knudsen cell. If p_B inside the cell is lowered, then p_{Gd} will increase. However, since no Gd(l,s) was observed in the cell with GdB_4, p_{Gd} did not increase to the gadolinium vapor pressure.

The free energy of congruent vaporization of GdB_4 at 2200°K. was estimated from the entropy and heat of sublimation data of Table 1. 2 with the heat of formation of GdB_4 taken as -45 kcal./mole. Setting the gadolinium pressure equal to the vapor pressure of gadolinium at 2200°K., as given by Stull and Sinke (65), one establishes a lower limit on p_B inside the cell as 4×10^{-7} atm. Since p_B over GdB_4 must be less than p_B over B_4C, an upper limit of 8×10^{-7} atm. is established. Hence, the boron pressure corresponding to the measured gadolinium pressure in the reactive ZrB_2 crucible is between 4 and 8×10^{-7} atm., which is less than a decade lower than the apparent p_B.

Thus, all the inconsistencies in the partial pressures are comfortably explained. While the decreased boron pressure over GdB_4 will produce higher heats of vaporization for GdB_4, since the pressure changes are less than a decade, the change will be less than 10 kcal./total gas atom at 2200°K. Further, the stabilities of GdB_6 and GdB_{100} with respect to gaseous elements are still fairly restricted.

CHAPTER 14

TERNARY COMPATIBILITY STUDIES

14. 1 Thermodynamic Basis

In order to determine the relative stability of the lanthanide borides and to select a crucible material in which to study the vaporization of lanthanide borides, compatibility tests between various lanthanide tetra- and hexaborides and the metals W, Zr and Ta were made. Compatibility studies with graphite were discussed in Part I, Chapter 3. The equilibria observed in these ternary systems, coupled with a knowledge of the heats of formation of the non-lanthanide metal borides, define the range on the heats of formation of the lanthanide borides. This same technique was used by Brewer and Heraldsen (20) to determine the relative stabilities of transition metal borides, carbides and nitrides. A more sophisticated discussion of this technique is given by Rudy (19).

The thermochemical basis for this study lies in the following considerations: Consider the process in equation 14. 1.

$$AB_x\ (s) + A'\ (s) = AB_{x-y}\ (s) + A'B_y(s). \qquad (14.\ 1)$$

The free energy change for this process at any temperature is given by equation 6.18. The Neumann-Kopp Rule states that for the formation from the constituent elements of alloys of the metallic type and compounds with a co-ordination lattice, ΔCp at all temperatures is essentially zero (179).

With the assumption of this Rule, the free energy change for process 14. 1 is

$$\Delta F_T = \Delta H_{298^oK.} - T \Delta S_{298^oK.} \quad . \qquad (14.\ 2)$$

Since the reactants and products are all condensed phases, the entropy change for the process is assumed zero. Thus, the free energy for this process, to a first approximation, is determined by the heat of the reaction at 298°K. Observation of ternary equilibria in the A'-A-B system from compatibility studies defines a set of reactions which will or will not proceed. Then the sign of ΔF_T for these processes and, thus, of $\Delta H_{298^oK.}$ is established. A knowledge of the heats of formation of the borides in the A-B system coupled with the determination of the direction of the reaction in equation 14. 1, would, therefore, prescribe a limit on the heat of formation of $A'B_y(s)$. Judiciously chosen reference systems, A-B, can define the limits on the heat of formation of a boride, $A'B_y$, fairly closely from observation of ternary equilibria.

The validity of these assumptions for boride materials is discussed in Chapters 12. 3 and 15. 1. 3. In these studies equilibrium was assumed in the arc melting. Further, it was assumed that the equilibrium observed in the quenched samples is the same at all temperatures. Solid solution effects were considered second order. Ternary compounds were not observed in the equilibrium triangles used to derive heats of formation.

14. 2 Experimental

With the use of the reagents of Chapter 2. 2. 1, compacted mixtures of 325 mesh powdered samples, in proportions such that the synthetic

compositions were in the center of suspected ternary equilibrium triangles, were melted in an argon atmosphere purged of oxygen in the arc melting furnace described in Chapter 2. 2. 2. The quenched "buttons" were crushed in a hardened steel mortar, ground in an agate mortar to 325 mesh and analyzed with a Guinier or Debye-Scherrer powder X-ray diffraction technique ($Cu\text{-}K_{\alpha_u}$, 1.54178Å, radiation) to reveal the resultant phases.

In addition to the arc melter experiments in Table 14. 1, involving principally gadolinium, several lanthanide borides were heated in tungsten or graphite crucibles in the temperature range 1300 to 2200°K. The residues were examined by X-ray powder diffraction techniques for the phases present. While it was the intention of these studies to examine the vaporization process for the lanthanide boride, the presence of tungsten borides or a LnB_2C_2 phase demonstrated the reaction of tungsten or graphite crucibles with the lanthanide boride.

14. 3 Results

Table 14. 1 contains all of the information relating to the interactions between lanthanide borides and C, Zr, Ta or W. Columns one and two list the lanthanide and the experiment number. The initial phase content, conditions and synthetic compositions (where determined) are contained in column three. The phases present after reaction and the accompanying X-ray film number are listed in columns four and five. Column six describes whether the experiments were performed with arc melting techniques or are vaporization experiments using Knudsen crucibles. It should be noted that most of the observations regarding the interactions of the lanthanides other than gadolinium are taken from Tables 3. 1, Part I (graphite inter-

TABLE 14. 1

Ternary Compatibility Observations Involving Lanthanide Borides

Ln	Experiment	Initial Phases	Final Phases	Film	Method
La	1LaAMa1	LaB_6 in W cruc.	LaB_4 layer on LaB_6	C-2297	Knudsen
	1LaAMb1	LaB_4 on LaB_6 in W	LaB_4 layer thicker	C-2301	Knudsen
	2LaAM	(cf. Table 3. 1, Part I)			
	6LaAM	(cf. Table 4. 1)			
	6LaAM2	(cf. Table 4. 2)			
	7LaAM	LaB_6, Ta	$Ta_{2.4}B$, mjr. Ta, mnr. TaB and La_2O_3, mnr. to tr.	C-2629	Arc Melt
Ce	1CeAM	(cf. Table 4. 1)			
	863CeAM	(cf. Table 4. 2)			
Pr	1PrAM	(cf. Table 4. 1)			
	1PrAMb	(cf. Table 4. 2)			
Nd	0NdIH	NdB_6, mjr. NdB_4, mnr. in W cruc.	NdB_6, mjr. NdB_4, mnr. δ-WB, mnr. γ-W_2B, mnr.	C-1503	Knudsen
	2NdAM1	NdB_6 and NdB_4 in C cruc.	NdB_6 and C on lid	C-1683	Knudsen
	6NdAM	(cf. Table 4. 1)			
	6NdAM1	(cf. Table 4. 2)			
	7NdAM	(cf. Table 3. 1)			
	7NdAMa	(cf. Table 4. 1)			
	8NdAM	(cf. Table 3. 1, Part I)			
	763NdAM	NdB_6 and ZrB_2	NdB_6 and ZrB_2	C-2869	Arc Melt

TABLE 14. 1, continued

Ln	Experiment	Initial Phases	Final Phases	Film	Method
Sm	2SmAM	(cf. Table 3. 1, Part I)			
Gd	(Several compatibilities are noted in each of the Tables 3. 1 (Part I), 4. 1, 4. 2 and 3.)				
	4GdAMa2	GdB_4 in W cruc.	γ-W_2B and unknown	C-2049	Knudsen
	39GdAM	GdB_4 and W	GdB_4 and β-WB, mjr. δ-WB, mnr.	C-2376	Arc Melt
	40'GdAM	GdB_6 and W in W cruc.	β-WB, mjr. δ-WB, mnr. GdB_4, tr.	C-2445	Knudsen
	41GdAMb	GdB_4 and C in W cruc.	β-WB and GdB_2C_2, eqc. δ-WB, mnr. WC, tr.	D-1170	Knudsen
	41IHa4	GdB_4 and C in W cruc.	GdB_6 and δ-WB	D-1090	Knudsen
	60GdAM	W and GdB_6 $(W_{.035}{}^{Gd}{}_{.138}{}^{B}{}_{.828})$	GdB_6, mjr. GdB_4, mnr. W_2B_5, mnr.	C-2657	Arc Melt
	61GdAM	W_2B_5 and GdB_4 $(W_{.213}{}^{Gd}{}_{.069}{}^{B}{}_{.718})$	W_2B_5, mjr. GdB_4, GdB_6, β-WB and δ-WB, mnr.	C-2657	Arc Melt
	62GdAM	W and GdB_6 $(W_{.300}{}^{Gd}{}_{.100}{}^{B}{}_{.600})$	β-WB, mjr. δ-WB, mnr. unknown, mnr.	C-2666	Arc Melt
	63GdAM	W and GdB_6 $(W_{.327}{}^{Gd}{}_{.096}{}^{B}{}_{.577})$	β-WB, mjr. δ-WB, mnr. unknown, mnr.	C-2676	Arc Melt
	64GdAM	Ta, B and GdB_6 $(Ta_{.182}{}^{Gd}{}_{.091}{}^{B}{}_{.727})$	TaB_2, mjr. GdB_4, mnr. unknown, mnr.	C-2675	Arc Melt
	65GdAM	Ta, B, GdB_6 and GdB_4 $(Ta_{.071}{}^{Gd}{}_{.143}{}^{B}{}_{.785})$	TaB_2, mjr. GdB_4 and GdB_6, mnr.	C-2678	Arc Melt

TABLE 14. 1, continued

Ln	Experiment	Initial Phases	Final Phases	Film	Method
Gd	66GdAM	Ta, B and GdB_4 ($Ta_{.271}Gd_{.104}B_{.625}$)	Ta, TaB_2 and Ta_3B_4, mjr. GdB_4, tr.	C-2674	Arc Melt
	67GdAM	Ta and GdB_4 ($Ta_{.138}Gd_{.172}B_{.690}$)	TaB_2, mjr. GdB_4, mnr. unknown, mnr.	C-2679	Arc Melt
	68GdAM	Ta and GdB_4 ($Ta_{.615}Gd_{.077}B_{.308}$)	Ta_2B, mjr. TaB, mnr. unknown, mnr.	C-2673	Arc Melt
	69GdAM	GdB_6, Zr and B ($Zr_{.087}Gd_{.044}B_{.869}$)	GdB_6, ZrB_{12} and ZrB_2, eqc.	C-2690	Arc Melt
	70GdAM	GdB_6 and Zr ($Zr_{.067}Gd_{.134}B_{.800}$)	GdB_6, GdB_4 and ZrB_2, eqc.	C-2692	Arc Melt
	71GdAM	GdB_6 and Zr ($Zr_{.222}Gd_{.111}B_{.666}$)	ZrB_2, mjr. GdB_4, tr.	C-2691	Arc Melt
Tb	1TbAM2	(cf. Table 4. 1)			
	1TbAMaMS	TbB_6 in W cruc.	TbB_4 and TbB_6	visual	Knudsen
	2TbAM	(cf. Table 4. 1)			
	3TbAM	(cf. Table 3. 1, Part I)			
	741TbAM	(cf. Table 4. 1)			
Dy	1DyAMd	DyB_6 and DyB_4 in W cruc.	Unidentified Visible crucible interaction	C-2172	Knudsen
	2DyAM	(cf. Table 3. 1, Part I)			
	3DyAMa	(cf. Table 4. 1)			
	4DyAM	(cf. Table 3. 1)			

TABLE 14. 1, continued

Ln	Experiment	Initial Phases	Final Phases	Film	Method
Ho	2HoAM	(cf. Table 3. 1, Part I)			
Er	2ErAM	(cf. Table 3. 1, Part I)			
Yb	1YbAMal	YbB_6 in W cruc.	YbB_6, mjr. YbB_4, mnr.	C-2347 C-2350	Knudsen
	2YbAM	(cf. Table 3. 1, Part I)			
	3YbAMa	(cf. Table 4. 1)			
	5YbAM	(cf. Table 3. 1, Part I)			
	5YbAMa	(cf. Table 3. 1, Part I)			
Y	1YAM	(cf. Table 4. 1)			

action), 4. 1 (ZrB_2 interaction) and 4. 2 (ZrB_2 interaction).

The vaporization behavior of lanthanide borides either in tungsten or in graphite Knudsen crucibles was quite different from the behavior in the inert ZrB_2 crucibles. Hexaborides of all lanthanides studied (La, Nd, Gd, Tb, Dy, Yb) were reduced by tungsten with tetraboride layers appearing on hexaboride-tetraboride pelleted mixtures or on granule cores. The vaporizing area for the boron was the reactive wall and lid area of the tungsten crucible, while the metal vaporized through the area of the orifice. This observation accounts for the apparent preferential loss of boron from LaB_6 (1LaAMal,bl), NdB_6 (ONdIH) and YbB_6 (1YbAMal) (cf. Table 14. 1), which is contrary to the Langmuir observations and Knudsen observations on these borides in ZrB_2 crucibles (cf. Chapter 4). Vaporization from graphite crucibles showed reaction of tetraboride with graphite to form LnB_2C_2 in several cases, leading to preliminary interpretations that GdB_4 and TbB_4 lost metal preferentially; this conclusion was contradicted by the observations of congruent vaporization of GdB_4 and TbB_4 in Chapter 4.

Lanthanum: The equilibrium between graphite and LaB_6 was demonstrated in Part I and again in Table 14. 1, where, in experiment 6LaAM2, the graphite outer crucible lid did not react with an LaB_6 deposit from a ZrB_2 crucible containing LaB_6. In view of the formation of a tetraboride layer on LaB_6 granules after reaction in tungsten Knudsen crucibles and from the realization that this loss of boron from LaB_6 in 1LaAMal and 1LaAMbl is contrary to the congruent vaporization of LaB_6 demonstrated in Chapter 4, the tungsten reduction of LaB_6 to LaB_4 is concluded. X-ray analysis of lid deposits of LaB_6 heated in ZrB_2 crucibles and analysis of

the $ZrB_2/LaB_{4,6}$ interface in Langmuir heatings indicated LaB_6 and LaB_4 exist in equilibrium with ZrB_2 (cf. Chapter 4, Tables 4. 1 and 4. 2).

In the arc melting of an arbitrary mixture of tantalum metal and LaB_6 (7LaAM), the presence of $Ta_{2.4}B$, Ta, TaB and La_2O_3 in the product indicated that tantalum metal reduces LaB_6 and LaB_4 to lanthanum metal and TaB. The presence of small amounts of tantalum is attributed to incomplete reaction. La_2O_3 would result on exposure of lanthanum metal to air after melting. Below 2040°C. Ta and $Ta_{1.60}$ exist in equilibrium; however, according to Leitnaker (54), above 2180°C. $Ta_{1.60}B$ disproportionates into $Ta_{2.4}B$ and TaB, as was observed in this arc melting experiment. Thus, tantalum reduces LaB_6 and LaB_4 to lanthanum metal with the formation of TaB, $Ta_{1.6}B$ or $Ta_{2.4}B$, depending on the temperature and stoichiometry.

Cerium: The equilibrium between CeB_4, CeB_6 and ZrB_2 was demonstrated in Chapter 4, Tables 4. 1 and 4. 2.

Praseodymium: As in the case of lanthanum and cerium, PrB_6 and PrB_4 were found to exist in equilibrium with ZrB_2 (cf. Tables 4. 1 and 4. 2).

Neodymium: From the free evaporation experiments in Table 4. 1 the ZrB_2/NdB_6 interface did show some reaction to NdB_4 and ZrB_{12} on one occasion; however, on another occasion, no reaction was observed. In 763NdAM, Table 14. 1, an arc melting of NdB_6 with ZrB_2 failed to show any interaction. In Part I, Table 3. 1, and in Table 14. 1 for sample 2NdAM1, evidence for the reaction of graphite with NdB_4 to form NdB_2C_2 and the NdB_6-C equilibrium was presented. The walls of a tungsten crucible revealed δ-WB and γ-W_2B, after extensive heating of NdB_6 and NdB_4 mixtures in the crucible (ONdIH). From this observation and the observations of

gray tetraboride layers on hexaboride/tetraboride pellet cores that appear from heatings in tungsten crucibles, it is concluded that tungsten reduces NdB_6 to NdB_4 with the formation of δ-WB.

Promethium: Promethium was not investigated.

Samarium: The equilibrium between SmB_6 and graphite was demonstrated in Part I, Table 3. 1.

Europium: Europium was not investigated.

Gadolinium: Most of these ternary studies were performed with GdB_6 and GdB_4. To a first approximation, the heats of formation of the lanthanide tetraborides are all nearly the same, and the heats of formation of the lanthanide hexaborides are all nearly the same. Thus, the equilibria observed in the gadolinium systems will probably reflect the behavior of all lanthanide tetra- and hexaborides in ternary behavior with C, Zr, Ta or W except in some specific instances discussed later in this chapter.

Reaction of graphite with GdB_4 to form GdB_2C_2 and the GdB_6-graphite equilibrium were reported in Part I. While some Knudsen and Langmuir vaporizations in tungsten and ZrB_2 crucibles and the studies of Chapter 5 indicated tungsten does reduce GdB_6 and GdB_4 and that ZrB_2 does not, the arc melting experiments of Table 14. 1 were designed specifically to define the equilibria in the W-, Zr- and Ta-Gd-B systems.

Sample 60GdAM was a reaction product of tungsten and GdB_6 with a synthetic stoichiometry within the ternary triangle, W_2B_5-GdB_4-GdB_6. The observation of only these three phases in the arc melted product confirmed this equilibrium triangle. In the reaction of W_2B_5 with GdB_4 in experiment 61GdAM, the presence of GdB_6 in the product is inexplicable in view

of the results for experiment 60GdAM. However, the presence of high- and low-temperature WB in the residue of experiment 61GdAM and in tungsten crucibles in which GdB_4 was vaporized and, also, the observation of the W_2B_5-GdB_4 join in experiment 60GdAM force the conclusion of the equilibrium triangle, W_2B_5-GdB_4-WB. Finally, in two experiments, 62- and 63GdAM, tungsten and GdB_6 were allowed to react in proportions such that the synthetic composition was on the metal-rich side of the WB-GdB_4 join. It was the intention here to demonstrate WB-Gd-GdB_4 equilibrium. In both cases high- and low-temperature WB were observed. Further, a complex pattern of an unidentified phase or phases was present in the diffraction record. These diffraction lines could have represented a mixture of Gd_2O_3 and GdB_4, but the pattern was too poor to allow firm interpretation. At any rate, the Knudsen heatings of GdB_4 in tungsten crucibles (excess tungsten) do reveal WB formation. Therefore, the WB-Gd join does exist.

In the Zr-Gd-B system, the binary joins ZrB_2-GdB_4 and ZrB_2-GdB_6 were demonstrated in Chapter 4. Experiment 69GdAM with synthetic composition in the GdB_6-ZrB_2-ZrB_{12} triangle did, in fact, demonstrate this three-phase equilibrium. The arc melting experiment, 70GdAM, confirmed the GdB_4-GdB_6-ZrB_2 ternary equilibrium. Finally, a synthetic composition in the Gd-GdB_4-ZrB_2 region revealed GdB_4 and ZrB_2 on examination. Gadolinium could have been present in small amounts as Gd_2O_3 and, therefore, not observed; or gadolinium metal could have distilled out. If zirconium were the third phase, it would not oxidize on exposure to air and should be detectable by X-ray diffraction methods. Thus, the ternary equilibrium, Gd-GdB_4-ZrB_2, exists. The absence of ZrB, as pointed out by Glaser and

Post (129), is explained by instability with respect to Zr and ZrB_2, except over a narrow range of temperature.

The TaB_2-GdB_4-GdB_6 equilibrium was demonstrated by experiments 64- and 65GdAM, although in the latter experiment the low concentration of GdB_6 precluded its observation in the diffraction pattern. An attempt in experiment 66GdAM to determine the equilibria in the TaB_2-Gd-GdB_4 region revealed Ta_3B_4, TaB_2, Ta and GdB_4 present in the product. The presence of tantalum metal lines in the X-ray pattern is explained by the adherence of unreacted metal to the bottom of the arc melted button. The presence of Ta_3B_4 or TaB_2 eliminates the possibility of a TaB-GdB_4 join. Gadolinium could have been present below the limits of detection as Gd_2O_3 or could have been distilled out.

In the TaB_2-GdB_4-Gd region, the reduction of GdB_4 by Ta in experiment 67GdAM revealed TaB_2 and GdB_4 plus a phase with a complicated and poor X-ray pattern, a phase which probably was Gd_2O_3 and certainly was not a boride or Ta metal. The presence of TaB_2 in this experiment is in conflict with the observations of experiment 66GdAM, if the Ta_3B_4-GdB_4 join is assumed established in that experiment.

A more satisfactory interpretation which satisfies both experiments 66- and 67GdAM is that the ternary triangles, GdB_4-Ta_3B_4-Gd and, by implication, Ta_3B_4-TaB-Gd, exist at low temperatures. Schwarzkopf and Glaser (134) reported that the only borides in the Ta-B system that exist up to their melting points are TaB and TaB_2. Thus, at some as yet undefined temperature, Ta_3B_4 would disproportionate to TaB and TaB_2. At a sufficiently high temperature such that Ta_3B_4 does not exist, the observed equilibrium triangles would be GdB_4-TaB_2-Gd and TaB_2-TaB-Gd. Such a high

temperature was achieved in the 67GdAM melting and the equilibrium quenched in. Therefore, the most probable high temperature equilibrium triangles are GdB_4-TaB_2-Gd and TaB_2-Gd-TaB. Assuming that the temperature in the 66GdAM experiment was not uniform or that the back reaction for the cooling rate in experiment 66GdAM was not negligible, then one can explain the presence of both TaB_2 and Ta_3B_4 with GdB_4 and Gd.

Reaction of tantalum with GdB_4 in a synthetic composition in the $Ta_{1.60}B$-Gd-$Ta_{2.40}B$ triangle (68GdAM) revealed on X-ray diffraction analysis $Ta_{2.40}B$, TaB and weak lines which again probably were from Gd_2O_3. The absence of $Ta_{1.60}B$ was explained by its disproportionation above 2180°C. to TaB and $Ta_{2.40}B$, as demonstrated by Leitnaker (54). No gadolinium boride was observed. Thus, above 2180°C. the triangle $Ta_{2.4}B$-TaB-Gd exists. This observation implies the Ta-$Ta_{2.4}B$-Gd triangle.

Terbium: The equilibrium between ZrB_2 and TbB_4 and between ZrB_2 and TbB_6 was demonstrated in Table 4. 1. The reaction of graphite with TbB_4 to form TbB_2C_2 was revealed in Part I, Table 3. 1. Finally, evidence for the reduction of TbB_6 by tungsten was found in the low B^+/Tb^+ intensity ratios in a mass spectrometric study of TbB_6 in a tungsten crucible.

Dysprosium: The equilibrium of DyB_4 and DyB_6 with ZrB_2 and graphite was summarized in preceding sections. Further, a mixture of DyB_6 and DyB_4 heated in a tungsten cell was observed to interact with the tungsten, forming a gray DyB_4 layer on a DyB_4/DyB_6 pellet. No such kinetic problem arose in the use of a ZrB_2 cell.

Holmium and Erbium: The reaction of HoB_4 and ErB_4 with graphite to form HoB_2C_2 and ErB_2C_2 was discussed in Part I.

Thulium: The behavior of Tm was not investigated.

Ytterbium: The equilibrium between YbB_6 and ZrB_2 and between YbB_{12} and ZrB_2 was implied in Table 4. 1. The behavior of YbB_6/YbB_4 with graphite also was discussed in Part I, Table 3. 1. When a YbB_6 sample was heated in a tungsten crucible, YbB_4 layers formed on a YbB_6 pellet, which was contrary to the observed vaporization processes of Chapter 4, and indicated reaction of W with YbB_6.

Lutetium: Lu was not investigated.

Yttrium: Finally, the YB_6-ZrB_2 and YB_4-ZrB_2 equilibria were observed in Table 4. 1.

14. 4 Other Compatibility Information

Brewer and Heraldsen (20) found that CeB_6 did not react with graphite while CeB_4 did react to form some unidentified ternary borocarbide. This fact agrees with the observations in this work on other lanthanides (Part I). Nowotny, et al. (17), found that graphite did not react with UB_4 or UB_{12}. Further, Glaser (06) and Nowotny, et al. (18), reported that graphite would not reduce ThB_6 or ThB_4. Lafferty (103) demonstrated equilibrium between LaB_6 and graphite. In their investigation of the La-B system, Johnson and Daane reported no serious attack on the crucible when lanthanum and boron were melted in a tantalum crucible to prepare LaB_4, unless the La contained appreciable carbon. However, this investigation demonstrated that tantalum metal will reduce both LaB_6 and LaB_4 if intimate contact is achieved. Galloway and Eick (117) reported the reaction of molybdenum crucibles with SmB_4 and SmB_6 samples indicated by the appearance of δ-MoB on the crucible walls. Since tungsten is more reducing than molybdenum, certainly tungsten reduces these borides.

14. 5 Schematic Ternary Diagrams

The equilibria observed in this investigation may be catalogued into ternary diagrams, which do not represent isotherms or isobars, but do illustrate the reactions that can occur at high temperatures. Within each triangle in the diagrams only those condensed phases representing the corners of that triangle may be in equilibrium. Similarly, along the two condensed phase joins, only those phases at the ends of the join may exist together at equilibrium. These diagrams are illustrated in Figures 14. 1 to 14.14.

In Figures 14. 1 to 14.14 the lanthanides are divided into three groups according to the borides existing in the particular lanthanide-boron binary system (cf. Chapter 2). The first group contains La, Ce, Pr, Nd, Sm, Eu, Gd and Sc borides. These boride systems contain a well characterized tetra- and hexaboride and, apparently, no dodecaboride. Europium and scandium were included in this group for convenience, even though EuB_4 and ScB_4 have not been made. The second group, consisting of Tb, Dy, Ho, Yb and Y, exhibits tetra-, hexa- and dodecaborides. Finally, the third group, Er, Tm and Lu, do not form hexaborides but do exhibit tetra- and dodecaborides. Lanthanide diborides are omitted from these diagrams since they probably disproportionate to Ln(l) and LnB_4 at the temperatures of the arc melting experiments. It is believed that all lanthanides will be proved to exhibit a hectoboride. Thus, LnB_{100} is included in all groups. Discussions of the existence of these borides are found in Chapters 2 and 15. 1. 7. 2.

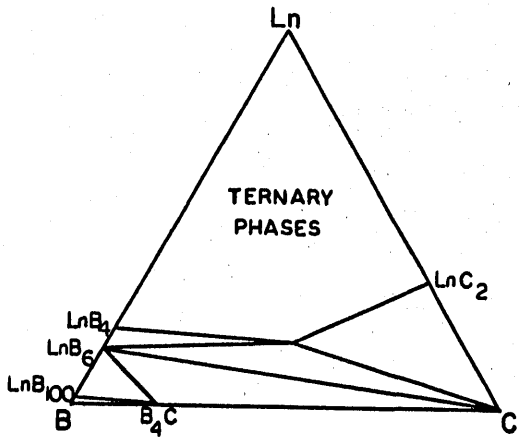

La, Ce, Pr, Nd, Sm, Eu, Gd, Sc

FIGURE 14. 1

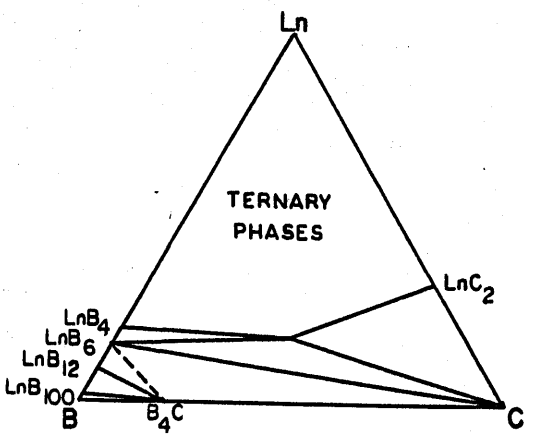

Tb, Dy, Ho, Yb, Y

FIGURE 14. 2

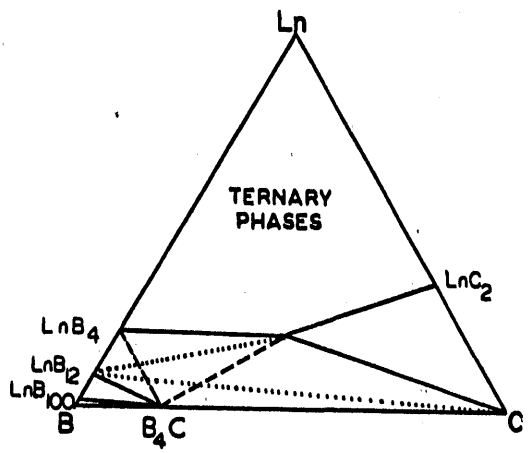

Er, Tm, Lu

FIGURE 14. 3

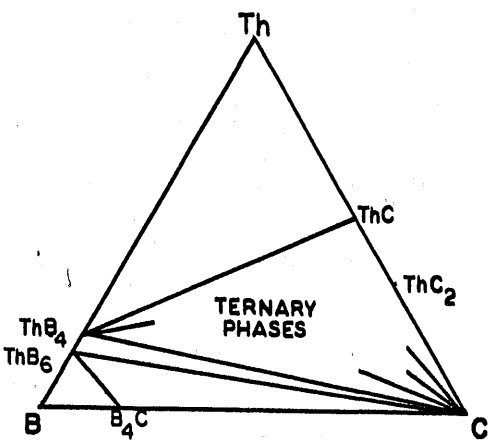

Th

FIGURE 14. 4

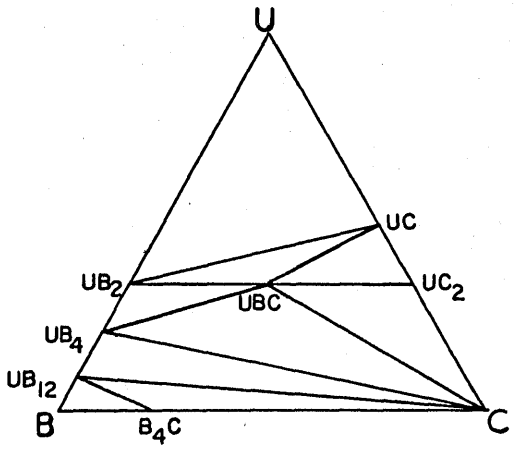

U

FIGURE 14. 5

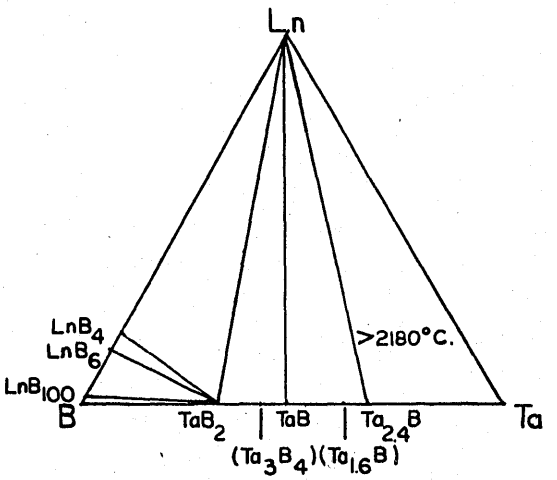

La, Ce, Pr, Nd, Sm, Eu, Gd, Sc

FIGURE 14. 6

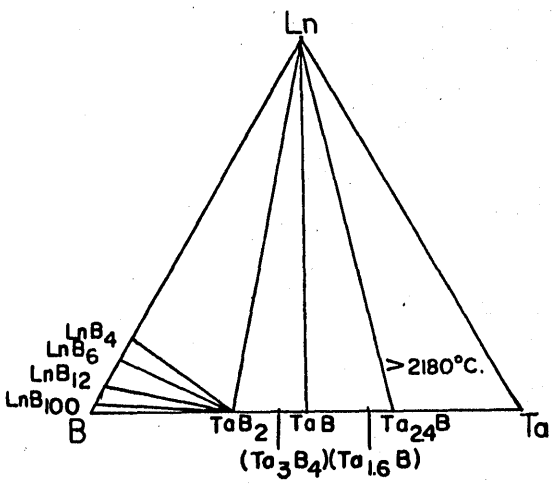

Tb, Dy, Ho, Yb, Y

FIGURE 14. 7

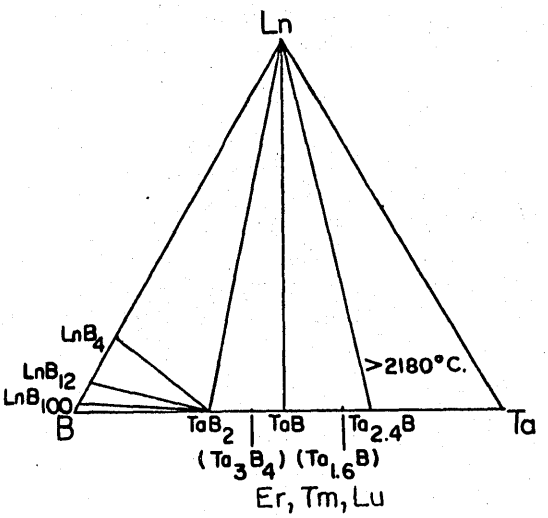

Er, Tm, Lu

FIGURE 14. 8

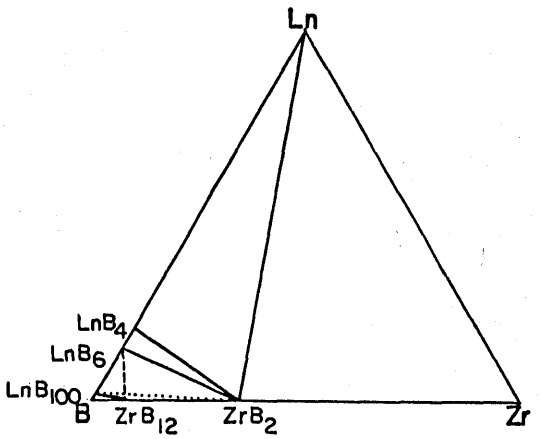

La, Ce, Pr, Nd, Sm, Eu, Gd, Sc

FIGURE 14. 9

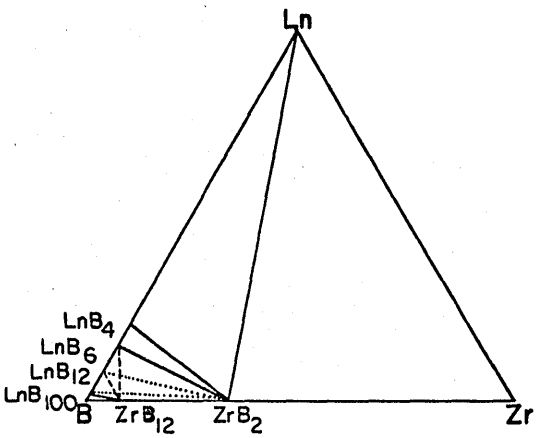

Tb, Dy, Ho, Yb, Y

FIGURE 14. 10

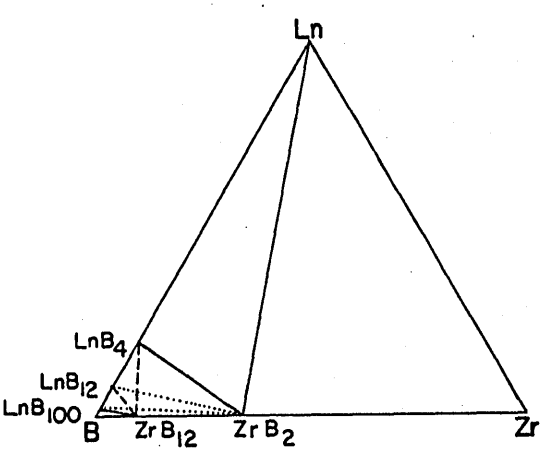

Er, Tm, Lu

FIGURE 14. 11

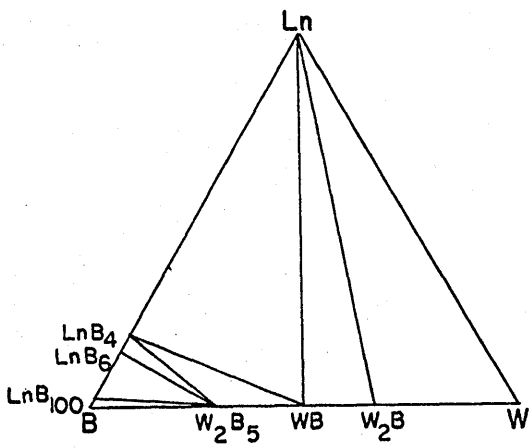

La, Ce, Pr, Nd, Sm, Eu, Gd, Sc

FIGURE 14. 12

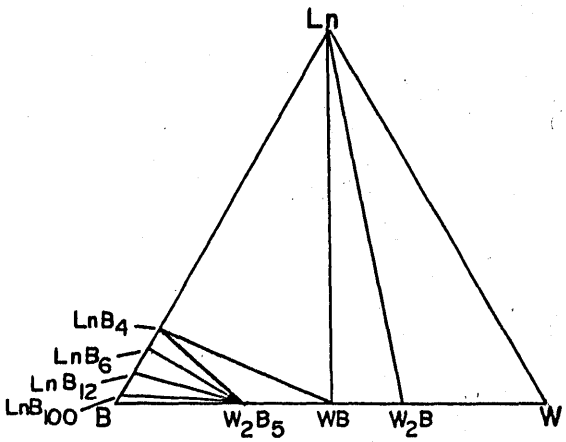

Tb, Dy, Ho, Yb, Y

FIGURE 14. 13

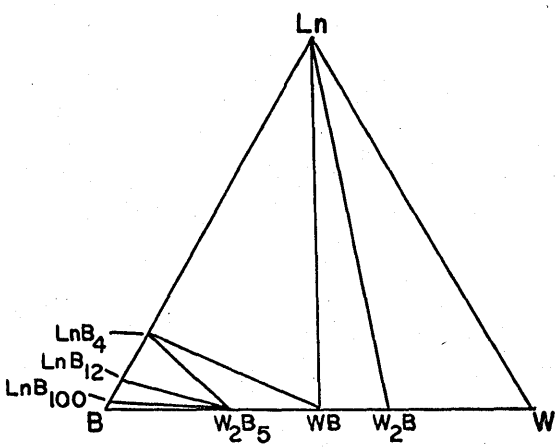

Er, Tm, Lu

FIGURE 14. 14

There are several ternary phases in the Ln-B-C and Th-B-C systems (cf. Part I). In view of their poor definition, undefined phase relations and their failure to contribute, as yet, to the understanding of lanthanide boride stability, the portions of Figures 14. 1 to 14. 4 in which these ternary phases occur are left blank. The U-B-C diagram is taken from Nowotny's work (17).

In the Ln-B-C system of Figure 14. 1, the triangles LnB_4-LnB_6-LnB_2C_2, LnB_6-C-LnB_2C_2, LnB_6-B_4C-LnB_{100} and LnB_2C_2-LnC_2-C have been observed for gadolinium. The other joins are fixed by inference. The LnB_6-C, LnB_6-LnB_2C_2, LnB_4-LnB_2C_2 joins were observed for several other metals in the group of Figure 14. 1 as well as for the lanthanides in Figure 14. 2. While the LnB_{100}-B_4C and LnB_{12}-B_4C joins must exist by inference in Figure 14. 2, no experiments on the Figure 14. 2 group lanthanides were performed to decide whether there is a B_4C-LnB_6 or a LnB_{12}-C join. The LnB_6-B_4C join is chosen for this group. This choice assumes that LnB_{12} is not sufficiently stable, with respect to the condensed elements, to prevent the reaction,

$$2\ LnB_{12}(s) + 3\ C\ (s) = 2\ LnB_6(s) + 3\ B_4C(s), \qquad (14.3)$$

from occurring. While this assumption is risky, some evidence on the stability of these borides with respect to solid elements is presented to support this assumption in Chapter 15. 1. 7. 2.

There are two joins to be established in Figure 14. 3. A decision as to which equilibria exist must await further arc melter experiments attempting to prepare LnB_2C_2 from C and LnB_4 (equation 14. 4) and to

$$2\ LnB_4(s) + 5\ C\ (s) = 2\ LnB_2C_2(s) + B_4C(s) \qquad (14.\ 4)$$

$$2\ C\ (s) + LnB_{12}(s) = LnB_4(s) + 2\ B_4C(s) \qquad (14.\ 5)$$

effect the reaction of graphite with LnB_{12} (equation 14. 5). The thermochemical implications of this choice are discussed in Chapter 14. 7.

The equilibria in Figures 14. 6 through 14. 8 for the Ln-Ta-B systems are fairly well established. Both GdB_4 and GdB_6 exist in equilibrium with TaB_2. Since TaB_2 is the highest tantalum boride, its equilibrium with other lanthanide group higher borides is implied. The TaB_2-Gd join was established at a sufficiently high temperature such that Ta_3B_4 decomposes to TaB_2 and TaB. The TaB-Gd-TaB_2 triangle exists by inference. From the experimentally determined triangle, TaB-Gd-$Ta_{2.4}B$, the triangle, $Ta_{2.4}B$-Gd-Ta, exists by implication at temperatures over 2180°C. The phase, $Ta_{2.4}B$, disproportionates into $Ta_{1.6}B$ and Ta below 2180°C. Figures 14. 6 to 14. 8 are drawn arbitrarily for a temperature greater than 2180°C. with the additional requirement that the temperature be above the Ta_3B_4 decomposition temperature.

Ternary behavior in the Ln-Zr-B system needs further characterization. The ZrB_2-LnB_6-LnB_4 and ZrB_2-GdB_4-Gd triangles are clearly established, as well as the Zr-Gd-ZrB_2 triangle by inference. However, the joins, other than the implied LnB_{100}-ZrB_{12} join, that exist in the boron-rich corner have yet to be defined. Solid solution between ZrB_{12} and LnB_{12} will be a problem. The use of this region to delineate the stability of the lanthanide borides is discussed in Chapter 14. 7.

Figures 14.12 through 14.14 illustrate the Ln-W-B systems. All equilibria are unequivocably assigned. The boron-rich joins are established by implication, as in the Ln-Ta-B systems. Presumably the Ln-Mo-B equilibria would be identical to the Ln-W-B system.

14. 6 Thermodynamic Implications

Table 14. 2 contains a listing of available heats of formation pertinent to this investigation. The data are listed on a per gram-atom of boron (or per metal for carbides) basis, since the reactions to be considered will involve the competition between two different metals for boron. Which metal is more reducing in a bimetal competition for boron may be simply determined by finding which of two metal borides in equilibrium has the more negative heat of formation per gram-atom of boron. Reactions involving three or more metal borides are not so simply predicted from Table 14. 2. Balanced reactions must be considered in order to weight properly the influence of the stability of each boride on the sign of ΔH for the reaction (cf. Chapter 14. 8).

Using the available data of Table 14. 2 and a judicious selection of reactants and products in the ternary equilibria of Figures 14. 1 to 14.14, one may place limits on the heats of formation of the lanthanide borides within the limits of the assumptions in Chapter 14. 1 and the accuracy of the data in Table 14. 2. Table 14. 3 lists all the possible reactions which will proceed as written as indicated in Figures 14. 1 to 14.14. Of all the possible processes in Table 14. 3, those providing the best limits on the heats of formation are illustrated below.

TABLE 14. 2

Summary of ΔH of Formation of Metal Borides, GdC_2, ThC_2, and UC.

Boride	ΔH_f (kcal./g.-at. B)	Reference
$1/2MgB_2$	-8.95 ± 1.5 (298°K.)	69
$1/4MgB_4$	-5.25 ± 1.25 (298°K.)	69
$1/6CaB_6$	$> 1/6SrB_6$	104, 180, 105
$1/6SrB_6$	-8.40	181
$1/6BaB_6$	$< 1/6SrB_6$	104, 180, 105
$1/6YB_6$	-4	182
$1/4LnB_4$	-15 ± 3	133
$1/6LnB_6$	-12 ± 2	133
$1/6LaB_6$	-11.7 ± 1.7	133
$1/4CeB_4$	> -21	20
$1/6CeB_6$	(-13.5 ± 2.5)	183
$1/4ThB_4$	< -13	20
$1/6ThB_6$	< -11	20
$1/2UB_2$	$-19.7 + 1.5T$, (ΔF)	184
$1/4UB_4$	$-15.1 + .0011T$, (ΔF)	184
$1/12UB_{12}$	$-8.83 + .00090T$, (ΔF)	184
TiB	-41.0 ± 9 (298°K.)	69
$1/2TiB_2$	-33.43 ± 1.5 (298°K.)	132
$1/2TiB_2$	< -25	20

TABLE 14. 2, continued

Boride	ΔH_f (kcal./g.-at. B)	Reference
$1/2TiB_2$	(-36)	20
$1/5Ti_2B_5$	< -21	20
ZrB	<-39/2	20
$1/2ZrB_2$	-36.5	132
$1/2ZrB_2$	-38.4 ± .8	54
$1/2ZrB_2$	<-39/2	20
$1/12ZrB_{12}$	> -10	20
$1/2HfB_2$	-40	30
$1/xNbB_x$, x<2	<-18	20
$1/2NbB_2$	<-18	20
TaB	-64.9 to -38.4	54
$Ta_{1.6}B$	-64.9 to -38.4	54
$Ta_{2.4}B$	-64.9 to -38.4	54
$1/xTaB_x$, x<2	<-26	20
$1/2TaB_2$	<-26	20
$1/2TaB_2$	<-45	20
$1/2TaB_2$	-51.7 to -22.7	54
$1/xCrB_x$, x<2	<-15	20
$1/2CrB_2$	<-15	20
Mo_2B	-25.5 (298°K.)	185
$1/2Mo_3B_2$	-21 (298°K.)	185

TABLE 14. 2, continued

Boride	ΔH_f (kcal./g.-at. B)	Reference
MoB	-16.3 (298°K.)	185
$1/2MoB_2$	-11.5 (298°K.)	185
$1/5Mo_2B_5$	-10 (298°K.)	185
W_2B	-26.0 to -20	20, 54
WB	-22 to -12	20
$1/5W_2B_5$	-9 to -5	20
$1/4B_4C$	-3.45 ± .675	186
$1/6SiB_6$	-1.17 (298°K.)	187
Carbide	**(kcal./g.-at. metal)**	
GdC_2	-22.5 to -29.9 (2045°K.)	49
ThC_2	-46.1 to -51.1 (298°K.)	49
UC	-18 ± 4 (298°K.)	49

TABLE 14. 3

Reactions Implied by Ternary Compatibilities Observed in Figures 15. 1 to 15.14. $\Delta F^{o} < 0$ for Each Reaction Written. All Reactants and Products are in the Condensed State.

Metal	Reaction	Process											
Ta	Ta-1	2 Ta	+	GdB_4	=	2 TaB_2	+	Gd					High Temperatures
	Ta-2	4 Ta	+	GdB_4	=	4 TaB	+	Gd					
	Ta-3	3 Ta	+	GdB_6	=	3 TaB_2	+	Gd					
	Ta-4	Ta	+	GdB_6	=	GdB_4	+	TaB_2					
	Ta-5	9.6 Ta	+	GdB_4	=	4 $Ta_{2.4}B$	+	Gd					
	Ta-6	6 Ta	+	GdB_6	=	6 TaB	+	Gd					
	Ta-7	14.4 Ta	+	GdB_6	=	6 $Ta_{2.4}B$	+	Gd					
	Ta-8	28.8 $Ta_{2.4}B$	+	7.57 GdB_4	=	69.2 TaB	+	7.57 Gd					
	Ta-9	$Ta_{2.4}B$	+	GdB_6	=	TaB_2	+	Gd					
	Ta-10	$Ta_{2.4}B$	+	GdB_6	=	TaB_2	+	GdB_4					
	Ta-11	$Ta_{2.4}B$	+	GdB_4	=	TaB_2	+	Gd					
	Ta-12	2 TaB	+	GdB_6	=	2 TaB_2	+	GdB_4					
	Ta-13	4 TaB	+	GdB_4	=	4 TaB_2	+	Gd					
	Ta-14	3 Ta	+	2 GdB_6	=	Ta_3B_4	+	2 GdB_4					Low Temperatures
	Ta-15	Ta	+	GdB_4	=	$Ta_{1.6}B$	+	Gd					
	Ta-16	Ta	+	GdB_6	=	$Ta_{1.6}B$	+	Gd					
	Ta-17	$Ta_{1.6}B$	+	GdB_6	=	TaB_2	+	GdB_4					
	Ta-18	30 $Ta_{1.6}B$	+	11 GdB_6	=	48 TaB_2	+	11 Gd					
	Ta-19	30 $Ta_{1.6}B$	+	3 GdB_6	=	48 TaB	+	3 Gd					
	Ta-20	10 $Ta_{1.6}B$	+	3/2 GdB_4	=	16 TaB	+	3/2 Gd					
	Ta-21	20 $Ta_{1.6}B$	+	11 GdB_4	=	32 TaB_2	+	11 Gd					

TABLE 14. 3, continued

Metal	Reaction	Process
C	C-1	$2\ Gd + 3\ B_4C = 2\ GdB_6 + 3\ C$
	C-2	$2\ GdC_2 + 3\ B_4C = 2\ GdB_6 + 7\ C$
	C-3	$GdC_2 + 14\ B = 2\ B_4C + GdB_6$
	C-4	$2\ GdB_4 + B_4C = 2\ GdB_6 + C$
	C-5	$GdC_2 + 6\ B = GdB_6 + 2\ C$
Zr	Zr-1	$Zr + GdB_6 = ZrB_2 + GdB_4$
	Zr-2	$3\ Zr + GdB_6 = 3\ ZrB_2 + Gd$
	Zr-3	$2\ Zr + GdB_4 = 2\ ZrB_2 + Gd$
	Zr-4	$5\ Gd + 2\ ZrB_{12} = 2\ ZrB_2 + 5\ GdB_4$
	Zr-5	$5\ Gd + 3\ ZrB_{12} = 3\ ZrB_2 + 5\ GdB_6$
	Zr-6	$5\ GdB_4 + ZrB_{12} = ZrB_2 + 5\ GdB_6$
W	W-1	$4\ W + GdB_4 = 4\ WB + Gd$
	W-2	$8\ W + GdB_4 = 4\ W_2B + Gd$
	W-3	$4\ W + 5\ GdB_6 = 2\ W_2B_5 + 5\ GdB_4$
	W-4	$2\ W + GdB_6 = 2\ WB + GdB_4$
	W-5	$12\ W + GdB_6 = 6\ W_2B + Gd$
	W-6	$6\ W + GdB_6 = 6\ WB + Gd$
	W-7	$3\ Gd + 4\ W_2B_5 = 3\ GdB_4 + 8\ WB$
	W-8	$4\ WB + 3\ GdB_6 = 3\ GdB_4 + 2\ W_2B_5$
	W-9	$W_2B + 2\ GdB_6 = 2\ GdB_4 + W_2B_5$
	W-10	$2\ W_2B + GdB_6 = GdB_4 + 4\ WB$
	W-11	$6\ W_2B + GdB_6 = Gd + 12\ WB$
	W-12	$4\ W_2B + GdB_4 = Gd + 8\ WB$

TABLE 14. 3, continued

Metal	Reaction	Process
Mo	Mo-1	$2\ Mo + SmB_6 = SmB_4 + 2\ MoB$
	Mo-2	$Sm + 4\ MoB_2 = 4\ MoB + SmB_4$
	Mo-3	$3\ Sm + 4\ Mo_2B_5 = 8\ MoB + 3\ SmB_4$
	Mo-4	$2\ Mo_2B + SmB_6 = 4\ MoB + SmB_4$
	Mo-5	$2\ Mo_3B_2 + SmB_6 = 6\ MoB + SmB_4$

$$2GdC_2(s) + 3B_4C(s) = 2GdB_6(s) + 7C(s) \qquad (C\text{-}3)$$

$$\Delta F \backsim \Delta H = 2\,\Delta H_{f_{GdB_6}} - 2\,\Delta H_{f_{GdC_2}} - 3\,\Delta H_{f_{B_4C}} < 0$$

$$2\,\Delta H_{f_{GdB_6}} < 2\,\Delta H_{f_{GdC_2}} + 3\,\Delta H_{f_{B_4C}}$$

$$< 2(-22.5 \text{ to } -29.9) + 3(-11.1 \text{ to } -16.5)$$

$$< -78.3$$

$$\therefore \quad \Delta H_{f_{GdB_6}} < -39.2 \text{ kcal./mole}$$

$$W_2B(s) + 2GdB_6(s) = W_2B_5(s) + 2GdB_4(s). \qquad (W\text{-}9)$$

$$\Delta F \backsim \Delta H = 2\,\Delta H_{f_{GdB_4}} - 2\Delta H_{f_{GdB_6}} + \Delta H_{f_{W_2B_5}} - \Delta H_{f_{W_2B}} < 0$$

$$2(\Delta H_{f_{GdB_4}} - \Delta H_{f_{GdB_6}}) < \Delta H_{f_{W_2B}} - \Delta H_{f_{W_2B_5}}$$

$$< (-20 \text{ to } -26) - (25 \text{ to } -45)$$

$$< -20 + 45$$

$$< 25 \text{ kcal./mole}$$

Hence,

$$\Delta H_{f_{GdB_4}} - \Delta H_{f_{GdB_6}} < 12.5 \text{ kcal./mole}$$

Realizing that W_2B must be less stable per mole than WB in order for WB and W to react, one can further restrict the limit in process W-9 to:

$$2(\Delta H_{f_{GdB_4}} - \Delta H_{f_{GdB_6}}) < -22 + 45; \text{ or}$$

$$2(\Delta H_{f_{GdB_4}} - \Delta H_{f_{GdB_6}}) < 23 \text{ kcal./mole.}$$

Hence,

$$\Delta H_{f_{GdB_4}} - \Delta H_{f_{GdB_6}} < 11.5 \text{ kcal./mole.}$$

Further,

$$\Delta H_{f_{GdB_4}} - 11.5 < \Delta H_{f_{GdB_6}} < -39.2 \text{ kcal./mole}$$

from the above considered process C-3. Thus,

$$\Delta H_{f_{GdB_4}} < -39.2 + 11.5$$

$$< -27.7 \text{ kcal./mole.}$$

$$W_2B(s) + 1/4GdB_4(s) = 2WB(s) + 1/4\ Gd(s,l) \qquad \text{(W-12)}$$

$$\Delta F \backsim \Delta H = 2\ \Delta H_{f_{WB}} - \Delta H_{f_{W_2B}} - 1/4\ \Delta H_{f_{GdB_4}} < 0;$$

$$2\ \Delta H_{f_{WB}} - \Delta H_{f_{W_2B}} < 1/4\ \Delta H_{f_{GdB_4}}.$$

Further,

$$\Delta H_{f_{W_2B}} < \Delta H_{f_{WB}}.$$

Hence,

$$2(-22) - (-22) < 1/4\ \Delta H_{f_{GdB_4}},$$

$$-22 < 1/4\ \Delta H_{f_{GdB_4}},$$

$$-88 \text{ kcal./mole} < \Delta H_{f_{GdB_4}}.$$

And,

$$-88 \text{ kcal./mole} < \Delta H_{f_{GdB_4}} < 11.5 + \Delta H_{f_{GdB_6}}.$$

Thus,

$$-88 - 11.5 < \Delta H_{f_{GdB_6}}; \text{ or}$$

$$-99.5 \text{ kcal./mole} < \Delta H_{f_{GdB_6}}.$$

$$2GdB_4(s) + B_4C(s) = 2GdB_6(s) + C(s) \qquad (C\text{-}4)$$

$$\Delta F \backsim \Delta H = 2\ \Delta H_{f_{GdB_6}} - 2\ \Delta H_{f_{GdB_4}} - \Delta H_{f_{B_4C}} < 0;$$

$$2(\Delta H_{f_{GdB_6}} - \Delta H_{f_{GdB_4}}) < \Delta H_{f_{B_4C}}$$

$$< -11.1.$$

Hence,

$$\Delta H_{f_{GdB_6}} - \Delta H_{f_{GdB_4}} < -5.6; \text{ or}$$

$$5.6 \text{ kcal./mole} < \Delta H_{f_{GdB_4}} - \Delta H_{f_{GdB_6}}.$$

From the gadolinium reactions of Table 14. 4 the following series of inequality relations among the gadolinium boride stabilities exists:

$$3\Delta H_{f_{GdB_4}} < 2\Delta H_{f_{GdB_6}} < 4\Delta H_{f_{GdB_6}} - 3\Delta H_{f_{GdB_4}} < \Delta H_{f_{GdB_6}} < \Delta H_{f_{GdB_4}}$$

$$< \Delta H_{f_{GdB_{12}}} < 2/3\Delta H_{f_{GdB_6}} < 1/3\Delta H_{f_{GdB_{12}}} < 0. \qquad (14.6)$$

Therefore, ΔH_f of GdB_4 lies between -22 and -6.9 kcal./g.-at. B; ΔH_f of GdB_6 lies between -16.6 and -6.5 kcal./g.-at. B; and the difference between the heats of formation of GdB_4 and GdB_6 lies between 5.6 and 11.5 kcal./mole. These limits are the least upper and greatest lower bounds on the heats of formation of GdB_4 and GdB_6 and their difference that can be obtained from the set of possible equations in Table 14. 3.

Using the molydenum reactions in Table 14. 3, one may establish an upper limit on $\Delta H_{f_{SmB_4}}$ and the difference between the heats of formation of SmB_4 and SmB_6.

$$Sm\ (s,l) + 4MoB_2(s) = 4MoB(s) + SmB_4(s) \qquad (Mo\text{-}2)$$

$$\Delta F \backsim \Delta H = 4\Delta H_{f_{MoB}} + \Delta H_{f_{SmB_4}} - 4\Delta H_{f_{MoB_2}} < 0;$$

$$\Delta H_{f_{SmB_4}} < 4\Delta H_{f_{MoB_2}} - 4\Delta H_{f_{MoB}},$$

$$< 4(-23.0) + 4(16.3),$$

$$< -26.8.$$

Hence,

$$\Delta H_{f_{SmB_4}} < -26.8 \text{ kcal./mole.}$$

$$2Mo_3B_2(s) + SmB_6(s) = 6MoB(s) + SmB_4(s) \qquad \text{(Mo-5)}$$

$$\Delta F \backsim \Delta H = 6\Delta H_{f_{MoB}} + \Delta H_{f_{SmB_4}} - \Delta H_{f_{SmB_6}} - 2\,\Delta H_{f_{Mo_3B_2}} < 0;$$

$$\Delta H_{f_{SmB_4}} - \Delta H_{f_{SmB_6}} < 2\Delta H_{f_{Mo_3B_2}} - 6\Delta H_{f_{MoB}},$$

$$< 2(-42) + 6(16.3).$$

Thus,

$$\Delta H_{f_{SmB_4}} - \Delta H_{f_{SmB_6}} < 13.8 \text{ kcal./mole.}$$

From the behavior of Er, Tm and Lu borides, discussed by Eick and Sturgeon (101), the processes written in Table 14.4 will proceed as written. From these processes the following relation among the heats of formation may be concluded:

TABLE 14. 4

Reactions with Negative Free Energies Within the Binary Lanthanide-Boron Systems. All Reactants and Products are in the Condensed State.

Lanthanide	Reaction	Process
Gd	Gd-1	$GdB_4 + 2\,B = GdB_6$
	Gd-2	$2\,GdB_6 + Gd = 3\,GdB_4$
	Gd-3	$Gd + 6\,B = GdB_6$
	Gd-4	$Gd + 4\,B = GdB_4$
	Gd-5	$GdB_{12} = GdB_6 + 6B$
	Gd-6	$GdB_{12} = GdB_4 + 8B$
	Gd-7	$GdB_{12} + 3\,GdB_4 = 4\,GdB_6$
	Gd-8	$GdB_{12} + 2\,Gd = 3\,GdB_4$
	Gd-9	$GdB_{12} + Gd = 2\,GdB_6$
Er, Tm, Lu	Ln-1	$2\,LnB_6 + Ln = 3\,LnB_4$
	Ln-2	$LnB_4 + 8\,B = LnB_{12}$
	Ln-3	$4\,LnB_6 = 3\,LnB_4 + LnB_{12}$
	Ln-4	$LnB_{12} + 2\,Ln = 3\,LnB_4$
	Ln-5	$Ln + 6\,B = LnB_6$
	Ln-6	$LnB_6 + 6\,B = LnB_{12}$
	Ln-7	$Ln + 12\,B = LnB_{12}$
	Ln-8	$Ln + 4\,B = LnB_4$

$$3\Delta H_{f_{LnB_{12}}} < 3\Delta H_{f_{LnB_4}} < 2\Delta H_{f_{LnB_6}} < 4\Delta H_{f_{LnB_6}} - 3\Delta H_{f_{LnB_4}}$$

$$< \Delta H_{f_{LnB_{12}}} < \Delta H_{f_{LnB_6}} < 0. \qquad (14.7)$$

A consideration of the many possible processes that may be written for the ternary behavior of Er, Tm and Lu borides from Figures 14. 3, 14. 8, 14.11 and 14.14 provides some information about the stability of the dodecaboride with respect to the solid elements.

$$12W(s) + LnB_{12}(s) = 12WB(s) + Ln(s), \qquad (14.8)$$

$$\Delta F \backsim \Delta H = 12\Delta H_{f_{WB}} - \Delta H_{f_{LnB_{12}}} < 0;$$

$$12\Delta H_{f_{WB}} < \Delta H_{f_{LnB_{12}}},$$

$$12(-12 \text{ to } -22) < \quad .$$

Hence,

$$-244 \text{ kcal./mole} < \Delta H_{f_{LnB_{12}}}.$$

$$2W_2B(s) + LnB_{12}(s) = LnB_4(s) + 2W_2B_5(s) \qquad (14.9)$$

$$\Delta F \backsim \Delta H = \Delta H_{f_{LnB_4}} + 2\Delta H_{f_{W_2B_5}} - 2\Delta H_{f_{W_2B}} - \Delta H_{f_{LnB_{12}}} < 0;$$

$$\Delta H_{f_{LnB_4}} - \Delta H_{f_{LnB_{12}}} < 2\Delta H_{f_{W_2B}} - 2\Delta H_{f_{W_2B_5}},$$

$$< 2(-20 \text{ to } -26) - 2(-25 \text{ to } -45),$$

$$< -40 + 90.$$

Hence,

$$\Delta H_{f_{LnB_4}} - \Delta H_{f_{LnB_{12}}} < 50 \text{ kcal./mole}.$$

The stability limits obtained for GdB_4 and GdB_6 are applicable in the case of Er, Tm and Lu tetra- and hexaborides except for the lower bound on the LnB_4-LnB_6 difference and for the upper bound on the LnB_6 stability. No information concerning the former limit is available, since one cannot be certain that process Zr-6 will proceed as written for these lanthanide borides. Similarly, in the latter case reaction C-3 may not proceed as written.

Thus, a combination of the stabilities of process 14. 9 with the lower limit on the LnB_4 stability allows the following statement to be made:

$$-88 < \Delta H_{f_{LnB_4}} < 50 + \Delta H_{f_{LnB_{12}}}.$$

Hence,

$$-138 \text{ kcal./mole} < \Delta H_{f_{LnB_{12}}}.$$

Further, since

$$\Delta H_{f_{LnB_{12}}} < \Delta H_{f_{LnB_4}} < -27.7 \text{ kcal./mole},$$

then

$$\Delta H_{f_{LnB_{12}}} < -27.7 \text{ kcal./mole.}$$

In summary, the lanthanide tetraborides are less stable than -88 kcal./mole, since the tetraborides will react with W_2B to form lanthanide metal and WB. Lanthanide hexaborides from La to Ho and also Yb are more stable than -39.2 kcal./mole, established by their formation with graphite from LnC_2 and B_4C. Further, from the reaction of W_2B and GdB_6 to form W_2B_5 and GdB_4 and from the reaction of GdB_4 with B_4C to form GdB_6 and graphite, the relation -11.5 kcal. $< \Delta H_{f_{GdB_6}} < \Delta H_{f_{GdB_4}}$ -5.6 kcal. was established. Therefore, GdB_4 is more stable than -27.7 kcal./mole and GdB_6 is less stable than -99.5 kcal./mole. Since W_2B reacts with LnB_{12} to form LnB_4 and W_2B_5, $\Delta H_{f_{LnB_4}} - \Delta H_{f_{LnB_{12}}} < 50$ kcal. Then from the LnB_4 stability limits and from $\Delta H_{f_{LnB_{12}}} < \Delta H_{f_{LnB_4}}$, $-138 < \Delta H_{f_{LnB_{12}}} < -27.7$ kcal./mole.

No attempt has been made to determine the stability range for LnB_{100} in view of its indefinite composition and the large limit values that would arise from the large coefficients in the balanced processes. In the ternary systems in which LnB_{100} exists, LnB_{100} would be in equilibrium with ZrB_2, W_2B_5, B_4C and TaB_2 in each respective ternary diagram.

The stability of LnB_2 may be determined. The diborides would be in equilibrium with WB, ZrB_2 and TaB_2 at low temperature. The graphite and molybdenum systems need further clarification. Should LnB_2 exist, then

$$LnB_2(s) + 2B(s) = LnB_4(s),$$

and

$$LnB_4(s) + Ln(s,l) = 2LnB_2(s),$$

will proceed as written. Thus,

$$\Delta H_{f_{LnB_4}} < \Delta H_{f_{LnB_2}} < 1/2\ \Delta H_{f_{LnB_4}} < 0.$$

Consider the reaction,

$$W(s) + LnB_4(s) = 2WB(s) + LnB_2(s). \qquad (14.10)$$

$$\Delta F \backsim \Delta H = \Delta H_{f_{LnB_2}} + 2\Delta H_{f_{WB}} - \Delta H_{f_{LnB_4}} < 0;$$

$$\Delta H_{f_{LnB_2}} - \Delta H_{f_{LnB_4}} < -2\Delta H_{f_{WB}} < 24 \text{ kcal.}$$

Hence,

$$\Delta H_{f_{LnB_2}} - \Delta H_{f_{LnB_4}} < 24 \text{ kcal./mole.}$$

In addition,

$$2W_2B(s) + LnB_2(s) = Ln(l,s) + 4WB(s). \qquad (14.11)$$

$$\Delta F \backsim \Delta H = 4\Delta H_{f_{WB}} - 2\Delta H_{f_{W_2B}} - \Delta H_{f_{LnB_2}} < 0;$$

$$4\Delta H_{f_{WB}} - 2\Delta H_{f_{W_2B}} < \Delta H_{f_{LnB_2}},$$

$$4(-22) - 2(-20) <$$

$$-48 < \quad .$$

Hence,

$$-48 \text{ kcal./mole} < \Delta H_{f_{LnB_2}} .$$

With the use of the limits on $\Delta H_{f_{LnB_4}}$ from above,

$$0 < \Delta H_{f_{LnB_2}} - \Delta H_{f_{LnB_4}} < 24 \text{ kcal./mole;}$$

and

$$-48 < \Delta H_{f_{LnB_2}} < -26.7 \text{ kcal./mole,}$$

or

$$-24 < 1/2 \Delta H_{f_{LnB_2}} < -13.4 \text{ kcal./g.-at. boron.}$$

It is interesting to establish limits on the stability of GdB_2C_2. From the reaction of GdC_2 and B_4C to form GdB_2C_2 and graphite, $\Delta H_{f_{GdB_2C_2}}$ <-28.0 kcal./mole. Further, the reaction of W_2B with GdB_2C_2 to form GdC_2 and WB fixes the GdB_2C_2 stability as greater than -78 kcal./mole. A more restrictive definition of the GdB_2C_2 stability and the trend of LnB_2C_2 stability with lanthanide can be found by combining WB and LnB_2C_2 to note

if W_2B_5 and LnC_2 are formed. The borocarbide, GdB_2C_2, then, is comparable in stability to the lanthanide tetraboride.

14. 7 Other Restricting Compatibility Tests

It was hoped that the equilibria observed in these ternary systems might distinguish the variation in the stability of the lanthanide borides with respect to their solid components as a function of the lanthanide. However, the wide limits on the heats of formation of the reference transition metal borides, the large coefficients in the inequalities, the small differences in stability between the lanthanide borides and the large differences in stability between the reference metal borides preclude this distinction.

A simpler method to determine the variation in the stability of lanthanide borides as a function of atomic number would seem to be available in the reaction of borides of different lanthanide metals and the observation of the ternary equilibria. However, the isomorphic character of lanthanide borides of the same stoichiometry allows for continuous solid solutions. Further, by X-ray diffraction, one could not distinguish between different lanthanide borides of the same composition. The same problems occur if the relative stabilities with respect to the gaseous elements are studied in a vapor phase equilibrium between physically separated different lanthanide borides. Therefore, one is limited to studying the relative stabilities indirectly through some reference system, as in the case of the ternary studies above, or to determining the relative volatilities, absolute heats of formation or some property for each lanthanide boride (cf. Chapter 17).

Considerable information concerning the variation of stability with atomic number could be obtained from the following disproportionation processes:

$$4LnB_6(s) = 3LnB_4(s) + LnB_{12}(s)$$

$$2LnB_2(s) = Ln(s,l) + LnB_4(s)$$

$$LnB_{12}(s) = LnB_6(s) + LnB_{100}(s)$$

Apparently, from Eick and Galloway's observations (101) at Er or Ho, LnB_6 becomes unstable with respect to LnB_4 and LnB_{12}. A definition of where in the lanthanides disproportionation of LnB_6 occurs and does not occur, coupled with a knowledge of the heats of formation of LnB_4 and LnB_{12}, would provide a very good value for the heat of formation of LnB_6. Similarly, a determination of where in the lanthanides LnB_2 becomes unstable with respect to Ln and LnB_4 would provide information on the stability of LnB_2 or LnB_4 if the stability of either LnB_4 or LnB_2 were known. The heat for this process is near zero somewhere early in the lanthanides, i. e., at NdB_2 or PrB_2. Further, disproportionation of the dodecaboride becomes important at gadolinium. Establishing these points of appearance or disappearance of borides in the lanthanide series could provide information about the stability of all lanthanide borides.

Other ternary systems might provide a sufficient test for variations in the stability of the lanthide borides. For instance, if LnB_4 were in equilibrium with MB_x for some of the lanthanides, but at one point $Ln'B_4$ could no longer be in equilibrium with MB_x because of the change in heat of formation of lanthanide tetraborides as a function of lanthanide,

then, if the heats of formation of the MB_x compounds were known, the heat of formation of $Ln'B_4$ at the transition lanthanide could be determined. This observation would aid in establishing the trend for the lanthanide tetraboride stabilities as a function of lanthanide.

For instance, consider process Mo-2 (Table 14. 3). In the case of samarium, the process is exothermic. Thus, the heat of formation of SmB_4 was less than -27.7 kcal./mole. Now consider a tetraboride not as stable with respect to condensed elements as SmB_4. The process above might become endothermic, thus precluding the MoB-LnB_4 equilibrium and demanding the Ln-MoB_2 and LnB_4-MoB_2 equilibria. Then the heat of formation of this LnB_4 would be greater than -27.7 kcal./mole. At the lanthanide where this change of behavior occurs the heat of formation is very nearly -27.7 kcal./mole.

Another significant process to determine the relative stability of LnB_4 and LnB_{12} can be found in equation (14.12).

$$4ZrB_2(s) + 5LnB_{12}(s) = 4ZrB_{12}(s) + 5LnB_4(s). \qquad (14.12)$$

Whether this process is endothermic or exothermic will allow one to predict whether $\Delta H_{f_{LnB_4}} - \Delta H_{f_{LnB_{12}}}$ is greater or less than $4/5(\Delta H_{f_{ZrB_{12}}} - \Delta H_{f_{ZrB_2}})$ and to note the trend of divergence or convergence of this difference between Er, Tm and Lu. If the heat of formation of LnB_4 is about -40kcal./mole and that of LnB_{12} is about -80kcal./mole, this test is very useful. Note that these binary joins are omitted from Figures 14. 9 through 14.11.

Another sensitive test for $\Delta H_{f_{LnB_4}} - \Delta H_{f_{LnB_{12}}}$ limits, where Ln is Er, Tm or Lu, may be found in process 14.13.

$$LnB_4(s) + 2B_4C(s) = 2C(s) + LnB_{12}(s). \qquad (14.13)$$

Depending on whether the process is endo- or exothermic, this difference will be less than or greater than 22.2 kcal./mole, again a sensitive test.

14. 8 General Thermodynamic Considerations

In the development of the use of ternary compatibility studies for gaining information about binary phase stability by examining the phase's compatibility with reference system borides, it became apparent that, while a table such as Table 14. 2 would serve to catalogue the stability of metal borides with respect to the solid elements, it is not very useful in predicting the equilibria in ternary or higher component fields. For instance, if LnB_{12} were less stable per boron atom than ZrB_{12}, Zr metal would certainly reduce LnB_{12}, but not necessarily to ZrB_{12} and Ln metal. Further, if one wishes to make a judicious choice of a reference system to determine as closely as possible the stabilities in an unknown system, such a method of tabulation is not very fruitful.

It is not sufficient to select a test boride comparable in stability to the unknown metal boride. The best choice would be a reference system which contained two borides whose stabilities per boron atom and whose stoichiometries were close together, and yet whose stabilities bracketed the stability of the unknown boride. For instance, the most valuable reference borides in the above study were the tungsten borides and B_4C. W_2B_5 is less stable per boron atom than GdB_4, but WB is more stable than GdB_4 per boron atom. The difference in stability per boron atom between W_2B_5 and WB is small and brackets that of GdB_4. Further, the fairly close stoichiometry

allows one to write balanced equations for processes with small coefficients which will not amplify the ranges of reference boride stability into too wide a set of bounds on the heat of formation of GdB_4. The high stability and the extreme gap in stability per boron atom and in composition between ZrB_2 and ZrB_{12} rendered the use of the Zr-B system as a reference set fairly limited. The high stability of the tantalum borides compared to the lanthanide borides precluded the utility of tantalum borides as a reference system.

A more revealing organization of boride stability data appears in Table 14. 5. This table organizes reaction couples according to their potential for formation of one mole of elemental boron. Those couples showing the lowest potential are at the bottom with increasing potential going up the table. The ordering of the potentials was established from the ternary compatibility studies of this chapter. For instance, the B_4C-C couple is higher in the table than the LnB_6-LnB_4 couple. Hence, B_4C should react with LnB_4 to form LnB_6 and C, as was indeed observed to be the case in this work. Clearly the most useful couples in establishing the relative position of the lanthanide boride potentials are the closest-lying couples, i. e., W-B and C-B couples.

Hence, boride stabilities can be organized, just as are reduction potentials of metals, into an electromotive displacement series involving boron instead of electrons. All borides and boron-containing compounds could be placed into such an organization, as well as other compounds in other series related by a common element. This kind of a series not only defines boride stability, but predicts the equilibrium phases in multi-component systems.

TABLE 14. 5

Boron Potential Series in Order of Decreasing Potential.

Brackets Imply the Inability to Assign Relative Position.

	$1/88\ LnB_{100}$	$= 1/88\ LnB_{12}$	$+ B$	
	$1/94\ LnB_{100}$	$= 1/94\ LnB_{6}$	$+ B$	
	$[1/16\ LnB_{12}$	$= 1/16\ LnB_{6}$	$+ B]$	
	$[1/6\ ZrB_{12}$	$= 1/6\ ZrB_{2}$	$+ B]$	
	$1/4\ B_4C$	$= 1/4\ C$	$+ B$	
$1/2\ C$	$+ 1/4\ LnB_6$	$= 1/4\ LnB_2C_2$	$+ B$	
	$1/2\ LnB_6$	$= 1/2\ LnB_4$	$+ B$	
	$[1/3\ W_2B_5$	$= 2/3\ WB$	$+ B]$	
	$[1/2\ LnB_2C_2$	$= 1/2\ LnC_2$	$+ B]$	
	$1/4\ LnB_4$	$= 1/4\ Ln$	$+ B$	
	$2\ WB$	$= W_2B$	$+ B$	
	W_2B	$= 2\ W$	$+ B$	
	$3/2\ TaB_2$	$= 1/2\ Ta_3B_4$	$+ B$	
	$[TiB_2$	$= TiB$	$+ B]$	
	$[TaB_2$	$= TaB$	$+ B]$	
	Ta_3B_4	$= 3\ TaB$	$+ B$	
	ZrB	$= Zr$	$+ B$	
	$1/2\ ZrB_2$	$= 1/2\ Zr$	$+ B$	
	$[ZrB_2$	$= ZrB$	$+ B]$	
	$[TiB$	$= Ti$	$+ B]$	
	$3\ TaB$	$= Ta_3B_2$	$+ B$	
	$2\ Ta_3B_2$	$= 3\ Ta_2B$	$+ B$	
	Ta_2B	$= 2\ Ta$	$+ B$	

There is a more revealing way to express the above considerations. At equilibrium the chemical potential of each of the components is the same in each phase in the system. In particular, in systems involving borides at equilibrium, the chemical potential of boron in each phase is the same. Consider Figure 14.15. 1. This is a schematic diagram of boron chemical potential normalized to range between zero and 1.00 referred to solid elemental boron at the same temperature of the isothermal diagram, versus the mole fraction or any composition units in the tungsten-boron system. Also included is a similar possible schematic in the lanthanide-boron system with the same ordinate scale and at the same temperature. Horizontal lines in such diagrams define the chemical potential of boron in the equilibrium between the two solid phases whose compositions are specified by the ends of the line. A vertical line shows the variation of chemical potential across the infinitely-narrow solid solution range of the single solid phase at that composition. A sloped line represents the chemical potential change across a single solid phase of detectable solid solution range.

In order to determine the ternary equilibria in the Ln-W-B system, the two diagrams are superimposed and shifted horizontally. The intersection of lines defines a chemical potential common to all phases at the ends of the horizontal lines and in the vertical line. Therefore, as noted in Figure 14.15. 1, the boron chemical potential in W_2B_5 can be the same as that in the B-LnB_{100}, LnB_{100}-LnB_{12}, LnB_{12}-LnB_6 and LnB_6-LnB_4 equilibria, if one shifts the diagrams to the respective intersections. Thus, a ternary diagram would contain the W_2B_5-B-LnB_{100}, W_2B_5-LnB_{100}-LnB_{12}, W_2B_5-LnB_{12}-LnB_6, and W_2B_5-LnB_6-LnB_4 equilibrium triangles at this temperature.

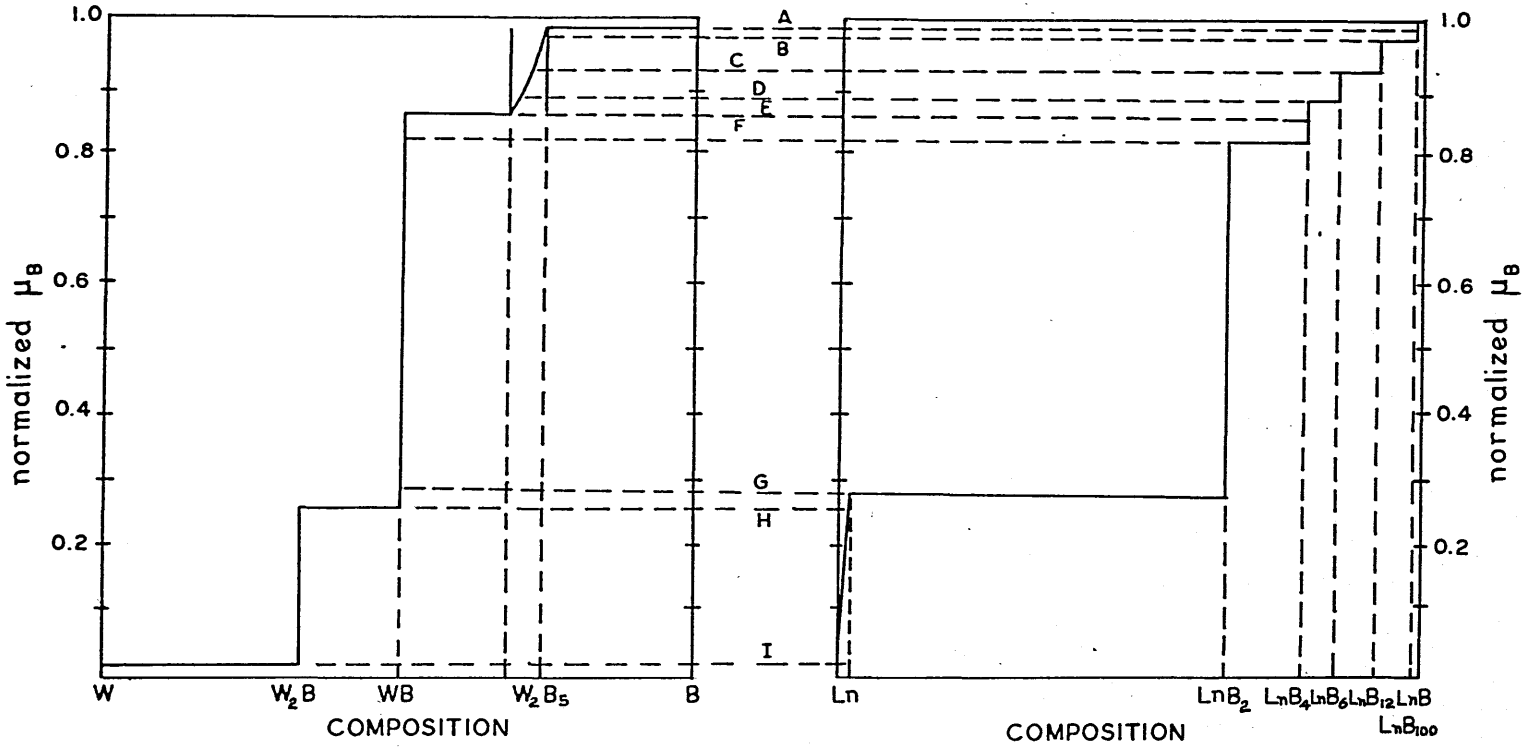

A; $W_2B_5-B-LnB_{100}$

B; $W_2B_5-LnB_{100}-LnB_{12}$

C; $W_2B_5-LnB_4-LnB_6$

D; $W_2B_5-LnB_4-LnB_6$

E; $W_2B_5-WB-LnB_4$

F; $WB-LnB_4-LnB_2$

G; $WB-LnB_2-Ln$

H; $WB-W_2B-Ln$

I; $W-W_2B-Ln$

Graphical Determination of Ternary Equilibria in Metal-Metal-Boron Systems

FIGURE 14. 15. 1

Figure 14.15. 2 demonstrates schematically the relation of the binary chemical potential systems to the ternary equilibria.

Since chemical potential data of boron in solid boride systems are totally lacking and extremely difficult to obtain, a more practical use of this technique would be to consider the stability of these solid borides with respect to boron gas whose pressure can be experimentally determined as a function of composition. Instead of boron chemical potential in the solid, the pressure of boron over the boride systems at constant temperature could be graphed. As in the chemical potential consideration, whenever the pressure of boron over different boride systems is the same, those borides will exist together in equilibrium.

Such a technique is not limited to the prediction of the three solid phase equilibria in three component systems. If vertical lines representing single solid phases from two binary systems can be made to superimpose, those two solid phases will exist together in equilibrium with a gas phase in which the boron pressure may vary over the range of common overlap at that temperature. In other words, an insufficient number of phases are present to fix the system. The system still contains three components. If the composition of the gas can be expressed from the compositions of the solid phases, the system reduces to two components and the range of pressure overlap would be limited to a single point.

Two superimposed horizontal lines represent an invariant system of four solid phases and a gas phase containing three components. Only at one particular temperature can this situation occur.

Quaternary and higher component systems may be treated in like fashion simply by overlaying the binary pressure-composition schematics

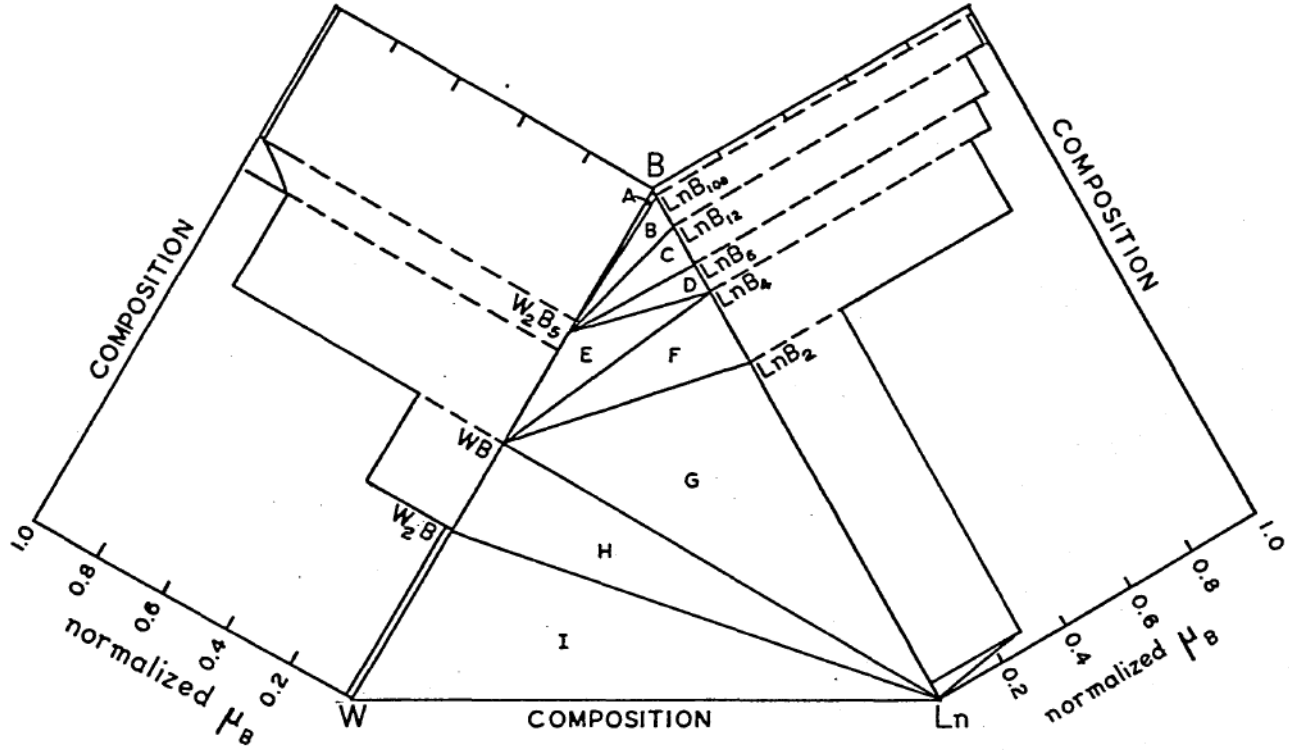

Relation Between Metal Boride Binary and Ternary Equilibria

FIGURE 14. 15. 2

all at the same temperature. One must be careful in using the Phase Rule in these considerations. Solid solutions and multicomponent compounds may exist which would complicate matters.

One should realize that the composition axis is totally artificial. The diagrams are equally useful if projected onto the boron-pressure axis. Two solid phase equilibrium would then be represented as a point, and single solid phases represented by a vertical line. The points and lines could be labeled for the phases they represent. Thus, one could use the abscissa to determine the variation of boron pressure with temperature in the particular two solid phase equilibrium by generating a plot of $-RT\ln p_B$ versus $1/T$. This kind of graph is discussed for metal oxides and sulfides by Darken and Gurry (68). The slopes of such plots are defined by the heats of vaporization of the higher boride to the lower boride with the loss of one mole of boron gas. Invariant points would be determined by the intersection of two lines in the same or different binary systems.

In such a way, all boride systems could be charted on the same diagram, although the chart would be cumbersome if all single solid phase bands were included with the two solid phase equilibria lines. In order to construct such diagrams, one would need to know the heats and entropies of formation of the solid phases and of gaseous boron at some temperature and the associated free-energy-functions. The pressure of boron can then be calculated from the Third Law.

Thus, with the diagrams discussed above, ternary equilibria could be predicted barring solid solution effects. However, in this work the ternary equilibria are established by experiment and one binary diagram

known. In particular, from Figure 14.15. 2 the pressure of boron at this temperature over a two solid phase mixture of LnB_4 and LnB_6 must be greater than that over WB-W_2B_5, but less than that over W_2B_5-B, both of which are known. If the reference system were judiciously chosen, this would prescribe the boron pressure over LnB_4-LnB_6 fairly precisely. Thus, limits on the free energy of the reaction

$$1/2\ LnB_6(s) = 1/2\ LnB_4(s) + B(g) \qquad (14.14)$$

may be set. Subtracting out the free energy of formation of B(g) at this temperature, assuming the entropy change for solid reactants is zero, assuming ΔC_p^o of formation of the solid compounds is also zero, one may set limits on the difference between the heats of formation of LnB_4 and LnB_6 at 298°K. This is precisely how the limits on the stabilities of the lanthanide borides were obtained in the preceding observations.

The thermochemical data available on boride systems are extremely meager and not very precise. As more boride systems are described in detail, this tool to determine stabilities of other borides will become more powerful. In fact, heats of formation of borides determined in this way may be as good as those determined from absolute pressure measurements at high temperatures. The technique is certainly much easier and considerably shorter than a high temperature vaporization rate study. Further, this technique is independent of errors in the heats of sublimation and free-energy-functions of boron, since pressures are matched with comparison systems and the contribution of B(g) is removed with the same error that was engendered in the reference system. In the determination of the heat of formation from the measured heat of vaporization, any errors in the

thermochemical data on boron gas or solid are included, and, possibly, those for the metal also. One should be critical of the quality of the thermochemical data used to construct the reference system.

CHAPTER 15

INTERPRETATION

15. 1 Significance of Vaporization Processes

15. 1. 1 Review of Hypothesis

As suspected in Chapter 1, the vaporization processes illustrated in Figure 4 should be explicable from a consideration of the variation in the volatility of the metal. This hypothesis assumed the absence of significant variation in the stability of corresponding borides with respect to the condensed elements as the lanthanide is varied. It was further assumed that the entropy change is the same for each possible reaction written to form one total mole of gas. Finally, it was assumed that all processes were studied at the same temperature or that, as a function of temperature, differences in free-energy-functions are negligibly small for different metal gases or compounds of different metals.

Recall from Chapter 1 the processes being considered (cf. Figure 15. 2):

$$3\ LnB_4(s) = 2\ LnB_6(s) + Ln(g) \qquad (1.\ 1)$$

$$1/5\ LnB_4(s) = 1/5\ Ln(g) + 4/5\ B(g) \qquad (1.\ 2)$$

$$1/4\ LnB_4(s) = 1/4\ Ln(l) + B(g) \qquad (1.\ 3)$$

$$2\ LnB_6(s) = LnB_{12}(s) + Ln(g) \qquad (1.\ 4)$$

$$1/7\ LnB_6(s) = 1/7\ Ln(g) + 6/7\ B(g) \qquad (1.\ 5)$$

$$1/2\ LnB_6(s) = 1/2\ LnB_4(s) + B(g) \qquad (1.\ 6)$$

15. 1. 2 Influence of Metal Volatility

It is clear from the observations described in Figure 4 that the variation in the metal volatility alone cannot explain the observed vaporization behavior of LnB_4 and LnB_6. For example, lanthanum, the most involatile of the lanthanide metals, would be expected to lose boron gas from the hexaboride to form LaB_4, if GdB_6 loses boron gas preferentially. However, it was observed to lose La(g) preferentially with $LaB_6(s)$ vaporizing congruently.

This apparent anomaly may be demonstrated more effectively by considering the enthalpies of vaporization at 2200°K. for the processes in equations 1. 1 to 1. 6 for different lanthanide metals. Since the principal process, i.e., the one with the smallest free energy change, was postulated to be dependent only on the metal volatility, the heat of formation of LnB_4 may be assumed constant at, say, -45 kcal./mole for every lanthanide, in order to estimate enthalpies for the six possible vaporization processes. Similarly, the heat of formation of LnB_6 may be assumed constant at -55 kcal./mole for every lanthanide and the heat of formation of LnB_{12} assumed constant at -50 kcal./mole for every lanthanide. The heat of vaporization of boron at 2200°K. from JANAF (69) is 130.3 kcal./g-at. The heats of vaporization of the lanthanide metals are taken from Table 1. 2. Figure 15. 1 describes the estimated enthalpy variation.

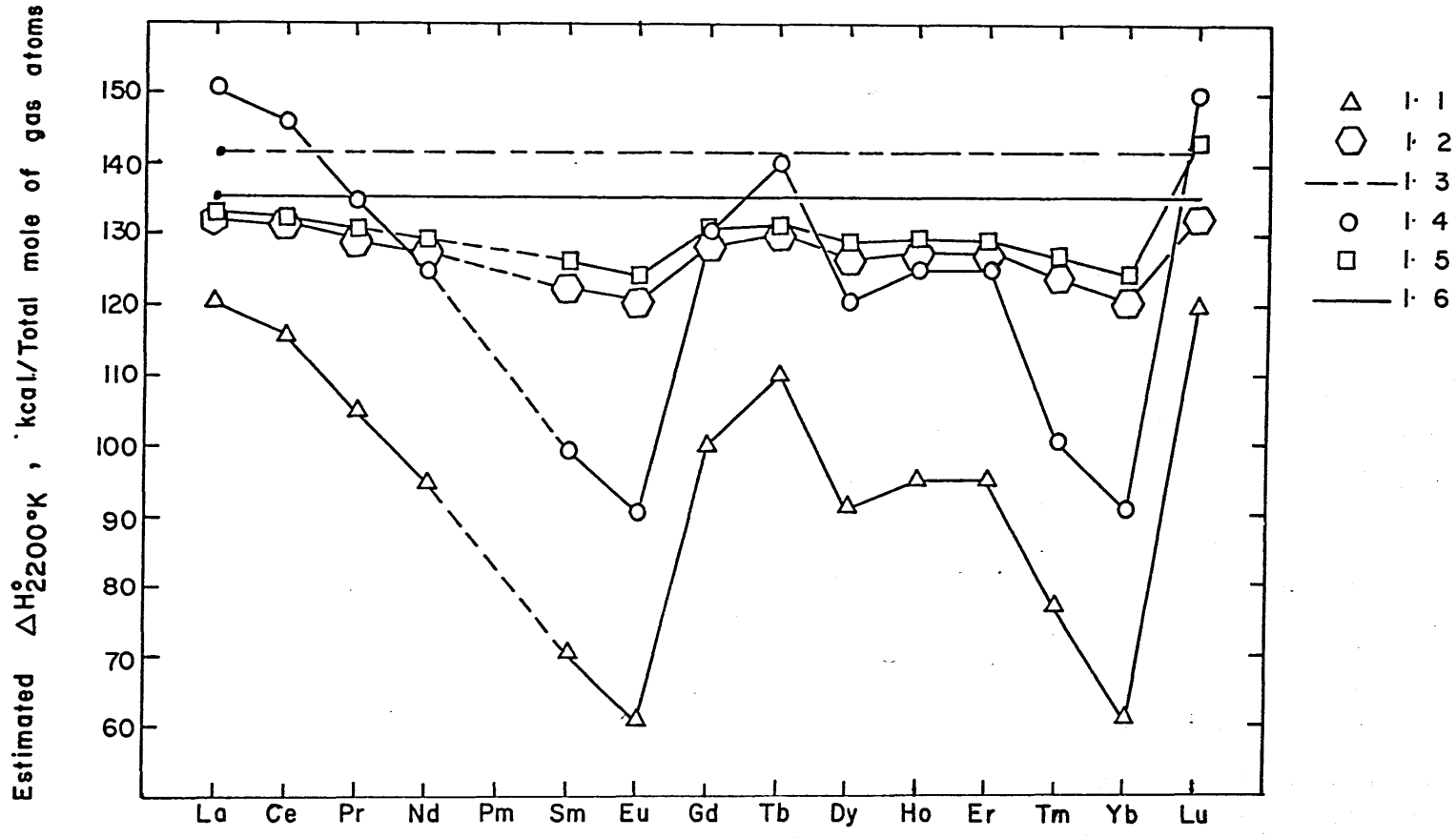

ESTIMATED $\Delta H^{\circ}_{2200^{\circ}K}$ VERSUS LANTHANIDE FOR POSSIBLE LnB_4 AND LnB_6 VAPORIZATION PROCESSES WITH CONSTANT BORIDE HEATS OF FORMATION

FIGURE 15. 1

It is obvious that the processes with the smallest enthalpy change, i.e., requiring the least amount of heat to form a mole of gaseous atoms, do not conform to the experimental observations. In particular, this scheme predicts that GdB_4(s) will lose Gd(g)(equation 1. 1) rather than vaporize congruently (equation 1. 2) as is observed experimentally. One may attempt to make the process in equation 1. 2 more important than that in equation 1. 1 by reassigning the heats of formation of LnB_4 and LnB_6 to account for the 30 kcal. difference in the two processes for GdB_4 vaporization. However, with the above assumption of constant heats of corresponding boride formation this reassignment would affect the LaB_4 behavior by the same 30 kcal. and allow the prediction that LaB_4 would vaporize congruently instead of losing La(g) as is observed experimentally. Similarly, any attempt to force congruent vaporization of SmB_6 over preferential loss of Sm(g) from SmB_6 by redefining the heats of formation of LnB_6 and LnB_{12} would force a contradiction of the observed loss of B(g) from Gd, Tb, Dy and Ho hexaborides.

Other similar anomalies in the scheme of Figure 15. 1 force the conclusion that there is no set of constant values for the heats of formation of LnB_4, LnB_6 and LnB_{12}, respectively, that can be chosen which will allow a match of the observed principal vaporization processes with the calculated principal processes within the limits of error in the metal volatilities. Thus, the conclusion that metal volatility alone does not determine the process by which the lanthanide borides vaporize is reached. This conclusion disproves the original hypothesis of this thesis. Possible variation in the heats of formation of the metal

borides and a reconsideration of the assumption of constant entropy change for the processes must be examined.

15. 1. 3 Entropy Estimation and Importance

15. 1. 3. 1 Entropy of Gaseous Atoms. Realizing that the principal vaporization process for a particular boride is that process with the smallest free energy change per mole of gas, i.e., the process which develops the largest total pressure, one must examine the entropy contribution to the free energy of vaporization for these processes and test the validity of the constant entropy assumption.

Consider as a first approximation that the entropy contribution to the processes from condensed phases is negligible compared to that of the gas. The composition of the gas varies from pure Ln(g) in processes 1. 1 and 1. 4 to pure B(g) in processes 1. 3 and 1. 6. Therefore, for the entropy change to be identical for the six processes, and for the free energy changes to be ordered according to the enthalpy changes, the entropies of the gaseous lanthanide metals must be equal to each other and equal to that of boron gas at the same temperature. However, an examination of Table 1. 2 reveals that at 2200°K. $S^{o}_{Yb(g)}$ differs from $S^{o}_{Gd(g)}$ by 7.5 eu. At 2200°K. this difference leads to an effect of 16.5 kcal. in the free energy. This wide variation in entropy of Ln(g) arises from the multiplicity of the ground state of the gaseous lanthanide atoms as discussed by Herzberg (188). Further, the entropy difference between B(g) and Ln(g) at 2200°K. may be as large as 12.2 eu. or 26.8 kcal./gas atom contribution to the free energy. Obviously, the

assumption of equal entropy for the six processes for all lanthanides is incorrect. The effect of 26.8 kcal. difference between a process involving pure boron gas and a process forming only lanthanide gas is quite appreciable compared to the enthalpy changes of the order of 100 kcal. estimated in Figure 15. 1.

15. 1. 3. 2 Entropy of Condensed Phases. It is necessary to examine to what extent the entropy contribution of the condensed phases may be ignored compared to the entropy of the gaseous atoms in the vaporization processes. Essentially no heat capacity data exist for the lanthanide borides. Therefore, the entropies of these borides must be estimated. There are three questions which must be considered in the estimation.

First, how precise is $S^{o}_{298^{o}K.}$ for the lanthanide borides calculated by assuming the standard entropy of formation at 298°K. to be zero, and in what way does $S^{o}_{298^{o}K.}$ deviate from this assumption? Fairly reliable estimates, by Mezaki, Tilleux, Barnes and Margrave (189), of $S^{o}_{298^{o}K.}$ for transition metal borides, based on the empirical scheme of elemental contribution to the entropy presented by Latimer and on the measured value of $S^{o}_{298^{o}K.}$ for ZrB_2, have been made and are listed in Table 15. 1, column two. Also included are the measured value by Swift (69) on MgB_4 and the measured value on LaB_6 by Westrum (190). It is clear from these data that the energy state of metal and boron atoms in the borides is significantly different from the pure elements. In particular, as the boron content increases, the entropy of the boride, determined from the assumption that ΔS^{o}_{298} of formation is zero (column three),

TABLE 15. 1

A Comparison of Literature Values of Entropies of Various Borides with those Estimated by Assuming ΔS_f^o and ΔC_p^o Are Zero.

Boride	$S^o_{298^oK.}$ (lit)[a] (eu.)		$S^o_{298^oK.}$ (est) (eu.)	$(S^o(lit)-S^o(est))_{298}$ (eu.)	% Deviation from lit (%)	$S^o_T-S^o_{298}$ (lit)[a] (eu.)	$S^o_T-S^o_{298}$ (est) (eu.)	$\left[S^o_T-S^o_{298}(lit)\right]-\left[S^o_T-S^o_{298}(est)\right]$ (eu.)	% Deviation from lit (%)
Mo_2B	22.8	± 2	15.05	- 7.7	-34	18.83	16.34	+ 2.49	+13.3
W_2B	28.2		17.47	-10.7	-38	25.35	24.05	+ 1.30	+ 5.13
TaB	13.1	± 1	11.29	- 1.8	-14	16.53	15.74	+ 0.79	+ 4.78
CrB	8.4		7.09	- 1.3	-16	16.28	16.02	+ 0.26	+ 1.60
MoB	10.5		8.22	- 2.3	-23	15.79	15.51	+ 0.28	+ 1.78
WB	13.2		9.43	- 3.8	-29	15.99	15.41	+ 0.58	+ 3.63
TiB_2	6.2	± 1	10.11	3.9	63	21.61	23.89	- 2.28	-10.55
ZrB_2	8.5		10.07	1.6	19	23.94	24.11	- 0.17	- 0.71
HfB_2	11.2		13.69	2.5	23	23.64	22.62	+ 1.02	+ 4.31
NbB_2	8.6		11.51	1.9	22	22.85	22.29	+ 0.56	+ 2.45
TaB_2	11.3		12.68	1.4	12	23.75	22.51	+ 1.24	+ 5.22
CrB_2	6.6		8.48	1.9	29	23.05	22.79	+ 0.26	+ 1.13
MoB_2	8.7		9.61	0.9	10	23.50	22.28	+ 1.22	+ 5.19
W_2B_5	21	± 2	23.04	2	10	47.73	51.13	- 3.40	- 7.12
MgB_4	12.41		13.41	1.00	8.1				
LaB_6	19.88		21.98	2.10	10.5				

a, Transition metal borides, 189; MgB_4, 69; LaB_6, 190.

becomes larger than the estimated values of column two. This difference is listed in column four. A rough extrapolation of the percent deviation of the entropy from this assumption, listed in column five, into the MB_4/MB_6 boron compositions indicates that $S^o_{298^oK.}$ for LnB_4 and LnB_6 may be estimated within 15 percent by correcting the value calculated from the assumption of zero entropy of formation downwards by 20 percent.

A further test of this assumption lies in a comparison of experimental data on $S^o_{298^oK.}$ for LaB_6 with the estimated entropy. Westrum, Clever, Andrews and Feick (190) have determined $S^o_{298^oK.}$ for LaB_6 as 19.88 eu. The value derived from assuming a zero entropy of formation is 22.0 eu. With a downwards correction of 20 percent, or 4.4 eu., the estimated value is 17.6 eu., which is 2.3 eu. smaller than the measured value, but within the estimated 15 percent error.

The second question to be answered is this: What is the value of $S^o_{2200^oK.} - S^o_{298^oK.}$? Measured heat capacity data in the range 298 to 1200°K. for transition metal borides by Mezaki, et al. (189), reveal the $S^o_T - S^o_{298^oK.}$ data listed in Table 15. 1, column six. These measured data are compared with data calculated from the assumption of the Neumann-Kopp Rule at 1200 and 298°K. with elemental heat capacities taken from Stull and Sinke (65) for the metals and from JANAF (69) for elemental boron (column seven). Notice the TiB_2—ZrB_2—HfB_2, CrB_2—MoB_2, CrB—MoB—WB and NbB_2—TaB_2 trends (column eight). These differences indicate that the assumption of ΔC^o_p equal to zero gives $S^o_T - S^o_{298^oK.}$ values increasingly too low as one goes down the groups in the Periodic Table. There is no significant trend with boron content.

The difference between calculated and observed values for S^{o}_{T} - $S^{o}_{298^{o}K.}$ at 1000°K. revealed that this difference was the same as the difference observed at 1200°K. Thus, it is believed that the deviation observed at 1200°K. may be assumed identical with that at 2200°K., even through the melting points of the metals. From a consideration of the position of the lanthanides in the Periodic Table, it would appear that the $S^{o}_{2200^{o}K.}$ - $S^{o}_{298^{o}K.}$ values, calculated from the assumption of zero for ΔC^{o}_{p} for formation at any temperature, are five percent lower than the actual values.

From a combination of the 20 percent correction downwards on $S^{o}_{298^{o}K.}$ determined from $\Delta S^{o}_{298} = 0$ with the 5 percent correction upwards on $S^{o}_{2200^{o}K.}$ - $S^{o}_{298^{o}K.}$ determined from $\Delta C^{o}_{p} = 0$, the formula used for obtaining the entropy of $LnB_4(s)$ and $LnB_6(s)$ and for LnB_{12}, as well, is:

$$S^{o}_{2200^{o}K} = 0.88\ (AS^{o}_{2200^{o}K.,B(s)} + S^{o}_{2200^{o}K.,Ln(l)}) \quad , \qquad (15.\ 1)$$

where A is four, six or twelve for LnB_4, LnB_6 or LnB_{12}, respectively. The error in the accuracy of these entropies is estimated liberally at 20 percent.

A third question remains to be answered. How systematic is the error in the entropy estimates of equation 15. 1? In other words, does the variation in entropy of the lanthanide borides with metal show the same trend as the variation in entropy of the pure condensed metal with atomic number? This observation is vitally important in establishing the trends of the free energies of the vaporization processes with lanthanide metal. If the large errors in the estimated entropies of the

borides can be shown to be systematic with varying metal, the influence of changes in the entropy from metal to metal for a particular vaporization process may be evaluated within the errors of the elemental lanthanide entropy only.

Borides of the same composition are isostructural as a function of lanthanide; and, therefore, the boron field into which metal ions must go is the same for each metal. Thus, it seems reasonable to suspect that, except for small size differences, the change in the entropy for metals going from isostructural solids or liquids into isostructural boride structures is influenced to the same extent by the boron matrix and is, therefore, constant with varying lanthanide metal. In other words, $\Delta S^{o}_{2200^{o}K.}$ for formation of lanthanide borides of the same composition is a constant as a function of lanthanide.

It is important to consider the change in the ground states of the metals on going into the boron field. The lanthanide metals are complicated by $R\ln(2J+1)$ magnetic entropy contributions from close-lying energy levels arising from unpaired 4f and 5d electrons. While it is certain that the boron field will influence these energy levels to a different extent for different lanthanides, any such changes should be small at 2200°K., even though the magnetic entropy of the lanthanides can be as much as 30 percent of the total entropy.

Further, the entropy due to the metal vibrations in the boride and due to conduction electrons might be influenced by the boron field to different extents for different metals. For instance, while other lanthanides show plus three valency, Sm, Eu and Yb retain quite a bit of

their alkaline earth character in alloys, but do not show divalency in ionic compounds such as oxides. Does this varied behavior imply varied entropy of formation with lanthanide metal, depending on whether the boride is ionic or metallic in nature?

It would appear that the most severe test of the constancy of ΔS_f^o would be found by examining the experimental data for a highly ionic compound such as the sesquioxide where severe restrictions are imposed on the metal valency in the oxide. Magnetic data, low electrical conductivity values, and linear lattice-parameter graphs, reported by Gschneidner (30), indicate that in every lanthanide sesquioxide the metal is constrained to a trivalent oxidation state. On the other hand, the lanthanide metals show significant metal divalency at Eu and Yb and tetravalency at Ce. Further, the metallic radius varies considerably from a linear function of atomic number at Ce, Eu and Yb. In view of the valency constriction on Ce, Eu and Yb in sesquioxide formation, perhaps deviation from a constant $\Delta S^o_{298^oK.}$ for formation will be revealed.

Westrum and Grönvold (61) have considered these factors and determined $\Delta S^o_{298^oK.}$ for formation of $Ln_2O_3(s)$ from a large amount of experimental data and some empirical estimations. These data are shown in Table 15. 2. Column two lists the entropy of the lanthanide metals taken from Stull and Sinke (65). Experimental values for the entropy of Ln_2O_3 are contained in column three. These are to be compared with values estimated by Grönvold and Westrum in column four. The entropy of formation of Ln_2O_3 is listed in column five. Column six tests the constancy of $S^o(Ln_2O_3) - 2\ S^o(Ln)$, where only experimental data are

TABLE 15. 2

Variation of the Standard Entropy of Formation of Lanthanide Sesquioxides with Lanthanide (61)

Metal	Metal $S^{o}_{298^{o}K.}$ (expt.) (eu.)	Sesquioxide $S^{o}_{298^{o}K.}$ (expt.) (eu.)	Sesquioxide $S^{o}_{298^{o}K.}$ (est.) (eu.)	Sesquioxide $-\Delta S^{o}_{298^{o}K.}$ (form.) (eu.)	$S^{o}_{298^{o}K.}(M_2O_3)-S^{o}_{298^{o}K.}(2M)$ (eu.)
Sc	(8.5)		19.4	(35.6)	
Y	10.63	23.69	22.4	35.54	2.43
La	13.64	30.43, 30.58	30.4	35.18	3.15
Ce	16.68		36.4	(35.2)	
Pr	17.49		37.9	(35.4)	
Nd	17.54	37.9, 36.92	38.0	(35.3)	2.8
Pm	(17.2)			(35.4)	
Sm	16.64	36.1	35.4	(35.4)	2.8
Eu	(17.0)		35	(36)	
Gd	15.77	36.0	36.3	(34.4)	4.5
Tb	17.48		37.5	(35.8)	
Dy	17.87	35.8	38.1	(35.7)	.1
Ho	18.00	37.8	38.2	(35.7)	1.8
Er	17.52	36.6	37.6	(35.5)	1.6
Tm	17.37		36.5	(35.7)	
Yb	(15.0)	31.8	34.5	(34.5)	1.8
Lu	12.19		26.0	(35.6)	

available. Parentheses imply estimated values or poor experimental data. Their work concludes that $\Delta S^{o}_{298^{o}K.}$ for formation of Ln_2O_3 (column five) is a constant within $\pm$ 0.6 eu., even for Eu and Yb. Experimental data support this conclusion, showing a variance of $\pm$ 1.5 eu. from constancy at 298°K.

While lanthanide ion in tetraborides is trivalent and ionic rather than metallic, some alkaline earth character, typical of the lanthanide metals, is observed at Yb and Eu (cf. Chapter 2). The valence of the metal in hexaborides is very close to that of the metals themselves, as shown by the lattice parameter variation, conductivity and magnetic measurements in Gschneidner (30). Considerably less is known about dodecaborides; however, the metal bonding in dodecaborides is probably similar to that in the tetraborides. Then, since the bonding in lanthanide borides is between the ionic bonding in Ln_2O_3 and the bonding in the metals, it appears reasonable to assume that ΔS^{o}_{f} at 298°K. and 2200°K. is a constant with lanthanide for corresponding lanthanide borides. Thus, a large step is taken in rendering the percentage errors in the boride entropy estimates constant.

The entropies for tetra-, hexa- and dodecaborides at 2200°K., estimated by equation 15. 1, are listed in Table 15. 3. With the use of the boride entropies in Table 15. 3, the heats of vaporization of lanthanide metals and boron, and the entropies of the elemental species at 2200°K. as listed in Table 1. 2, the standard free energies of vaporization for the six vaporization processes in equations 1. 1 to 1. 6 were calculated with equation 6.18 for the various lanthanides, excluding the

TABLE 15. 3

Estimated Entropies of Solid Lanthanide Tetra-, Hexa- and Dodecaborides at 2200°K.

Ln	$S^{o}_{LnB_4}$ (eu.)	$S^{o}_{LnB_6}$ (eu.)	$S^{o}_{LnB_{12}}$ (eu.)
La	70.8	92.6	158.0
Ce	74.5	96.2	161.6
Pr	74.5	86.2	161.6
Nd	76.1	98.1	163.5
Pm	74.2	96.0	161.4
Sm*	73.6	95.4	160.8
Eu*	74.0	95.8	161.2
Gd	73.3	95.1	160.5
Tb	74.3	96.1	161.5
Dy	74.6	96.3	161.7
Ho	74.5	96.2	161.6
Er	74.4	96.2	161.6
Tm	73.7	95.5	160.9
Yb*	71.4	92.8	158.2
Lu	69.0	91.7	157.1

* Liquid metal reference state

terms involving the heats of formation of the borides at this temperature. The estimated free energies, exclusive of the heats of formation of the borides, are tabulated in Table 15. 4 for all the lanthanide metals.

15. 1. 4 Systematic and Random Errors

In order to determine what reliance can be placed on the estimated data of Table 15.4 for use in the following arguments, it is necessary to discuss the magnitude of the errors involved in these estimations. In view of the lack of spectroscopic data and the ambiguity in interpretation of the spectra (Landolt and Börnstein (191)), entropy data on Ce, Pr, Tb, Dy, Ho, Er and Tm are not available. Based on the range of entropies in Table 1. 2, the entropy values for these gaseous elements at 2200°K. have been taken as 57 eu. with an uncertainty of $\pm$ 2 eu. The random error in the gaseous entropies of the other lanthanides and in the entropies of the liquid lanthanides at 2200°K., taken from Stull and Sinke (65), is liberally estimated at $\pm$ 0.5 eu. For Sm, Eu and Yb a liquid reference state has been taken by extrapolating the liquid standard state data to 2200°K., which is above the normal boiling point for these lanthanides. The entropy error in B(g) and B(s) at 2200°K. is taken as $\pm$ 0.1 eu. with the data taken from JANAF (69). The error in $\Delta H^{o}_{vap.}$ for boron at 2200°K. is taken as $\pm$ 4 kcal./g-at., according to Schick (132). Standard heats of sublimation of the lanthanide metals at 2200°K. were taken from Stull and Sinke (65) or estimated from more recent data (cf. Table 1. 2). These data are reliable to $\pm$ 2 kcal./g-at. random error. The uncertainties in the boride entropies were previously estimated as 20%. All these uncertainties are listed in Table 15. 5.

TABLE 15. 4

Free Energy Changes, Exclusive of Heats of Boride Formation, for the Six Possible Vaporization Processes of LnB_4 and LnB_6 at 2200°K.

			La	Ce	Pr	Nd	Pm	Sm	Eu	Gd	Tb	Dy	Ho	Er	Tm	Yb	Lu
LnB_4	1.1	$\Delta F^o-(2\Delta H^o_{LnB_6}-3\Delta H^o_{LnB_4})$	29.9	34.0	23.0	13.0		-16.2	-18.7	11.3	27.1	9.24	12.6	12.4	-7.2	-13.9	24.4
		Loss of Ln(g)															
	1.2	$\Delta F^o-(-1/5\Delta H^o_{LnB_4})$	47.2	48.0	45.8	44.1		38.1	37.6	43.8	46.8	43.0	43.8	43.8	39.8	38.4	47.1
		Congruent															
	1.3	$\Delta F^o-(-1/4\Delta H^o_{LnB_4})$	49.8	49.6	49.6	49.6		49.6	49.6	49.6	49.6	49.6	49.6	49.6	49.6	49.8	50.0
		Loss of B(g)															
LnB_6	1.4	$\Delta F^o-(\Delta H^o_{LnB_{12}}-2\Delta H^o_{LnB_6})$	29.9	33.4	22.4	14.3		-16.2	-18.7	11.3	27.1	8.6	12.4	12.4	-7.0	-16.6	30.3
		Loss of Ln(g)															
	1.5	$\Delta F^o-(-1/7\Delta H^o_{LnB_6})$	48.7	49.2	47.6	46.5		42.1	41.8	46.4	48.3	45.6	46.2	46.2	43.4	42.0	48.7
		Congruent															
	1.6	$\Delta F^o-(1/2\Delta H^o_{LnB_4}-1/2\Delta H^o_{LnB_6})$	51.8	51.8	51.8	51.8		51.8	51.8	51.8	51.8	51.8	51.8	51.8	51.8	51.8	51.8
		Loss of B(g)															

For these calculations $\Delta H^o_{298°K.}$ for boron vaporization was taken from JANAF (69) as 132.6 kcal./g.-at. If $\Delta H^o_{298°K.}$ for boron vaporization were 135.0 kcal./g.-at., reported by Robson and Gilles (178), then the values for processes 1. 2, 1. 3, 1. 5 and 1. 6 would be increased by 2.0, 2.4, 2.0 and 2.4 kcal., respectively. See Table 16. 6 for the uncertainties.

Collecting these errors, weighted for their contribution to the free energies, one obtains the total uncertainty in the free energies of vaporization for each of the six processes under consideration, exclusive of errors in the heats of formation of the boride. These uncertainties are contained in Table 15. 5. It is obvious that these uncertainties are too large to allow the prediction of behavior trends as the thermochemical properties of the lanthanides change. However, a great portion of these errors is systematic with atomic number, especially when comparing free energies for a particular vaporization process with varying lanthanide. Since the entropy of the borides varies with lanthanide in the same fashion as the entropy of the liquid lanthanide metal, the error from the estimation of S^{o} for LnB_4, LnB_6 and LnB_{12} is systematic and cancels in corresponding processes with different metals. The errors in $\Delta H^{o}_{vap.}$ of boron and in $S^{o}_{B(g)}$ and $S^{o}_{B(s)}$ are also systematic and cancel as two different lanthanides are compared in the same process. The sums of the remaining uncertainties between any two lanthanides for the six vaporization processes are shown in Table 15. 5. Since these uncertainties are smaller than the variations in $\Delta S^{o}_{vap.}$ and $\Delta H^{o}_{vap.}$ of the lanthanide metal at 2200°K., a test of the influence of variation in these contributions with atomic number is quite possible; the trend of stabilities of tetra- and hexaboride with respect to the gaseous elements may also be described.

It is also necessary to determine the uncertainties involved on intercomparing each of the six different processes all involving the same lanthanide. This determination is necessary in deciding the process of

TABLE 15. 5

Uncertainties in Estimated Free Energies of Vaporization

Uncertainties in component terms for the estimated free energies for the six LnB_4 and LnB_6 vaporization processes at 2200°K.

$S^\circ_{LnB_4}$ (eu.)	$S^\circ_{LnB_6}$ (eu.)	$S^\circ_{LnB_{12}}$ (eu.)	$\Delta H^\circ_{vap.Ln}$ (kcal./gat.)	$\Delta H^\circ_{vap.B}$ (kcal./gat.)	$S^\circ_{Ln(g)}$ (eu.)	$S^\circ_{Ln(l)}$ (eu.)	$S^\circ_{B(s)}$ (eu.)	$S^\circ_{B(l)}$ (eu.)
16.0	20.2	34.0	2	4	2	0.5	0.1	0.1

Uncertainty, exclusive of errors in heats of boride formation, in the estimated free energies of the possible vaporization processes of LnB_6 and LnB_4 at 2200°K.

$\Delta F^\circ_{1.1}$	$\Delta F^\circ_{1.2}$	$\Delta F^\circ_{1.3}$	$\Delta F^\circ_{1.4}$	$\Delta F^\circ_{1.5}$	$\Delta F^\circ_{1.6}$
20.0	11.3	13.3	17.2	10.7	8.8 kcal.

Uncertainty in the difference in estimated free energies, exclusive of heats of boride formation, between any two lanthanides vaporizing by one of the six possible processes at 2200°K.

$\Delta F^\circ_{1.1}$	$\Delta F^\circ_{1.2}$	$\Delta F^\circ_{1.3}$	$\Delta F^\circ_{1.4}$	$\Delta F^\circ_{1.5}$	$\Delta F^\circ_{1.6}$
3.0	0.9	0.3	3.1	0.5	0 kcal.

smallest free energy, i.e., the principal vaporization process. It is clear that while any errors in the entropies and heats of vaporization of a particular lanthanide are certainly systematic in their contribution to the different vaporization processes, terms with systematic errors, however, because of the varied stoichiometry for the processes, occur to different extents for different processes and do not cancel in general. Thus, the errors between free energies of different processes with the same lanthanides are larger than errors between free energies for the same process with different lanthanides. The errors remaining after elimination of systematic contributions are shown in Figure 15. 2.

While these uncertainties are generally large relative to the variation in the free energy of vaporization between processes, the total result on fitting the observed principal vaporization processes of Chapter 4 to estimated free energies affords a much more reliable interpretation than these uncertainties would indicate.

15. 1. 5 Condensed Phase Entropy Influence

While the entropies of the gaseous atoms are the principal contributions to the total entropy of vaporization, the entropies of the condensed phases and their variation with lanthanide and with process are certainly not negligible contributions to the free energies, but represent an appreciable contribution to the variation in free energy between the vaporization processes for different lanthanides. More specifically, the vaporization process for the tetra- and hexaboride is not determined by the variation in the heat of vaporization of the lanthanide metal alone, but also by the variation in entropy of lanthanide

1.1 $3LnB_4(s) = 2LnB_6(s) + Ln(g)$

1.2 $1/5LnB_4(s) = 1/5Ln\ (g) + 4/5B\ (g)$

1.3 $1/4LnB_4(s) = 1/4Ln(s,l) + B\ (g)$

1.4 $2LnB_6(s) = LnB_{12}(s) + Ln(g)$

1.5 $1/7LnB_6(s) = 1/7Ln\ (g) + 6/7B\ (g)$

1.6 $1/2LnB_6(s) = 1/2LnB_4(s) + B\ (g)$

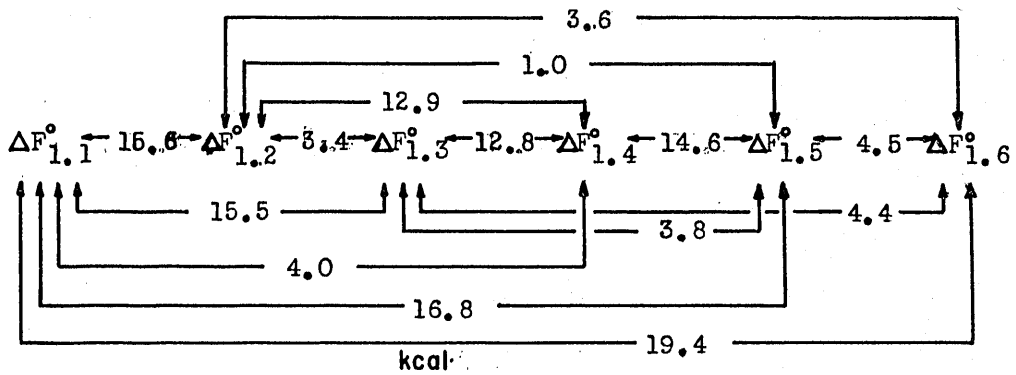

Non-Systematic Errors Between $\Delta F^\circ_{2200\,^\circ K}$ Values For Vaporization Processes of LnB_4 and LnB_6

FIGURE 15. 2

gas and lanthanide borides.

15. 1. 6 Influence of Boride Heat of Formation

If the metal volatilities and entropy considerations alone are sufficient to interpret the observed principal vaporization processes, then within the framework of assumptions and errors above one should find a value for the heat of formation of the solid tetraboride, a value for the solid hexaboride and a value for the solid dodecaboride, which, when considered as constants for all lanthanides, will allow the experimentally observed principal vaporization processes to match the predicted minimum free energy process in all lanthanide systems. Consider, as an example, the free energies of vaporization listed in Table 15. 6. These data were calculated assuming that $\Delta H^{o}_{f_{LnB_4}}$, $\Delta H^{o}_{f_{LnB_6}}$ and $\Delta H^{o}_{f_{LnB_{12}}}$ all are -50 kcal./mole at 2200°K. Notice that while some of the predicted minimum free energies match the observed processes for vaporization of tetra- and hexaboride, others fail to match by as much as 20 kcal. per total gas atom, which is beyond the estimated non-systematic errors.

It can be demonstrated that no such set of constant values for the heats of formation of the borides can be assigned, even outside the stability limits established in Chapter 14 for these borides, that will allow an agreement between observed and predicted minimum free energies in all cases. Consider processes 1. 1 and 1. 2. The heat of formation

TABLE 15. 6

Free Energies of LnB_4 and LnB_6 Possible Vaporization Processes at 2200°K., Heats of Formation of the Borides Assumed to be -50 kcal./mole

Ln	$\Delta F^{\circ}_{1.1}$ (kcal.)	$\Delta F^{\circ}_{1.2}$ (kcal.)	$\Delta F^{\circ}_{1.3}$ (kcal.)	$\Delta F^{\circ}_{1.4}$ (kcal.)	$\Delta F^{\circ}_{1.5}$ (kcal.)	$\Delta F^{\circ}_{1.6}$ (kcal.)
La	79.9 *	57.2 #	62.3	79.9	55.8 *	51.8 #
Ce	84.0 *	58.0 #	62.1	83.4	56.3 *	51.8 #
Pr	73.0 *	55.8 #	62.1	72.4	54.7 *	51.8 #
Pm						
Sm	33.8 *#	48.1	62.1	33.8 #	49.2 *	51.8
Eu	31.3(*)#	47.6	62.1	31.3 #	48.9	51.8
Gd	61.3	53.8 *#	62.1	61.3	53.4	51.8 *#
Tb	77.1	56.8 *#	62.1	77.1	57.4	51.8 *#
Dy	59.2	53.0 *#	62.1	58.6	52.7	51.8 *#
Ho	62.6	53.8(*)#	62.1	62.4	53.3	51.8(*)#
Er	62.4	53.8(*)#	62.1	62.4	53.3	51.8(*)#
Tm	42.8 #	49.8	62.1	43.0 #	50.5	51.8
Yb	36.1 *#	48.4	62.3	33.4 *#	49.1	51.8
Lu	74.4	57.1 #	62.5	80.3	55.8	51.8 #

#, Calculated principal process

*, Observed principal process

term which must be added to complete the free energy expression in process 1. 1 is $(2\ \Delta H^{o}_{f_{LnB_6}} - 3\Delta H^{o}_{f_{LnB_4}})$. To process 1. 2 must be added the term $(-1/5\ \Delta H^{o}_{f_{LnB_4}})$. In order for LaB_4 to lose La(g) preferentially (cf. Table 15. 4),

$$29.9 \text{ kcal.} + (2\Delta H^{o}_{f_{LaB_6}} - 3\Delta H^{o}_{f_{LaB_4}}) < 47.2 \text{ kcal.} + (-1/5\Delta H^{o}_{f_{LaB_4}}). \quad (15.\ 2)$$

And for, say, dysprosium tetraboride to vaporize congruently, as is experimentally observed,

$$43.0 + (-1/5\ \Delta H^{o}_{f_{DyB_4}}) < 9.2 + (2\Delta H^{o}_{f_{DyB_6}} - 3\Delta H^{o}_{f_{DyB_4}}) \quad (15.\ 3)$$

After collecting terms, one observes that $(2\ \Delta H^{o}_{f_{LnB_6}} - 14/5\ \Delta H^{o}_{f_{LnB_4}})$ must be greater than 33.8 kcal. for dysprosium, yet less than 17.3 kcal. for lanthanum. Clearly, no constant value for $\Delta H^{o}_{f_{LnB_6}}$ and for $\Delta H^{o}_{f_{LnB_4}}$ as a function of lanthanide will satisfy both requirements. Recalling from Figure 15. 2 that the random error for the difference in free energies between processes 1. 1 and 1. 2 is 15.6 kcal., one notes that the discrepancy in the above relation, 16.5 kcal., is outside this error. Further, as noted above, the existence of such a large collection of experimental observations and thermochemical data has the effect of reducing this particular error estimate, thus rendering the observation

more reliable. Clearly, then, a variation in the heats of formation of the lanthanide borides is a necessary criterion in the interpretation of the observed vaporization processes.

15. 1. 7 Variation in Boride Heat of Formation

15. 1. 7. 1 Background. While there are no precise data in the literature on the stability of the lanthanide borides with respect to solid elements, much less the variation with lanthanide, some idea of how these heats of formation will vary may be conceived from a consideration of other properties of these borides and of related materials.

It is apparent that the stability of metal borides, particularly those with high boron content, is principally due to the covalently-bound chains, nets and cages of boron atoms. This view is supported by the high melting points, extreme hardness, low thermal expansion, and low volatilities exhibited by metal borides. While the metal ions are necessary in these structures to meet the electronic demands for boron-boron bonds, the percentage contribution of boron-metal bonds to the stability of the boride is small compared to that of the boron-boron covalent bonds. Thus, the variations in stability of these borides between different lanthanides will be small because of the low metal concentration and the many boron-boron covalent bonds. However, variations must exist in order to explain the vaporization trends and other trends noted later for lanthanide borides.

Brewer and Engel (192) have described a correlation between electronic and crystal structure, and bond character and thermodynamic

stability of metallic and intermetallic phases. From their interpretation s and p-orbital electrons are structure determining, while the d-orbital electrons, which are restricted to nearest neighbor interactions, do not influence structure. However, the d-orbital electrons do contribute importantly to the binding energy in transition metals and intermetallic compounds. The d-orbital contribution increases with atomic number, while s and p-orbital contributions decrease with atomic number. The bond energy or stability is generally determined by the average number of unpaired electrons per atom available for bonding. The effects of size, internal pressure and promotion energies to higher electronic states must also be considered, but are second order.

Brewer (193) pointed out that in the lanthanides the 5d unpaired electrons do extensively contribute to bonding in lanthanide alloys. However, these 5d orbitals generally become less available for bonding as atomic number increases because of the increasing divergence between the 4f and 5d energy levels. Therefore, with the assumption that the s and p-orbital conditions are essentially the same as atomic number increases through the lanthanides, the contribution of 5d electrons to the compound stability should decrease. Thus, all borides might be expected to show a decrease in stability as z increases, with the most rapidly decreasing stability being exhibited by the boride with highest metal content. This argument would be the same for stabilities with respect to gaseous elements or to solid elements. The boron contribution to stability in a particular boride should be the same for each lanthanide. Some size effects might interfere with this argument.

Many research workers have discussed the electron configurations, bond types, structures and electrical or metallic properties of the MB_2, MB_4, MB_6 and MB_{12} borides and boron (104, 73, 105, 194, 106, 107, 108). These papers support the existence of covalently-bound boron atoms involving s, p and d-orbitals with two electrons per metal atom needed to satisfy the electron requirements of the boron-boron bonds. The third valence electron in the case of the lanthanide borides is not needed in the boron structure and accounts for the metallic properties of the lanthanide borides. The divalent nature of the alkaline earth hexaborides accounts for their semiconductor properties.

Flodmark (105,104) in a valence bond treatment of MB_6 crystals found that the stability of the hexaboride phase increases with decreasing ionization potential for the two electrons required per metal atom. Thus, the stability of the alkaline earth hexaborides increases going down the alkaline earth group. In trivalent metal hexaborides, there is a sufficiently large bonding energy for the third electron to compensate the larger ionization energy and Coulomb repulsion energy so that lanthanide hexaborides meet the requirements of Flodmark's valence bond model. This view of the existence and stability of the hexaboride depending on ionization potential is supported by Samsonov (195). The lack of ionization potential information (cf. Table 1. 2) and the small variation of ionization potential between lanthanides preclude any interpretation prescribing the variation of lanthanide hexaboride stability with lanthanide.

Russian authors (195) believe that La, Pr, Sm and Eu hexaborides are the most stable of the lanthanides, since the first ionization

potentials are low for these metals (5.6-5.7 ev.). The stability of Ce, Nd, Gd, Tb, Dy and YbB_6 is thought by these authors to be lower in view of the high ionization potentials of these metals (6.2-6.7 ev.). They further state that hexaboride phases are always more stable than tetra- and diboride phases, as demonstrated by their observations of loss of metal preferentially from lower borides to hexaborides (196). However, their observations ignore the second ionization potential, size effects, metal volatility variations and entropy effects. It is not clear whether their intention is to predict boride stability with respect to gaseous atoms or with respect to solid elements.

In summary, then, the lack of thermochemical data on specific borides and the inability of theory and of measured physical properties related to stability to distinguish the small variations in bond strengths between corresponding borides of different lanthanide metals preclude reaching any firm conclusion regarding the variation of the heat of formation of lanthanide borides as a function of atomic number.

15. 1. 7. 2 Empirical Evidence for Variations in Boride Stability. There are certain relationships between lanthanide borides established in this research and in others, which, when considered by themselves, do not establish the relative stability of lanthanide borides. However, a consideration of these relationships as a whole indicates how the heats of formation of lanthanide borides probably vary with atomic number.

Consider Figure 15. 3. This graph illustrates the heat of formation at 298°K. of lanthanide sesquioxides, trichlorides and aluminides versus lanthanide (30). Notice the trend of decreasing stability of the

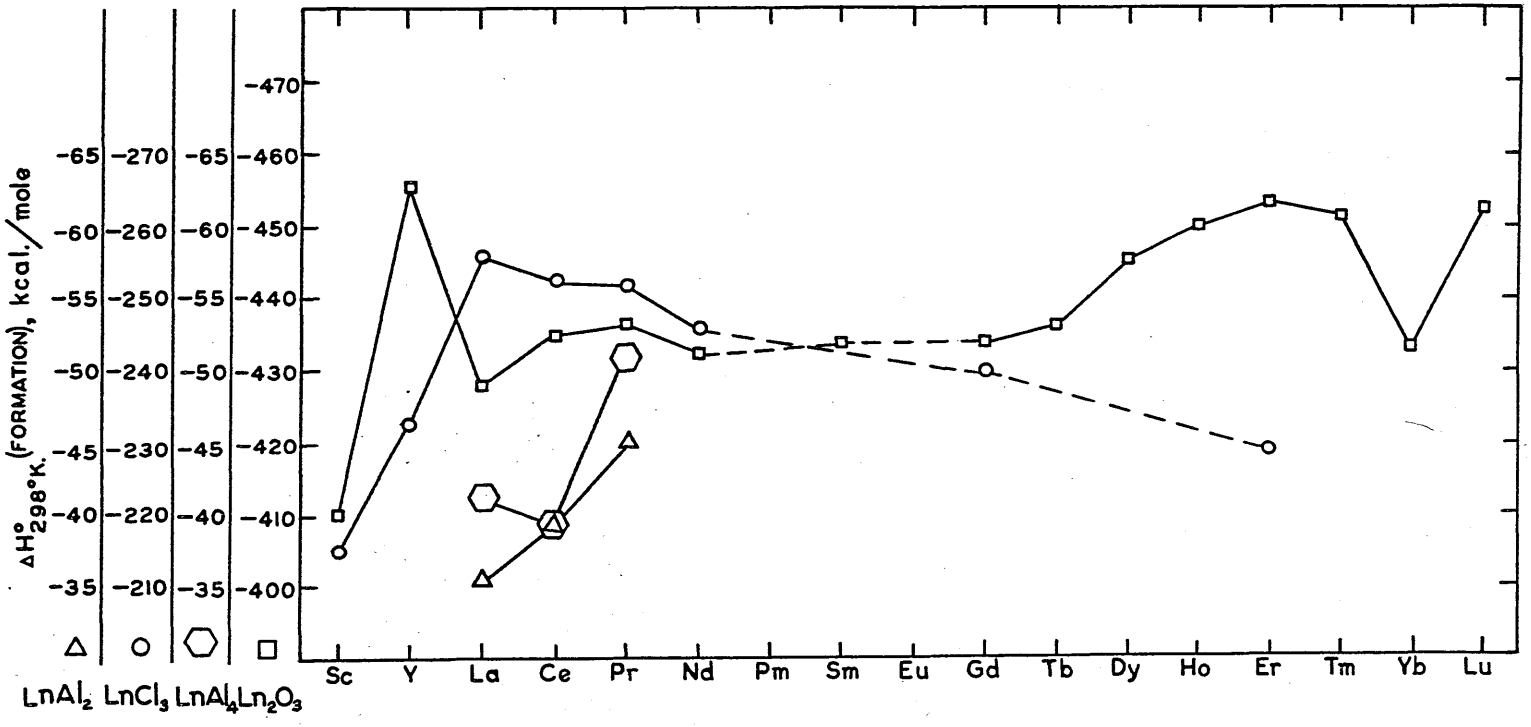

Standard Heats of Formation at 298°K. of Ln_2O_3, $LnCl_3$, $LnAl_2$, and $LnAl_4$ Versus Ln

FIGURE 15. 3

trichlorides with increasing atomic number. While there is a decreasing stability of sesquioxide in the first half of the lanthanide series, the second half does not show a similar trend. It is interesting to note that the heat of formation of the sesquioxides varies only very little with lanthanide, i.e., $\pm$ 10 kcal./mole in 450 kcal./mole or 2 percent. Recall from Part I, Chapter 7, that the lattice parameters for these sesquioxides vary strictly linearly with atomic number, even through Sm, Eu and Yb. Therefore, the sesquioxides are strictly ionic compounds. Notice further, that the aluminides exhibit an increasing stability with Z, a variation in the heats of formation of $\pm$ 12 percent, and metallic like deviations in lattice parameter at Sm (cf. Gschneidner, (30)). This correlation indicates that lanthanide compounds of metallic character exhibit wider fluctuations in stability with lanthanide than do ionic compounds.

The lanthanide tetraborides, dodecaborides and probably the hectoborides show linear behavior of their lattice parameters with lanthanide even through Tm and Yb (cf. Table 2.1). These phases, then, are fairly ionic. On the other hand, hexaboride lattice parameter variation is metallic in nature. Thus, perhaps hexaborides would have stabilities which would exhibit a greater variation from lanthanide to lanthanide than would the other lanthanide borides. Further, these variations may show decreasing boride stabilities with increasing Z.

Consider the requirements of equations 15. 2 and 15. 3. The quantity, $(2\Delta H^{o}_{f_{LnB_6}} - 14/5\Delta H^{o}_{f_{LnB_4}})$, must be less than 17.3 kcal. at La and greater than 33.8 kcal. at Dy. Therefore, $(2\Delta H^{o}_{f_{LnB_6}} - 14/5\Delta H^{o}_{f_{LnB_4}})$

must get larger with increasing atomic number.

If it is assumed that the variations in the tetra- and hexaboride stabilities are in the same direction, there exist two possible interpretations. First, if LnB_4 is getting more stable across the lanthanides, then LnB_6 must get more stable at a slower rate with increasing atomic number (weighted for the coefficients). However, the idea of increasing stability with Z seems improbable in view of Brewer's remarks above and other observations later. Further, between the two borides the tetraborides should show the slowest variation in stability because of their ionic character. The second possibility, and the more acceptable, requires the stability of hexaboride to decrease faster with increasing atomic number than that of the tetraboride.

Recall from Chapter 2 which borides exist in the lanthanide-boron systems. The diborides of Gd, Tb, Dy, Ho and Er have been made. Others certainly exist, e.g., Nordine reports the existence of SmB_2 (197). All tetraborides except EuB_4 have been observed. All hexaborides except those at the end of the series (Er, Tm and Lu) have been made. While hectoborides of only Sm, Gd, Tb, Ho, Yb and perhaps La have been found, they will all probably be found in time.

Post has indicated dodecaborides involving metal radii greater than that of Tb probably do not exist because the ionic size of the lanthanide is too large. Such a radius dependence implies that the dodecaborides are getting more stable as the ionic radius decreases or as Z increases. While size effects are important, the idea of increasing stability with Z is not appealing on the basis of the above discussion and because another more plausible explanation is available.

Consider the process,

$$LnB_{12}(s) = 3/47\ LnB_{100}(s) + 44/47\ LnB_6(s). \qquad (15.\ 4)$$

The free energy for this process early in the lanthanide series is negative, i.e., LnB_{12} cannot be prepared. At Gd or Tb the free energy becomes positive and LnB_{12} is stable with respect to LnB_{100} and LnB_6. The value of ΔS^o_T for this condensed phase process is assumed zero, and then the behavior can be explained by an increasing dodecaboride stability (decreasing $\Delta H^o_{f_{LnB_{12}}}$) with Z as Post's size restriction suggests. However, another possibility would be that the heat of formation of LnB_6 becomes less negative (less stable) faster than that of LnB_{12}. The heat of formation of LnB_{100} is not going to change much with lanthanide, simply because of the low metal concentration; but ΔH^o_f of LnB_6 might be expected to vary faster than the LnB_{12} stability, in view of the above discussion relating bonding to stability variation.

Consider further the process,

$$4\,LnB_6(s) = LnB_{12}(s) + 3\ LnB_4(s). \qquad (15.\ 5)$$

This process has a positive free energy for most of the lanthanide series so that LnB_6 is stable relative to LnB_{12} and LnB_4. However, the free energy of this process approaches zero at Ho where HoB_6 preparations contain all of the three phases in process 15. 5, and becomes negative for Er, Tm and Lu. This observation explains the inability to prepare hexaborides of Er, Tm and Lu. Here again an explanation based on an

increasing stability of dodecaboride with Z could explain this observation. However, LnB_{12} with its ionic character and low metal content should not influence the variation of free energy for this process nearly as much as should LnB_4 and LnB_6. Again, the satisfying choice is a more rapidly decreasing stability of LnB_6 with increasing atomic number.

These criteria are illustrated in the free energy diagram of Figure 15. 4. These five isothermal diagrams show schematically the borides existing in the Sc, Y and lanthanide systems. The ordinate defines the free energy (or enthalpy) of formation of a mole of boride from the condensed elements. These values are thought accurate to $\pm$ 10 kcal. Composition is indicated in weight percent boron rather than mole percent in order to separate the free energy curves on the diagram conveniently. The extent of solid solution indicated in the figure is, of course, unrealistic, but serves to define the tangents to the free energy curves and the influence of the shape of the free energy curve more clearly. The temperature is assumed to be below the melting points of the borides and above the disproportionation temperatures of LnB_2 for the lighter lanthanides. These diagrams are not the usual free energy diagrams which plot kcal./g-at., nor do the ordinate intercepts bear the usual significance as partial molal quantities.

The phases in equilibrium at this temperature for a particular synthetic composition are the two boride compositions defined by the tangent line to the free energy curves. These tangent lines represent the lowest free energy or most stable condition for that synthetic composition. For example, a mixture of CeB_6 and CeB_{12} on heating to this

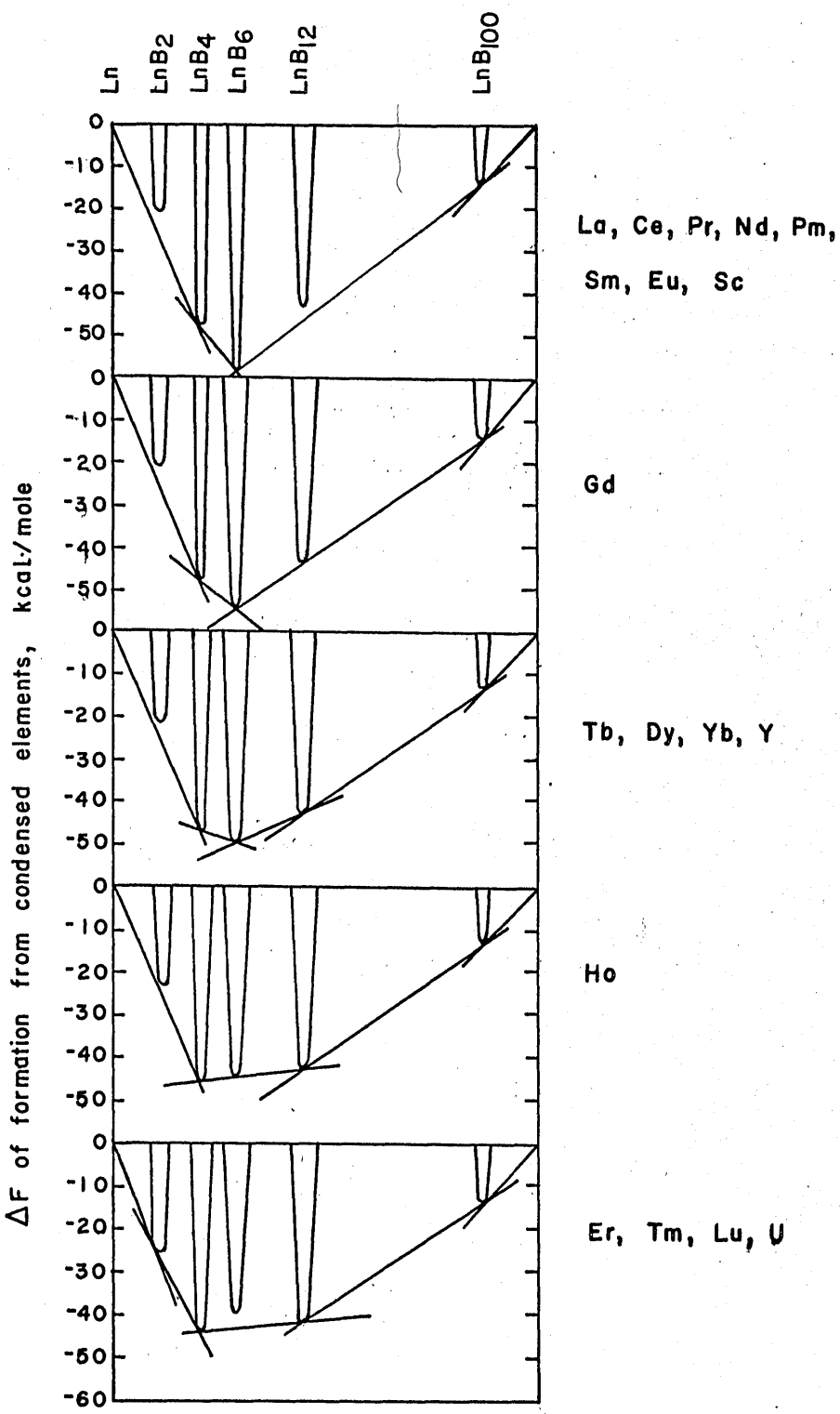

FREE ENERGY DIAGRAM FOR RELATIVE STABILITY OF LANTHANIDE BORIDES WITH RESPECT TO CONDENSED ELEMENTS

FIGURE 15. 4

temperature will show CeB_6 and CeB_{100} in the product, rather than a CeB_6-CeB_{12} mixture. The tangent line between the CeB_6 and CeB_{12} free energy curves does not represent the smallest free energy of the mixture; rather, the CeB_6-CeB_{100} tangent curve has a lower free energy. Therefore, CeB_{12} is unstable with respect to CeB_6 and CeB_{100}. In general, these diagrams assume that the depths of the free energy curves decrease for increasing atomic number of the metal. The decrease in LnB_6 free energy at a rate relatively faster with Z than for the other borides explains the boride behaviors noted in the above discussion.

Another indication of the higher stability of LnB_6 relative to LnB_4 at La is manifested by the difficulty of preparing LaB_4 from a mixture of La and boron, as reported by Felten, Binder and Post (76). The product invariably contains considerable LaB_6 indicating loss of La(g). The higher stability of LaB_6 accounts for the disproportionation of LaB_4(s) into La(l) and LaB_6(s). The free energy for this melting process must be close to zero and varies with temperature sufficiently to allow for LaB_4 preparation from La and LaB_6 at lower temperatures.

The inability to prepare EuB_4, where all attempts produce EuB_6, is a matter of high europium metal volatility and a more stable hexaboride than tetraboride. In the case of Yb where YbB_4 can be prepared, but is difficult to prepare free of YbB_6, the Yb volatility certainly is influencing the loss of Yb(g) from YbB_4 preferentially. However, the stability difference between YbB_6 and YbB_4 is not as large as the EuB_6-EuB_4 relative stability difference. Therefore, the free energy of the process,

$$3LnB_4(s) = 2LnB_6(s) + Ln(g) \qquad (15.6)$$

is larger for the Yb case than for the Eu case, even though Yb metal is more volatile than Eu metal (cf. Table 1. 2). Hence, again a more rapidly decreasing stability of LnB_6 relative to LnB_4 is indicated.

While the conclusions above are not binding when each point is made separately, the combination of the heat of formation-lattice parameter correlation, Brewer's discussion, the restrictions from observed vaporization processes, the two boride disproportionation reactions, and the LaB_4, EuB_4, and YbB_4 behaviors all indicate a larger decrease in LnB_6 stability with respect to the solid elements, as a function of Z, compared to the decrease in stabilities of the other lanthanide borides with Z.

It is not implied that the variation of stabilities with respect to condensed elements is strictly linear with atomic number. The ability to prepare YbB_6 and not TmB_6 or LuB_6 on either side of YbB_6 is indicative of a deviation from linearity at Yb. This same variation probably exists at Ce, Sm and Eu. The extent of the double periodicity effect, noted in the heats of vaporization of the lanthanide metals, Figure 1. 1, is not known. However, the double periodicity effect is not as large in the stabilities of the borides with respect to condensed elements as it is in the stability of the solid borides with respect to the gaseous elements. In general, the conclusion is reached that the stability of the lanthanide borides with respect to solid elements decreases as atomic number increases with ΔH_f^o of LnB_6 increasing with Z more rapidly per mole than ΔH_f^o for the other lanthanide borides.

15. 1. 7. 3 Matching Calculated and Observed Vaporization Processes. In Chapter 15. 1. 6, it was demonstrated that variation in

the heat of formation of LnB_4 and LnB_6 was necessary to explain the observed vaporization processes. Chapter 15. 1. 7. 2 prescribed how this variation goes with lanthanide. This section describes how the observed and calculated principal vaporization processes can be matched by properly assigning boride heats of formation. The severe limitation on the boride stabilities is also emphasized.

In order to get some idea of the variation in the free energies of the six vaporization processes in equations 1. 1 to 1. 6, a linear decrease in the stability, i.e., increase towards zero in ΔH_f^o, of LnB_6 with a constant value for ΔH_f^o of LnB_4 and LnB_{12} might be chosen. Such a choice for the heats of formation of LnB_4, LnB_6 and LnB_{12} can be made that does, indeed, match the minimum estimated free energies with the observed principal vaporization processes. Imposing the restriction that the heats of formation must not deviate outside the limits established in the metal-lanthanide-boron studies of Chapter 14, assuming constant values for ΔH_f^o of LnB_4 and LnB_{12} and assuming the previously discussed errors in the components of the free energies, one can calculate the free energies for all the six vaporization processes for all the lanthanides. Such calculated free energies, representing typical stabilities with the above restrictions, are shown in Table 15. 7. The heat of formation of LnB_4 is assumed constant at -48.5 kcal./mole and that of LnB_{12} at -43.7 kcal./mole. The assumed hexaboride stabilities are shown in column eight of the table. In every case the calculated principal process matches the observed principal vaporization process.

Various attempts to fit other heats of formation values to this scheme with the above assumptions and restrictions fail for variations

TABLE 15. 7

Free Energies of LnB_4 and LnB_6 Possible Vaporization Processes at 2200°K., Based on the Assumptions that $\Delta H^{\circ}_{LnB_4}$ = - 48.5 kcal./mole and $\Delta H^{\circ}_{LnB_{12}}$ =-43.7 kcal./mole

Ln	$\Delta F^{\circ}_{1.1}$ (kcal.)	$\Delta F^{\circ}_{1.2}$ (kcal.)	$\Delta F^{\circ}_{1.3}$ (kcal.)	$\Delta F^{\circ}_{1.4}$ (kcal.)	$\Delta F^{\circ}_{1.5}$ (kcal.)	$\Delta F^{\circ}_{1.6}$ (kcal.)	$-\Delta H^{\circ}_{f}(LnB_6)$ (kcal./mole)
La	51.4 *#	56.9	61.9	110.2	57.6 *#	58.7	62.0
Ce	57.5 *#	57.7	61.7	111.7	58.0 *#	58.0	61.0
Pr	50.5 *#	55.5	61.7	96.7	56.0 *#	57.3	59.0
Nd	43.5 *#	53.8	61.7	85.6	54.7 *#	56.3	57.5
Pm							
Sm	19.3 *#	47.8	61.7	50.1	50.0 *#	55.0	55.0
Eu	19.8(*)#	47.3	61.7	44.6 #	49.4	54.3	53.5
Gd	53.0	53.0 *#	61.7	71.6	53.8	53.5 *#	52.0
Tb	70.6	56.5 *#	61.7	85.4	55.6	53.0 *#	51.0
Dy	56.7	52.7 *#	61.7	62.9	52.6	52.0 *#	49.0
Ho	63.1	53.5(*)#	61.7	63.7	53.0	51.3(*)#	47.5
Er	65.9	53.5(*)#	61.7	60.7	52.8	50.5(*)#	46.0
Tm	49.3	47.5 #	61.7	38.3 #	49.7	49.8	44.5
Yb	45.6 *#	48.1	61.9	25.7 *#	48.1	49.0	43.0
Lu	86.9	56.8 #	62.1	69.6	54.6	48.3 #	41.5

#, Calculated principal process

*, Observed principal process

10 kcal./mole on either side of the values given in Table 15. 7 for the heats of formation of the tetra- and hexaboride. Attempts to fit calculated and observed processes with less stable tetra- and hexaborides reduces the required stability of LnB_{12} rapidly to the lowest possible limit determined from ternary studies. However, as noted in Figure 15. 2, the error between processes 1. 4 and 1. 5 or 1. 6 is of the order of 15 kcal., which could allow for a higher dodecaboride stability by 15 kcal./mole. Changes in LnB_4 and LnB_6 stabilities affect process 1. 1 considerably more than processes 1. 2 or 1. 3 because of the stoichiometry. Thus, boride stabilities greater by 10 kcal. than those in Table 15. 7 prevent the assignment of the lowest free energy to process 1. 1 for the lighter lanthanides. Therefore, within this framework the heats of formation at 2200°K. of these borides are those used in Table 15. 7 within 10 kcal./mole.

Notice that under these assumptions hexaboride becomes less stable per mole than tetraboride at Ho. This observation is in contradiction to the Russian statement (cf. Chapter 15. 1. 7. 1) that hexaborides are always more stable than tetraborides.

Notice too, that the free energy change for the congruent vaporization of GdB_4 estimated in Table 15. 7 is 53.0 kcal. per 1/5 mole. With consideration for the errors involved in this estimate, the agreement with the measured value of 55.3 kcal. per 1/5 mole at 2200°K. (cf. Chapter 13) is really remarkable. This satisfying agreement provides more confidence in the estimations of Table 15. 7.

A graphical summary of the estimated free energy changes of

Table 15. 7, shown in Figure 15. 5, also orders the total pressures developed in each of the three possible vaporization processes either for tetraboride or for hexaboride for each lanthanide system. Total pressure increases up the ordinate with decreasing free energy. The principal processes are those with the smallest free energy change or developing the highest total pressure or appearing the highest on the graph for a particular boride.

This graph does not necessarily order the component partial pressures. For instance, the total pressure of process 1. 2 for Dy is larger than that of process 1. 1. However, the Dy partial pressure may be higher in process 1. 1 than in process 1. 2. The variation with lanthanide in the free energies for each process in Figure 15. 5 is generally the same as the variation in free energy change in vaporization of the metal (cf. Figure 15. 6), with the damping of the variation increasing with boron content of the gas.

15. 1. 8 Boride Stability With Respect to Gaseous Elements; Relation to Vaporization Process

The stability of LnB_4 and of LnB_6 with respect to the gaseous elements is indicated in Table 15. 7 by processes 1. 2 and 1. 5, the congruent processes. The variations with lanthanide of the boride stabilities with respect to gas atoms are shown graphically in Figure 15. 6. The variations in metal pressures over pure metal, as determined by ordering the heat of vaporization on the right-hand ordinate, are included. Also, from the free energy of vaporization at 2200°K. for the metals, the actual metal pressures are given. Notice that the variation

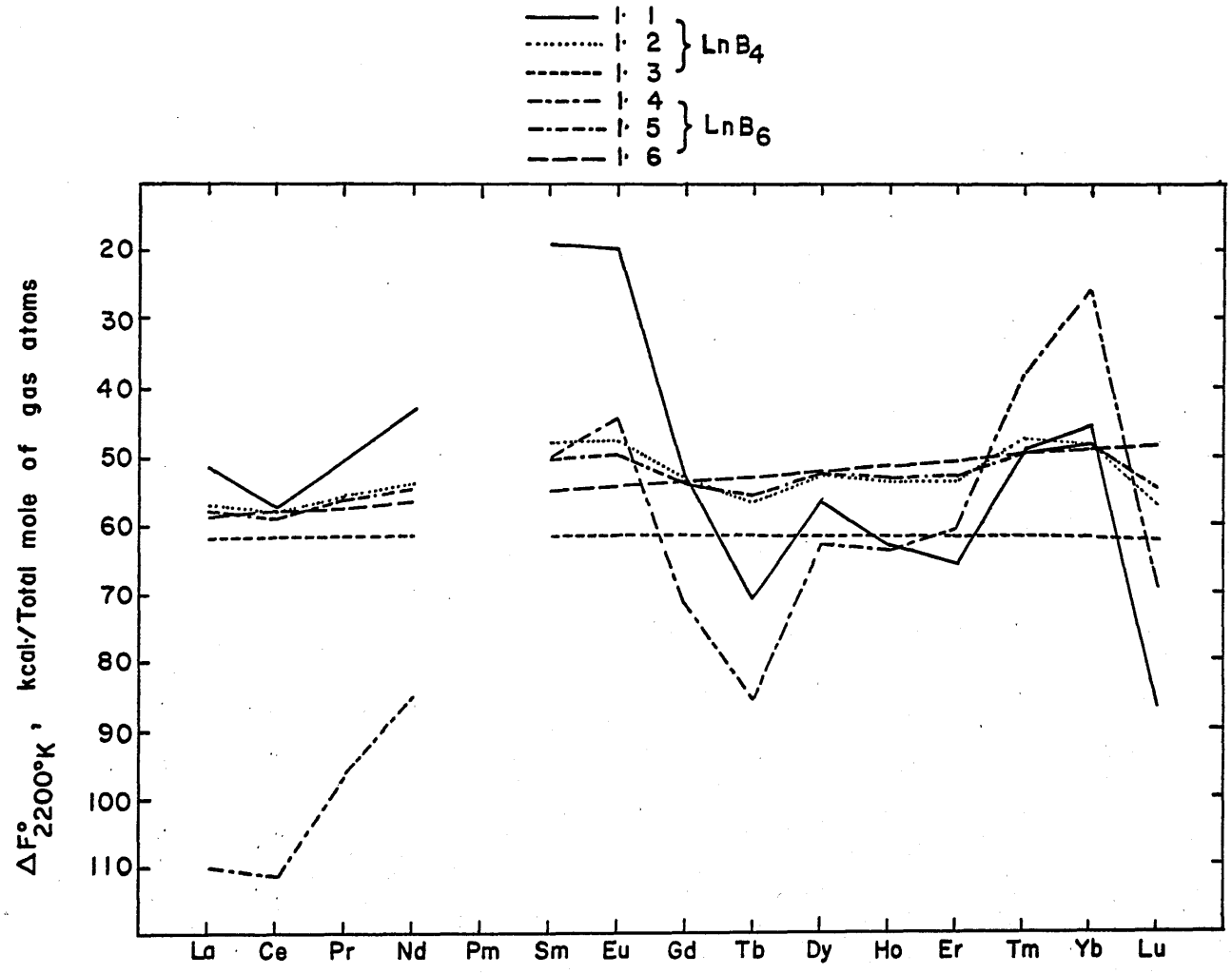

ESTIMATED $\Delta F^{\circ}_{2200\,^{\circ}K}$ VERSUS LANTHANIDE FOR POSSIBLE LnB_4 AND LnB_6 VAPORIZATION PROCESSES

FIGURE 15. 5

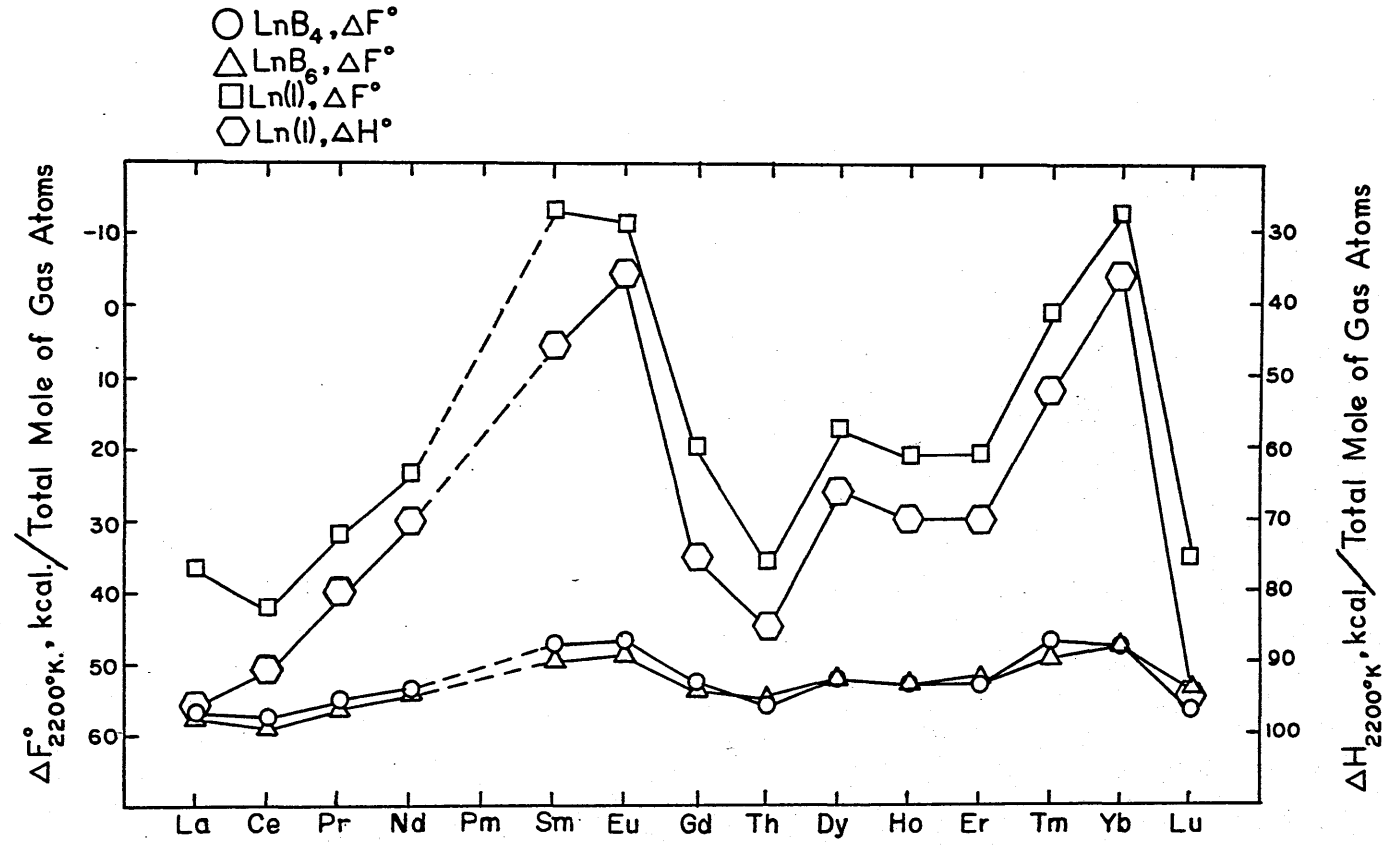

Volatility of Ln(l), ΔF° (Vap.) Ln(l) and ΔF° For Formation of One Total Mole of Gas Atoms From LnB_4 and LnB_6 Versus Ln All at 2200°K.

FIGURE 15. 6

in stability of the borides goes as the variation in the free energy of vaporization of the metal, as expected.

An ordering of the free energy changes, as in Figure 15. 6, also orders the total pressure exhibited by corresponding borides in different lanthanide systems. Borides or metals developing the highest pressure among corresponding compounds have the largest equilibrium constant, and, hence, the smallest free energy in Figure 15. 6. Thus, the most volatile metals at this temperature are Sm, Eu and Yb. Of the tetraborides, EuB_4 is the least stable and CeB_4 is the most stable with respect to gaseous elements. Similarly, YbB_6 and CeB_6 are, respectively, the least and most stable hexaborides with respect to gaseous elements. Comparison of tetraboride to hexaboride stability must include consideration for the difference in equilibrium constants for the two vaporization processes. However, hexaborides are more stable than tetraborides for the light lanthanides. For the heavy lanthanides there is a tendency for tetraborides to show greater stability except at Yb.

It is interesting to examine the observed vaporization processes for the lanthanide borides in terms of free energy diagrams similar to those for boride stability with respect to the solids (cf. Figure 15. 4). Such a diagram at 2200°K. is Figure 15. 7. The abscissa defines increasing boron composition in atomic percent. The gas phase is taken as the separated ideal gases, boron and lanthanide metal, at a total pressure of one atmosphere. The ordinate defines the free energies of formation of one total mole of gas atoms from the condensed phases. In other words, the figure describes the standard free energy change on congruent vaporization to the elements (the stability).

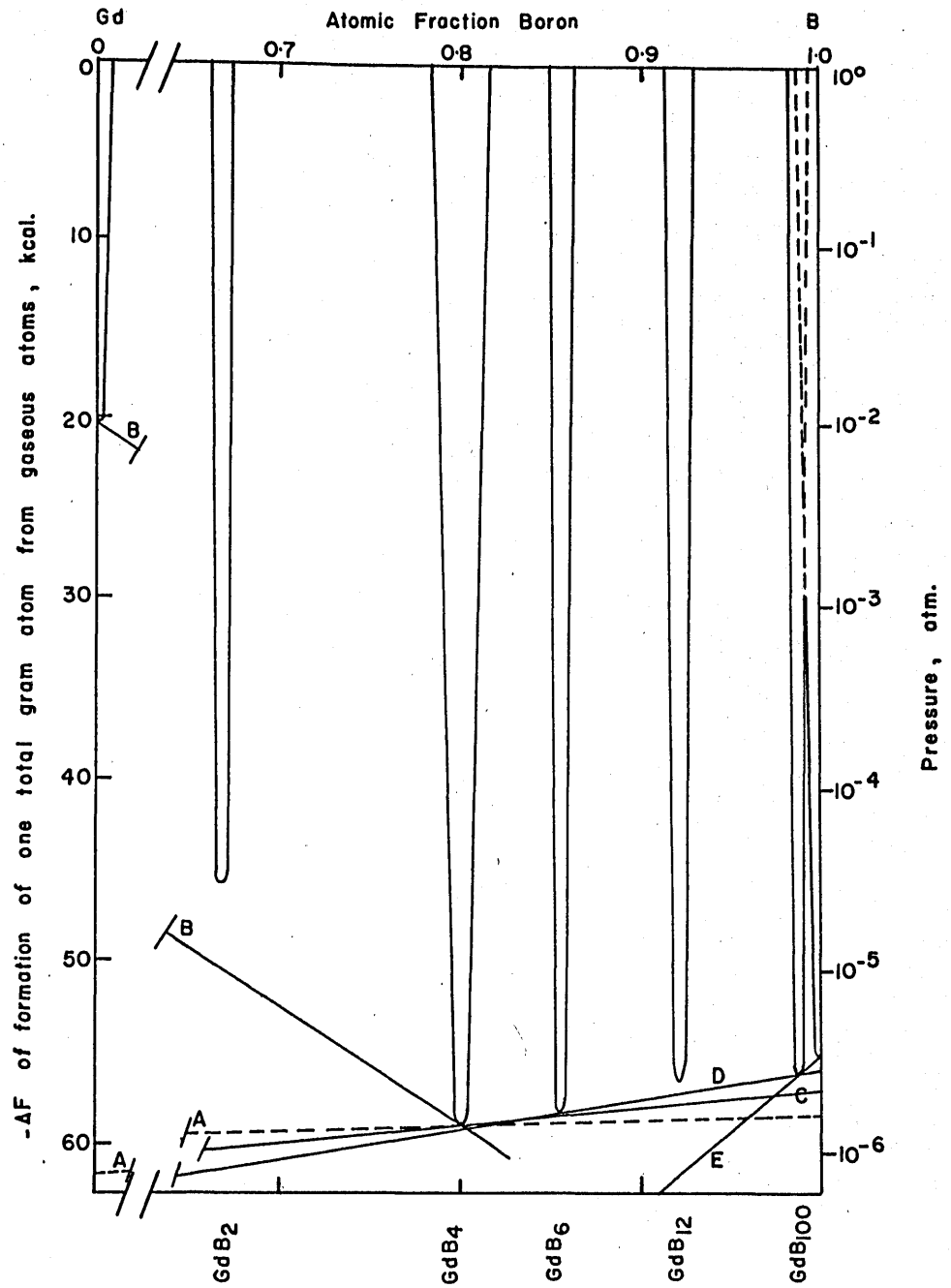

FREE ENERGY DIAGRAM AT 2200 °K FOR GADOLINIUM BORIDE STABILITIES WITH RESPECT TO GASEOUS COMPONENTS

FIGURE · 15. 7

At the temperature of the figure, 2200°K., a 10 kcal. increase in the free energy corresponds fairly closely to a pressure drop of one decade. Thus, in addition to a free energy ordinate the ordinate may be labeled with pressure decreasing as free energy increases. Therefore, tangents, representing minimum free energy, drawn to the solid free energy curves have intercepts on either side of the diagram which define the pressures of lanthanide and boron in equilibrium with the solid boride or borides at this temperature.

The principal problem in this work is to determine the relative depths of the boride free energy curves below the free energy of the gas. In order to correlate the observed vaporization processes with the stabilities, consider the vaporization behavior of the gadolinium-boron system as an example, as shown schematically in Figure 15. 7.

The boride, GdB_4, has been observed to vaporize congruently to gaseous elements with a measured standard free energy change of 55.3 kcal. per 1/5 mole at 2200°K. (cf. Chapter 13). The partial pressures of gadolinium and boron are defined by the ordinate intersections of a tangent, A, to the GdB_4 free energy curve restricted to a slope with the ratio of boron to gadolinium pressure equal to four. Since GdB_6 has been observed to lose boron preferentially on vaporization, the free energy curve for solid GdB_6 has a closely restricted depth in relation to the free energy of the gaseous elements. In particular, the tangent line, C, to both the GdB_4(s) free energy curve and the GdB_6(s) free energy curve must intersect the elemental pressure scale in such a way that the boron pressure is less than the vapor pressure of boron, but greater than the partial

pressure of boron over GdB_4, tangent A.

Similarly, the gadolinium pressure over GdB_6-GdB_4 is less than the partial pressure of gadolinium over GdB_4. If the boron partial pressure over the GdB_4-GdB_6 two-condensed-phase mixture, defined by tangent C, were greater than the vapor pressure of pure boron, then GdB_6 would be unstable at this temperature with respect to GdB_4 and boron solid. Similarly, a pressure of gadolinium over the GdB_4-GdB_6 mixture greater than the pressure of Gd over GdB_4 would predict that GdB_4 would lose Gd(g) preferentially to form GdB_6, which contradicts experiment. A boron partial pressure below that of the boron pressure over GdB_4 would indicate that GdB_4 is unstable with respect to loss of Gd(g) to form GdB_6(s).

The above discussion must be qualified somewhat. It is not strictly true that the partial pressures interact as depicted. The vaporization process for a particular boride developing the largest total pressure is the important process. Because of the different expressions for the equilibrium constants for the three possible processes by which a boride may vaporize, the partial pressures of lanthanide or boron may, in fact, be slightly larger in a process that is not the principal process, and yet the total pressure still be less.

The phase, GdB_{100}, as well as GdB_6, exists at this temperature. Therefore, the limitation on the boron pressure over a GdB_4-GdB_6 mixture is more restrictive than indicated above. This boron partial pressure must be greater than the boron partial pressure over GdB_4 (weighted for the equilibrium constant differences) but less than the boron pressure

over GdB_6-GdB_{100} mixtures, tangent D. Similarly, the pressure of boron over a GdB_6-GdB_{100} mixture must be less than the pressure of boron over a GdB_{100}-B mixture, tangent C. Only with these restrictions will all borides with more boron content than GdB_4 lose boron preferentially. Thus, the observed vaporization processes in the Gd-B system establish restricting limits on the relative stability of all the gadolinium borides with respect to the gaseous elements.

As can be seen from the proximity of the GdB_4 free energy curve to that of pure boron, the stabilities of higher borides than GdB_4 with respect to gaseous elements are restricted to a narrow range. Thus, the relative volatilities of these borides are close together, separated only by a few kcal. per gas atom (cf. Chapter 13).

The phases, GdB_2 and GdB_{12}, cannot be prepared at this temperature and pressure. Thus, tangents between either Gd(1) and GdB_2 or GdB_4 and GdB_2 define higher free energies than the GdB_4-Gd tangent curve, B. Hence, GdB_2 is unstable with respect to Gd(1) and GdB_4. Similar arguments establish the instability of GdB_{12} with respect to GdB_6 and GdB_{100}. Therefore, lower limits on the stability of GdB_2 and GdB_{12} can be established. For GdB_2, ΔF° of formation of one total gram atom of boride must be greater than -45 kcal. at 2200°K. And for GdB_{12} the stability of one gram atom of boride with respect to gaseous elements is greater than -55 kcal. at 2200°K. This same scheme holds for the other lanthanide borides. With the measured value for $\Delta F^\circ_{2200°K.}$ for congruent GdB_4 vaporization as a reference point, with a knowledge of the free energies of vaporization of the elements at this temperature, and with the free energy variations

of Table 15. 7 established from the observed vaporization processes, significant definitions of the limits on the stabilities of all the lanthanide borides with respect to their gaseous elements have been established. In particular, if the standard free energy of vaporization of boron at 2200°K. is taken from JANAF (69) as 55.09 kcal./g-at., the standard free energies of vaporization of GdB_6, GdB_{12} (if it exists) and GdB_{100} to the gaseous elements at 2200°K. must lie in decreasing order of free energies between 55.3 and 55.1 kcal./one total gas atom. However, the errors in ΔF^o for boron vaporization and for GdB_4 vaporization expand this limiting range. Accepting the postulated free energies in Table 15. 7, one can make similar more or less restrictive statements concerning other lanthanide borides.

In conclusion, the free energies of the LnB_4 and LnB_6 vaporization processes, contained in Table 15. 7 and shown schematically in Figures 15. 5 and 15. 6, are required by the observed vaporization processes. To establish the absolute values of these free energies one must consider not only the metal volatility, but also the entropy of the lanthanide gas, the entropy of the lanthanide borides and the variations in the stability of the borides with respect to the condensed elements, all of which are important.

15. 2 Ancillary Vaporization Observations

15. 2. 1 Temperature Effect on Vaporization Process

It is interesting to note that the difference in free energies between two possible vaporization processes involving the same lanthanide

boride is sometimes small (cf. Table 15. 7). If the free energy functions for two processes, which proceed nearly to the same extent, are not the same as a function of temperature, at a temperature different from 2200°K. the observed principal vaporization process might change. In other words, while the conditions required to observe two congruently-vaporizing single-phase compositions in the same lanthanide-boron system are very restrictive, two such phases could be observed to vaporize congruently at a different temperature.

Consider the vaporization of SmB_6 at 2200°K. According to Table 15. 7, congruent vaporization is the dominant process by only 0.1 kcal. over preferential loss of Sm(g) into the vapor. From free-energy-functions, estimated in the same fashion as the data employed in the calculations of Chapter 15. 2. 4, one predicts that SmB_6 will change from congruent vaporization to a preferential loss of Sm(g) at a temperature near 1000°K. Then SmB_{12} or SmB_{100} will vaporize congruently below this temperature. This temperature may be high enough to allow observation of this change of process with a mass spectrometer.

The explanation of this behavior lies in the implication that the partial molal entropy change on vaporization of samarium from the congruently vaporizing SmB_6 is different from that of boron vaporizing from SmB_6. Hence, the partial molal heats of vaporization of Sm and of B from SmB_6 are slightly different. The Clapeyron plot of log p versus 1/T will show slightly different slopes for samarium gas and for boron gas. The boron partial pressure decreases with temperature at a rate less than that of samarium until the ratio of boron partial pressure to samarium partial pressure is twelve at some particular temperature. At this

invariant temperature, solid SmB_6 and SmB_{12} are in equilibrium with a vapor of composition twelve parts boron to one part samarium. Below this temperature SmB_6 vaporizes with such a relatively high samarium partial pressure that samarium is lost preferentially from SmB_6 to form SmB_{12} solid, which will vaporize congruently.

Similar transitions to different vaporization processes with varying temperature might be observed for CeB_4, GdB_4, CeB_6, GdB_6 or DyB_6.

15. 2. 2 Vaporization of Sc and Y Borides

All the boride phases found in the lanthanide-boron systems have been found in the Y-B system. The heat of vaporization of yttrium metal is comparable to that of lanthanum metal, while the entropy of gaseous yttrium at 2200°K. is almost exactly that of lanthanum gas (cf. Table 1. 2). In the absence of data on the heat of formation of the yttrium borides, one is tempted to assume stabilities comparable to lanthanum borides. If so, the vaporization of the yttrium borides should show loss of metal preferentially from YB_2 and YB_4, congruent vaporization of YB_6, and preferential loss of boron from all higher borides, just as in the lanthanum-boron system.

However, the experiments in Chapter 4 reveal a net loss of boron from YB_6 to YB_4. In view of the entropy and volatility agreement between yttrium and lanthanum metals, the explanation of the contrasting vaporization behavior of YB_6 probably lies in a relatively higher stability of YB_4 with respect to the solid elements compared to YB_6 stability. This behavior is typical of the boride stabilities in the last half of the

lanthanide series. Considering the free energies for LaB_4 vaporization listed in Table 15. 7, one notes that to bring process 1. 2 (congruence) into predominance over process 1. 1 (loss of metal) requires only an increase in the stability of LaB_4 over LaB_6 by 2 kcal. or more per mole. At the same time this would make process 1. 6 (loss of boron) more important than process 1. 5 (congruence) for LaB_6, thus explaining the observed vaporization processes for YB_4 and YB_6.

In the Sc-B system only ScB_2 and ScB_6 have been reported. Post, et al. (113), were unable to make ScB_{12}. The higher volatility of Sc metal over Y metal with the entropy of vaporization of the metals nearly the same would lead one to suspect that the congruently vaporizing single-phase composition in this system is ScB_6. This observation is supported by Samsonov, Markovskiĭ, Zhigach and Valyashko (195), who observed the formation of ScB_6 as ScB_2 was allowed to vaporize from a hot tantalum wire.

15. 2. 3. Vaporization of Alkaline Earth Borides

Apparently, very little effort has been made to prepare borides in alkaline earth systems. As noted in Chapter 2, the hexaboride is known to exist for Be, Mg, Ca, Sr and Ba. Only the hexaboride has been found in the case of Sr and Ba. CaB_4 and CaB_6 are known to exist. More recently the Mg-B and Be-B systems have been investigated in greater detail with the discovery of MgB_2, MgB_4, MgB_6 and MgB_{12} by Samsonav, et al. (195) and by Post (46). Many Be borides exist but will be excluded from this discussion in view of the singular chemical character of Be. One wonders if

the borides in the Mg-B system cannot be prepared for the other alkaline earths.

Some information is available concerning the stabilities of these borides with respect to the solid elements. Wright and Walsh (69) measured the heats of formation, entropies and heat capacities for MgB_2 and MgB_4 up to 300°K. The heats of formation (Table 14. 2) are -17.9±3.0 and -21.0± 5.0 kcal./mole, respectively, at 298°K. Samsonov, Serebryakova and Bolgar (181) measured the heat of formation of SrB_6 at 298°K. as -50.4 kcal./mole. A previous discussion in Chapter 15. 2. 7. 1 suggested that the stability of the alkaline earth hexaborides decreases in the order $BaB_6 > SrB_6 > CaB_6 > MgB_6$, according to the difficulty in removal of two electrons from the metal.

Consider the vaporization of the magnesium borides below 1200°K., which is below the melting points of the magnesium borides. The possible vaporization modes for MgB_2 are:

$$1/2\ MgB_2(s) = 1/2\ Mg(s,1) + B(g), \qquad (15.\ 7)$$

$$1/3\ MgB_2(s) = 1/3\ Mg(g) + 2/3\ B(g), \qquad (15.\ 8)$$

and

$$2\ MgB_2(s) = MgB_4(s) + Mg(g). \qquad (15.\ 9)$$

With the use of thermochemical data for B, MgB_2 and MgB_4 from JANAF (69) and data on magnesium from Stull and Sinke (65), the standard free energy changes for these processes were calculated as 96.2, 53.7 and 14.3 kcal., respectively. By far the predominant process is the loss of magnesium from $MgB_2(s)$ to form $MgB_4(s)$.

Next consider the vaporization of $MgB_4(s)$.

$$3\ MgB_4(s) = 2\ MgB_6(s) + Mg(g). \quad (15.10)$$

$$1/5 MgB_4(s) = 1/5\ Mg(g) + 4/5\ B(g). \quad (15.11)$$

$$1/2 MgB_4(s) = 1/2\ MgB_2(s) + B(g). \quad (15.12)$$

In order to calculate the free energy of the first possible process the entropy of MgB_6 is assumed to be 0.88 times the entropy determined from the assumption that $\Delta S_f^o(MgB_6)$ is zero (cf. Chapter 15. 1. 3. 2). Further, ΔH_f^o of MgB_6 is taken as -40 kcal./mole, less than that of SrB_6. Then the free energy values calculated for reactions 15.10, 15.11 and 15.12 are -25.5, 76.5 and 91.2 kcal., respectively. Again the loss of metal from MgB_4 is by far the most important process, even if MgB_6 has a zero heat of formation.

In the consideration of MgB_6 vaporization, the possible processes are:

$$2\ MgB_6(s) = MgB_{12}(s) + Mg(g), \quad (15.13)$$

$$1/7 MgB_6(s) = 1/7\ Mg(g) + 6/7\ B(g) \quad (15.14)$$

and

$$1/2 MgB_6(s) = 1/2\ MgB_4(s) + B(g). \quad (15.15)$$

Making the same assumptions for $S^o_{MgB_{12}}$ as for $S^o_{MgB_6}$ and assuming $\Delta H^o_{f_{MgB_{12}}}$ is -100 kcal./mole, one calculates the respective free energies to be 11.4, 124 and 139 kcal. Even if MgB_{12} had a heat of formation of zero, loss of metal from MgB_6 to form MgB_{12} would still predominate.

Because of the absence of stability data on MgB_{12}, no calculations to predict its vaporization behavior are worthwhile. It is probable that MgB_{12} will also lose magnesium preferentially. However, it is certain that all magnesium borides on the metal side of MgB_{12} will lose Mg(g) preferentially. Indeed, this statement is supported by Samsonov's observation that MgB_2 loses Mg to form MgB_6 on heating at 1200°C. in vacuo; and MgB_{12} continues to lose Mg to pure elemental boron at 1700°C. in vacuo (195).

Clearly the overwhelming volatility of Mg metal ($\Delta H^{o}_{vap.298°K.}$ = 35.60 kcal./g-at.) accounts for the vaporization behavior. In addition, the magnesium borides are not as stable with respect to the solid elements as are the lanthanide borides. Further, there is no unusual entropy effect on the free energies of vaporization, since the entropy of magnesium gas is within one entropy unit of that of boron gas (cf. Table 1. 2).

Now consider the behavior of Ca, Sr and Ba hexaborides on vaporization. In the absence of evidence for the existence of other borides in these systems, except CaB_4, the pertinent processes to be considered, again at 1200°K., are:

$$MB_6(s) = 6B(s) + M(g), \qquad (15.16)$$

$$1/7MB_6(s) = 1/7M(g) + 6/7\ B(g) \qquad (15.17)$$

and

$$1/6MB_6(s) = 1/6M(l) + B(g). \qquad (15.18)$$

Assuming heats of formation comparable to SrB_6 and estimating the entropy of MB_6 just as above for MgB_6, one calculates the standard free energy changes for these processes to be 65 to 85 kcal., 120 to 130 kcal. and 139

kcal., respectively. Consequently, hexaborides of Ca, Sr or Ba will lose metal gas preferentially to boron solid.

Samsonov, et al. (181), determined the heat of vaporization of SrB_6 by a Langmuir method. They interpreted their temperature-coefficient data in terms of vaporization to SrB_6 molecules and implied the vaporization was congruent. Their Second Law value was 97.2 $\pm$ 3.0 kcal./mole in the range 1400-2100°K. However, this heat of vaporization is not even sufficient to vaporize a gram atom of boron, much less a mole of SrB_6. Consequently, Samsonov's data are severely in question.

The discussion indicates clearly that all known alkaline earth borides lose metal to form boron solid. Metal volatility alone apparently governs the vaporization behavior of alkaline earth borides, in contrast to the lanthanide borides, where entropy variations and boride heats of formation are important.

15. 2. 4 Vaporization of Uranium Borides

It is interesting to examine the vaporization processes exhibited in the uranium-boron system in comparison to the lanthanide behaviors found in this work. The borides in the uranium-boron system are UB_2, UB_4 and UB_{12}.

Recently, Alcock and Grieveson (184) have determined free energies of formation as a function of temperature for UB_2, UB_4 and UB_{12} based on a Knudsen effusion technique. They determined the U(g) and B(g) pressures over a UB_4-UB_{12} mixture in tungsten crucibles. Uranium boride entropies were calculated as for the lanthanide borides (cf. Chapter 15. 1. 3. 2)

from the elemental entropy data listed in Table 1. 2. With these entropies and the uranium volatility of Table 1. 2 the heat of formation of UB_4 at 2200°K. was determined from Alcock and Grieveson's free energy of formation as -72.7 kcal./mole. The heat of formation of UB_{12} was estimated at -127 kcal./mole from its reported free energy of formation. However, a calculation of the free energy change with these heats and entropies for the process,

$$3/2\ UB_4(s) = 1/2UB_{12}(s) + U(g)\ , \qquad (15.19)$$

failed to duplicate Alcock and Grieveson's free energy change for this process (84.0 kcal.) by 4.8 kcal. (88.8 kcal. on back calculation). While this small disagreement reflects a fundamental inconsistency in their data, the observation that UB_4 and UB_{12} are much more stable with respect to the condensed elements than their lanthanide counterparts is secure. The high stability of UB_4 and UB_{12} explains why attempts to prepare UB_6 produce only UB_4 and UB_{12}.

Another anomaly in Alcock and Grieveson's measurements arises in using their data to define the principal vaporization process for UB_{12}. By adding the appropriate reactions, and, hence, the free energies, one may calculate from their data the free energy changes at 2200°K. for the processes,

$$1/13UB_{12}(s) = 1/13U(g) + 12/13B(g),\ \Delta F^\circ = 61.0\ \text{kcal.}, \qquad (15.20)$$

$$1/8\ UB_{12}(s) = 1/8\ UB_4(s) + B(g),\ \Delta F^\circ = 66.7\ \text{kcal.}, \qquad (15.21)$$

and

$$UB_{12}(s) = 12\ B(s) + U(g),\ \Delta F^\circ = 132.3\ \text{kcal.} \qquad (15.22)$$

Since process 15.20 proceeds with the smallest free energy, one predicts from their data that UB_{12} will vaporize congruently. However, Brewer, et al. (74), indicated that UB_{12} probably loses B(g) preferentially on sintering compositions of UB_{12} synthetic composition to form UB_4(s). In view of the small difference in free energies between processes 15.20 and 15.21, a simple vaporization experiment to define the principal vaporization process for UB_{12} should define the heat of formation of UB_{12} fairly precisely.

CHAPTER 16

SUMMARY AND CONCLUSIONS

The phases of the rare earth-boron systems are presented in Table 2. 1. In the course of a cursory investigation of the rare-earth borides, cubic dodecaborides of Ho, Er and Yb were found. Gadolinium dodecaboride could not be made. An extremely boron-rich phase with composition LnB_{100} was identified for Gd and Yb. The primitive cubic unit cell for this hectoboride has edges of 16.50 ± 0.02 and 16.56 ± 0.01 Å, respectively. The failure to observe GdB_2 and the many tetraborides and hexaborides found generally confirmed the results of previous research in the field.

The high temperature vaporization processes for La, Ce, Pr, Nd, Sm, Gd, Tb, Dy, Yb, and Y borides were established and are depicted in Figure 4. Free evaporation experiments and Knudsen effusion experiments using ZrB_2 crucibles demonstrated the preferential loss of lanthanide metal to the gas phase from the tetraborides of La, Ce, Pr, Nd and Sm and demonstrated the congruent vaporization of hexaborides for these lanthanides. Hexaborides of Gd, Tb, Dy and Y were found to lose boron gas preferentially to form tetraborides, which then vaporized congruently. Ytterbium tetra-, hexa- and dodecaboride all lost ytterbium preferentially on vaporization with YbB_{100} probably the congruently vaporizing phase.

A mass spectrometric study of the vaporization of a GdB_4/GdB_6 mixture and a TbB_4/TbB_6 mixture in tungsten and ZrB_2 crucibles demonstrated

that the vapor phase over these borides contained only the gaseous elements. When background pressures in the mass spectrometer were high at crucible temperatures over 1900°K., GdO^+ (and TbO^+) and GdO_2^+ ion currents in appreciable proportions to Gd^+ were observed. From this demonstration of only atomic species in the vapor over lanthanide borides, the vaporization reactions of the lanthanide borides may be written.

The stability of GdB_4 with respect to the gaseous elements was determined. Gadolinium and boron pressures over congruently vaporizing GdB_4 were determined in the temperature range 1600 to 2500°K. by Langmuir, mass spectrometric and Knudsen effusion techniques. The temperature coefficient graphs are shown in Figure 13. These data were treated by Second and Third Law techniques in each of the three kinds of experiments. The low gadolinium pressures found in the Langmuir free evaporation experiments demonstrated a vaporization coefficient of about 0. 1. The mass spectrometric studies suffered from reaction of background water or oxygen gas with the sample, forming GdO(g) and possibly $Gd_2O_3(s)$, and effecting high apparent gadolinium pressures. Consequently, the mass spectrometrically-determined gadolinium pressures were not reliable.

The Knudsen experiments provided the most reliable measure of GdB_4 stability. From the Knudsen experimental data in the range 2047 to 2362°K., ΔH° from the temperature coefficient is 121.2 $\pm$ 16.6 kcal. for the vaporization of 1/5 mole of GdB_4 to gaseous elements. The value of $\Delta S^\circ_{2200°K.}$ from the intercept is 31.6 $\pm$ 7.4 eu. An $S^\circ_{298°K.}$ was obtained for GdB_4 by taking the sum of the elemental values and correcting it as indicated from a consideration of MgB_4 for which measurements have been made. From this value together with the assumption that $\Delta C_p^\circ = 0$ at each

temperature for the formation of GdB_4 and with the entropies of the gaseous elements, the Third Law $\Delta H^8_{2200°K.}$ is 124.8 ± 3.6 kcal.; and the Third Law $\Delta H^8_{2980°K.}$ is 128.9 ± 3.7 kcal., both for formation of a total mole of gas. The gadolinium pressure over $GdB_{4.00}$ is 3.2×10^{-6} atm. within a factor of 2.2 at 2200°K. The agreement between the Second and Third Law values for the heat of vaporization of 1/5 mole of GdB_4 from Knudsen effusion data is very good, and also the agreement between these values and the value of 127.6 to 139.8 estimated from ternary equilibrium studies is good. The agreement of the Second Law entropy with the value of 32.4 eu., determined above from the estimated S^o for $GdB_4(s)$, is good. The high pressure of boron over $GdB_4(s)$ compared to the vapor pressure of boron fixes the stability of GdB_6 and GdB_{100} with respect to the gaseous elements fairly closely, i. e., between -55.3 and -55.1 kcal. for $\Delta F^o_{2200°K.}$ per total mole of gas atoms. However, a lower boron pressure over GdB_4 than that corresponding to the measured gadolinium pressure can be expected from reaction of boron with the ZrB_2 crucible.

Within the analytical experimental accuracy of ± 1 atomic percent boron and ± 0.5 atomic percent gadolinium in the boride, chemical analyses for gadolinium and boron in GdB_6 and GdB_4 samples supported the congruence of GdB_4 vaporization, the stoichiometry of the borides, and the existence of a narrow solid solution range.

Ternary compatibility studies involving lanthanide borides arc melted with the metals, Zr, Ta, W, or their borides and with graphite established the ternary equilibria in these systems. These equilibria are shown in Figures 14. 1 to 14.14. From a knowledge of the equilibria and the heats of formation of the non-lanthanide borides, the following limits

on the heats of formation of lanthanide borides were established.

For all Ln,

$$-24 < 1/2\Delta H_{f_{LnB_2}} < -13.4 \text{ kcal./g.-at. boron,}$$

$$-22 < 1/4\Delta H_{f_{LnB_4}} < 0 \text{ kcal./g.-at. boron,}$$

$$0 < \Delta H_{f_{LnB_2}} - \Delta H_{f_{LnB_4}} < 24 \text{ kcal./mole,}$$

$$-16.7 < 1/6\Delta H_{f_{LnB_6}} < 0 \text{ kcal./g.-at. boron,}$$

$$\Delta H_{f_{LnB_4}} - \Delta H_{f_{LnB_6}} < 12.5 \text{ kcal./mole}$$

and

$$-11.5 < 1/12\ \Delta H_{f_{LnB_{12}}} < -2.2 \text{ kcal./g.-at. boron .}$$

More specifically, for all lanthanides except Er, Tm and Lu,

$$-16.7 < 1/6\Delta H_{f_{LnB_6}} < -6.5 \text{ kcal./g.-at. boron,}$$

$$-22 < 1/4\Delta H_{f_{LnB_4}} < -6.9 \text{ kcal./g.-at. boron}$$

and

$$5.6 < \Delta H_{f_{LnB_4}} - \Delta H_{f_{LnB_6}} < 11.5 \text{ kcal./mole .}$$

And for Er, Tm and Lu,

$$\Delta H_{f_{LnB_4}} - \Delta H_{f_{LnB_{12}}} < 50 \text{ kcal./mole.}$$

At a temperature above that for disproportionation of GdB_2 into Gd and GdB_4, with no consideration of GdB_{100}, the heats of formation of the gadolinium borides are related in the following manner:

$$3\Delta H_{f_{GdB_4}} < 2\Delta H_{f_{GdB_6}} < 4\Delta H_{f_{GdB_6}} - 3\Delta H_{f_{GdB_4}} < \Delta H_{f_{GdB_6}}$$

$$< \Delta H_{f_{GdB_4}} < \Delta H_{f_{GdB_{12}}} < 2/3\Delta H_{f_{GdB_6}} < 1/3\Delta H_{f_{GdB_{12}}} < 0.$$

Similar series of inequalities can be written for other lanthanide systems, depending on which borides exist.

The heat of formation of GdB_2C_2 must lie between -78 and -28 kcal./mole, according to its reaction with W_2B to form WB and GdC_2 and its formation with graphite from B_4C and GdC_2. Hence, GdB_2C_2 is comparable in stability to lanthanide tetraborides.

These limits compare favorably with a broader limit on $\Delta H_f(CeB_4)$ > -21 kcal./g.-at. B established by Brewer and Heraldsen (20), with an estimate for $\Delta H_f(CeB_6)$ of -81 ± 15 kcal./mole by Samsonov and Grodshtein (183), with estimates by Leitnaker (133) of -15 ± 3 and -12 ± 2 kcal./g.-at. of boron for ΔH_f of lanthanide tetra- and hexaborides, respectively, and with Leitnaker's estimate for $\Delta H_f(LaB_6)$ as -70 ± 10 kcal./mole.

Considerable discussion on the use of metal boride reference systems to establish heats of formation for borides in other metal-boron

systems was presented. The concept of a boron potential series consisting of metal boride couples, which would catalogue the stability of metal borides and predict equilibria in multicomponent boride diagrams, was expounded. The series is given in Table 14. 5.

The factors influencing the vaporization behavior of the lanthanide borides were established. The principal vaporization processes exhibited by the lanthanide tetra- and hexaborides cannot be explained solely on the basis of metal volatility as was supposed at the outset of this work. Of the three processes by which a boride may vaporize, i. e, loss of metal gas, congruent vaporization, or loss of boron gas, the principal process cannot be established by choice of the vaporization process with the smallest enthalpy change. Because of the large differences in the entropy among the lanthanide metal gases and the larger entropy differences between the metal gas entropies and that of boron gas, the $T\Delta S^{o}$ contribution to the free energies of vaporization is different for different lanthanides, for different borides, and for different vaporization processes. This factor influences the vaporization behavior exhibited by the various lanthanide borides quite markedly. Further, the variation with lanthanide in the entropy of the solid borides, and the contribution of the boride entropy to the free energies of vaporization are also important in defining the principal vaporization process. These boride entropies have been estimated at 2200°K. for LnB_4, LnB_6 and LnB_{12}.

Totaling these three contributions to the free energy of vaporization for the possible vaporization processes of LnB_4 and LnB_6 still does not allow the calculated principal vaporization processes to match the observed processes. Variation with lanthanide in the heats of formation of

the tetra- and hexaborides must be prescribed such that $\Delta H_{f_{LnB_4}} - \Delta H_{f_{LnB_6}}$ becomes smaller, in general, across the lanthanide series. Arguments supporting the decrease in stability of LnB_6 with respect to condensed elements at a rate faster than that of LnB_4 as a function of atomic number were presented. The calculated and observed principal vaporization processes could be made to agree (cf. Table 15. 7) by restricting the heat of formation of LnB_4 between -55 to -40 kcal./mole and of LnB_6 between -65 to -40 kcal./mole with LnB_6 becoming less stable with Z faster than LnB_4. These limits on the heats of formation for LnB_4 and LnB_6 are not independent, but are subject to the inequalities which arise from the existence of the various phases for the particular metal.

A more rapidly decreasing stability of LnB_6 than LnB_4 stability would explain the instability of Er, Tm and LuB_6 with respect to the tetra- and dodecaborides. Further, the inability to prepare EuB_4, the difficulty in preparing LaB_4, and the ability to prepare YbB_4 when Yb has a higher metal volatility than Eu, can all be explained by a decreasing hexaboride stability across the lanthanides relative to LnB_4 stability. A more rapidly decreasing stability of LnB_6 than that of LnB_{12} would explain the instability of dodecaborides of the lighter lanthanide metals with respect to LnB_6 and LnB_{100} (or boron) formation.

The stabilities of the tetra- and hexaborides with respect to gaseous elements were described by the free energies for the congruent vaporization processes, calculated in the fitting of calculated to observed principal vaporization processes. These stabilities are shown in Figure 15. 6. The stabilities were found to vary with the same double

periodicity over the lanthanides as does the stability of the lanthanide metals with respect to lanthanide metal gas. However, this variation was considerably damped compared to the metal variation.

The agreement of the predicted stability of GdB_4 at 2200°K. of 53.0 kcal./per total mole of gas formed with the measured value of 55.3 kcal. from the Knudsen pressure measurements supports the analysis of the tetra- and hexaboride vaporization behavior in this work. Further, with the measured GdB_4 stability as a reference, the absolute stabilities of other lanthanide hexa- and tetraborides, rather than their relative stabilities as defined by the observed vaporization processes, are defined.

The stabilities of the lanthanide tetra- and hexaborides with respect to the gaseous elements lie between -45 and -60 kcal. for formation of one total gram atom of the boride at 2200°K. Hexaborides are two or three kcal. more stable with respect to gaseous elements than tetraborides per gram atom of gas for the lighter lanthanide metals. However, in general the tetraborides are more stable with respect to gaseous atoms by one or two kcal. per gram atom of gas than are the hexaborides for the heavier lanthanides. The most stable hexaboride and tetraboride with respect to the gaseous elements are CeB_6 and CeB_4 or LuB_4, respectively, reflecting principally the high heats of sublimation of Ce and Lu metals. The least stable corresponding borides are EuB_4 or YbB_4 and YbB_6, reflecting the low heat of vaporization of Eu and Yb metals.

To predict the vaporization process from these stabilities the appropriate vaporization equations must be written and the free energies calculated. Then the process with the smallest free energy per gram atom of gas will predominate.

The vaporization processes for Sc, Y and the alkaline earth and uranium borides were described. Agreement with reported vaporization behaviors lends even more confidence in the interpretation of the factors influencing boride vaporization processes discussed above.

CHAPTER 17

RELATED FUTURE RESEARCH

The overwhelming limitation of any discussion of boride behavior is the absence of thermochemical data such as heats of formation, heat capacities, entropies and decomposition pressures. While the need for thermochemical information has been recognized, as indicated by the increased effort in this direction in the past fifteen years, data are still woefully lacking.

This deficiency is particularly true in the lanthanide systems. Lanthanide borides are still to be discovered, much less to be characterized thermochemically. Even the heats of vaporization of the lanthanide metals are not well established. Further, the ground states of several of the lanthanide gaseous metals have not been interpreted, making entropy factors only roughly estimable.

Several people have measured boron pressures over elemental boron to determine its heat of vaporization. Yet, currently, scientists disagree about the heat of vaporization of boron. For the most part, the disagreement lies in a controversy between mass spectrometric interpretations and Knudsen effusion measurements. Values for $\Delta H^{\circ}_{298^{\circ}K.}$ (vap.) of boron have been proposed in the range 133 ± 4 kcal./g.-at.

Certainly one large limiting factor in determining thermochemical data on boron and its metal compounds is the purity of materials. The

purity of reagent-grade boron, until recently, was only 95 to 98% at best. The large stability and low volatility of boron oxides precludes removal of all oxygen by ordinary vacuum distillation techniques. Future studies must be done on materials prepared in extremely-deficient oxygen atmospheres, i. e., ultra-high vacuum. The ability to analyze boron precisely is needed to confirm phase compositions, solid solution effects and establish net reactions.

Attempts to prepare the diborides and dodecaborides of the lanthanides early in the lanthanide series should be made. The recent work in this area has been done with arc melting preparations or with vacuum firings above 1400°C. At such high temperatures these borides are probably unstable with respect to adjacent borides. If the free-energy-function of the disproportionation reaction changes with temperature, the diborides and dodecaborides of the lighter lanthanides might well be observed at lower preparation temperatures.

In view of the discussion of hectoborides contained above, it is believed that all lanthanides will exhibit a LnB_{100} phase. In the past, the complex diffraction records for both boron and LnB_{100} and the high boron content of this phase led research workers to postulate boron allotropes rather than a boride. On close examination of boron-rich preparations with longer wavelength X-radiation and X-ray focusing cameras or with metallographic analysis, other LnB_{100} phases may be distinguished. In view of the very high boron content of LnB_{100}, a single crystal analysis possibly can locate both metal and boron atoms in the crystal structure. When electrical and thermochemical properties of these materials become available, quantum mechanics can be applied to a new series of

similar borides to sharpen the interpretation of bonding in the solid state. This phase may exist for other transition metals, whose radii are comparable to the radii of the lanthanide metals.

Considerable effort should be made to develop the temperature-composition phase diagrams in these systems. Variations of melting points, eutectic temperatures and eutectoid temperatures with lanthanide would provide valuable insight into the relative stabilities of these borides. Solid solution effects should be characterized to establish the precise stoichiometry of net chemical processes.

While this work described the general vaporization behavior in most of the lanthanide boride and other metal-boron systems, there is much to be done establishing the pressure-composition diagrams in more detail. In particular, consider the estimations of the free energies for the possible vaporization processes of LnB_4 and LnB_6 in Table 15. 7. Where the free energies for two possible vaporization processes are nearly the same, establishing the principal vaporization process for these borides will further define the limits on the stability of the lanthanide borides. Judicious choices are EuB_6, HoB_6, ErB_{12}, TmB_4 and LuB_{12}. These studies are simple, rapid experiments with a large leverage towards understanding the variations in boride relative stability with lanthanide.

In view of the close competition between possible vaporization processes for some borides and in view of the difference in free-energy-functions between gaseous boron and gaseous lanthanide, it is possible that the differences in free-energy-functions for the competing vaporization processes are sufficient to allow two different single-phase congruently-vaporizing compositions in the same system but at different tempera-

tures. As discussed in the samarium-boron system, these temperatures may be within 1000° of each other, and both congruently vaporizing borides may develop pressures detectable with a mass spectrometer.

It does not seem practical to continue Knudsen effusion pressure measurements on these borides in order to distinguish the small variations in stability of these borides with respect to solid or gaseous elements as a function of lanthanide. The free energy differences between the congruent vaporization process of a lanthanide boride and the same process for the corresponding boride of an adjacent lanthanide are usually of the order of 2 kcal. at most. At 2000°K. this is a difference in the equilibrium constants and the pressures of a factor of 1.7, which is not easily measureable in these boride systems with Knudsen effusion techniques and ZrB_2 crucibles. Further, the Knudsen experiments may define the pressures, but the current lack of thermochemical data for the borides, in particular, entropies and heat capacities, prevents the precise determination of the heat of formation of the boride. However, Knudsen experiments, judiciously chosen to establish the limits in which these boride stabilities must vary, are advantageous, e. g., Yb pressures over YbB_6-YbB_{12} mixtures and congruent vaporization of CeB_6.

An isopiestic method for establishing relative boride volatilities seems inviting in principle. In this technique, two corresponding borides of different lanthanide metals would be physically separated in an isothermal, evacuated, sealed system. When the boron pressures have equilibrated, the boride phases would be identified to discover which boride developed the higher boron pressure. However, large metal partial pressures and

solid solutions between isomorphic corresponding borides of the different lanthanides would prevent boride identification.

If the difference in total pressures developed by corresponding lanthanide borides of different lanthanides could be determined, relative stabilities of the borides with respect to gas atoms would be established. Perhaps the simplest means of determining relative volatility of the lanthanide borides would be found in the torsion effusion technique. A ZrB_2 or HfB_2 torsion cell, whose null point had been determined by loading both sides with one of the materials to be intercompared and heating to the temperature of interest, could be loaded with, say, CeB_6 on one side and LaB_6 on the other side. When the cell is heated to the same temperature used in null point determination, a deviation from the null point would be exhibited. The direction and magnitude of this deflection would be determined by the difference in the total pressures exhibited by the borides. Hence, differences in equilibrium constants and free energies of vaporization would be directly determined. Care should be used in determining the relative volatility of non-corresponding borides of different lanthanides, e. g., GdB_4 with LaB_6. While the disparity in total pressures can be fixed, because of the different equilibrium constant expressions the relative free energies may not be fixed.

In order to distinguish the relative stabilities of the borides with respect to the condensed elements, there are many more simple ternary compatibility experiments that can be done. The use of this technique was discussed in detail in Chapter 14. Judiciously chosen reference metal-boron systems might be chosen, which would separate the stabilities of the lanthanide borides into groups and point out the trends for variation

of ΔH_f of the borides with atomic number. As noted in Chapter 14. 7, immediately obvious experiments involve the use of B_4C as a reference to set limits on the difference in LnB_4 and LnB_{12} stabilities for Er, Tm and Lu systems. A second set of experiments to define the same limits involves the reaction of ZrB_2 and LnB_{12} and noting if ZrB_{12} and LnB_4 are formed or not. Finally, MoB-LnB_4 or MoB_2-Ln equilibria might distinguish stabilities of lanthanide tetraborides. Of course, as additional and more precise heats of formation are determined for metal borides, additional compatibility studies can be made to establish closer limits on the lanthanide boride heats of formation.

Mass spectrometer ion current ratio measurements, coupled with the boron pressure over GdB_4 deduced from the measured p_{Gd} in this work and the vapor pressure of boron, can yield the pressure of boron over GdB_4-GdB_6, GdB_6-GdB_{100} and GdB_{100}-B two-phase regions. The ratios of boron ion currents, arising from the two-phase condensed systems, would describe the boron partial pressure ratios over these systems. A mixture of GdB_{100} and boron could be vaporized by loss of boron to produce the GdB_{100}-B, GdB_{100}-GdB_6 and GdB_6-GdB_4 ion currents. These pressure determinations could establish the stabilities of these borides with respect to the gaseous elements.

Other experiments, more remotely related to the central effort of describing the influence of different lanthanides on boride stability, might be interesting. First, a quantitative kinetic study of the free evaporation rates as a function of temperature for different-sized lanthanide ions in corresponding borides may lead to an understanding of the mechanism of vaporization of these materials and explain the variation of

evaporation coefficient with temperature. These experiments would be quite easily performed and would be very significant in understanding gas-solid interactions.

Second, the inability to observe BO^+, $B_2O_2^+$ or other boron-oxygen species in the mass spectrum of an oxiding atmosphere over GdB_4, when GdO^+ and TbO^+ have been observed, is baffling. How is the boron transported? Third, a study of the LnO_2 and ZrO_2 molecules by mass spectrometry would be interesting in view of their importance relative to LnO and ZrO. Previous workers failed to observe these molecules because studies were performed under the reducing conditions of a metal crucible.

In conclusion, all of the experiments described in this work are bent towards understanding boride behaviors at high temperature. Hopefully, this effort and future contributions will eventually lead to a clearer interpretation of the chemical binding in the solid state. The fourteen lanthanides and lanthanum provide a wonderful opportunity to study the influence of small variations in size, valence and electronic configuration of metals in borides with generally the same gross properties of the metals and the borides. Hopefully, clarification of the influence of these variations on chemical behavior will lead to theories or correlations which will allow the prediction of such thermochemical properties as entropy, heat capacity and heat of formation and the prediction of such physical properties as electrical and thermal conductance, structure, hardness, thermal expansion and non-stoichiometry for borides or refractories in general.

REFERENCES

1. P. Schwarzkopf and R. Kieffer, Refractory Hard Metals, The MacMillan Company, New York, 1953

2. H. A. Eick and P. W. Gilles, J. Am. Chem. Soc. 81, 5030 (1959)

3. R. Steinitz, Powder Met. Bull. 6, 54 (1951)

4. J. A. Nelson, T. A. Willmore, and R. C. Womeldorph, J. Electrochem. Soc. 98, 465 (1951)

5. H. M. Greenhouse, O. E. Accountius, and H. H. Sisler, J. Am. Chem. Soc. 73, 5086 (1951)

6. F. W. Glaser, J. Metals 4, 391 (1952)

7. H. Nowotny, E. Rudy, and F. Benesovsky, Monatshefte Für chemie 91, 963 (1960)

8. H. Nowotny, E. Rudy, and F. Benesovsky, Monatshefte Für chemie 92, 393 (1961)

9. H. Nowotny, F. Benesovsky, C. Brukl, and O. Schob, Monatshefte Für chemie 92, 403 (1961)

10. E. Rudy, F. Benesovsky, and L. E. Toth, Z. Metallkde. 54, 345 (1963)

11. E. Rudy, F. Benesovsky, and L. E. Toth, Z. Metallkde. 54, 348 (1963)

12. W. Jeitschko, H. Nowotny, and F. Benesovsky, Monatshefte Für chemie 94, 565 (1963)

13. H. H. Stadelmaier, Metall. 17, 412 (1963)

14. L. Ya. Markovskiĭ and N. V. Vekshina, Zhur. Priklad. Khim. 34, 242 (1961)

15. N. V. Vekshina and L. Ya. Markovskiĭ, Zhur. Priklad. Khim. 35, 30 (1962)

16. L. Ya. Markovskiĭ, N. V. Vekshina, and G. F. Pron, Zhur. Priklad. Khim. 35, 2090 (1962)

17. L. Toth, H. Nowotny, F. Benesovsky, and E. Rudy, Monatshefte Für chemie 92, 794 (1961)

18. L. E. Toth, H. Nowotny, F. Benesovsky, and E. Rudy, Monatshefte Für chemie 92, 956 (1961)

19. E. Rudy, "Thermodynamics of High-Melting Uranium and Thorium Compounds," The Symposium on Thermodynamics of Nuclear Materials, Proceedings, May, 1962, International Atomic Energy Agency, Vienna, 1962, pp. 243-269

20. L. Brewer and H. Heraldsen, J. Electrochem. Soc. 102, 399 (1955)

21. E. W. Hoyt, J. Chorné, and W. V. Cummings, A. E. C. Research and Development Report, GEAP-3548, Vallecitos Atomic Laboratory, General Electric Co., Pleasanton, Calif., 1962

22. B. Post, D. Moskowitz, and F. W. Glaser, J. Am. Chem. Soc. 78, 1800 (1956)

23. I. Binder, Powder Met. Bull. 7, 74 (1956)

24. I. Binder, J. Am. Ceram. Soc. 43, 287 (1960)

25. R. W. Johnson and A. H. Daane, J. Phys. Chem. 65, 909 (1961)

26. P.M. de Wolff, Acta Cryst. 1, 207 (1948)

27. E. B. Hunt and R. Rundle, J. Am. Chem. Soc. 73, 4777 (1951)

28. F. H. Spedding, K. Gschneidner, and A. H. Daane, J. Am. Chem. Soc. 80, 4499 (1958)

29. J. B. Hess, Acta Cryst. 4, 209 (1951)

30. K. A. Gschneidner, Jr., Rare Earth Alloys, D. Van Nostrand Co., Inc., Princeton, 1961

31. M. J. Buerger, X-Ray Crystallography, John Wiley and Sons, Inc., New York, 1942

32. M. J. Buerger, Crystal-Structure Analysis, John Wiley and Sons, Inc., New York, 1960

33. International Tables for X-Ray Crystallography, International Union of Crystallography, Kynoch Press, Birmingham, England, 1952

34. M. J. Buerger, Vector Space, John Wiley and Sons, Inc., New York, 1959

35. N. F. M. Henry, H. Lipson, and W. A. Wooster, The Interpretation of X-Ray Diffraction Photographs, D. Van Nostrand Co., Inc., New York, 1951

36. J. A. Ibers, Acta Cryst. 10, 86 (1957)

37. J. Berghuis, I. J. Bertha, M. Haanappel, M. Potters, B. O. Loopstra, C. H. MacGillavry, and A. L. Veenendaal, Acta Cryst. 8, 478 (1955)

38. Internationale Tabellen zur Bestimmung von Kristallstruckturen, 1944 Edition, vol. 2, Gebruder Borntraeger, Berlin, 1935, p. 573

39. P. Blum and F. Bertaut, Acta Cryst. 7, 81 (1954)

40. A. Zalkin and D. H. Templeton, Acta Cryst. 6, 269 (1953)

41. S. La Placa, I. Binder, and B. Post, J. Inorg. Nucl. Chem. 18, 113 (1961)

42. M. Atoji, K. Gschneidner, Jr., A. H. Daane, R. E. Rundle, and F. H. Spedding, J. Am. Chem. Soc. 80, 1804 (1958)

43. R. C. Vickery, R. Sedlacek, and A. Ruben, J. Chem. Soc. 103, 498 (1959)

44. J. L. Hoard, "Structure and Polymorphism in Elemental Boron," Borax to Boranes, No. 32, Advances in Chemistry Series, American Chemical Society, Washington, D. C., 1961, p. 42

45. Therald Moeller, Inorganic Chemistry, John Wiley and Sons, Inc., New York, 1952

46. Ben Post, Refractory Binary Borides, Technical Report No. 6, NR 032-414, under Contract Nonr 839 (12) between the Polytechnic Institute of Brooklyn and the Office of Naval Research (1962)

47. E. Hückel, Z. Phys. 70, 204 (1931)

48. E. J. Felten, J. Inorg. Nucl. Chem. 19, 61 (1961)

49. D. D. Jackson, G. W. Barton, Jr., O.H. Krikorian, and R. S. Newbury, "Vaporization of Gadolinium and Thorium Dicarbides," The Symposium on Thermodynamics of Nuclear Materials, Proceedings, May, 1962, International Atomic Energy Agency, Vienna, 1962, pp. 529-548

50. J. Drowart, private communication, Université Libre de Bruxelles, 1963

51. A. Büchler and J. B. Berkowitz-Mattuck, Bull. of Thermodynamics and Thermochemistry, IUPAC Committee on Thermodynamics and Thermochemistry, 5, 4 (1962)

52. D. White, P. N. Walsh, L. L. Ames, and H. W. Goldstein, "Thermodynamics of Vaporization of the Rare-Earth Oxides at Elevated Temperatures; Dissociation Energies of the Gaseous Monoxides," The Symposium on Thermodynamics of Nuclear Materials, Proceedings, May 1962, International Atomic Energy Agency, Vienna, 1962, pp. 417-440

53. P. N. Walsh, H. W. Goldstein, and D. White, J. Am. Ceram. Soc. 43, 229 (1960)

54. J. M. Leitnaker, M. G. Bowman, and P. W. Gilles, J. Electrochem. Soc. 109, 441 (1962)

55. D. White, P. N. Walsh, H. W. Goldstein, and D. F. Dever, J. Phys. Chem. 65, 1408 (1961)

56. O. C. Trulson, D. E. Hudson, and G. H. Spedding, J. Chem. Phys. 35, 1024 (1961)

57. A. H. Daane and F. H. Spedding, abstract of paper presented at the American Chemical Society Meeting, Chicago, Sept., 1958

58. W. R. Savage, D. E. Hudson, and F. H. Spedding, J. Chem. Phys. 30, 221 (1959)

59. F. H. Spedding, J. J. Hanak, and A. H. Daane, Trans. AIME 212, 379 (1958)

60. R. J. Johnson, D. E. Hudson, W. C, Caldwell, F. H. Spedding, and W. R. Savage, J. Chem. Phys. 25, 917 (1956)

61. E. F. Westrum, Jr., and F. Grönvold, "Chemical Thermodynamics of the Actinide Element Chalcogenides," The Symposium on Thermodynamics of Nuclear Materials, Proceedings, May, 1962, International Atomic Energy Agency, Vienna, 1962, pp. 3-36

62. M. H. Rand, "Some Inconsistencies in the Thermodynamic Data for Uranium Compounds," The Symposium on Thermodynamics of Nuclear Materials, Proceedings, May, 1962, International Atomic Energy Agency, Vienna, 1962, pp. 71-80.

63. R. J. Ackermann and R. J. Thorn, "Thermodynamic Properties of Compounds of Actinide Elements," The Symposium on Thermodynamics of Nuclear Materials, Proceedings, May, 1962, International Atomic Energy Agency, Vienna, 1962, pp. 39-59

64. F. H. Spedding and A. H. Daane, The Rare Earths, John Wiley and Sons, Inc., New York, 1961

65. D. R. Stull and G. C. Sinke, Thermodynamic Properties of the Elements, No. 18, Advances in Chemistry Series, American Chemical Society, Washington, D. C., 1956

66. H. L. Schick, et al., "Thermodynamics of Certain Refractory Compounds, Part II," Second Quarterly Progress Report, RAD-SR-62-251, Research and Advanced Development Division, AVCO Corp., Wilmington, Mass., September, 1962

67. J. Kleinberg, W. J. Argersinger, Jr., and E. Griswold, Inorganic Chemistry, D. C. Heath & Co., Boston, 1960

68. L. S. Darken and R. W. Gurry, Physical Chemistry of Metals, McGraw-Hill Book Co., Inc., New York, 1953

69. JANAF Interim Thermochemical Tables, vol. 1, Interim Table Issued December 31, 1960, Joint Army-Navy-Air Force Thermochemical Panel, ARPA-USAF Contract No. AF33 (616)-6149 with the Dow Chemical Company, Midland, Mich.

70. G. N. Lewis, M. Randall, K. S. Pitzer, and L. Brewer, Thermodynamics, McGraw-Hill Book Co., Inc., New York, 1961

71. No author, FS-LA-1, Final Prog. Rept. of Electro Metal Div. of Firth Sterling, Inc., March, 1958

72. N. N. Zhuravlov and A. A. Stepanova, Kristallografiya 3, 94 (1958)

73. R. W. Johnson and A. H. Daane, J. Chem. Phys. 38, 425 (1963)

74. L. Brewer, D. L. Sawyer, D. H. Templeton, and C. H. Dauben, J. Am. Ceram. Soc. 34, 173 (1951)

75. A. Zalkin and D. H. Templeton, Acta Cryst. 6, 269 (1953)

76. E. J. Felten, I. Binder, and B. Post, J. Am. Chem. Soc. 80, 3479 (1958)

77. E. J. Felten, I. Binder, and B. Post, "Cemented Metallic Borides," Final Report, Nonr 2218(00), NR-039-001, 1958

78. V. S. Neshpor and G. V. Samsonov, Dopovidi Akad. Nauk Ukr., R. S. R., 1957, p. 478

79. V. S. Neshpor and G. V. Samsonov, Zhur. Fiz. Khim. 32, 1328 (1958)

80. C. E. Lundin, "Rare Earth Metal Phase Diagrams," paper given at the Rare Earth Symposium, Annual Meeting Am. Soc. Metals, Chicago, November, 1959

81. H. A. Eick, "Rare Earth Borides and Nitrides," paper given at the Rare Earth Research and Development Conference, Lake Arrowhead, Cal., October, 1960

82. H. Moissan and P. Williams, Compt. rend. 125, 629 (1897)

83. M. Geelmuyden, Compt. rend. 130, 1026 (1900)

84. E. Jungst and R. Meines, Chem. Zentr. 1, 195 (1905)

85. A. Stock and W. Holle, Ber. deut. chem. Ges. 41, 2095 (1908)

86. L. Andrieux, Ann. chim. 12, 423-507 (1929)

87. G. Allard, Bull. Soc. chim. France 51, 1213-15 (1932)

88. a. M. V. Stackelburg and F. Neumann, Z. physik. Chem. B19, 314-320 (1932)

b. M. V. Stackelburg and F. Neumann, Ceram. Abstr. 12, 206 (1933)

89. a. F. Laves, Z. physik. Chem. B22, 114-16 (1933)

b. F. Laves, Ceram. Abstr. 13, 73 (1934)

90. R. Kiessling, Acta Chem. Scand. 4, 209-27 (1950)

91. F. Bertaut and P. Blum, Compt. rend. 234, 2621 (1952)

92. G. V. Samsonov, Yu. B. Paderno, and T. I. Serebryakova, Kristallografiya 4, 542 (1959)

93. N. N. Tvorogov, Zhur. Neorg. Khim. 4, 1961 (1959)

94. G. V. Samsonov, Yu. B. Paderno, and T. I. Serebryakova, Kristallografiya 4, 546 (1959)

95. G. V. Samsonov, V. P. Dzeganovskii, and I. A. Semashko, Doklady Akad. Nauk S. S. S. R. 119, 506 (1958)

96. G. V. Samsonov, V. P. Dzeganovskii, and I. A. Semashko, Kristallografiya 4, 119 (1959)

97. I. Binder and R. Steinitz, Plansuber. Pulvermet. 7, 18 (1959)

98. G. V. Samsonov, Uspekhi Khim. 28, 189 (1959)

99. G. A. Kudintseva, M. D. Polyakova, G. V. Samsonov, and B. M. Tsarev, Fiz. Metal. i. Metalloved. 6, 272 (1958)

100. Yu. B. Paderno, T. I. Serebryakova, and G. V. Samsonov, Doklady Akad. Nauk S. S. S. R. 125, 317 (1959)

101. H. A. Eick and G. D. Sturgeon, Inorg. Chem. 2, 430 (1963)

102. F. H. Spedding, A. H. Daane, and K. W. Herrman, Acta Cryst. 9, 559 (1956)

103. J. M. Lafferty, J. Appl. Phys. 22, 299 (1951)

104. S. Flodmark, Arkiv Fysik. 14, 513 (1959)

105. S. Flodmark, Arkiv Fysik. 9, 357 (1954)

106. H. C. Longuet-Higgins and M. deV. Roberts, Proc. Roy. Soc. (London) A224, 336 (1954)

107. W. N. Lipscomb and D. Britton, J. Chem. Phys. 33, 275 (1960)

108. H. C. Longuet-Higgins and M. deV. Roberts, Proc. Roy. Soc. (London) A230, 110 (1955)

109. F. Bertaut and P. Blum, Compt. rend. 229, 666 (1949)

110. L. Andrieux and P. Blum, Compt. rend. 229, 210 (1949)

111. B. Post and F. W. Glaser, Trans. Amer. Inst. Mech. Engrs. 194, 631 (1952)

112. B. Post and F. W. Glaser, J. Metals 4, 631 (1952)

113. B. Post, D. Moskowitz, and F. W. Glaser, J. Am. Chem. Soc. 78, 1800 (1956)

114. A. V. Seybolt, Trans. Am. Soc. Met. 52, 971 (1960)

115. S. LaPlaca, D. Noonan, and B. Post, Acta Cryst. 16, 1182 (1963)

116. F. W. Glaser and B. Post, J. Metals 5, 1117 (1953)

117. Gordon L. Galloway, Ph. D. Dissertation, Michigan State Univ., 1961

118. J. L. Hoard, J. Am. Chem. Soc. 82, 70 (1960)

119. J. L. Hoard, "Remarks on Structure and Polymorphism in Boron," Boron, Synthesis, Structure, and Properties, (J. A. Kohn, W. F. Nye, and G. K. Gaulé), Plenum Press, Inc., New York, 1960, p. 1

120. B. F. Decker and J. S. Kasper, Acta Cryst. 12, 503 (1959)

121. J. L. Hoard, S. Geller, and R. E. Hughes, J. Am. Chem. Soc. 80, 4507 (1958)

122. D. E. Sands and J. L. Hoard, J. Am. Chem. Soc. 79, 5582 (1957)

123. C. P. Talley, Acta Cryst. 13, 271 (1960)

124. St. V. Náray-Szabó and C. W. Tobias, J. Am. Chem. Soc. 71, 1882 (1949)

125. M. A. Rollier, Proc. XIth Int. Cong. Pure and Applied Chem., London 5, 935 (1947), published 1953; Chem. Abs. 47 (1953) 11941h

126. D. R. Stern and L. Lynds, J. Electrochem. Soc. 105, 676 (1958)

127. J. L. Hoard and R. E. Hughes, J. Am. Chem. Soc. 85, 361 (1963)

128. P. W. Gilles, "High Temperature Chemistry of the Binary Compounds of Boron," Borax to Boranes, No. 32, Advances in Chemistry Series, American Chemical Society, Washington, D. C., 1961

129. F. W. Glaser and B. Post, Trans. AIME 197, 117 (1953)

130. H. L. Schick, et al., "Thermodynamics of Certain Refractory Compounds, Part II, "Fourth Quarterly Progress Report, RAD-SR-63-105, Research and Advanced Development Division, AVCO Corp., Wilmington, Mass., June, 1963

131. J. M. Leitnaker, M. G. Bowman and P. W. Gilles, J. Chem. Phys. 36, 350 (1962)

132. H. L. Schick, et al., "Thermodynamics of Certain Refractory Compounds, Part II," Third Quarterly Progress Report, RAD-SR-63-52, Research and Advanced Development Division, AVCO Corp., Wilmington, Mass., March, 1963

133. J. M. Leitnaker, N. H. Krikorian, and M. G. Bowman, "High Temperature Poisons," Symposium on Recent Developments in Materials for Nuclear Applications, American Society of Metals, Albuquerque, New Mexico, February, 1961

134. P. Schwarzkopf and F. W. Glaser, Z. Metalkunde 44, 353 (1953)

135. A. W. Searcy and C. E. Myers, J. Phys. Chem. 61, 957 (1957)

136. J. M. Leitnaker, Ph. D. Dissertation, University of Kansas, 1960

137. V. A. Epel'baum and M. A. Gurevich, Zhur. Fiz Khim. 32, 2274 (1958)

138. L. Brewer, D. L. Sawyer, D. H. Templeton, and C. H. Dauben, J. Am. Ceram. Soc. 34, 173 (1951)

139. H. A. Eick and P. W. Gilles, unpublished work, Eick N. B. p. 368, University of Kansas, 1959

140. L. Y. Markovsky, Y. D. Kondrashev, and G. V. Kaputovskaya, Zhur. Obshchei Khim. 25, 409 (1955)

141. P. Blum and F. Bertaut, Acta Cryst. 7, 81 (1954)

142. P. W. Gilles, "Vaporization Processes of Refractory Materials," The Symposium on Thermodynamics of Nuclear Materials, Proceedings, May, 1962, International Atomic Energy Agency, Vienna, 1962, pp. 401-413

143. W. A. Chupka, ANL-5667, Argonne National Laboratory Report, Argonne, Illinois, 1957, p. 75

144. W. A. Chupka, J. Berkowitz, M. Giese, and M. G. Inghram, J. Phys. Chem. 62, 611 (1958)

145. M. G. Inghram and R. J. Haydon, Publication 311, National Academy of Science and National Research Council, 1954

146. W. A. Chupka and M. G. Inghram, J. Phys. Chem. 59, 100 (1955)

147. H. J. Kostkowski and R. D. Lee, "Theory and Methods of Optical Pyrometry," National Bureau of Standards Monograph 41, March, 1962

148. J. O'M. Bockris, J. L. White, and J. D. MacKenzie, Physiochemical Measurements at High Temperatures, Butterworths Scientific Publications, London, 1959

149. Irving Langmuir, Phys. Rev. 2, 329 (1913)

150. M. Knudsen, Ann. Phys. 28, 75 (1909); 28, 299 (1909); 29, 179 (1909)

151. M. Knudsen, Kinetic Theory of Gases, Methuen, Ltd., London, 1934

152. M. G. Inghram and J. Drowart, "Mass Spectrometry Applied to High Temperature Chemistry," High Temperature Technology, McGraw-Hill Book Co., Inc., 1960

153. W. A. Chupka and M. G. Inghram, J. Phys. Chem. 59, 104 (1959)

154. J. Drowart and P. Goldfinger, Jour. de Chimie Physique 7, 721 (1958)

155. J. W. Otvos and D. P. Stevenson, J. Am. Chem. Soc. 78, 546 (1956)

156. J. Drowart, private communication, Université Libre de Bruxelles, 1963

157. M. Knudsen, Ann. Physik 28, 999 (1909)

158. R. J. Thorn, ANL-5417, Argonne National Laboratory Report, Argonne, Illinois, March, 1955

159. P. Clausing, Ann. Physik 12, 961 (1932)

160. Saul Dushman, Scientific Foundations of Vacuum Techniques, John Wiley and Sons, Inc., New York, 1949

161. Ketil Motzfeldt, J. Phys. Chem. 59, 139 (1955)

162. K. D. Carlson, P. W. Gilles, and R. J. Thorn, paper presented at the High Temperature Symposium of the Division of Inorganic Chemistry, 135th Meeting of the American Chemical Society, Boston, Mass., April, 1959

163. O. Knacke and I. N. Stranski, Progr. Metal. Phys. 6, 181 (1956)

164. J. P. Hirth and G. M. Pound, J. Chem. Phys. 26, 1216 (1957)

165. L. Brewer, XVI International Congress of Pure and Applied Chemistry, Paris, 1957, Birkhauser Verlag, Basel and Stuttgart, 1957, p. 227

166. R. J. Ackermann and R. J. Thorn, XVI International Congress of Pure and Applied Chemistry, Memoire presente a la section Chimie Minerale, Paris, 1957, Birkhauser Verlag, Basel and Stuttgart, 1957, p. 609

167. E. F. Northrop, Trans, Am. Electrochem. Soc. 25, 69 (1919)

168. G. Babat and M. Losinsky, J. App., Phys. 11, 816 (1940)

169. D. L. Hildenbrand, L. P. Theard, W. F. Hall, F. Ju, F. S. LaViola, and N. D. Potter, First Quarterly Technical Report, Section 4, ARPA No. 22-62, Aeronutronic Division of Ford Motor Company, Newport Beach, Cal., September, 1962

170. M. G. Inghram, private communication, University of Chicago, 1963.

171. A. Büchler and J. B. Berkowitz-Mattuck, J. Chem. Phys. 39, 286 (1963)

172. M. B. Panish, J. Chem. Eng. Data 6, 592 (1961)

173. M. G. Inghram, R. J. Haydon, and P. Hess, "Mass Spectrometry in Physics Research," National Bureau of Standards (U. S.) Circular 522, 257 (1963)

174. R. D. Freeman and A. W. Searcy, J. Chem. Phys. 22, 1137 (1954)

175. H. N. Russell, J. Opt. Soc. Amer. 40, 550 (1950)

176. R. M. Swift and D. White, J. Am. Chem. Soc. 79, 3641 (1957)

177. J. G. Edwards, Ph. D. Dissertation, Oklahoma State University, 1964

178. H. E. Robson and P. W. Gilles, "The High Temperature Vaporization of Boron Carbide and the Heat of Sublimation of Boron," to be published in J. Phys. Chem., June, 1964

179. O. Kubaschewski and E. LL. Evans, Metallurgical Thermochemisty, Third Edition, Pergamon Press, New York, 1958, p. 185

180. G. V. Samsonov and V. S. Neshpor, Zhur. Neorg. Khim. 4, 1956 (1959)

181. G. V. Samsonov, T. I. Serebryakova and A. S. Bolgar, Zhur. Neorg. Khim. 6, 1142 (1961)

182. G. A. Kudintseva, M. D. Polyakova, G. V. Samsonov, and B. Tsarev, Fiz. Metal. i. Metalloved, 6, 275 (1958)

183. G. V. Samsonov and A. E. Grodshtein, Zhur. Fiz. Khim. 30, 379 (1956)

184. C. Alcock and P. Grieveson, "A Study of Uranium Borides and Carbides by Means of the Knudsen Effusion Technique," The Symposium on Thermodynamics of Nuclear Materials, Proceedings, May, 1962, International Atomic Energy Agency, Vienna, 1962, pp. 563-578.

185. P. Gilles and D. Pollock, Trans. Am. Inst. Mining Met. Engrs. 197, 1537 (1953); unpublished work

186. D. Smith, A. S. Dworkin, and E. R. Van Artsdalen, J. Am. Chem. Soc. 77, 2654 (1955)

187. W. A. Knarr, Ph. D. Dissertation, University of Kansas, 1959

188. Gerhard Herzberg, Atomic Spectra and Atomic Structure, Dover Publications, New York, 1944

189. R. Mezaki, E. W. Tilleux, D. W. Barnes, and J. L. Margrave, "High-Temperature Heat Contents of Some Refractory Borides," The Symposium on Thermodynamics of Nuclear Materials, Proceedings, May, 1962, International Atomic Energy Agency, Vienna, 1962, pp. 775-789

190. E. F. Westrum, Jr., H. L. Clever, J. T. S. Andrews, and G. Feick, "Thermodynamics of Lanthanum and Neodymium Hexaborides," 4th Rare Earth Research Conference, Phoenix, Arizona, April, 1964

191. Landolt-Börnstein, Zahlenwerte und Funktionen, 6. Auflage, 1. Band, "Atom- und Molekularphysik," 1. Teil, "Atome und Ionen," Springer-Verlag, Berlin, 1950

192. Leo Brewer, "Thermodynamic Stability and Bond Character in Relation to Electronic Structure and Crystal Structure," Electronic Structure and Alloy Chemistry of the Transition Elements, (P. A. Beck), Interscience Publishers, New York, 1963, p. 221

193. Leo Brewer, private communication, University of California, 1963

194. W. H. Eberhardt, B. L. Crawford, and W. H. Lipscomb, J. Chem. Phys. 22, 989 (1954)

195. G. V. Samsonov, L. Ya. Markovskiĭ, A. F. Zhigach, and M. G. Valyashko, Boron, Its Compounds and Alloys, AEC-tr-5032 (Book 2), translated from a publication of the Publishing House of the Academy of Sciences of the Ukrainian S. S. R., Kiev, 1960

196. G. A. Kudintseva, et al., in the collection High Temperature Ceramic Materials, Publishing House of the Academy of Sciences, Ukrainian S. S. R., Kiev, 1960

197. P. C. Nordine, private communication, University of Kansas, 1964

198. R. P. Iczkowski, J. L. Margrave, and S. M. Robinson, J. Phys. Chem. 67, 229 (1963)